LINKING THERMAL VARIABILTY AND CHANGE TO URBAN GROWTH IN HARARE METROPOLITAN CITY USING REMOTELY SENSED DATA

Terence Darlington Mushore

A thesis submitted to the College of Agriculture, Engineering and Science, at the University of KwaZulu-Natal, in fulfilment of the academic requirements for the degree of Doctor of Philosophy in Environmental Science

Supervisors: Professor Onisimo Mutanga and Dr John Odindi

Pietermaritzburg
South Africa

September 2017

ABSTRACT

Urban growth, which involves Land Use and Land Cover Changes (LULCC), alters land surface thermal properties. Within the framework of rapid urban growth and global warming, land surface temperature (LST) and its elevation have potential significant socio-economic and environmental implications. Hence the main objectives of this study were to (i) map urban growth, (ii) link urban growth with indoor and outdoor thermal conditions and (iii) estimate implications of thermal trends on household energy consumption as well as predict future urban growth and temperature patterns in Harare Metropolitan, Zimbabwe. To achieve these objectives, broadband multi-spectral Landsat 5, 7 and 8, in-situ LULC observations, air temperature (Ta) and humidity data were integrated. LULC maps were obtained from multi-spectral remote sensing data and derived indices using the Support Vector Machine Algorithm, while LST were derived by applying single channel and split window algorithms. To improve remote sensing based urban growth mapping, a method of combining multi-spectral reflective data with thermal data and vegetation indices was tested. Vegetation indices were also combined with socio-demographic data to map the spatial distribution of heat vulnerability in Harare. Changes in outdoor human thermal discomfort in response to seasonal LULCC were evaluated, using the Discomfort Index (DI) derived parsimoniously from LST retrieved from Landsat 8 data. Responses of LST to long term urban growth were analysed for the period from 1984 to 2015. The implications of urban growth induced temperature changes on household air-conditioning energy demand were analysed using Landsat derived land surface temperature based Degree Days. Finally, the Cellular Automata Markov Chain (CAMC) analysis was used to predict future landscape transformation at 10-year time steps from 2015 to 2045.

Results showed high overall accuracy of 89.33% and kappa index above 0.86 obtained, using Landsat 8 bands and indices. Similar results were observed when indices were used as stand-alone dataset (above 80%). Landsat 8 derived bio-physical surface properties and socio-demographic factors, showed that heat vulnerability was high in over 40% in densely built-up areas with low-income when compared to "leafy" suburbs. A strong spatial correlation (α = 0.61) between heat vulnerability and surface temperatures in the hot season was obtained, implying that LST is a good indicator of heat vulnerability in the area. LST based discomfort assessment approach retrieved DI with high accuracy as indicated by mean percentage error of less than 20% for each sub-season. Outdoor thermal discomfort was high in hot dry season (mean DI of 31^{o}C), while the post rainy season was the most comfortable (mean DI of 19.9^{o}C). During the hot season, thermal discomfort was very low in low density residential areas, which are characterised by forests and well maintained parks (DI $\leq$27^{o}C). Long term changes results showed that high density residential areas increased by 92% between 1984 and 2016 at the expense of cooler green-spaces, which decreased by 75.5%, translating to a 1.98^{o}C mean surface temperature increase. Due to surface alterations from urban growth between 1984 and 2015, LST increased by an average of 2.26^{o}C and 4.10^{o}C in the cool and hot season, respectively. This decreased potential indoor heating energy needed in the cool season by 1 degree day and increased indoor cooling energy during the hot season by 3 degree days. Spatial analysis showed that during the hot season, actual energy consumption was low in high temperature zones. This coincided with areas occupied by low income strata indicating that they do not afford as much energy and air conditioning facilities as expected. Besides quantifying and strongly relating with energy requirement, degree days provided a quantitative measure of heat vulnerability in Harare.

Testing vegetation indices for predictive power showed that the Urban Index (UI) was comparatively the best predictor of future urban surface temperature (r = 0.98). The mean absolute percentage error of the UI derived temperature was 5.27% when tested against

temperature derived from thermal band in October 2015. Using UI as predictor variable in CAMC analysis, we predicted that the low surface temperature class (18-28^{o}C) will decrease in coverage, while the high temperature category (36-45^{o}C) will increase in proportion covered from 42.5 to 58% of city, indicating further warming as the city continues to grow between 2015 and 2040.

Overall, the findings of this study showed that LST, human thermal comfort and air-conditioning energy demand are strongly affected by seasonal and urban growth induced land cover changes. It can be observed that urban greenery and wetlands play a significant role of reducing LST and heat transfer between the surface and lower atmosphere and LST may continue unless effective mitigation strategies, such as effective vegetation cover spatial configuration are adopted. Limitations to the study included inadequate spatial and low temporal resolution of Landsat data, few in-situ observations of temperature and LULC classification which was area specific thus difficult for global comparison. Recommendations for future studies included data merging to improve spatial and temporal representation of remote sensing data, resource mobilization to increase urban weather station density and image classification into local climate zones which are of easy global interpretation and comparison.

PREFACE

This research was carried out in the School of Agricultural, Earth and Environmental Sciences (SAEES), University of KwaZulu-Natal, Pietermaritzburg, from January 2015 to June 2017, under the supervision of Prof. Onisimo Mutanga and Dr. John Odindi.

I would like to declare that the research reported in this thesis has never been submitted in any form to any other university and represents my original work, except where due acknowledgments are made.

Terence Darlington Mushore

Signed: _Tmushore_____ Date: _27/02/2018__

As the candidate's supervisor, I certify the above statement and have approved this thesis for submission.

Prof. Onisimo Mutanga

Signed: _____ Date: _____

Dr. John Odindi

Signed: _____ Date: _____

DECLARATION 1 - PLAGIARISM

I, **Terence Darlington Mushore**, declare that:

1. The research reported in this thesis, except where otherwise indicated, is my original research,

2. This thesis has not been submitted for any degree or examination at any other university,

3. This thesis does not contain other persons' data, pictures, graphs, or other information, unless specifically acknowledged as being sourced from other persons,

4. This thesis does not contain other persons' writing, unless specifically acknowledged as being sourced from other researchers. Where other written sources have been quoted, then:

    a. Their words have been re-written, but the general information attributed to them has been referenced;

    b. Where their exact words have been used, then their writing has been placed in italics and inside quotation marks, and referenced;

5. This thesis does not contain text, graphics, or tables copied and pasted from the internet, unless specifically acknowledged and the source detailed in the thesis and in the references section.

Signed:_____

DECLARATION 2 - PUBLICATIONS AND MANUSCRIPTS

1. **Mushore T. D**., Odindi J., Dube T., Matongera T., Mutanga O. (**2017)** Remote sensing applications for monitoring urban growth impacts on in-and-out door thermal conditions: A state of the art review. *Remote Sensing Applications: Society and Environment, 8, 83-93,* https://doi.org/10.1016/j.rsase.2017.08.001

2. **Mushore T. D**., Mutanga O., Odindi J., Dube T. (**2017**). Assessing the potential of integrated Landsat 8 thermal bands, with the traditional reflective bands and derived vegetation indices in classifying urban landscapes. *Geocarto International*, 32(8), 886-899, http://dx.doi.org/10.1080/10106049.2016.1188168

3. **Mushore T. D**., Mutanga O., Odindi J., Dube T. (**2018**). Determining extreme heat vulnerability of Harare Metropolitan City using multispectral remote sensing and socio-economic data. *Journal of Spatial Science*, 63(1), 173-191. http://dx.doi.org/10.1080/14498596.2017.1290558

4. **Mushore T. D.**, Odindi J., Dube T., Mutanga O. (**in press**). Outdoor thermal discomfort analysis in Harare, Zimbabwe in Southern Africa. *South African Geographical Journal*, http://dx.doi.org/10.1080/03736245.2017.1339630.

5. **Mushore T. D.**, Mutanga O., Odindi J., Dube T. (**2017**). Linking major shifts in land surface temperatures to long term land use and land cover changes in Harare, Zimbabwe. *Urban Climate*, 20, 120–134, http://dx.doi.org/10.1016/j.uclim.2017.04.005

6. **Mushore T. D.**, Odindi J., Dube T., Mutanga O. (**2017**). Understanding the relationship between urban outdoor temperatures and indoor air-conditioning energy demand in Zimbabwe. *Sustainable Cities and Society*, 34, 97-108, http://dx.doi.org/10.1016/j.scs.2017.06.007

7. **Mushore T. D.**, Odindi J., Dube T., Mutanga O. (**2017**). Prediction of future urban surface temperatures using medium resolution satellite data in Harare Metropolitan City, Zimbabwe. *Building and Environment Journal*, 122, 397-410, http://dx.doi.org/10.1016/j.buildenv.2017.06.033

Signed: _____

DEDICATION

This thesis is dedicated to my wife Placxedes, daughter Anotidaishe Divine Mushore, my parents Mr Terence (senior) and Mrs Cathrine Mushore as well as to my family, inlaws and friends!!!

ACKNOWLEDGEMENTS

But he said to me, "My grace is sufficient for you, for my power is made perfect in weakness."- 2 Corinthians 12:9. I would like to give all thanks to the Almighty God for even during my toughest moments he helped me to rise to the occasion. I would like to express great appreciation to the Government of the Republic of South Africa for availing resources such as the fees remission and peaceful environment which made my studies a success. I would like to thank all members of staff of the Geography department of UKZN Pietermaritzburg Campus for every support. I am grateful for every service rendered to me by the departmental secretary, Mrs Shanita Ramroop, throughout the study period. PhD indeed has heavy demands which I would never have tackled without the supervision and support of the dedicated and very generous Professor Onisimo Mutanga and Dr. John Odindi. God bless you all.

My wife Placxedes and child Anotidaishe deserve a special mention. I started leaving them alone going to South Africa when our marriage was just a few months old and also when my daughter was less than a year old. A special mention also goes to my parents, brothers, sisters and in-laws for encouraging me to push on. Dr Washington Mushore, Professor Arthur Rwafa and Professor Maurice Vambe are family members who inspired me through their academic achievements. Friends were also a pillar of strength throughout my PhD studies. Dr Timothy Dube, Dr Mbulisi Sibanda and Dr Abel Chemura stood by me from the onset and made me believe that things will work out. My sincere gratitude also goes to my all weather friends and colleagues whom I can never finish mentioning by names for boosting my morale and keeping me keeping on.

I acknowledge the generosity of United State Geological Survey Earth Resources Observation and Science (USGS-EROS) for providing Landsat archival data freely online. The Metetorological Services Department of Zimbabwe assisted with meteorological data. I appreciate the support from Zimbabwe Electricity Transmission and Distribution Company (ZETDC) specifically the Tariffs Department for providing energy consumption data for Harare. My sincere gratitude also goes to members of staff of the Physics Department at the University of Zimbabwe for encouraging me to finish the race. Members of the Geography Department of Bindura University of Science Education are thanked for moral support.

I would like to thank Professor Pavari, Pastor (Professor) Shaun and Shani Ramroop, Pastor Mupa, Pastor and the Late Mai Chipangura as well as the assemblies they are or were leading for spiritual guidance during our times of interaction. I thank the Lord Almighty for it is finished!!!!

TABLE OF CONTENTS

LIST OF FIGURES

LIST OF TABLES

LIST OF ACRONYMS

NDBaI	Normalized Difference Bareness Index
NDBI	Normalized Difference Built-up Index
BI	Bare Soil Index
UI	Urban Index
IBI	Index-based Built-up Index
EBBI	Enhanced Built-up and Bareness Index
NBI	Normalized Built Index
NDVI	Normalized Difference Vegetation Index
EVI	Enhanced Vegetation Index
SAVI	Soil Adjusted Vegetation Index
NDWI	Normalized Difference Water Index
MNDWI	Modified Normalized Difference Water Index
FVG	Vegetation Fraction
LST	Land Surface Temperature
CBD	Central Business District
LULC	Land Use and Land Cover
USGS-EROS	United States Global Survey Earth Resources System
CA	Cellular Automata
UN	United Nations
TIR	Thermal infrared
NIR	Near infrared
ETM	Earth thematic mapper
OLI	Operational Land Imager
ASTER	Advanced Space-borne Thermal Emission and Reflection Radiometer
AVHRR	Advanced Very High Resolution Radiometer
ATLAS	Advanced Thermal and Land Applications Sensor
NOAA	North Oceanic Atlantic Administration
MSI	Multi-Spectral Instrument
MSS	Multi-Spectral Scanner
MODIS	Moderate resolution Imaging Spectrometer
HAMO	Harare Airport Meteorological Office
HDD	Heating Degree Days
CDD	Cooling Degree Days
ENVI	Environment for Visualizing Images
GOES	Geostationary Operational Environmental Satellite
SVM	Support Vector Machines
ANN	Artificial Neural Networks
MLC	Maximum Likelihood Classifier
WRF	Weather Research and Forecasting
WUDAPT	World Urban Database and Access Portal Tool
UFP	Urban Footprint Product
LCZ	Local Climate Zone
TEB	Town Energy Balance

CHAPTER 1: GENERAL INTRODUCTION

1.0 Introduction

Climate change threatens sustainable development at global and local scales. Increasing frequency and intensity of extreme events has potential to worsen existing natural hazards, especially in densely populated areas such as cities (Brown. et al., 2012). Globally, average temperatures are rising while the frequency and intensity of heat waves seems to be also on the rise (De-Simone et al., 2011; IPCC, 2007). The contribution of human activities such as land use and land cover (LULC) changes may also significantly modify temperatures such as by altering the energy and water balance of converted areas (Nayak & Mandal, 2012). These changes may increase public health risks such as by increasing diseases, especially where high levels of poverty reduce adaptation options (Dube & Phiri, 2013; McMichael & Confalonieri, 2012; Brown., et al., 2012). According to Newland (2011), it is estimated that 200 million people could be displaced by harsh environmental conditions due to climate change, globally. Concerning is that temperature changes observed over southern Africa were found to be higher than those reported for other parts of the world (IPCC, 2007). Furthermore, Africa is one of the most vulnerable regions in the world due to widespread poverty, limited coping capacity and highly variable climate (Brown., et al., 2012). Therefore, understanding factors contributing to climate dynamics is important for establishing adaptation and mitigation mechanisms, especially in resource constrained regions.

At a local scale, the impacts of climate change are likely to be worsened by alterations to the energy and water balance caused by urbanization. Ogrin and Krevs (2015) observed that temperature changes are faster in urbanized than other areas. High density of population and economic activity in urban areas lead to intense anthropogenic heat release within small spatial scales (Blake, Curitiba, et al., 2011). Replacement of natural soil and vegetation with impervious surfaces reduces latent heat cooling and increases surface and near surface temperatures. Preferential heating of the cities against surroundings increases convection currents which further trap the heat (Tursilowati, 2007). According to Tursilowati (2007), the effect is even worse in central business areas where tall buildings absorb large amounts of heat while reducing ventilation and sensible heat cooling process. The severity of warming in urban areas depends on city size, population density, industrialization, seasonality of climate and structure of roads and transport system, thus differ from city to city (Odindi et al., 2015). According to Gusso et al. (2014), monitoring of local environmental challenges is an important tool for developing policies and strategies for sustainable development. This is also important

for determining internal climate within buildings and energy exchanges that influence comfort of city dwellers (Voogt & Oke, 2003).

While conditions in urban microclimate affect the health and comfort of the residents, energy consumption and air quality, the areas are growing in population and coverage globally. Growth has become remarkable in developing countries over recent decades due to pursuit for fast economic growth (Zhou & Wang, 2011a; Yuen & Kong, 2009). For example, in 2008 more than 50% of the world population were already living in cities (De-Simone, et al., 2011) while projections are that the population will grow to 70% by 2050 (Blake, Curitiba, et al., 2011). In developing countries, urbanization offers increase in opportunities for employment, specialization, better education as well as production of goods and services, however it also brings a variety of environmental challenges (Acharya et al., 2015). Urban growth causes surface temperatures to increase, which modulates air temperature in the lower atmosphere (Zhou & Wang, 2011a). Warming in cities affects much large number of people due to concentrated populations, especially in low to medium income countries where slum dwellers make up about 60% of the urban population (De-Simone, et al., 2011). This increases vulnerability of urban dwellers to heat related risks, unless adequate adaptation and mitigation measures are adopted. For example, urbanization induced warming will be superimposed on projected increases in frequency and intensity of heat waves, globally (Reid et al., 2012). Therefore, the large proportion of the world's population, economic activities and physical infrastructure are at increasing risk to heat and other changes associated with urban growth. Analysis of thermal conditions, especially in low income cities will provide quantitative understanding of the effect of growth patterns on temperatures and thermal comfort. This will help in planning for further growth, for sustainable development as well as in ensuring thermal comfort and reduced heat vulnerability to urban dwellers.

1.1 Temperature measurement using remote sensing

Remote sensing plays a critical role in the study of responses of land and near surface temperatures to land use and land cover dynamics. Conventionally, in situ temperature observations are used in thermal analysis. However, although they usually have high temporal resolution, in-situ meteorological observations are limited in spatial coverage, such that it becomes unviable to use them to monitor large areas (Zhou & Wang, 2011a; Mohamed et al., 2016). Urban areas are characterised by high spatial variability in surface thermal properties, which require a large number of in-situ observation points (Sattari & Hashim, 2014). In

analysis of long term temperature changes, in-situ measurements are therefore less reliable as they may change in location over time or are affected by land use and land cover changes of the surroundings (Ogrin & Krevs, 2015). According to Ogrin and Krevs (2015), in order to obtain reliable analysis for long term changes, meteorological stations must have operated at same place all the time and conditions around them should not have significantly changed over time. However, this is not always the case, especially in dynamic environments such as urban areas. In addition, values measured at a single location are also difficult to extend to the scale of an area making them less representative (Cai et al., 2011). Furthermore, in-situ observations describe response rather than the forcing of surface energy fluxes over urbanized areas (Owen et al., 1998). On the other hand, remote sensing offers benefits which include wide spatial coverage, digital data format easy to integrate with other digital data forms as well as advances in sensor technology, implying improvements in data quality (Odindi, et al., 2015; Dube et al., 2016). Remote sensing also allows measurements to be repeated over the same area, which is important for detection of changes such as impacts of urban growth (Dube, et al., 2016). Therefore, remote sensing presents a practical approach for analysing land surface temperatures on wide spatial and temporal scales (Abutaleb et al., 2015). Furthermore, due to increased sensor resolution and low altitude flight, it has become possible to extract temperatures from localized regions such as urban areas (Voogt & Oke, 2003). Algorithms have also been developed to sharpen satellite data and improve spatial resolution (Dominguez et al., 2011; Tomlinson et al., 2011).

Land surface temperatures are mostly derived from thermal infrared data in the 8-15μm window. However, passive microwave sensors are also used for monitoring temperatures, although they are limited due to coarse spatial resolution which is usually in the order of tens of kilometres (Tomlinson, et al., 2011; Sattari & Hashim, 2014). Therefore, passive microwaves are mostly suitable over large areas hence the common usage of thermal infrared sensors, which offer higher spatial resolution (Tomlinson, et al., 2011). The thermal infrared sensors measure radiance at the top of the atmosphere from which blackbody/brightness temperatures can be derived using Planck's law (Franco et al., 2015; Dash et al., 2007). The main algorithms used to retrieve temperature from thermal infrared data are the radiative transfer equation and the split window algorithm (Tomlinson, et al., 2011; McMillin, 1975; Qin et al., 2001; Rozenstein et al., 2014; Yang, Cao, et al., 2014). The split window algorithms are only applicable to sensors such as Landsat 8, ASTER, NOAA AVHRR and MODIS which

have at least two thermal bands (Sattari & Hashim, 2014). With the exception of Landsat 8, most of these sensors with at least two thermal infrared bands suffer from low spatial resolution. For example, MODIS determines surface temperature using the split window algorithm at a spatial resolution of 1km (Odindi, et al., 2015). Since the earth's surface is not a blackbody and due to variations in spectral properties between land use and land cover types, emissivity correction is necessary (Abutaleb, et al., 2015). According to Qiao et al. (2013), without emissivity correction, retrieved surface temperatures may have an error of about 1.4^{o}C. There are several ways of obtaining emissivity maps which include derivation from NDVI maps, NDWI maps as well as assigning emissivity values to a land use and land cover map (Southworth, 2004; Wu et al., 2014; Yang, Cao, et al., 2014; Wang, Liu, et al., 2010). Accurate surface temperature is obtained from brightness temperature by correcting for differences in emissivity between surface types. Therefore, remote sensing offers easily accessible data options and great potential for monitoring effects of land cover conversion on near surface temperature at a wide variety of spatial and temporal scales. This is important for resource constrained African nations, where the distribution of in-situ stations is sparse while vulnerability to extreme weather events is high.

The need for this study arises from rapid urban growth which threatens to magnify the warming effect already imposed by other natural and anthropogenic factors in the lower atmosphere. Temperature elevation has devastating effects, especially in developing countries where pressure from other socio-economic stressors is high, reducing capacity for adaptation and mitigation. The thermal conditions in urban areas of most developing countries such as in Zimbabwe are under-studied, which increases residents' exposure and vulnerability. There is thus need to understand thermal conditions to enable sustainable growth and formulation of effective adaptation and mitigation strategies. Resource constrained countries also suffer from largely inadequate meteorological station network which makes it difficult to perform spatial thermal analysis such as in complex urban setting. On the other hand, remote sensing provides a cost effective data option useful at landscape scale, whose potential needs to be fully exploited for urban thermal analysis such as in Harare.

1.2 Aim of the study

The study aimed at analysing the impact of urban growth on the indoor and outdoor thermal environment of the Metropolitan City of Harare using freely accessible medium resolution multi-spectral data from space-borne sensors.

1.3 Objectives of the thesis

The main objectives of the study were;

1. To assess the potential of fusing thermal infrared data with vegetation indices and multi-spectral remotely sensed data in improving urban land use/cover mapping
2. To determine extreme heat vulnerability of Harare metropolitan city using multi-spectral remote sensing and socio-economic data
3. To assess seasonal and spatial daytime outdoor thermal comfort variations using recently launched and improved Landsat 8 data
4. To link major dynamics in urban near-surface temperatures to long term changes in land use/cover
5. To determine the link between built-up density and indoor air-conditioning energy demand in Harare using degree days derived from remote sensing and in-situ data
6. To predict future land use/cover distribution and implications on near-surface temperatures in Harare.

1.4 Scope of the study

The study was aimed at investigating the impact of urban growth and differences in the spatial structure of built-up areas on the thermal conditions of Harare Metropolitan City, Zimbabwe. The study focuses mainly on the potential of medium resolution multi-spectral Landsat series to determine land use and land cover regimes as well as related responses of indoor and outdoor temperatures and thermal comfort. Urban growth and temperature mapping relies greatly on accurate land use and land cover mapping. Therefore, the study commences by assessing the potential of combining newly launched Landsat 8 multi-spectral data with vegetation indices in improving mapping accuracy. Taking advantage of archival data, seasonal and long term responses of urban temperatures to land use and land cover changes is also assessed. Socio-economic impacts of temperature patterns are also investigated by ways of heat vulnerability mapping, outdoor thermal discomfort assessment and estimation of effects of temperatures on air-conditioning energy demand. In order to provide insight into the future, land cover and urban indices are used to predict future LULC and temperature patterns using Cellular Automata Markov Chain modelling.

1.5 Thesis outline

This thesis consists of seven semi-autonomous chapters which are either published or at different stages of publication. Six of the manuscripts have already been published while one is in press (published online). Each chapter can be read and considered independently but

contributes to the overall introduction (Chapter one) and synthesis (Chapter nine). Since the content of the manuscripts has been retained as submitted to journals, duplications and overlaps are found between them, especially in the introduction and method sections. This is of little consequence considering that the articles are peer reviewed and can be read separately without losing overall context. The thesis can be split into sections namely (i) General introduction (ii) Remote sensing applications for monitoring the impacts of urban growth on in-and-out door thermal conditions: A review of limitations and opportunities (iii) Improved urban land use and land cover (LULC) classification (iv) Spatial variations in extreme heat vulnerability and link to LULC distribution (v) Remote sensing of seasonal variations in urban outdoor thermal discomfort (vi) Quantification of long term effect of LULC changes on urban heat island (vii) Implications of urban surface changes on air conditioning energy demand (viii) Remote sensing based future prediction of LULC and land surface temperature distribution (ix) Synthesis and conclusion.

1.6 Chapter 1: General introduction

This chapter introduces and contextualizes the study. It highlights the importance of mapping urban growth and its implications on climate. The chapter also expresses the value and potential of remote sensing to detect landscape scale changes in land- and near-surface temperature, especially against a background of scarcity of in-situ observations in developing countries. Research problem, aim and objectives are also detailed in this chapter.

1.7 Chapter 2: Remote sensing applications for monitoring the impacts of urban growth on in-and-out door thermal conditions: A review of limitations and opportunities

In order to address the objectives identified in Chapter one, this chapter provides a review of progress made in the study of implications of urban growth on in- and out-door thermal conditions. The chapter identifies methods used for urban growth, temperature and human thermal comfort assessment. The methods and roles of remote sensing are evaluated while at the same time challenges, gaps and need to develop other approaches are highlighted.

1.8 Chapter 3: Improved land use and land cover (LULC) classification for urban growth mapping

This chapter assesses the potential of multi-spectral Landsat data and derived vegetation indices to improve urban land use and land cover classification. This is aimed at identifying data combination which produces land use and land cover (LULC) classes at higher

classification accuracy than the traditional methods of using multi-spectral visible and infra-red (VIS/IR) data. Traditional methods of Landsat-based LULC classification do not combine reflective VIS/IR data with thermal infra-red or vegetation indices. Therefore, methods tested include based on a combination of reflective with vegetation indices, reflective with thermal data and reflective with both thermal data vegetation indices as input data to urban LULC classification. The indices considered include the normalized difference vegetation index (NDVI), normalized difference built-up index (NDBI), normalized difference bareness index (NDBaI) and the normalized difference water index (NDWI). The best methods with high accuracy identified in this chapter were be used for urban LULC classification in the other chapters of the thesis.

1.9 Chapter 4: Spatial variations in extreme heat vulnerability and link to LULC distribution

Land surface properties such as wetness, density of buildings and vegetation cover fraction affect surface energy balance. This chapter determines spatial distribution of heat vulnerability by combining surface bio-physical properties with socio-demographic factors. Indices such as NDBI, NDVI and NDWI are used to determine level of physical exposure at 30m resolution, which characterizes reflective Landsat data. This enables detailed mapping of heat vulnerability as opposed to the use of the spatial scale of census blocks for instance, which is too broad and general. The chapter provides a description of the link between urban socio-economic patterns, land use/cover distribution (mapped in Chapter three), land surface temperature and heat vulnerability.

1.10 Chapter 5: Remote sensing of seasonal variations in urban outdoor thermal discomfort

Chapter four focuses on the link between spatial distribution of temperatures and LULC during the hot season, without addressing the influence of seasonality in this link. Therefore, Chapter five explains how seasonal changes in land cover may affect outdoor thermal discomfort. In-situ air temperature data are commonly used to monitor outdoor thermal discomfort, such as for the computation of the Discomfort Index (DI). However, in-situ data are limited in spatial coverage and do not sufficiently cover all the land cover types in complex urban settings. In this chapter, the DI is mapped in different seasons by replacing air temperature with land surface temperature derived from Landsat data. Land surface properties are used to explain the differences in the spatial distribution of outdoor thermal discomfort between seasons.

1.11 Chapter 6: Quantification of long term effect of LULC changes on urban heat island

Besides seasonal changes in land use and land cover obtained in Chapter five, city growth is associated with LULC conversions over long periods. Natural covers such as vegetation and wetlands are usually replaced by man-made impervious surfaces and buildings. Since different surfaces differ in interaction with electromagnetic radiation, long term changes in LULC distribution affects urban spatial and temporal thermal patterns. This chapter, therefore, links historical changes in LULC to changes in surface urban heat island. The chapter further separates land surface temperature changes due to LULC conversion from changes due to background warming using a temperature normalization approach.

1.12 Chapter 7: Implications of urban surface changes on air conditioning energy demand

Long term changes in land surface temperature due to urban growth (chapter six) are linked to near-surface air temperature changes and potential responses of air-conditioning energy demand in this chapter. Heating Degree Days (HDD) and Cooling Degree Days (CDD) are mapped using land surface temperature to represent spatial distribution of energy requirements for space heating and cooling, respectively. The spatial distribution of HDD and CDD is analysed and linked with LULC trends over a period from 1984 to 2015. HDD and CDD are further linked with actual mean household energy consumption for different residential set-ups. The chapter is relevant in linking urban growth, air-conditioning energy demand trends with spatial distribution in socio-economic status in an urban area. The analysis also provides an indication of societies at risk by linking thermal comfort, air-conditioning energy requirement to ensure human comfort and whether communities afford to match the costs of the energy needed. The study identifies, by location, communities in higher need of space heating and space cooling in the cool and hot seasons, respectively. The chapter also determines residential types that are energy efficient, important for urban planning and management.

1.13 Chapter 8: Remote sensing based future prediction of LULC and land surface temperature distribution

Globally, urban growth is expected to continue infinitely. Earlier chapters provided an understanding of the effect of LULC distribution on the urban thermal environment, without a predictive component. This chapter uses the understanding of historical LULC and land surface temperature patterns developed in preceding chapters to predict future growth and its implications on spatial distribution of land surface temperature. The potential of a variety of

land cover and vegetation indices to predict future urban growth and land surface temperature patterns is tested. The best predictor index is selected and used to predict future responses of land surface temperature to urban growth from 2015 to 2045. The Cellular Automata Markov Chain model is used, assuming that future growth will follow similar trends to those observed in historical analysis.

1.14 Chapter 9: Synthesis and conclusion

The chapter provides a synthesis of the finding and conclusions drawn in preceding chapters. Recommendations for future studies are made based on limitations of this study and other gaps identified in the review chapter but not tackled by the study. The thesis concludes by providing a list of references.

CHAPTER 2: A REVIEW OF IMPLICATIONS OF URBAN GROWTH ON INDOOR AND OUTDOOR THERMAL ENVIRONMENT

This chapter is based on:

Mushore T. D., Odindi J., Dube T., Matongera T., Mutanga O. (**2017):** Remote sensing applications for monitoring urban growth impacts on in-and-out door thermal conditions: A state of the art review. *Remote Sensing Applications: Society and Environment, 8, 83-93,* https://doi.org/10.1016/j.rsase.2017.08.001

2.0 Abstract

Urban growth and the consequent expansion of impervious surfaces influence a landscape's thermal characteristics by raising Land Surface Temperatures (LST). Resultant warming may cause among others, thermal discomfort, high prevalence of heat related health conditions, air pollution, increased water usage and energy demand for air-conditioning. Recently, studies aimed at understanding the impacts of urbanization and subsequent landscape transformation on in-and-out door temperature have increased significantly. This review therefore provides synthesis on the progress of space-borne remote sensing in monitoring the implications of urban growth on thermal characteristics. It was observed that despite the relative coarse spatial properties; medium resolution sensors (i.e. Landsat and MODIS) have become valuable in characterizing urban thermal conditions, especially in data-limited areas. More importantly, literature shows that thermal assessments have been confined to examination of historical and current conditions, without considering current research studies. This work identifies low temporal resolution that characterizes the commonly used medium spatial resolution thermal sensors as a major limitation to mapping urban surface temperature. There is therefore need for future studies to shift towards integrating new crop of high resolution satellite data with existing high temporal and low spatial resolution sensors. Such techniques can lead to the development of robust spatial datasets suitable for improved seasonal and long term monitoring of urban thermal patterns.

Keywords: Surface temperature; urban growth, thermal discomfort; land cover; land use; vulnerability

2.1 Introduction

Studies have shown that the spatial extent and population of urban areas are increasing globally, and the growth is expected to continue beyond the year 2100 (De-Simone, et al., 2011; Blake, Curitiba, et al., 2011; Seto et al., 2012). By the year 2008 for instance, more than 50% of the world's population was already living in cities and their immediate surroundings (De-Simone, et al., 2011). Urban population is projected to increase by a further 10% by 2030, reaching 70% in 2050 (Blake, Curitiba, et al., 2011; UNFPA, 2007; United Nations, 2014). According to Seto et al (2012), urban areas are expanding twice faster than population growth and are a major driver of environmental change. For instance, due to the characteristic conversion of natural landscapes to impervious surfaces, urbanization has been linked to an increase in size and intensity of the Urban Heat Island (UHI), which is associated with an increase in water and energy demand, high levels of air pollution and increased heat related health risk (Guhathakurta & Gober, 2007; Blake, Curitiba, et al., 2011; Zhang, Schaaf, et al., 2013; Saitoh et al., 1996; Tran et al., 2006). Other impacts include depletion of freshwater resources, uncomfortable sleeping nights, increase in heat related mortality and habitat loss (Seto, et al., 2012; Luber & McGeehin, 2008; McDonald et al., 2011b; Kusaka et al., 2012). Furthermore, elevated temperatures increase the exposure of the society vulnerable, due to their low coping strategies and mechanisms (Newland, 2011). Monitoring and forecasting urban growth patterns and their implication on urban thermal characteristics is therefore valuable for planning and optimization of physical landscapes and socio-economic services (Bhattacharjee and Ghosh (2015).

Recently, the use of remotely sensed data has emerged as a reliable approach for assessing urban landscape transformation and its implication on urban climate. Remotely sensed data offers better prospects in providing up to date spatial and temporal data necessary for understanding the complex relationship between urban growth and in-and-out door thermal conditions. Recent studies that evaluated the utility of remotely sensed data in urban climate studies have shown great promise (Acharya, et al., 2015; Cai, et al., 2011; Franco, et al., 2015; Zhou & Wang, 2011a; Amiri et al., 2009). Zhou and Wang (2011a) for instance assessed the dynamics of LST in response to land cover change in rapidly urbanizing city of Kunming, China, while Zhang et al. (2009) investigated bi-temporal characterization of LST in relation to impervious surface area, Normalised Difference Vegetation Index (NDVI) and Normalised Difference Built Index (NDBI) using sub-pixel image analysis. They managed to map urban growth, using both qualitative (general Land Use and Land Cover [LULC] classes) and quantitaive measures (indices). The changes in vegetation spatial structure and impervious

areas were, therefore, monitored using change detection methods. This indicated that there is a wide variety of remote sensing approaches that can be used to depict LULC changes. The growth patterns observed in these studies managed to explain changes in surface temperature. Also, Amiri, et al. (2009) analyzed the spatial and temporal dynamics of LST in relation to fractional vegetation cover and land cover in Tabriz, Iran. In their quantitative approach, they found out that LST was high in areas where vegetation fractional cover was low. Recently Lin et al. (2016) focused on winter in-door thermal and heating demand of urban residential buildings in China during the hot and cold seasons in relation to LST changes. that the study showed that warming, due to urban growth and land surface alteration, increased energy demand for in-door cooling in the hot season. Other studies on the implication of urbanization on urban thermal properties include Voogt and Oke (2003), Rizwan et al. (2008) and Goshayeshi et al. (2013b). The aforementioned studies revealed that urban land cover dynamics modify urban thermal conditions, by elevating surface temperatures at an alarming rate. In this regard, there is need to assess these impacts on a city's specific local temperatures to ensure sustainable growth and adoption of relevant mitigation measures.

Previous studies that adopted remotely sensed data indicated that the spatial structure of impervious surfaces, wetlands and vegetation has a direct influence on LST (Connors et al., 2012; Hasanlou & Mostofi, 2015; Keramitsoglou et al., 2011). Green areas and water bodies have low temperatures and act as cool islands during the day and also alleviate heat by fragmenting the urban thermal island and vice-versa (Rasul et al., 2015; Zhang et al., 2012). Conversely, built up areas absorb high amounts of heat and are regarded as a major source of heat in urban zones (Sithole & Odindi, 2015). Studies have also revealed that the net effect of buildings and vegetation in an area depends on their density (Odindi, et al., 2015; Jalan & Sharma, 2014; Hu & Jia, 2010). For example, in a study conducted in South Africa, Odindi, et al. (2015) observed that moderately built "leafy" suburbs were slightly cooler than areas with sparse vegetation, while temperature increased with building density. This is also confirmed by the study by Jalan & Sharma (2014) who observed that expansion of built-up areas at the expense of green-spaces resulted in warming of the city of Jaipur in India by an average of 2.99 ^{o}C. A number of studies (Jenerette et al., 2007; Collatz et al., 2000; Ganopolski et al., 1998) have demonstrated this inverse influence of vegetation on LST. These studies indicated that, within a city, areas with high vegetation cover proportion experience high extent of cooling by evaporation, resulting in low surface temperatures.

Review papers on urban surface temperature have mostly focused on spatial and temporal LST variations and heat island retrieval, using remote sensing (Mohamed, et al., 2016; Sattari & Hashim, 2014; Voogt & Oke, 2003; Weng et al., 2004). For example, Mohamed, et al. (2016) recently reviewed methods of LST and emissivity retrieval, using low and medium spatial resolution satellite data. However, previous reviews did not highlight on methods to quantify and link the long term changes in urban thermal characteristics to urban growth and socio-economic impacts. On the other hand, reviews on the implications of temperature on in-and-out door thermal comfort assessment have looked at models of thermal comfort analysis, as well as implications on energy consumptions (Goshayeshi, et al., 2013b; Kwong et al., 2014; Charles, 2003; García-Frapolli et al., 2007). However, the reviews did not include the methods on incorporation of remote sensing thermal data in estimating thermal comfort and impacts on energy consumption. For example, previous studies have quantified thermal comfort and energy consumption, using indices, such as Thom's Discomfort Index and Degree Days, respectively, which use in situ air temperature measurements. , There is therefore a need to identify robust remote sensing based approaches that can potentially quantify thermal comfort and energy consumption. To the best of our knowledge, no review to date has focused on approaches for predicting future LST and urban heat island patterns, using remotely sensing land use and land cover trends. In order for sustainable development to be achieved, it is necessary to consider future implications, by embracing predictive techniques that can link these changes with potential impacts.

Based on the aforementioned shortcomings, this paper therefore seeks to review the progress in remote sensing applications in monitoring the impacts of urban growth on in-and-out door thermal conditions. Firstly, the study provides a brief overview of the general implications of urban growth on in-and-outdoor thermal conditions, highlighting the contribution of impervious surfaces, buildings and urban vegetation on spatial temporal LSTs. Secondly, the study explores the utility of remotely sensed data in assessing the impacts of urban growth on in-and-outdoor thermal conditions, as well as examines available analytical algorithms for assessing urban growth and its influence on urban thermal conditions. Also, included in this review are remote sensing based prediction methods for future LST distribution, which can also be used for estimating the impact of urbanization on outdoor thermal discomfort. Finally, the review discusses the impact of urban growth on air-conditioning energy demand, as well as possible future directions in the applications of remotely sensed data in assessing and monitoring the impacts of urban growth on in-and-out door thermal conditions.

2.2 Implications of urban growth on in-and-outdoor thermal conditions

Urbanization is characterized by surface alterations, which mostly entails an increase in area covered by surfaces that absorb large amounts of heat (Sobrino et al., 2012; Amiri, et al., 2009; Zhang, et al., 2009). For example, vegetated areas are replaced with impervious surfaces and buildings, resulting in elevated surface temperatures much higher than the surrounding rural and undisturbed areas (Johnson et al., 2014; Steeneveld et al., 2014; Tomlinson, et al., 2011; Hua et al., 2013; Song & Wu, 2015; Sobrino, et al., 2012). For example, an increase in built-up area alters the energy balance by increasing heat absorption and heat transfer between the earth's surface and the lower atmosphere (Guan, 2011). According to Xian and Crane (2005), urbanization alters air temperature of the atmospheric boundary layer, making it a key component of the surface energy balance. Generally, the impact of elevated temperatures within cities varies spatially, as a consequence of differences in physical exposure, landscape characteristics and socio-demographic factors (Johnson, et al., 2014). Spatial variation in land cover distribution influences distribution of heat absorption rates and hence physical exposure patterns to extreme heat. Moreover, literature has revealed that the increase in surface temperatures have the potential to expose residents to heat related stress, especially the urban poor without air conditioning facilities (Parsons, 2014; Hsiang, 2010; Dokladny et al., 2006).

A frequently used international standard for indoor thermal conditions is the Fanger's predicted mean vote (PMV). Using PMV, comfort conditions are then assessed based on ASHRAE scale (Goshayeshi et al., 2013a; Madhumathi & Sundarraja, 2012). According to Goshayeshi, et al. (2013a), PMV was designed for indoor thermal comfort assessments and is not capable to explain outdoor and semi-outdoor conditions. In another approach, Humphreys (1978) discovered that indoor thermal comfort is linearly related to mean outdoor temperature; method referred to as Humphreys. In such analysis, mean outdoor temperature is computed as the average of maximum and minimum outdoor temperature (Humphreys, 1978; Madhumathi & Sundarraja, 2012). While PMV is based on complex representation of human heat balance Humphrey's is based on a simpler equation relating indoor comfort with outdoor ambient temperature taking into account adaptability of occupants (Shastry et al., 2016). According to Shastry, et al. (2016), PMV is predictive model whose applicability for tropical regions has been widely questioned while Humphreys is an evaluative model. This clearly shows that the Humphreys is a simple and parsimonious method to relate outdoor thermal conditions with indoor comfort of the occupants. However, the approach requires up scaling from point analysis

using in-situ observations of maximum and minimum temperature to aerial analysis. Techniques to improve this may include geo-statistical approaches such as interpolation and adoption of remotely sensed thermal infrared datasets. This will enable establishment of the link between outdoor temperature, indoor comfort and LULC distribution especially in built environments.

2.3 Remote sensing of impacts of urban growth on in-and-outdoor thermal conditions

Traditionally, in-situ meteorological observations have been used in near-surface (usually 2m above the ground) temperature analysis. These measurements were used to explain temporal patterns and sometimes interpolated in analyzing spatial LST (Owen, et al., 1998; Mohamed, et al., 2016). Effective thermal monitoring however requires a high density of surface monitoring equipment, seldom available, even in the developed world (Stathopoulou et al., 2006). In developing countries, especially in Africa, the coverage of meteorological stations is often in-adequate to effectively depict urban landscape heterogeneity (Owen, et al., 1998; Shahmohamadi et al., 2010; Tao et al., 2013; Zhou & Wang, 2011a). Commonly, existing observations focus on describing responses, rather than the partitioned surface energy fluxes over urbanized surface (Owen, et al., 1998). In-situ approaches are also affected by the surface heterogeneity, caused by non-climatic factors, such as changes in location of stations, time of observation, instrumentation and surrounding LULC types (Oort, 2005; Hamdi, 2010). In long term studies, this has potential to reduce accuracy of analysis as some of the changes may not be linked to climate change, but other effects, such as thestations location and instrumentation. Hence the reliability of results from such monitoring areas depends largely on long-term installations and technology uniformity (Salvati & Sabbi, 2011; Mohamed, et al., 2016; Hamdi, 2010). Challenges as also include the cost of data acquisition from private or public organizations which commonly impede effective adoption of in-situ meteorological data (Henry et al., 1989).

Conversely, due to synoptic coverage of large areas and reasonable temporal resolution, medium spatial resolution satellite data sets, such as Landsat have been found to be effective in depicting urban LULCs and thermal characteristics (Jia et al., 2014). Remote sensing allows repeated image acquisitions over the same area, which is necessary for monitoring urban growth patterns (Dube, et al., 2016). According to Dube, et al. (2016), the provision of spatial data in digital format, makes it easy to integrate with ancillary data in a GIS system for further analysis. Owing to these capabilities, remote sensing has increasingly gained popularity in

mapping qualitative and quantitative land surface properties. The most common remote sensing based sensors that have been utilized in land surface analysis, include Landsat series (Vlassova et al., 2014; Weng, et al., 2004), Advanced Very High Resolution Radiometer (Streutker, 2002; Gallo & Owen, 1998; Gillies & Carlson, 1995), Thermal Infrared Multispectral Scanner (Schmugge et al., 1998; Kealy & Hook, 1993; Kahle, 1987), MODIS (Vaughan et al., 2012; Wan et al., 2004; Tran, et al., 2006) and Advanced Space-borne Thermal Emission and Reflection Radiometer (ASTER) (Lu & Weng, 2006; Gluch et al., 2006; Gillespie et al., 1998).

Although LST is commonly monitored using the 8-15um thermal infrared range, using the radiative transfer algorithm (Tomlinson, et al., 2011; Mohamed, et al., 2016), the application of passive microwave sensors is also possible (McFarland et al., 1990; Peterson et al., 2000; Williams et al., 2000; Chen et al., 2011). However, passive microwave space-borne sensors have a poor spatial resolution (tens of kilometers), hence the wide usage of medium resolution thermal infrared data which have improved spatial, spectral, radiometric and temporal characteristics (Tomlinson, et al., 2011). Despite the fact that high spatial resolution thermal sensors are ideal for urban surface characterization, their utility is limited by cost, especially in resource constrained developing countries. Whereas studies like Lo et al. (1997) successfully used air-borne Advanced Thermal and Land Application Sensor (ATLAS) over Alabama, USA, their approach may not be viable in resource constrained areas. Hence, there is need to fully exploit freely available medium resolution thermal data, such as from Landsat archives. For example, Landsat data offers optimum spatial resolution for characterization of urban LST and provides archival data to enable historical analysis free of charge. On the other hand, MODIS is useful for monitoring general but frequent changes in LST due to daily revisit time step. Furthermore, data merging such as blending freely available Landsat with MODIS data may create dataset with high spatial and temporal resolution. This can improve spatial and temporal details of LST, especially in heterogeneous urban areas.

2.4 Challenges in remote sensing of the impacts of urban growth on in-and-out door thermal conditions

Despite the successful application of remote sensing technology in monitoring the impacts of urban growth on in- and outdoor temperatures of the lower atmosphere, remote sensing of the land surface properties are characterized by a number of limitations. For example, due to the requirement of clear skies, data is not always available for specific scenes and times hence revisit time may be affected by poor atmospheric conditions (Cai, et al., 2011; Mohamed, et

al., 2016). Archives may also be corrupt as in the case of Landsat 7 ETM+ images after 2003 in which 22% of the data are lost resulting from failure of scan line corrector (Shoko et al., 2016; Storey, 2005). According to Wu, et al. (2014), the major limitation of remote sensing is that high spatial resolution sensors have low temporal resolution and vice versa. For example, although some of the medium spatial resolution sensors provide thermal data with reasonable spatial resolution, they have poor temporal resolution when compared to geostationary satellites such as Meteosat 8 which provides data every 15 minutes (Table 1). This makes it challenging to use these sensors in monitoring rapid changes such short term variations. Despite the above limitations, remote sensing techniques remain useful for spatial analysis, especially where the scale of phenomena monitored is comparable with spatial and temporal resolution of selected sensor.

Table 2.1: Commonly used satellite sensors for land and near-surface thermal analysis

Satellite	Sensor	Spatial resolution (thermal data)	Temporal resolution	Overpass Time	Operational since	Number of thermal bands
Landsat	Landsat 8 TIRS	100 m	16 days	1000	2013	2
Landsat	ETM	60 m	16 days	1000	2009	1
Landsat	TM	120 m	16 days	1000	1984	1
Terra	MODIS	1 km	Twice daily	1030/2230	2000	2
Aqua	MODIS	1 km	Twice daily	1330/0130	2002	2
Terra	ASTER	90 m	Twice daily	Request only	1999	5
NOAA	AVHRR	1.1 km	Twice daily		1979	2
METOP	AVHRR	1.1 km	29 days	0930	1979	2
ENVISAT	AATSR	1 km	35 days	1000	2004	2
Meteosat 8	SEVIRI	3 km	Geostationary	Every 15 minutes	2005	2
GOES Network	GOES Imager	4 km	Geostationary	Every 3 hours	1974	2

2.5 Shift towards the use of broadband medium resolution

The applications of broadband medium spatial resolution sensors, such as National Oceanic and Atmospheric Administration's Advanced Very High Resolution Radiometer (NOAA AVHRR), MODIS and ASTER in urban LST analysis has significantly increased. The shift towards these broadband sensors can be attributed to improved sensing characteristics, such as high temporal resolution, strategically positioned thermal bands and wide swath width.. The use of sensors such as AVHRR and MODIS is only suitable for urban thermal studies, due to their rich archival data (since 1979), global coverage and high temporal resolution – twice daily (Sattari & Hashim, 2014). Specifically, NOAA AVHRR has two thermal infra-red bands useful for accurate retrieval of LST using the Split Window Algorithm. Moreover, AVHRR data sets are effective in regional scale applications due to their low spatial resolution. Similarly, MODIS datasets have two thermal bands and a high (twice daily) temporal resolution, thus suitable for both day- and night assessments of temperature patterns. They have low spatial resolution, slightly greater than AVHRR but comparatively limited archival data (2000 to present), thus limited in analysis for historical patterns (Tao et al., 2015). According to Shi et al (2015), the low spatial resolution MODIS data makes it difficult to construct the relationship between LULC and LST. High temporal resolution in combination with low spatial resolution is also characteristic of Geostationary Operational Environmental Satellite (GOES) imager and the Spinning Enhanced Visible and Infrared Imager (SEVIRI) sensor. For example, SEVIRI has a 15 minutes and 3km temporal and spatial resolution, respectively.

Compared to rural natural environments, the complexity of urban landscapes limit the use of low resolution remotely sensed data. Ideally, urban areas require high spatial resolution data (less than 10 m) to effectively deal with mixed pixels associated with lower spatial resolution data (Aplin, 2003; Salvati & Sabbi, 2011; Lo & Choi, 2004). However, high spatial resolution sensors are often associated with a number of challenges that include high acquisition costs, small swath width and low temporal resolution, which limit their value for change detection analysis studies, especially over large areas (Forkuor & Cofie, 2011). In urban surface temperature analysis, the major limitation with high resolution space-borne satellite data such as SPOT imagery is the absence of thermal infra-red data. Fortunately, medium resolution remote sensing datasets such Landsat, and ASTER allow cost effective monitoring responses of surface temperatures to land use and land cover changes, even in the often complex urban land use and land cover spatial structure (Owen, et al., 1998). Voogt and Oke (2003), pointed out that improvements in sensor spatial and spectral resolutions provide low cost detailed

surface representation. Specific advantages of Landsat include appropriate spatial resolution, free online access to archival data since 1972 and launch of advanced missions such as Landsat 8 with improved data quality (Tao, et al., 2013; Liu & Weng, 2009; Sithole & Odindi, 2015). Earlier missions had a single thermal band hence they were incompatible with split window algorithm. However, the recently launched Landsat 8 has two thermal bands which enable retrieval of temperature using both single band and split window techniques (Yang, Lin, et al., 2014; Rasul, et al., 2015). Landsat provides higher spatial resolution than sensors such as MODIS and NOAA. However it has a lower temporal resolution (16 days). ASTER is also widely used medium spectral (five thermal bands) and spatial (90 m) resolution sensor. ASTER's thermal data- has higher spatial resolution than Landsat TM (120 m) and Landsat 8 (100 m), but lower spatial resolution than Landsat ETM thermal data – 60 m (Mohamed, et al., 2016). Although ASTER's Terra platform has a twice-daily overpass, it is a commercial sensor and has limited archival data. Therefore, despite low temporal resolution, medium resolution multi-spectral data from Landsat is beneficial due to its appropriate spatial resolution, free access and rich historical data.

2.6 Analytical algorithms for assessing urban growth and thermal conditions

2.6.1 Land use and land cover classification for urban growth detection

In order to relate land cover distribution to corresponding land surface- and near-surface air temperatures, accurate LULC maps are needed. In thermal remote sensing, LULC maps are also reclassified into emissivity maps that can be used to convert brightness temperatures into surface temperature (Stathopoulou & Cartalis, 2007). Furthermore, a national repository of accurate LULC maps is necessary for change detection such as monitoring urban growth over time (Abegunde & Adedeji, 2015; Dube et al., 2014; Yu et al., 2013). To date, several efforts have been made to enhance the suitability of readily available dataset for LULC mapping in both homogeneous and complex landscapes. In Germany, Esch et al. (2013) used 12m resolution TerraSAR-X data to map built-up areas. The Germany TerraSAR-X data have a global coverage, are weather independent, have day and night acquisition capability and low sensitivity to atmospheric effect. The most common methods to improve classification accuracy include the enhancement of spectral, spatial and radiometric data properties. For example, Gervin et al. (1985) observed that Landsat MSS outperformed NOAA AVHRR for classification of heterogeneous areas due to its superior 80m compared to 1.1km spatial resolution. Owing to the improvements in radiometric resolution (8-bit to 12-bit), signal to

noise ratio and refined spectral range for Landsat 8 data a study by (Jia, et al., 2014) reported better classification performance compared to earlier missions.

Furthermore, data transformation techniques such as independent component analysis (CA), Principal Component Analysis (PCA), Tasseled Cap Transformation and Minimum Noise Function have been reported to increase mapping accuracy by reducing data redundancy and minimizing noise caused by correlation between multi-spectral bands (Namdar et al., 2014; Mallick et al., 2013; Forkuor & Cofie, 2011; Seto & Kaufmann, 2005). Data enhancement methods employed also includes a combination of different sensors, multispectral data with transformed data and multi-date data. There are several examples of successes of data merging in improving LULC classification accuracy. Several studies have successfully used data merging techniques in improving LULC classification in urban studies. For instance, Witt et al (2004) obtained a higher overall classification accuracy of 87.66% by combining Heat Capacity Mapping Mission (HCMM) thermal data using Landsat Multi-Spectral Scanner (MSS) visible and infrared bands in Bristol compared to 85.20% overall accuracy attained using MSS data alone. In another study, Lu and Weng (2005) noted that combining texture data derived from panchromatic image with Landsat 7 ETM multi-spectral bands significantly improved classification accuracy. Myint (2001) established that texture plays an important role in object recognition and image segmentation. Similarly, Geneletti and Gorte (2003) observed that combining Landsat data with high resolution data such as ortho-photos enhance classification results.

The use of Bayesian techniques, to account for error propagating from class definition and positional errors, has also demonstrated its ability to improve overall classification accuracy (Oort, 2005). Furthermore, other physical datasets, such as elevation and slope have also been combined with multi-spectral bands of Landsat to increase accuracy (Heinl & Tappeiner, 2012). The applications of spectral vegetation indices in assessing urban growth and thermal conditions have also significantly improved classification accuracy. Dash, et al. (2007) reported 73.2% accuracy using Medium Resolution Image Spectrometer (MERIS) derived multi-seasonal vegetation indices compared to 61.3% using multi-spectral bands of MERIS in Wisconsin. Stathakis et al. (2012) introduced the Vegetation Index Built-up Index (VIBI) which retrieved built-up areas more accurately (91.9%) than the Index Based Built-Up Index – IBI (88.6%) and the continuous Built-Up index – BUC – 54.5%. Chen et al. (2006) applied

Boolean logics on NDWI, NDBI, NDBaI and NDVI and retrieved LULC map with an overall accuracy of 92%. Therefore, based on the above successes, it can be assumed that combining a variety of land cover indices with multi-spectral data from improved sensors like Landsat OLI has potential to reliably map complex landscapes that characterize urban areas.

Apart from the data properties, both supervised and unsupervised classification accuracy depend on the algorithm used. Yu, et al. (2013) observed that the Support Vector Machine (92.99%) classifier performed better than the Artificial Neural Network with an overall accuracy of 91.96% using Landsat 7 ETM in Yantai, China. Seto and Kaufmann (2005) concluded that for general classification, the MLC outperformed a Logit model using data translated by tasseled cap transformation in Pearl River Delta, China. However, their study also proved that fewer training data improves Logit model performance. Discriminant Analysis (DA) has also been used in LULC analysis Lo and Choi (2004) performed a hybrid of ISODATA unsupervised classification with fuzzy supervised method achieving a higher accuracy using the hybrid method (91.5%) than using each of fuzzy supervised (77.8%), MLC (76.7%) or ISODATA (90.3%) separately. Kawakubo et al. (2013) showed that application of an unsupervised called ISOSEG classification approach on fraction imagery from multi-spectral bands of Landsat has potential to increase accuracy by over 10% more than the MLC. Merging of data such as combining multi-spectral images with land cover indices as well as hybridization of classification techniques has potential to further increase land use and land cover mapping even in complex urban landscapes. Therefore, even with medium resolution data, high urban classification accuracy has been achieved which can still be further improved.

2.6.2 Assessment techniques of urban growth induced extreme heat vulnerability

Physical and socio-economic conditions coincide at a given location to constitute a measure of heat vulnerability, which can be displayed as a thematic map to inform strategies. Heat vulnerability mapping is done using variables, such as heat islands, vegetation health and abundance and building density as contributing physical factors (Johnson, et al., 2014; Aubrecht & Özceylan, 2013; Uejio et al., 2011). Heat vulnerability mapping also incorporates economic and socio-demographic factors, such as exposure to hazard, sensitivity and adaptive capacity (Johnson, et al., 2014; Aubrecht & Özceylan, 2013; Uejio, et al., 2011).

Early heat vulnerability assessment studies mainly emphasized on the contribution of socio-demographic factors, such as age, race, gender, education, health and economic status to vulnerability placing little attention on physical factors (Cutter, 2009; Cutter et al., 2003;

Vescovi et al., 2005; Reid et al., 2009). Developments have seen an increased incorporation of biophysical variables in assessing heat related risks (van-Westen; Johnson, et al., 2014; Buscail et al., 2012). For example, recent studies have combined socio-demographic factors with remote sensing derived physical heat exposure factors, such as UHI, LULC maps, and land cover indices (Johnson, et al., 2014; Johnson et al., 2012; Johnson et al., 2009; Aubrecht & Özceylan, 2013; Uejio, et al., 2011; Wolf & McGregor, 2013; Depietri et al., 2013; Hansen et al., 2013; Buscail, et al., 2012; Reid, et al., 2012). Although data from space-based sensors like Landsat offers great potential in mapping localized complex phenomena such as in heterogeneous urban landscapes, the spatial resolution of heat vulnerability maps have remained coarse and generalized. Even where higher resolution physical factors are involved, heat vulnerability maps are at the low spatial resolution of demographic variables, such as census block and district level (Johnson, et al., 2014; Heaton et al., 2014; Buscail, et al., 2012). Variability of heat risk within each census block is thus ignored by assuming uniformity over large areas, which limits usefulness and precision of the derived maps. Dewan and Corner (2012) highlighted that use of census blocks causes spatial averaging over large areas which weakens the correlation between population density and LST because of variability of land cover within each census tract.

The use of remote sensing derived land cover indices as exposure factors in heat vulnerability assessments is still limited to a few studies (Johnson, et al., 2014; Johnson, et al., 2012; Johnson, et al., 2009; Buscail, et al., 2012; Chow et al., 2012; Harlan et al., 2006; Uejio, et al., 2011). While inclusion of a variety of indices in a single assessment should enhance land surface characterization, studies have been limited to two bio-physical indices per heat vulnerability analysis (Johnson, et al., 2012; Johnson, et al., 2014). As such, mostly NDVI which indicates vegetation abundance and health is commonly combined with socio-demographic factors in urban thermal vulnerability analysis (Uejio, et al., 2011; Buscail, et al., 2012; Chow, et al., 2012). However, similar to other previous studies, the vulnerability maps produced were at the resolution of census blocks despite the capability of remotely sensed variables to enhance spatial details of vulnerability factors. Vulnerability maps at improved spatial resolution are important for area specific interventions and avoidance of generalization which may disadvantage underprivileged communities.

2.6.3 Monitoring impact of land cover changes on LST using remote sensing

The NDVI has been proved to have strong negative relationship with temperature (Zhang, et al., 2012; Hung et al., 2006; Song & Wu, 2015; Jiang et al., 2005; Senanayake et al., 2013). However, land cover fraction indicators, such as vegetation fraction and percentage impervious surface area are more stable and less affected by seasons than NDVI. Generally, stronger relationships between temperature and other land cover indices than NDVI have also been reported. For example, Li and Liu (2008), using MODIS imagery, reported a stronger relationship between Normalized Difference Bareness Index (NDBI) and LST as indicators of surface urban heat island effect. Therefore, efforts to identify land cover indices which best quantitatively explain the effect of land cover on temperature are still growing and with impressive results to date. Apart from the use of indices and land cover fractions, LULC maps enhance the explanation of the effect of surface dynamics on the thermal environment. A number of studies have related LST to LULC spatial and temporal patterns using remote sensing (Odindi, et al., 2015; Zhou & Wang, 2011a; Jalan & Sharma, 2014; Omran, 2012). Spatial overlays are used to derive minimum, average and maximum temperature per LULC regime. Single date and multi-temporal analysis then allows understanding of diurnal, seasonal and long term trends in LULC and temperature. For example, in a single date analysis, Omran (2012) observed temperature ranges of 28.7–33^{o}C in vegetated areas and 37.7–43.9^{o}C in built-up areas. In a similar analysis, Sithole and Odindi (2015) concluded that surface temperatures were highest in central business district and lowest in high density vegetation and water bodies. However, although temperatures may be very high in densely built-up areas, the net effect on heat for the entire study area depends on the proportion they occupy. As such, Odindi, et al. (2015) used a Contribution Index (CI) which takes into account the proportion covered by the LULC and whether the LULC mitigates or increases heat. In this case, the CI is negative for dense vegetation and water bodies due to their cooling effect. The CI is an important indicator of the impact of LULC changes as it also changes in response to changes in proportional area per LULC type seasonally and in the long term. One of the limitations of the CI is its dependence on the accuracy of LULC classification which can be subjective. Another constrain to the use of CI to quantify long-term changes is the inability to separate temperature changes due to LULC conversion from changes caused by other factors observed within a class (Zhou & Wang, 2011a).

2.6.4 Remote sensing based prediction of future LST distribution

Traditionally, near-surface air temperature forecasts are done using global and regional climate models. The models mostly consider greenhouse gas emission scenarios as the major anthropogenic contribution to climate change (McCarthy et al., 2010; Saitoh, et al., 1996; Unganai, 1996). However, these models usually consider the effect of urban growth as negligible and are at coarse spatial scales of at least 1km. Global and regional climatic models require further downscaling or coupling with other local scale models such as urban models to depict phenomena at city scales. For example, Smith and Roebber (2011) coupled the Weather Research and Forecasting (WRF) model with an urban canopy model to investigate potential of green roof technology to mitigate warming. Another deficiency of general circulation models is that they ignore the impact of LULC changes on climate especially in small areas such as urban micro-climates (Hoffmann et al., 2012; Smith & Roebber, 2011). Despite the understanding of heat exchange between the land surface and the lower atmosphere, little emphasis has been placed on predicting future LST. LLST modulate near-surface air temperatures thus predicting has potential to improve climate change prediction scenarios. On the other hand, models such as Markov Chain, SLEUTH, Geomod, Multi-Layer Prediction and Cellular Automata have also been influential in predicting future LULC distribution (Fan et al., 2008). Due to simplicity, parsimony, repeatability and applicability, the models have successfully been used to, among others, predict LULC transitions due to urbanization, assess the impacts of LULC changes on biodiversity as well as on the distribution of water resources (Araya & Cabral, 2010; Li et al., 2011; Flamenco-Sandoval et al., 2007; Fan, et al., 2008; Elsner et al., 2004; Crow et al., 1975; García-Frapolli, et al., 2007). Additionally, the models have the capability to predict LULC changes at landscape scale using remote sensing variables in complex and heterogeneous urban landscapes. Therefore, future temperature predictions (both LST and near-surface air temperature) incorporating influence of LULC dynamics are needed. This will augment the available understanding of climate change and predictions which have mostly been based on effect of greenhouse gas concentrations.

2.6.5 Estimation of impact of urbanization on outdoor thermal discomfort

As aforementioned, the analysis of thermal comfort patterns is essential for addressing related problems such as health risks, global warming and increased energy demand for energy (Goshayeshi, et al., 2013b). Thermal discomfort is when 80 to 90% of residents express dissatisfaction with prevailing temperature at a given instant and location (Yilmaz, 2007). Several approaches such as Thom's Discomfort Index (DI), Physiological Equivalent

Temperature (PET), Universal Thermal Climate Index (UTCI), Apparent Temperature (AT), Thermo-hygrametric Index (THI), Humphreys, Predicted Mean Vote (PMV), Standard Effective Temperature (SET), Wet Bulb Globe Temperature (WBGT), Wind Chill Temperature (WCT) are used to assess outdoor thermal discomfort (Abdel-Ghany et al., 2014; Mohan et al., 2014; Yilmaz, 2007; Goshayeshi, et al., 2013b). However, indices such as the Humpreys, THI, PET and DI have been preferred in most studies due to simplicity and parsimony compared to the use of empirical methods such as PMV, which are complex and require significant parameterization (Mohan, et al., 2014; Roelofsen, 2015; Shastry, et al., 2016). Simple techniques such as PET and DI only require wind speed, air temperature and humidity while complex approaches such as PMV use more variables including human metabolism and insulation provided by clothing (Goshayeshi, et al., 2013b). Discomfort indices are commonly used due to parsimony because thermal comfort assessment using models such as the Rayman, ENVI-MET or other models requires parameterization and data (Mohan, et al., 2014; Roelofsen, 2015; Shastry, et al., 2016).

Outdoor thermal discomfort assessment have widely used in-situ meteorological measurements (Yousif & Tahir, 2013; Cheng et al., 2010; Abdel-Ghany, et al., 2014; Tulandi et al., 2012). One of the simplest indices is the Thom's Discomfort Index (DI) computed using air temperature and relative humidity. However, remote sensing enables synoptic measurement of intensity and spatial distribution of thermal discomfort for the whole city (Sobrino et al., 2004). A few studies on outdoor thermal discomfort using remote sensing have employed NOAA AVHRR and Multi-functional Transport Satellite (MTSAT) data whose low spatial resolution is too coarse for monitoring complex urban surface properties (Okamura et al., 2014; Polydoros & Cartalis, 2014). Ideally, spatial resolution greater than 50m is needed for urban thermal analysis (Sobrino, et al., 2004). Nevertheless, readily available medium resolution data such as from Landsat offers a better alternate for mapping and monitoring thermal discomfort at landscape scale than in-situ and low resolution space-borne thermal data.

2.6.6 Impact of urban growth related warming on air-conditioning energy demand

Several approaches have been used in estimating the impact of urbanization on energy consumption for indoor space heating, with varying strengths and limitations. One of the techniques involves the use of household electricity bills to monitor the responses of air-conditioning energy consumption to temperature elevation induced by urban growth (Hirano et al., 2009; Souza et al., 2009; Shahmohamadi, et al., 2010; Arifwidodo & Chandrasiri, 2015).

Shahmohamadi, et al. (2010) for instance established a positive correlation between urban heat island intensification and increased households energy consumption in the United Kingdom, United States of America and Sri Lanka. A major weakness of this technique is that household electricity usage is not restricted to air conditioning but also other purposes such as refrigeration, lighting and cooking (Ewing & Rong, 2008). Another popular approach involves the use of Degree Days derived from air temperature to quantify trends in energy for indoor cooling or heating (Vardoulakis et al., 2013; Arifwidodo & Chandrasiri, 2015; Ewing & Rong, 2008). Degree Days are calculated relative to a reference temperature below or above which human discomfort is triggered, making them a direct measure of energy consumption (Bolattürk, 2008). Cooling Degree Days (CDD) provides a measure for energy for space cooling while Heating Degree Days (HDD) infers energy for household warming (Christenson et al., 2006). The HDDs are calculated by subtracting the mean temperature from a reference (base) while CDDs are obtained by subtracting a base temperature from the mean air temperature. The base temperature is defined as the outdoor temperature above which ambient cooling is required and below which space heating is required (Eto, 1988). The choice of base temperature has been widely varied, as studies have used values ranging from 8 to 26^{o}C (Bolattürk, 2008; Christenson, et al., 2006; Büyükalaca et al., 2001; Durmayaz et al., 2000; Sarak, 2003; Dombaycı, 2009; Satman & Yalcinkaya, 1999; Papakostas & Kyriakis, 2005). The most widely used reference temperature is 18^{o}C, which is also recommended for global comparability (Santamouris et al., 2001; Sivak, 2009; Bolattürk, 2008; Sailor & Pavlova, 2003; Guerra Santin et al., 2009). Degree Days were proved to have a strong positive correlation with household energy consumptions in resourced countries such as in European cities (Balaras et al., 2005). The major constraint highlighted in previous studies on Degree Days is the use of in-situ measurements of temperature which limited spatial coverage (Stathopoulou, et al., 2006). Despite advantages over in-situ data in the analysis of spatially complex phenomena, to the best of our knowledge, only a single study has used space-borne satellite data to estimate degree days. Stathopoulou, et al. (2006) derived Degree Days using air temperature estimated from surface NOAA AVHRR's thermal data-based temperature using a linear regression model (R^2=0.78). Although the method showed great potential, the spatial resolution of NOAA AVHRR's thermal data has low spatial resolution (1.1 km), especially for applications in localized heterogeneous regions such as urban landscapes. Hence, better results can be achieved by merging in-situ observations of near surface air temperature with medium resolution surface temperature, especially from the easily accessible Landsat series. Such

analysis can also be further enhanced by adopting high resolution thermal infrared data where resources are available. This can be obtained such as by mounting thermal sensors on air planes which can fly at low altitude to obtain LST at high spatial resolution. For example, Lo, et al. (1997) analyzed day- and nighttime surface temperature in Alabama in United States of America using 5 m resolution remote sensing data from the air-bone Advanced Thermal and Land Application Sensor (ATLAS). However, this is an expensive exercise hence the popular use of medium resolution data such as from Landsat, ASTER and MODIS.

2.6.7 Local climate zoning and the World Urban Database and Access Portal Tools

Land use and land cover classifications discussed in this chapter so far create zones whose naming is culture and region specific and independent of climate. The schemes are not universal for example the vagueness of defining rural and urban areas in different parts of the globe (Stewart & Oke, 2012). The classifications were designed for other purposes not heat island fields which triggered the need to come up with a procedure for climate specific local area zoning. This can be done using Local Climate Zones (LCZ) which avoid the use of culture and region specific classifications (Stewart & Oke, 2012; Perera & Emmanuel, 2016). LCZ are inclusive of all regions, independent of culture, and quantifiable according to class properties that are relevant to surface thermal climate (Stewart & Oke, 2012). Oke (2004) developed nine urban climate zones which coincide with the first nine of the seventeen zones later developed by Stewart and Oke (2012). The names of zones developed by Stewart and Oke (2012) are local in scale, climatic in nature and zonal in presentation thus of a global standard. Thomas et al. (2014) linked LCZ with UHI and observed intense cooling in sparsely built regions and maximum intense heating in compact midrise. In another study done in Beirut, Lebanon the link between LCZ and modeling results from Town Energy Balance Model (TEB) was established (Kaloustian & Bechtel, 2016). Brousse et al. (2016) showed LCZ improves Weather Research and Forecasting (WRF) model output when compared with CORINE land cover data. There is a global call for studies which use LCZ in urban areas for input into World Urban Database and Access Portal Tools (WUDAPT) (Cai et al., 2016; Bechtel et al., 2015; Stewart & Oke, 2012). Currently, progress in urban climate science is strolled by lack of useful information that describes aspects of the form and function of cities at detailed spatial resolution hence the WUDAPT call (Bechtel, et al., 2015). WUDAPT is being developed to gather and disseminate LCZ information. Bechtel, et al. (2015) developed WUDAPT protocols which are easy to understand, use freely available data such as medium resolution remote sensing imageries) and can be applied by someone with limited knowledge in spatial analysis

or urban climate science. Scientists in developing countries should carry out studies which feed into the WUDAPT to inform global sustainable urban development.

2.7 Future recommendations

Although significant progress has been achieved in remote sensing based LULC mapping, accuracy in mapping urban landscapes stills needs further improvement. The urban landscape is characterized by complex changes in LULC in space and time. Such detection usually suffers from the mixed pixel challenge. In order to improve LULC mapping in urban areas, studies should focus on algorithms, data enhancement and data merging techniques using medium and high resolution remote sensing data sets. Future efforts must include LULC classification using data from recently launched freely available medium resolution sensors such as Sentinel and Landsat 8. Specifically, Landsat 8 has improvements which include improved noise-signal ratio, high radiometric resolution and improved spectral range. Additionally, the sensor has two thermal infra-red bands whose inclusion has the potential to increase mapping accuracy, given the strong relationship between LULC and LST (Xu et al., 2013; Larsen & Gunnarsson-Östling, 2009; Yuan & Bauer, 2007). The options for improving urban mapping include merging optical bands with indices such as NDBI, NDBaI, NDWI and NDVI (Chen, et al. 2006). Other high resolution data such as the 12m Germany TerraSAR-X with a global coverage also need to be tested even in mapping LULC of African and other cities. The potential of remote sensing based LCZ mapping to improve understanding of link between urban surface characteristics and near-surface temperatures needs to be tested especially in developing countries.

Lack of high spatial resolution thermal imagery has significantly constrained surface temperature characterization. Previous urban surface temperature studies have relied heavily on medium resolution sensors such as ASTER and Landsat series with spatial resolutions of at least 60m. As a result, urban surface covers and land cover indices are mapped at a higher resolution than thermal information which strongly affects attempts for their correlation. Engineering solutions should involve development of thermal sensors with higher spatial resolution. Options may also include launching other polar orbiting satellites with thermal sensors at lower altitude to reduce Instantaneous Field of View (IFOV), thereby increasing spatial resolution. Furthermore, using the relationship between LST and higher resolution variables such as vegetation indices may improve spatial resolution at which thermal conditions are characterized.

Although medium resolution thermal datasets are useful for urban surface temperature analysis, low temporal resolution limits their applications for temporal analysis. For example, the number of Landsat images available per period is limited by the 16-day revisit time. This is further worsened by the requirement for cloud free images in order analyze surface conditions (Sattari & Hashim, 2014). This makes it difficult to relate satellite observations from medium resolution sensors with in-situ air temperature data due to comparatively few coinciding observations. Seasonal analysis, for instance, requires a representative number of observations in order to calculate average conditions and avoid errors due to basing on random single date imagery to represent entire season. However, due to gaps caused by limited data quantity, it is difficult to accurately represent seasonal and long term surface temperature properties using medium resolution thermal data. High temporal resolution thermal data characterize low spatial resolution sensors such as geostationary satellites (Sattari & Hashim, 2014). For instance, SEVIRI sensor has a 15 minutes temporal resolution, but due to a very coarse spatial resolution (3km), the thermal data are not useful for characterizing thermal conditions in urban landscapes. Studies should focus on integrating low and medium resolution sensors to build thermal datasets with improved spatial and temporal resolution. This is capable of monitoring spatial and temporal variations of temperature in heterogeneous urban landscapes. This will improve temperature analysis at seasonal and longer time scales critical also for prediction of future thermal conditions.

Previous studies have attributed long term changes in urban surface temperature to LULC transitions without resolving the contribution of other factors such as global warming. Similarly, global and regional climate models have mostly left out urban meteorological stations and assumed that their contribution is negligible (Nayak & Mandal, 2012). Where urban areas are considered, emphasis is placed on the contribution of anthropogenic emissions to greenhouse gas concentration levels. However, studies like Pielke et al. (2011) have shown that impacts of LULC changes is superimposed on already changing temperatures due to among others the general global warming patterns. For example, Ogrin and Krevs (2015); Pielke et al. (2011) observed that long term changes in urban temperature were faster than other areas. Future studies need to develop methods to separate effects of LULC conversion from other causes of temperature increases such as changes in GHG concentrations and ozone

depletion in urban environments. This has potential to improve urban planning, growth policies and strategies as well as modeling of the urban micro-climatic changes.

Impact assessments such as extreme heat vulnerability mapping should enhance use of remotely sensed contributing factors and improve the spatial resolution. Available literature such as Johnson, et al. (2014) produced heat vulnerability maps at low spatial resolution for instance, at district and census block scale. However, socio-economic status and physical exposure are not uniform within each sub-division. Hence there is need to improve spatial details of input factors in order to produce maps that show variations found even with census blocks. Remote sensing, especially using medium and high spatial resolution sensors should be capable of mapping heat exposure factors at higher resolution than census blocks. Studies need to identify heat vulnerability factors detectable using medium and high resolution dataset and establish methods to combine them with other data to improve the mapping of heat vulnerability. Due to the link between surface properties and temperature, remotely sensed variables such as NDVI and NDBI have been incorporated in vulnerability studies. However, where this was done, focus was not placed on improving the spatial resolution of the maps generated. Detailed heat vulnerability maps are important for tailoring interventions based on levels of need, which eliminates poor strategies caused by generalization at coarse resolution.

Assessments of thermal discomfort and impact on air conditioning energy demand have most widely been executed using in-situ observations of temperature (Vardoulakis, et al., 2013). However, research has shown that surface temperature modulates near surface (2m) air temperature and there is strong correlation between the two (Pielke, et al., 2011; Marland et al., 2003; Cai, et al., 2011). Future studies should use this relationship to upscale temperature observations. In that case, the use of medium resolution thermal data will enable mapping of the spatial distribution of temperature as well as derivation of responses such as discomfort and energy consumption. For example, up-scaling temperature observation will enable analysis of the variations in degree days, hence air conditioning energy between urban landscapes. The use of medium resolution remotely sensed thermal imagery in estimating temperature has strong potential in mapping spatial variations with higher reliability than point data. This is also important for analysis of thermal conditions in resource constrained cities where stations are usually undesirably sparse.

Remote sensing based thermal studies have mostly been focused on single date, seasonal and long-term but historical analysis of the relationship between urban LULC patterns and LST (Xu, et al., 2013; Larsen & Gunnarsson-Östling, 2009; Yuan & Bauer, 2007). Land cover indices have also been used to show the quantitative relationship between LULC conversion and temperature (Weng, et al., 2004; Chen, et al., 2006; Yuan & Bauer, 2007; Tran, et al., 2006; Xiao et al., 2007; Zhang, et al., 2012; Hung, et al., 2006). Thus, previous studies have mostly stressed on historical changes in temperature in response to urban growth and proved that surface alterations result in warming (Yuan & Bauer, 2007; Hu & Jia, 2010; Valsson & Bharat, 2009; Odindi, et al., 2015). However, there is paucity of literature on future LULC and temperature patterns using remote sensing. Due to improvements in sensor technology, data availability and better spatial coverage than meteorological stations, there is need to use freely available medium spatial resolution remote sensing data sets such as Landsat and Sentinel-2 Multi-Spectral Instrument (MSI) in models to predict future LULC and temperature distribution. This is important for planning, especially in developing countries often characterized by rapid urban growth and limited spatial data.

Ahmed et al. (2013) used NDVI as a predictor of future LST using the Markov Chain Analysis. Although the approach is unique, NDVI has limitations which include saturation when vegetation fraction is high. The study did not test the potential of other indices, hence there is need to test other indices like NDBI and NDWI or a combination of various indices in multi-variate regression to predict future temperature. In cases where more than a single index is used, there is need to identify a set of indices that most accurately predict LST with optimal errors and minimal multiple collinearity issues. This will complement efforts made by greenhouse gas concentration based models to predict future temperatures. This will also enhance understanding of the implications of urban growth patterns and associated LULC changes on future climate even if greenhouse gas concentration levels are to remain constant or be reduced in effect.

2.8 Conclusion

The current study reviewed previous studies on monitoring the impacts of urban growth on in-and-out door thermal conditions using remote sensing tools. Specifically, the study focused on urban growth and changes in temperature covering topical issues of urban growth assessment methods such as, heat vulnerability mapping, outdoor thermal discomfort, heat island-related air conditioning energy consumption and prediction of future temperatures using space-borne

remote sensing data sets. Literature has revealed that improvements among others sensor properties and data quality as well as techniques such as data merging have increased accuracy for the determination of urban growth. Data merging techniques such as inclusion of land cover indices have potential to further improve LULC mapping. There is also need to improve temporal analysis of the urban thermal conditions such as by integrating data from polar orbiting with geostationary sensors. This has potential to create thermal datasets with high spatial and temporal resolution, useful for mapping spatial variations in urban temperatures at seasonal and longer timescales. Furthermore, heat vulnerability assessments still place much emphasis on socio-demographic factors with limited attention given to bio-physical factor. There is still need to enhance the use of medium and high spatial resolution data to improve the spatial resolution of heat vulnerability maps compared to the widely used census block level. The potential of medium resolution data, such as Landsat series, to map outdoor thermal discomfort and indoor air-conditioning energy demand still needs to be tested. To date, studies have dwelt on traditional methods therefore, it is necessary that thermal remote sensing be adopted for future temperature predictions. The potential of a variety of indices including NDBI to predict future temperatures needs to be assessed.

2.9 Link with other chapters

Chapter 2 highlighted remote sensing based and other techniques used to assess and quantify urban growth as well as its impacts on surface and near surface temperatures, thermal discomfort as well as other associated impacts. The chapter assessed the extent to which remote sensing can be and has been used to quantify urban growth and effects on temperatures. The next chapters build on identified strengths of remote sensing over in-situ based analysis as well as research gaps extracted from recommendations for future studies. For example, the review showed the complexity of urban LULC classification using medium resolution remotely sensed data and the need to improve mapping accuracy. Chapter 3 thus tests the potential of various combinations of optical, thermal infrared data and indices to improve urban mapping accuracy using recently launched Landsat 8 data.

CHAPTER 3: ENHANCED URBAN CLASSIFICATION USING MULTI-SPECTRAL MEDIUM RESOLUTION REMOTE SENSING DATASETS

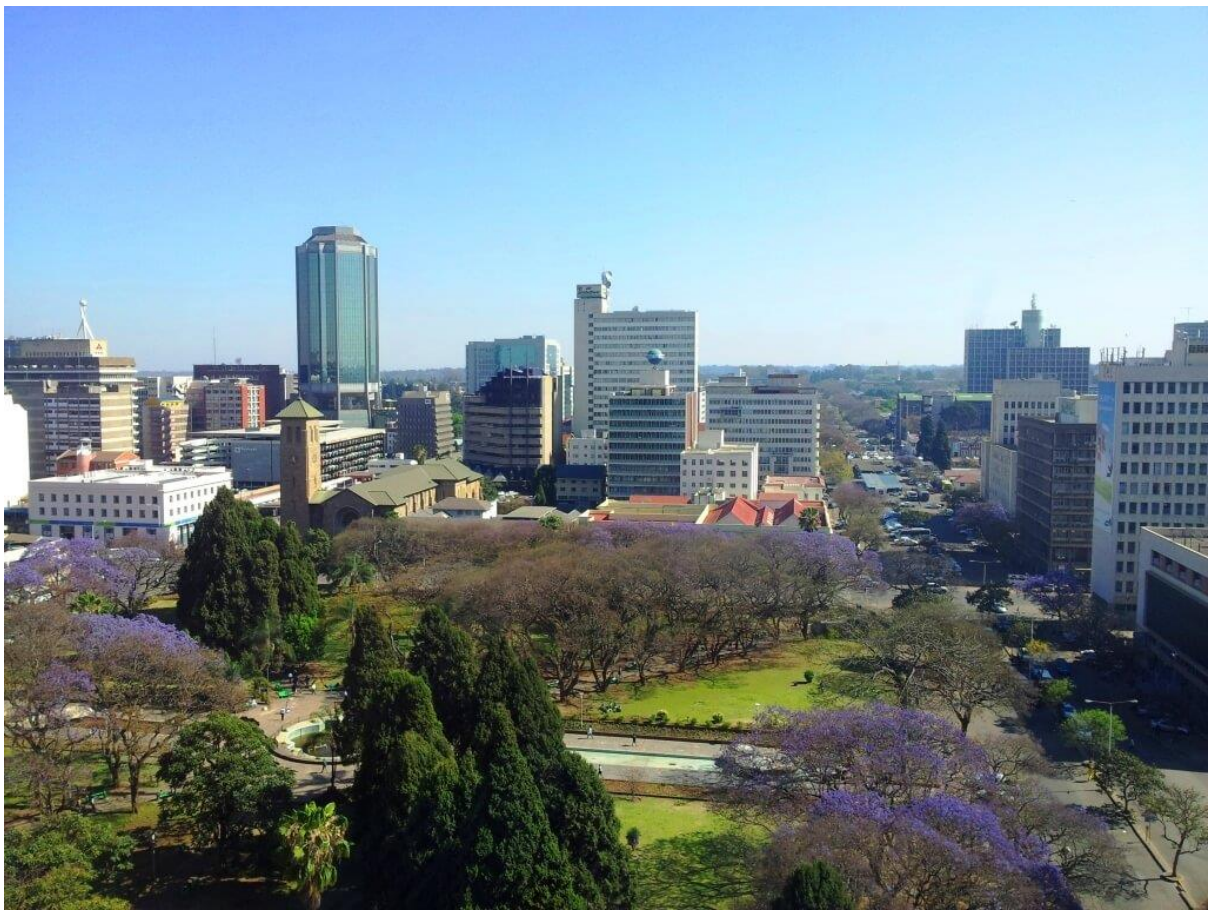

This chapter is based on:

Mushore T. D., Mutanga O., Odindi J., Dube T. (**2017**). Assessing the potential of integrated Landsat 8 thermal bands, with the traditional reflective bands and derived vegetation indices in classifying urban landscapes. *Geocarto International*, 32:8, 886-899, http://dx.doi.org/10.1080/10106049.2016.1188168

3.0 Abstract

Reliable and up-to-date urban land cover information is valuable in urban planning and policy development. Due to the increasing demand for reliable land cover information, there has been a growing need for robust methods and datasets to improve the classification accuracy from remotely sensed imagery. This study sought to assess the potential of the newly launched Landsat 8 sensor's thermal bands and derived vegetation indices in improving land cover classification in a complex urban landscape using the Support Vector Machine (SVM) classifier. This study compared the individual and combined performance of Landsat 8's reflective and thermal bands and vegetation indices in classifying urban land use-land cover (LULC). The integration of Landsat 8 reflective bands, derived vegetation indices and thermal bands produced significantly higher accuracy classification results than using traditional bands as standalone (i.e. overall, user and producer accuracies). An overall accuracy above 89.33% and a kappa index of 0.86, significantly higher than the one obtained with the use of the traditional reflective bands as a standalone dataset and other analysis stages was obtained. On average, the results also indicate high producer and user accuracies (i.e. above 80%) for most of the classes with a McNemar's Z score of 9.00 at 95% confidence interval, showing significant improvement compared with classification using reflective bands as standalone. Overall, the results of this study indicate that the integration of the Landsat 8's Operational Land Imager and Thermal Infrared data presents an invaluable potential for accurate and robust land cover classification in a complex urban landscape, especially in areas were the availability of high resolution datasets remains a challenge.

Keywords: Classification accuracy; complex urban landscapes; data integration; new generation sensor; resampled thermal bands; satellite data

3.1 Introduction

Accurate and updated urban Land Use-Land cover (LULC) information is important for optimal and sustainable land use planning (Hashem & Balakrishnan, 2015). For instance, in order to improve land use planning, accurate information on current land use is essential as this provide details needed for planning purposes and relevant policy development at a range of scales (Oort, 2005). Furthermore, a national database of accurate LULC maps is needed in order to detect changes over time, including urban growth in order to determine impacts on the environment and human livelihood (Yu, et al., 2013; Dube, et al., 2014; Abegunde & Adedeji, 2015). Besides, this information is crucial for monitoring and mitigating the impact of urban growth on the environment i.e. forests, agriculture and wetlands (Xian & Crane, 2005). Therefore, LULC mapping assists planners to project future trends of human activities, urban growth and land surface characteristics, in addition improving performance of ecosystem and atmospheric models amongst others (Hashem & Balakrishnan, 2015; Yu, et al., 2013). However, accuracy is affected by the scale, as well as by spatial and spectral data characteristics (Lo & Choi, 2004).

From a social perspective, urban planning is also related to the comfort of urban dwellers as increasing impervious surfaces at the expense of greenery results in surface temperature increases (Weng, et al., 2004; Odindi, et al., 2015; Rossi et al., 2014). Increases in surface temperature need to be accurately quantified as this escalates related impacts, like human thermal discomforts. Surface temperature changes resulting from increases in impervious areas due to urban growth raise costs associated with restoring thermal normalcy, such as air conditioning and resultant electricity bills (Larsen et al., 2008). For example, literature shows that hard or impervious surfaces have the potential to increase local temperature resulting in warmer environments than in areas with high vegetation fraction and water (Forkuor & Cofie, 2011; Deng & Wu, 2013; Zhang, Qi, et al., 2013). Accurate quantification of LULC changes and related changes in climate depends on the accurate mapping of the initial and final state of the distribution of the functional zones in an urban area, hence the need to improve LULC mapping (Xian & Crane, 2005; Abegunde & Adedeji, 2015; Juan-juan Li et al., 2009). If the derived maps are not accurate, the policy and technical measures implemented in an area based on them will also be very deceptive (Xian et al., 2012). However, the complexity of urban setups results in low accuracy maps from remotely sensed data, hence a constant need for improvement in classification accuracy.

Urban LULC mapping remains difficult due to heterogeneity of surface features and reduction in accuracy due to the presence of mixed pixels, especially when using images with coarse spatial resolutions (Lu & Weng, 2005). Whereas the adoption of higher spatial resolution data (less than 10 m) has been suggested as a solution to the mixed pixel problem, a number of studies have noted that lower classification accuracy persists as this may increase intra-and-interclass variability resulting in unreliable LULC information derived from satellite data (Aplin, 2003; Salvati & Sabbi, 2011; Lo & Choi, 2004). Furthermore, higher resolution imagery are often costly, have a small spatial coverage and poor temporal resolution, which does not adequately aid change analysis (Forkuor & Cofie, 2011). It is therefore important to explore the extent and potential to which the readily available datasets and affordable moderate resolution data, such as the recently launched Landsat 8 can be fully used to improve accuracy of mapping in urban areas (Lu & Weng, 2005). Moreover, Landsat 8 data have proved to perform very well in forest biomass related studies (Dube & Mutanga, 2015a), evaporation mapping (Shoko et al., 2015), as well as land surface temperature mapping (Yang, Lin, et al., 2014) when compared to the previous Landsat series data due to improved spectral and radiometric resolutions.

Based on this background, the newly-launched Landsat 8 multispectral sensor is hypothesized to present numerous and invaluable opportunities required for the derivation of up-to-date and crucial LULC information, particularly in complex urban environments. For instance, the inherent Landsat 8 sensor improvements i.e. radiometric, signal to noise ratios and the introduction of new thermal bands, is hypothesized to have the potential of improving the mapping accuracy of complex urban setups - a challenging task from the previous Landsat series data especially using the four spectral vegetation indices. The Landsat 8 reflective bands have mostly been used alone for urban LULC mapping and findings from literature have shown that this data alone is not sufficient for that purpose (Panah et al., 2001; Tucker et al., 1985; Lu et al., 2015; Pengra et al., 2015; Dube, et al., 2014). Although not fully explored, previous work demonstrates that the coarser spatial resolution Landsat 8 thermal bands have critical information linked to the land surface and vegetation biochemical properties (Sun & Schulz, 2015; Foody, 1996). The thermal information is usually left out of mapping procedures while landscapes, such as in urban areas, contain a variety of surfaces with contrasting properties to conduct and release heat during the day and night (Xian, et al., 2012).

In most heat island phenomena studies, surface temperatures have shown strong dependency on LULC types although LULC were mapped at higher spatial resolution than surface temperatures (Stathopoulou & Cartalis, 2007; Chen, et al., 2006; Yuan & Bauer, 2007; Klok et al., 2012; Wang & Zhu, 2011; Odindi, et al., 2015). The strong correlation between thermal capacity and LULC types can be utilized as additional information for thoroughly discriminating between surface cover types using low and moderate resolution satellite data (Ormsby, 2007). Although the thermal bands of Landsat 8 are at lower resolution than the optical bands, they should improve classification accuracy in this study because the classes considered at a broad scale are detectable at such low resolution. Rather than extracting single buildings that require high resolution, extraction of broad classes, such as high density residential, is very viable at the resolution of Landsat 8 thermal bands given that such classes are larger than the cell size of the thermal data. Also, in such broad scale classifications, the inclusion of thermal data should improve classification accuracy (Witt et al., 2007) given the clearly documented differences in thermal properties between LULC classes.

In addition, vegetation indices contain valuable information useful for LULC mapping. Indices, such as the Normalized Difference Vegetation Index (NDVI), are the most widely used in LULC studies as they relate to a number of vegetation characteristics, which include density, vegetation water content and chlorophyll content (Chen, et al., 2006; Stathakis, et al., 2012; Sharma et al., 2012). The NDVI best separates vegetation from other surface covers by utilizing the unique property that vegetation has very high reflectance in the near infrared range and reflects low amounts of visible red radiation. NDVI is thus high over vegetated areas, low over bare and built areas, and negative over areas covered by water (Chen, et al., 2006). The Normalized Difference Built Index (NDBI) is used to extract built up areas from remotely sensed data although it ignores the fact that besides built up areas, bare areas also reflect higher in the mid-infrared (MIR) than the near-infrared (NIR) band (Hua, et al., 2013). In order to adequately separate bare areas from built areas, the Normalized Difference Bareness Index (NDBaI) can be used based on the principle that bare soils reflect more in the thermal infrared than the MIR part of the spectrum. The Normalized Difference Wetness Index (NDWI) separates water from other surface cover types utilizing the principle that water reflects more in the visible spectrum than in the short wave infrared (Hua, et al., 2013; Stathakis, et al., 2012). Combined with the NDVI, the NDWI improves identification of vegetated areas as it also relates to vegetation water content (VWC) (Jackson et al., 2004) and it is deemed to equate to

thickness of water (Sharma, et al., 2012). Evidently, the four indices contain valuable information that if integrated with the traditional Landsat 8 reflective bands and thermal bands can be used to discriminate different land cover types, particularly in complex and heterogeneous urban areas with plausible accuracies.

This work aimed at assessing the potential of integrating Landsat 8 derived thermal bands, with the sensor's traditional reflective and computed vegetation indices in discriminating complex and heterogeneous urban landscapes. It was hypothesized that the inclusion of the Landsat 8 thermal bands together with the sensor's traditional reflective bands, as well as the computed vegetation indices has the potential to greatly improve the image classification of complex and heterogeneous urban landscapes.

3.2 Materials and methods

3.2.1 Description of study area

The study was conducted in the rural and urban districts of Harare, which form part of Harare Metropolitan City. Harare Metropolitan City occupies approximately 94 000 ha and, according to the 2012 national census, the entire city has a population of approximately 2 million (Wania et al., 2014) (Figure 3.1). Harare is experiencing growth as shown by increasing population and built-up extent. The city assumes the radial model with the central business district at the centre, with high built-up density. Residential setups are more spacious to the north of the city center where high income earners are found than in the southern areas (i.e. largely high density residential areas) where mostly low income earners live (Wania, et al., 2014). The period from mid-April to mid-September is generally cool with the major climatic hazard being frost, mainly on high ground. The city experiences high temperatures during the hot season between mid-September and mid-November with a peak in October. The month of October is the warmest with an average temperature of 28^{o}C (Manatsa et al., 2012) and during this period most croplands are uncultivated, cleared in preparation of the intra-urban farming activities. During the hot season, bare and sparsely vegetated surfaces are dry, thus further exacerbating surface warming. Vegetation growth is seasonal as the city receives rainfall between mid-November and April (Unganai, 1996; Manatsa, 2012; Mushore, 2013b). The city is also characterized by well-maintained parks located in the central business district and northern areas.

.

3.2.2. Field data collection and processing

Supervised image classification requires prior knowledge of LULC classes in the study area. It also requires coordinates of representative samples for each LULC type used for training the computer how to assign classes as well as to assess accuracy afterwards. In order to identify LULC classes in Harare and obtain coordinate of representative points per LULC class, field data collection was done between the 1 April and 30 April 2015. During data collection, 120 GPS points were collected for each land cover class using a hand-held Garmin eTrex30 GPS with ±3m accuracy. Field data collection followed a stratified random sampling approach to obtain sample from several locations across Harare. For each LULC type, sub-classes were also identified and coordinates of samples were collected. This was done to incorporate intra-class variability. For example, different types of vegetation were identified during field survey and data collection ensured that samples were taken from all possible sub-classes of vegetation (e.g. trees, shrubs, grassland). Although classes obtained in the field could be further disaggregated into several small sub classes, this study generalized them into seven major LULC types (Table 3.3). Seven land cover classes were used based on the recommendations that when using moderate to coarse resolution satellite data, such as Landsat series data, the generation of a large number of classes was inappropriate (Yu, et al., 2013).

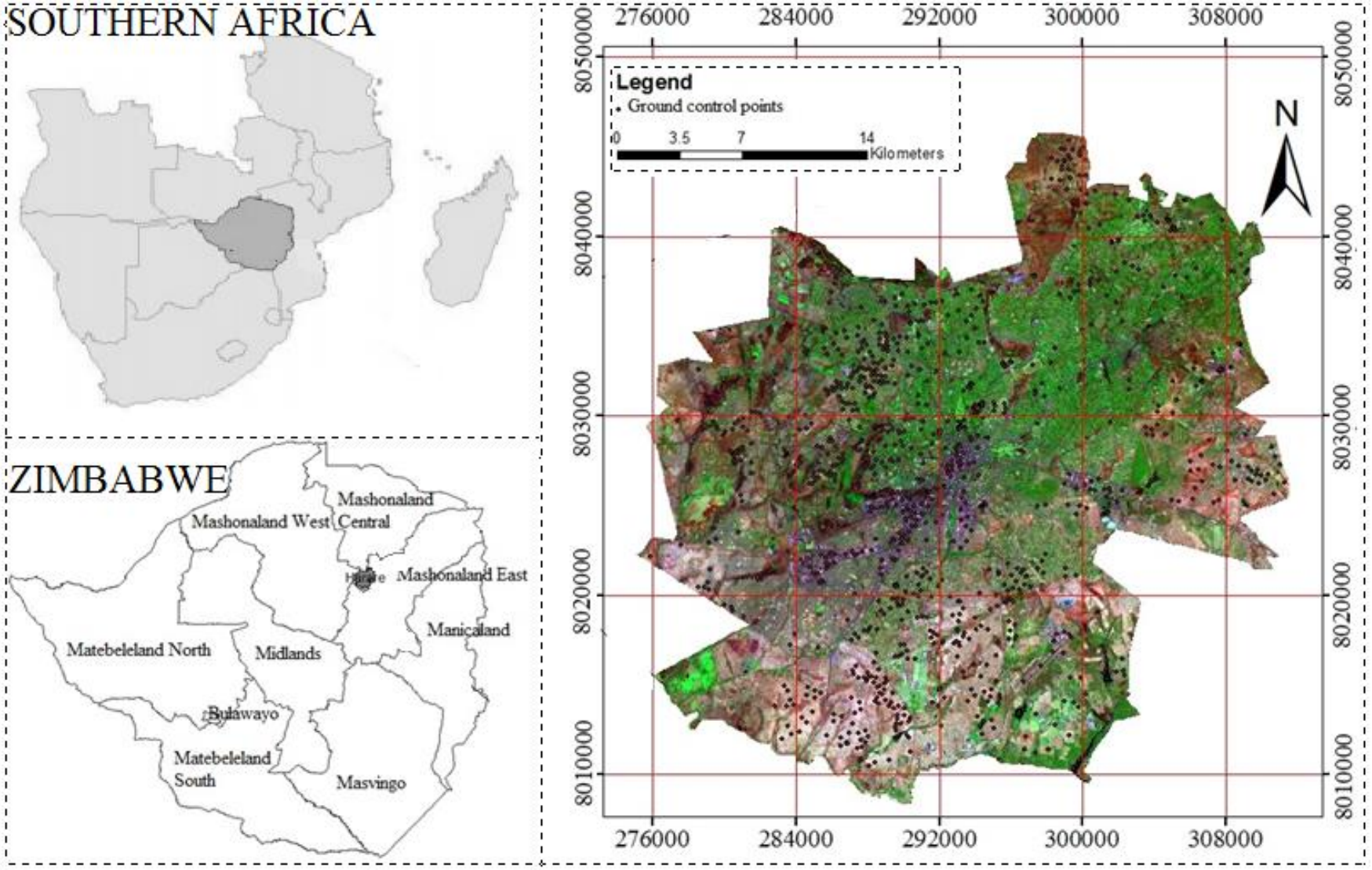

Figure 3.1: Location of the area under study area

3.2.3. Remote sensing data acquisition and pre-processing

A cloud free 30-m Landsat 8 image covering the entire study area was downloaded for free using 170/72 path/row from the earth explorer website courtesy of the USGS-EROS Centre archive (www.earthexplorer.usgs.gov). The image was acquired on 31st October 2014. The Landsat 8 Thermal Infrared Sensor (TIRS) bands are acquired at 100 metre resolution, but were provided already resampled to 30 metre spatial resolution (Table 3.1). The acquired image was corrected for geometric and radiometric errors. The image was rectified to UTM Zone 36S using 20 ground control points collected in the field at the intersection of major roads. Also, to ensure accurate retrieval of spectral information, the image was atmospherically corrected using the FLAASH module in ENVI 4.5 software and the parameters downloaded from AERONET website (Dube, et al., 2014).

Table 3.1: Properties of Landsat 8 data used in the study (Genc et al., 2014)

Band	Name	Bandwidth (µm)	GSD (m)
1	Coastal blue	0.435–0.451	30
2	Blue	0.452–0.512	30
3	Green	0.533–0.590	30
4	Red	0.636–0.673	30
5	NIR	0.851–0.879	30
6	SW1	1.566–1.651	30
7	SW2	2.107–2.294	30
8	Pan	0.503–0.676	15
9	Cirrus	1.363–1.384	30
10	TIRS 1	10.60-11.19	100 *(30)
11	TIRS 2	11.50-12.51	100 *(30)

*TIRS- Landsat 8 thermal Infra-red bands

3.2.4 Landsat 8 spectral bands and vegetation indices retrieval

Six simple spectral reflectance from the visible, near-infra-red short-wave (i.e. blue, green, red, nir, swir I, swir II and two thermal bands (*i.e.* TIR I and TIR II) were extracted from Landsat 8 OLI and TIR images. In addition, four spectral vegetation indices were computed using Landsat 8 OLI spectral bands. The choice of these indices was based on previous studies that demonstrated their reliable applications in land cover mapping (Chen, et al., 2006; Sharma, et al., 2012). The computed vegetation indices are summarized in Table 3.2. The Landsat 8 OLI and TIRS spectral bands and the computed vegetation indices selected for this study were extracted at each location based on points obtained during field data collection. 120 field-collected GPS points were first projected to the Landsat 8 OLI and TIRS image coordinate system for easy overlay and spectral extraction purposes. Since a point represents a single pixel,

a land cover may occupy a pixel and its neighbours, polygons were created by digitizing around each point on pixels falling within the same class. These regions of interest were created using the Region Of Interest (ROI) tool in ENVI 4.5. This was done for both training and validation datasets so that polygons instead of points were prepared as ground truth regions for classification and validation.

3.2.5 Image classification

The extracted Landsat 8 OLI and TIRS bands and computed vegetation indices were used in classifying the complex and heterogeneous urban settings. The analysis was done using seven different sets of both spectral and vegetation indices summarised in Table 3.2. The analysis procedure was done using the Support Vector Machine (SVM) classifier algorithm. The SVM is regarded as one of the most powerful and robust non-parametric machine learning algorithms in image classification studies when compared to the commonly used classification algorithms such as Maximum Likelihood, Random Forest, Artificial Neural Networks and Mahalanobis classifiers (Adelabu et al., 2013; Jia, et al., 2014). One of the major advantages of the SVM algorithm is that it requires comparatively low amounts of training data compared to its counterparts (Forkuor & Cofie, 2011; Yu, et al., 2013). The algorithm applies two classes, namely presence or absence of the training samples, within a multi-dimensional feature space to fit an optimal separating hyper-plane (i.e. in each dimension, vector component is image gray-level). During the process the algorithm attempts to maximize the distance between the closest training samples, or support vectors, and the hyper-plane.

The ground truth data for classification were used to classify each of the layer combinations shown on Table 3.2 using the SVM classifier (Gamma in Kennel function was set at 0.091, Penalty parameter was 100, Pyramid level were set at 0 and the Classification Probability threshold was also 0). The same settings were used in all the methods to eliminate the contribution of the SVM parameters on the accuracy since input band combinations were the only variable in this study. For this work, the dataset was randomly split into 70% (85) and 30% (36) training and testing datasets respectively (Adelabu, et al., 2013). The major land cover classes considered in this study are summarised in Table 3.

Table 3.2: OLI, TIRS spectral bands and computed vegetation indices

Data type	data source	variables applied	Analysis
SB	OLI	1-6: blue, green, red, NIR, SWIR I & II	I
	TIRS	1-2: TIRS I & II	II
	OLI & TIRS	1-8: blue, green, red, NIR, SWIR I, SWIR II, TIRS I & TIRS II	III
Vis	OLI	1-4: NDBaI, NDVI, NDBI & NDWI	IV
SB & Vis	OLI & TIRS	1-6: TIRS I, TIRS II, NDBaI, NDVI, NDBI & NDWI	V
SB & Vis	OLI	1-10: blue, green, red, NIR, SWIR I, SWIR II, NDBaI, NDVI, NDBI & NDWI	VI
All variables	OLI & TIRS	blue, green, red, NIR, SWIR I, SWIR II, TIRS I, TIRS II, NDBaI, NDVI, NDBI & NDWI	VII

*SB = spectral bands; Vis = Vegetation Indices; TIRS = Thermal Infrared Sensor; OLI = Operational Land Imager; NDBaI = Normalized Difference Bareness Index; NDVI = Normalized Difference Vegetation Index; NDWI = Normalized Difference Water Index; NDBI = Normalized Difference Built Index

Table 3.3: Description of the major land cover classes considered for this study

Class	**Description**
Densely built (DB)	Very high built density (CBD and industrial areas)
Low-medium density residential (LMR)	Low and medium density residential areas with higher vegetation fraction than high density residential
High density residential (HDR)	Built-up with higher density of building and lower vegetation cover than low-medium residential
Forested Areas (Fr)	moderate to dense forest cover
Development (Dv)	High density residential under development; mixture of bare and building with very low vegetation cover
Grasslands (Gr)	Grass covered areas with little or no trees
Water (Wt)	Water bodies

3.2.6 Accuracy assessment

To evaluate the reliability of the results obtained from this study, accuracy assessment was performed for each land cover class. An independent test dataset of LULC data consisting of 36 points per LULC type was used in the process. For each method, the obtained classes where cross tabulated on a confusion matrix against the ground truth classes for the corresponding pixels on a confusion matrix in order to determine classification accuracies (Yu, et al., 2013). The agreement between classification results and ground truth was measured using the producer accuracy, user's accuracy, overall accuracy and Kappa index generated from the confusion matrices (Jia, et al., 2014). Producer's accuracy is a measure of how correct the classification is, while user's accuracy is a measure of the reliability of the map for each class (Namdar, et al., 2014). The different classification methods were primarily compared in performance with the traditional method, which uses reflective bands only based on the

coverage per class (area), producer's accuracy, user's accuracy, overall accuracy and McNemar's tests.

3.2.7 Significance of the differences in accuracy between the classification methods

The significance of the differences in accuracy between the methods was tested based on the confusions tables, using the McNemar's test. The McNemar's test was used to compare each of the methods with the traditional method which uses only the reflective bands for classification to assess whether the other methods significantly differed in terms of accuracy. The McNemar's test is a better statistic for comparing accuracies of classification methods than the Kappa index and it is simple to compute (Petropoulos et al., 2012; Adelabu, et al., 2013). The Kappa chi-squared requires that independent data are used to assess accuracies, but in this study, the same points are used in all methods thus the McNemar's test was more appropriate as it is also more precise and sensitive (Manandhar et al., 2009).

Table 3.4: Comparison of two methods using the McNemar's test

		Method 2	
		Correctly classified	**Wrongly classified**
Method 1	Correctly classified	f_{11}	f_{12}
	Wrongly classified	f_{21}	f_{22}

McNemar's Chi squared statistic was computed using Equation 3.1 as:

$$\boldsymbol{Z^2} = \frac{(\boldsymbol{f_{12}} - \boldsymbol{f_{21}})^2}{\boldsymbol{f_{12}} + \boldsymbol{f_{21}}} \qquad \text{Equation 3.1}$$

where f_{12} denotes the number of cases that are wrongly classified by classifier 1 but correctly classified by classifier 2 (Table 3.4) and f_{21} denotes the number of cases that are correctly classified by classifier 1 and wrongly classified by classifier 2 (Petropoulos, et al., 2012). The difference in accuracies were tested at 95% significant level and deemed different if $Z > 1.96$. By comparing error matrix of each analysis with that of Analysis I, we obtained total number of cases correctly classified by the analysis and wrongly classified by Analysis I (f_{12}) and vice versa (f_{21}). The values of f_{12} and f_{21} thus obtained were used in equation one to test whether the accuracy of each analysis was significantly different with that of analysis I at 95% confidence intervals.

3.3 Results

3.3.1. Analysis I: Classification results using the traditional OLI spectral bands

Table 3.6 shows the classification accuracy results obtained using the traditional reflective bands of the Landsat 8 OLI sensor. The use of the Landsat 8 OLI derived reflective bands

produced an overall accuracy of 82.65% and Kappa index was 0.81. Further, producer accuracies greater than 75.0% for all the classes were obtained based on the use of reflective bands as independent datasets. Comparatively, the same dataset produced slightly lower user accuracy (65.7%) for the high density residential class and above 75.0% for the remaining classes. For example, densely built, forested and water classes, had significantly higher user and producer accuracies above 80.0%.

3.3.2. Analysis II: Classification results using TIRS spectral bands

Table 3.6 illustrates classification results (i.e. overall, producer and user accuracies) obtained from using Landsat 8 thermal bands. The use of thermal bands as standalone datasets overall yielded lower user and producer accuracies for almost all the classes considered under study except for the water class which had a producer accuracy of 87.5% and 86.5% user accuracy. For example, for grasslands, forested and high density residential classes, user accuracies were 33.3%, 35.6% and 45.5% respectively. Similarly, the standalone use of Landsat 8 thermal bands yielded low producer accuracies of 28.0% and 44.6% for forested and grassland classes respectively. The study produced 53.40% and 0.46 kappa index value as overall accuracy, significantly lower (i.e. McNemar's score was 9.98 at 95% confidence interval) when compared to the use of the traditional visible or reflective bands of the Landsat 8 OLI. Compared with the other methods, Analysis II produced areas per LULC class which were mostly very different from those obtained with the other methods (Table 3.5). For example, the development class had an area of 429.69km^2 using Analysis II while the area ranged between 287 and 300km^2 with the six other analysis.

3.3.3. Analysis III: Classification results using OLI & TIRS spectral bands

Table 3.6 demonstrates the urban landscape classification results based on the integration of thermal and reflective bands of the Landsat 8 sensor. Based on this analysis, an overall accuracy (84.03% and kappa index was 0.81) comparatively similar to the one obtained in the Analysis I using reflective bands as a standalone dataset. For example, high producer accuracies, mostly greater than 80%, were obtained for most of the classes i.e. water, forested and densely built classes except for development class which had producer accuracy of 72.6% (Table 3.6). User accuracies were also mostly above 80% except for development and grassland classes which had 62.8% and 76.7%, respectively.

3.3.4. Analysis IV: Classification results using spectral vegetation indices

The urban landscapes classification results obtained using Landsat 8 derived vegetation indices are shown in Table 3.6. Comparatively, the results indicate that the use of Landsat 8 derived vegetation indices produced slightly lower classification results (i.e. overall, user and producer accuracies), when compared to the use of traditional reflective bands (detail see Analysis I). For instance, user accuracies greater than 75% obtained for the majority of the classes, except for high density residential and grasslands classes where the user accuracies of 70.1% and 72.6% were respectively observed. Similarly, good producer's accuracy results (i.e. above 75%) for all the classes considered in this study were observed from the use of vegetation indices as standalone datasets. Furthermore, high overall accuracy (81.96%) and Kappa index (0.79) comparable to those obtained in Analysis I were obtained (McNemar's score was 6.93 at 95% confidence interval).

3.3.5. Analysis V: Classification results using TIRS spectral bands and VIs

Table 3.6 provides a summary of urban landscape classification results obtained based on the integration of Landsat 8 derived vegetation indices and thermal bands. The integration of Landsat 8 derived vegetation indices and thermal bands overall produced significantly higher classification accuracies (i.e. overall, user and producer accuracies). For example, an overall accuracy 82.97% and a kappa index of 0.82 was slightly higher than the result obtained in Analysis I based on the use of the traditional reflective bands as standalone dataset (McNemar's Z score of 20.70 at 95% confidence interval). The results also indicate high producer accuracies i.e. above 80% for almost all he classes except high density residential and development classes which had producer accuracies of 78.7% and 72.3%, respectively. Only the high density residential class had user accuracy below 75%.

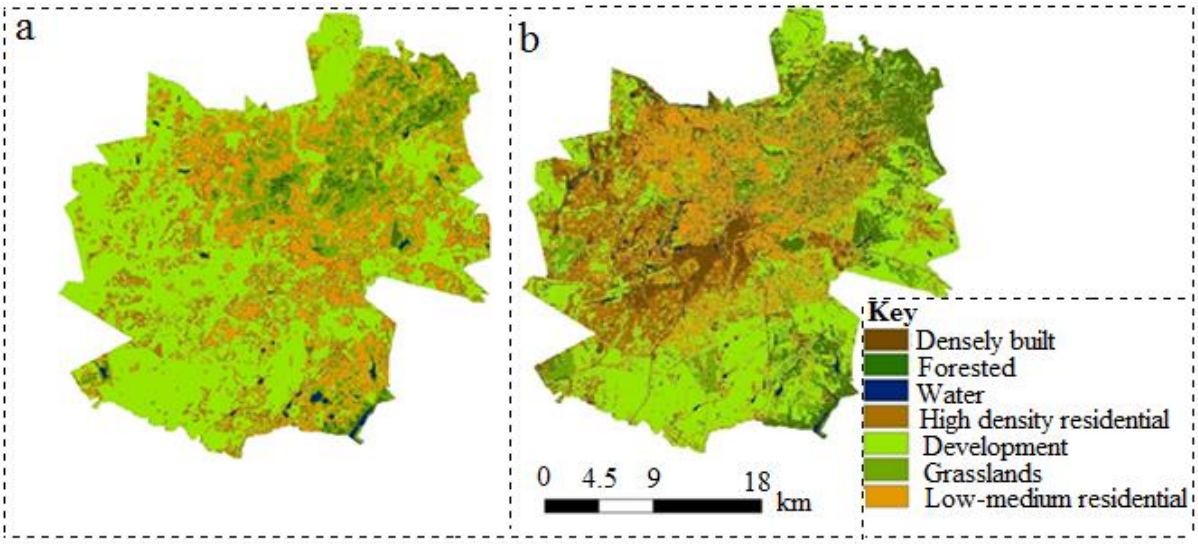

Figure 3.2: Urban landscapes lands cover classification results for obtained based on the classification models derived from analysis III and VII respectively.

Table 3.5: Areas per class obtained in the 7 analysis tested in this study

	Area covered by class (km^2)						
	Analysis I	Analysis II	Analysis III	Analysis IV	Analysis V	Analysis VI	Analysis VII
Densely Built	54.63	0.25	61.94	64.82	67.91	63.85	65.26
Low-medium residential	174.05	154.16	154.23	170.78	164.33	167.69	162.97
High density residential	139.96	126.05	156.77	143.48	142.79	130.81	133.68
Forested	129.80	31.78	126.39	124.04	121.17	126.39	126.75
Development	287.20	429.69	288.74	295.88	299.00	299.57	299.87
Grassland	53.08	107.79	54.84	49.71	50.71	55.89	55.47
Water/wetlands	17.81	5.80	12.61	6.82	9.62	11.71	11.52
McNemar's Z score	-	9.98	3.47	6.93	20.70	10.00	9.00

Table 3.6: Accuracies obtained and used to assess the impact of the inclusion of thermal band and vegetation indices on urban mapping accuracy (UA=User's accuracy, PA=Producer's accuracy and OA is the Overall Accuracy of the classification)

	Analysis I		**Analysis II**		**Analysis III**		**Analysis IV**		**Analysis V**		**Analysis VI**		**Analysis VII**	
	PA	**UA**	**PA**	**UA**	**PA**	**UA**	**PA**	**UA**	**PA**	**UA**	**PA**	**UA**	**PA**	**UA**
DB	84.8	87.1	0.0	0.0	88.8	88.7	80.0	77.6	83.0	79.4	88.1	87.2	90.9	88.8
FR	90.1	86.3	28.0	35.6	86.4	88.2	87.6	89.2	90.0	89.7	96.9	89.1	96.9	89.0
WT	89.2	90.6	87.5	86.5	82.1	98.6	89.4	91.2	96.6	90.2	92.7	98.8	97.0	98.9
HDR	79.2	65.7	61.7	45.5	80.4	62.8	78.7	70.1	78.7	71.7	79.4	75.7	79.8	75.0
Dv	75.9	84.4	71.3	54.9	72.6	82.7	76.2	86.7	72.3	86.4	79.3	86.4	79.1	86.4
LMR	84.5	84.6	66.6	58.7	81.4	85.4	84.0	81.2	83.3	82.8	87.2	86.0	86.4	85.9
GR	81.1	77.4	44.6	33.3	81.8	76.7	81.1	72.6	82.6	80.8	83.9	76.9	83.3	76.8
OA	**82.65**		**53.40**		**84.03**		**81.96**		**82.97**		**85.49**		**89.33**	
Kappa	**0.81**		**0.46**		**0.81**		**0.79**		**0.82**		**0.84**		**0.86**	

3.3.6. Analysis VI: Classification results using OLI spectral bands and VIs

The use of OLI spectral bands and the derived vegetation indices yielded high and comparative similar results with those obtained in Analysis I (i.e. use of reflective bands as standalone dataset) and Analysis V (i.e. use of Landsat 8 thermal bands and the derived vegetation indices). For example, high overall user (85.49%) and producer accuracies greater than 78% were obtained for all the classes considered under this study. Moreover, an overall accuracy and kappa index of 0.84 was attained (Table 3.6 and Figure 3.2). Producer and user accuracies were greater than 75% for all the LULC classes. A comparison of the results obtained from this analysis (i.e. OLI spectral bands and the derived vegetation indices) and those obtained from Analysis I (i.e. use of the traditional reflective bands as standalone datasets) show significant differences with the McNemar's Z score of 10 at 95% confidence interval.

3.3.7. Analysis VII: Classification results using OLI, TIRS spectral bands and VIs

Table 3.6 shows the urban landscape classification results obtained from running the model based on the integration of Landsat 8 derived OLI reflective bands, TIRS spectral bands and computed vegetation indices. The classification results demonstrate great improvement on the overall, user and producer accuracies for all the classes considered under this study. For example, significantly high user and producer accuracies, greater than 85% for low-medium density residential, water, forested and densely built classes were obtained. The results showed high overall accuracy of 89.33% and a kappa index of 0.86 (Table 3.6). Furthermore, when compared to Analyses 1, II, III, IV, V and VI, the urban landscape classification results obtained from the integration of Landsat 8 derived OLI reflective bands, TIRS spectral bands and computed vegetation indices (i.e. Analysis VII) yielded higher accuracies with McNemar's Z score of 9 at 95% confidence interval. Overall, these results demonstrate that the integration of TIRS spectral bands from the Landsat 8 sensor with the sensor's derived reflective bands and computed vegetation indices, improves the classification accuracy of urban landscapes compared to the use of these datasets as standalone datasets.

3.4 Discussion

Accurate and reliable information on urban land use-land cover is important for well-informed urban land use planning and for appropriate policy development at a range of scales. Besides, this information is urgently required for developing and updating the national LULC database, as well as assessing the current urban growth and for modeling future growth projection. This work thus aimed at assessing the potential of integrating Landsat 8 derived thermal bands with

the sensor's traditional reflective bands and computed vegetation indices in discriminating complex and heterogeneous urban landscapes.

The results of this study have shown that the recently-launched Landsat 8 with unique radiometric, as well as new thermal bands, present a strong capability of improving the classification of heterogeneous and complex urban landscapes; especially in areas where the availability of high resolution satellite datasets with strategically positioned spectral bands and band settings remains one of the major limiting factors. When Landsat 8 derived TIRS spectral bands were integrated with the traditional OLI reflective bands, as well as the computed vegetation indices, the classification of urban landscapes significantly improved when compared to the use of these variables as standalone datasets. For instance, based on the integrated datasets, significantly higher overall accuracy (89.33%), along with user and producer accuracies of about 85% were attained for the low-medium density residential, water, forested and densely built land cover classes. The McNemar's Z score was 9 at 95% confidence interval, implying that there was significant increase in classification accuracy when compared with the traditional use of reflective bands alone. Overall, the use of the integrated datasets outperformed the use of thermal bands and vegetation indices as standalone classification variables. The study showed that the results were almost comparable to those attained using traditional reflective and thermal bands. Higher classification accuracies (i.e. overall, kappa, user and producer) in mapping complex urban environments indicate the high performance associated with the improved Landsat 8 push broom scanner (Jia, et al., 2014).

Also, the performance observed from the results obtained based on the integration of the entire set of variables (i.e. derived thermal, traditional reflective bands, as well as the computed vegetation) concur with findings from the literature (Li et al., 2013; Sun & Schulz, 2015; Ormsby, 2007). The above studies concluded that thermal remote sensing has the capability of providing crucial information that can enhance robust and reliable monitoring of land cover dynamics. For example, Ormsby (2007) pointed out that the inclusion of thermal bands together with other spectral bands in remote sensing applications influences classification accuracies. Also, the increased performance based on the integrated datasets can be linked to the ability of thermal bands, despite the coarser resolution to separate or separate areas associated with low temperature areas (water, forests and low-medium residential) from high temperature areas (high density residential, grasslands, development areas and densely built

areas). The results of this study therefore clearly indicate the general importance of thermal bands from the new Landsat 8 sensor, through the provision of complementary information (Panah, et al., 2001), which greatly improves or aids the performance of the traditional reflective bands and the associated derived vegetation indices.

Furthermore, this work showed that merging the traditional reflective bands, with the four selected vegetation indices (NDVI, NDWI, NDBaI and NDBI) derived from the Landsat 8 OLI sensor for urban land cover mapping slightly increased the overall classification accuracy by 1.84% (i.e. from 82.65% to 85.49%) when compared to the use of the traditional reflective bands as a standalone dataset. For example, the test results showed that the inclusion of the four selected vegetation indices significantly (i.e. McNemar's Z score had a value of 9.98 at 95% confidence interval) increased the classification accuracy. These results demonstrate the importance of Landsat 8 computed vegetation indices. These findings are in line with findings from previous studies which have demonstrated and reported the unique strength and usefulness of the four indices in separating various land cover types (Chen, et al., 2006; Jia, et al., 2014). Moreover, literature shows that indices, such as the NDWI (Stathakis, et al., 2012; Jackson, et al., 2004; De Fries et al., 1998) and NDBI, have the capability to efficiently extract built up areas. The major limitation with these vegetation indices is that they do not consider that bare areas also exhibit similar properties with built up areas (Stathakis, et al., 2012). Thus, in this study, the inclusion of the NDBaI was useful in further separating bare areas from built up areas as it provides good contrast between bare and other surfaces (Sharma, et al., 2012).

Contrastingly, the use of four selected vegetation indices as a standalone dataset proved comparatively weak in discriminating the LULC of the complex and heterogeneous urban environments. However, comparatively the use of Landsat 8 derived vegetation indices alone produced slightly lower classification results (i.e. overall, user and producer accuracies), when compared to the use of traditional reflective bands (see Analysis I). For example, for the majority of the land cover classes considered in this study, user and producer accuracies slightly above 70% on average were observed. Similarly, the use of Landsat 8 derived thermal bands as a standalone dataset for classifying complex and heterogeneous LULC in urban environments overall yielded poor results except for water bodies where the model produced high user and producer accuracies above 90%. Effectiveness of thermal bands is thus dependent on land cover type, and climatic and geographic conditions (Panah, et al., 2001). Lo

et al. (2010) observed that although most land covers had similar thermal radiances at night, water was still separable from the rest as it had lowest thermal radiance values. This study, similarly, observed that based on temperature water was easily distinguishable from other classes as it had lowest temperatures.

Above all, the high overall classification accuracies obtained in this study from the integration of the Landsat 8 TIRs bands, the traditional reflective spectral bands, as well as the derived vegetation indices, although not tested, can hypothetically be largely associated with the sensor's unique design. For example, the recently-launched Landsat 8 sensor, unlike its predecessors, provides great improvement in numerous aspects. To begin with, Landsat 8 OLI and TIRs applies the push broom technique during data acquisition (Dube & Mutanga, 2015a, 2015b; Roy et al., 2014; Ke et al., 2015; Dube & Mutanga, 2015c). Sensors applying the push broom design in data acquisition are known to receive good and robust signals from the earth's surface since they use elongated and linear arrays of detectors (Roy, et al., 2014). For example, the study by Dube and Mutanga (2015a) reports that the Landsat 8 makes use of a multiple extended collection of detectors for each spectral waveband, which in turn provides a comprehensive scan of the earth's surface. Besides, the newly-launched 30m Landsat 8 sensor is associated with a narrower spectral range which is believed to be useful for this dataset to precisely detect and discriminate various land covers or earth surface features (Dube & Mutanga, 2015a, 2015c). The observed highly accurate land cover classification results (i.e. overall, kappa, user and producer accuracies) for complex and heterogeneous urban landscapes obtained in this study, projects the recently launched 30m Landsat 8 sensor as the best satellite data that can provide remarkable solutions and breakthroughs for land cover mapping, especially in environments where the availability of high resolution satellite data remains a daunting task due to cost and above all the restricted spatial coverage.

The observed higher accuracy classification results (i.e. overall, kappa, user and producer accuracies), although not tested in this study, can also be attributed to the strength and effectiveness of the SVM algorithm. Amongst most available classification algorithms, literature shows that the support vector machine classification algorithm is currently one of the most powerful and robust non-parametric machine learning algorithms in image classification studies when compared to the most commonly applied image classification techniques, such as Artificial Neural Networks and Mahalanobis classifiers, Maximum Likelihood, Random

Forest, among others (Adelabu, et al., 2013; Jia, et al., 2014; Forkuor & Cofie, 2011; Yu, et al., 2013).

3.5 Conclusion

We tested the potential of integrating the recently-launched 30-m Landsat 8 derived thermal bands, with the sensor's traditional reflective and computed vegetation indices in classifying complex and heterogeneous urban landscapes. The study was motivated by the need to identify an optimal, suitable and cheap remote sensing dataset that could improve the detection and classification of complex and heterogeneous urban landscapes in data-scarce environments with reasonable accuracy. Currently, as well as possibly in the near future, the application of high resolution imagery in these areas remains a challenge due to associated costs and the restricted availability, except for project based applications.

The findings of this study have shown that the integration of Landsat 8 derived TIRS spectral bands, OLI reflective bands and computed vegetation indices produced high classification results. Comparatively, the use of TIRS spectral bands, OLI reflective bands and computed vegetation indices as standalone variables produced slightly weaker overall classification results. Thermal remote sensing has the capability of providing crucial information that can enhance robust and reliable classification of land cover dynamics especially in data-scarce environments when applied together with the traditional reflective bands, as well as robust and effective non-parametric algorithms (i.e. SVM, and others). Overall, the findings of this research highlight the potential and needs of remote sensing communities in data-scarce environments to immediately embrace the use of thermal remote sensing datasets. Nonetheless, it is advisable to stress that further assessment and/or comparative experiments are conducted at landscape scales amongst the recently-launched 30-m Landsat 8's thermal and traditional spectral bands.

3.6 Link between Chapter 3 with other chapters

Chapter 3 showed that high urban LULC classification accuracy (overall accuracy above 80%) from Landsat data is achieved by i) the traditional method of using atmospherically corrected multi-spectral optical data excluding thermal data ii) combining these multi-spectral data with NDVI, NDBI, NDBaI and NDWI iii) combining multi-spectral optical data with thermal infra-red data and iv) merging multi-spectral optical data with indices and thermal infra-red data (highest accuracy of the methods tested). The next chapters will use LULC mapping

approaches proved highly reliable by Chapter 1 to map urban extent as well as urban growth and link to the thermal environment of the lower atmosphere. As such, the next chapter (Chapter 4) will relate heat vulnerability to LULC spatial structure derived from classification of Landsat multi-spectral data in Harare.

CHAPTER 4: SPATIAL DISTRIBUTION OF EXTREME HEAT VULNERABILITY AND ITS LINK WITH LANDUSE AND COVER REGIMES

This chapter is based on:

Mushore T. D., Mutanga O., Odindi J., Dube T. (**in press**). Determining extreme heat vulnerability of Harare Metropolitan City using multispectral remote sensing and socio-economic data. *Journal of Spatial Science*, 63(1), 173-191. http://dx.doi.org/10.1080/14498596.2017.1290558

4.0 Abstract

Urbanisation alters surface landscape characteristics through conversion of natural landscapes to impervious surfaces. Such changes alter the thermal properties of urban landscape mosaics, increasing the urban heat island intensity and population's vulnerability to heat related stress. This study aimed at deriving detailed area specific spatial information on the distribution of heat vulnerability in Harare city, Zimbabwe, valuable for informed urban thermal mitigation, planning and decision making. Using Landsat 8 derived bio-physical surface properties and socio-demographic factors, findings show that vulnerability to heat related distress was high in over 40% of the city, mainly in densely built-up areas with low-income groups. Comparatively, low to moderate heat vulnerability was observed in the high income northern suburbs with low physical exposure and population density. Results also showed a strong spatial correlation ($\alpha = 0.61$) between heat vulnerability and observed surface temperatures in the hot season, signifying that land surface temperature is a good indicator of heat vulnerability in the area. Furthermore, the study showed that indices derived from moderate resolution Landsat 8 data improve thermal risk assessment in areas of close proximity. These findings demonstrate the value of readily available multispectral data-sets in determining areas vulnerable to temperature extremes within a heterogeneous urban landscape. The findings are particularly valuable for designing heat mitigation strategies as well as identifying highly vulnerable areas during heat waves.

Keywords: Land surface temperature, vegetation indices, heat island, vulnerability, heat stress.

4.1 Introduction

Urbanization changes the distribution of surface land covers and alters landscape energy and water balance, which in turn alters surface thermal characteristics (Zhang, et al., 2009; Chen, et al., 2006; Sobrino, et al., 2012; Amiri, et al., 2009). Due to urban growth, natural surfaces such as forests are replaced with impervious surfaces that absorb and emit thermal energy, resulting in creation of Urban Heat Islands (UHI) (Johnson, et al., 2014; Steeneveld, et al., 2014; Tomlinson, et al., 2011; Hua, et al., 2013; Song & Wu, 2015; Sobrino, et al., 2012). Such thermal elevation exposes residents to heat related health risks, especially residents without air conditioning systems. Studies have shown that extreme temperatures result in reduced indoor and outdoor comfort and performance at work and increase morbidity and mortality (Tanabe et al., 2015; Humphreys, 2015; Lin, et al., 2016). Within cities in developing countries, vulnerability to elevated temperatures varies due to heterogeneity in surface bio-physical properties and socio-demographic factors (Johnson, et al., 2014). According to Wilhelmi and Hayden (2010), contextualizing vulnerability to local settings can influence formulation of successful approaches that are targeted locally using resources allocated at national level. Therefore, to design effective adaptation and mitigation measures for vulnerable areas, heat vulnerability maps are valuable in identifying high risk areas.

Urban geophysical (e.g. heat islands, vegetation health and abundance and building density) economic and socio-demographic factors constitute exposure to hazard, sensitivity and adaptive capacity, which determine differences in heat vulnerability between places (Johnson, et al., 2014; Aubrecht & Özceylan, 2013; Uejio, et al., 2011). Whereas earlier thermal vulnerability studies solely stressed the role of socio-demographic factors e.g. age, race, gender, education, health and economic status (Cutter, 2009; Cutter, et al., 2003; Vescovi, et al., 2005; Reid, et al., 2009), recent studies have sought to incorporate quantitative and qualitative socio-demographic and biophysical variables in risks associated with elevated urban temperatures (van-Westen; Johnson, et al., 2014; Buscail, et al., 2012). Recent studies have also sought to incorporate remote sensing derived heat exposure factors such as land surface temperature, land use and land cover maps, and land cover indices (Johnson, et al., 2014; Johnson, et al., 2012; Johnson, et al., 2009; Aubrecht & Özceylan, 2013; Uejio, et al., 2011; Wolf & McGregor, 2013; Depietri, et al., 2013; Hansen, et al., 2013; Buscail, et al., 2012; Reid, et al., 2012). Hence, space-borne remote sensing has the potential to yield a variety of spatial information valuable for reliable heat vulnerability mapping.

Remote sensing has several advantages in urban thermal studies. These include synoptic view of large areas, availability of archival data, and effectiveness in mapping land surface characteristics. In addition, medium resolution space-borne remote sensing detects localized variations in land surface characteristics even in complex urban areas where changes are observed within small distances. However, despite the reliability of space-based sensors like Landsat in mapping heterogeneous urban landscapes, heat vulnerability maps have remained largely coarse and generalized. For instance, previous studies have mapped vulnerability at the low spatial resolution of demographic variables, such as census block and district level (Johnson, et al., 2014; Heaton, et al., 2014; Buscail, et al., 2012). This has a major disadvantage of assuming uniform heat exposure over large regions thus ignoring variability within each block/district. For example, Dewan and Corner (2012) noted that use of census blocks weakened the correlation between population density and land surface temperature because of variability of land cover within each census tract. However, mapping risk using medium resolution remotely sensed data has the potential to improve area specific assessment interventions required to curb heat related stress in cities. Therefore, there is a need to improve the spatial resolution of heat vulnerability maps using spatial details of variations in heat exposure obtained from reputable medium resolution sensors such as Landsat missions.

Land cover indices such as Normalized Difference Vegetation Index (NDVI) provide quantitative and reliable information of surface physical characteristics. Compared to land use and land cover classification and retrieval of land surface temperature from thermal infra-red data, indices simplify heat vulnerability mapping as they are easy to compute (Sharma, et al., 2012; Chen, et al., 2006). According to Byomkesh et al. (2012), indices help to surmount the mixed pixel problem affecting accuracy of land cover identification using moderate resolution data in heterogeneous urban environments. Indices also match the criteria by Dewan and Yamaguchi (2009) that each vulnerability indicator should simplify a number of properties and be quantifiable using existing data. For instance, Chen et al (2006) used the Normalized Difference Vegetation Index (NDVI), Normalized Difference Bareness Index (NDBaI), Normalized Difference Water Index (NDWI) and Normalized Difference Built-up Index (NDBI) to map land use and land cover types with high accuracy. Besides land cover mapping, these indices are deemed capable of determining a variety of heat exposure factors as they are strongly correlated with land surface temperature (Chen, et al., 2006; Song & Wu, 2015; Kerchove et al., 2013; Essa et al., 2013; Xu, et al., 2013). As such, Johnson et al. (2014)

included surface temperature, NDVI, NDBI and socio-demographic variables among others, to determine urban heat vulnerability. However, the use of remote sensing derived land cover indices as exposure factors in heat vulnerability assessments is still limited to a few studies and indices hence the need to explore the utility of other indices (Johnson, et al., 2014; Johnson, et al., 2012; Johnson, et al., 2009; Buscail, et al., 2012; Chow, et al., 2012; Harlan, et al., 2006; Uejio, et al., 2011).

Although previous studies for instance combined NDBI, NDVI and Soil Adjusted Vegetation Index (SAVI) with socio-demographic urban thermal vulnerability mapping, the value of other indices in vulnerability assessment, such as the NDWI, remain unexplored. In addition, while inclusion of a variety of indices in a single assessment should enhance land surface characterization, the studies have been commonly confined to at most two indices per heat vulnerability analysis (Johnson, et al., 2012; Johnson, et al., 2014). Commonly, only NDVI is combined with socio-demographic factors in urban thermal vulnerability analysis (Uejio, et al., 2011; Buscail, et al., 2012; Chow, et al., 2012). However, whereas NDVI has been useful in mapping vegetation abundance and health, it saturates at high values of vegetation fraction. Therefore, this study proposes inclusion of NDWI which gives a measure of surface water content and is critical in heat vulnerability mapping. This index is best in quantifying water depth in plants which strongly relates to turgidity of cells and thus combines effectively with NDVI to quantify vegetation health (Jackson, et al., 2004). For example, combining NDVI and NDWI provides a more robust measure of vegetation abundance and health, which are key factors in heat exposure mapping, compared to use of NDVI alone (Chen, et al., 2006; Jackson, et al., 2004; Stathakis, et al., 2012). Furthermore, the index provides a measure of surface moisture (Cao et al., 2008; Xu, et al., 2013) required for evaporative cooling, hence is valuable for mitigation against extreme surface temperatures. We therefore hypothesize that combining NDWI with NDBI and NDVI should improve delineation of spatial variations in heat exposure in heterogeneous and complex urban environments.

In previous heat vulnerability studies researchers have mainly adopted heat exposure factors derived from earlier Landsat missions; Landsat 5 and Landsat 7 (Johnson, et al., 2014; Aubrecht & Özceylan, 2013; Harlan et al., 2013). For example, Johnson et al. (2013) derived NDBI and NDVI from optical information of Landsat 7 Earth Thematic Mapper Plus (ETM+). Unlike earlier Landsat satellite missions, Landsat 8 satellite data has several strengths, which

include improved radiometric and spectral resolution, signal to noise ratio, refined bandwidth and two thermal infra-red bands (Karlson et al., 2015; Almutairi, 2015; Dube & Mutanga, 2015a). Furthermore, land cover classes generated from Landsat 8 have been shown to be more accurate than the previous Landsat series and MODIS data (Mwaniki et al., 2015; Yu, et al., 2013; Jia, et al., 2014; Ke, et al., 2015). Due to these improvements, studies have shown that Landsat 8 data enhances the retrieval of surface features such as biomass estimation, land cover mapping, discrimination of crops, and active fire and volcano detection (Dube & Mutanga, 2015a; Jia, et al., 2014; Banskota et al., 2014; Oumar, 2015; Han & Nelson, 2015; Kharat & Musande, 2015; Blackett, 2014). Therefore, in this study, we hypothesize that the indices retrieved from Landsat 8 contain valuable information for characterization of landscapes useful for reliable urban heat vulnerability mapping.

The objective of this study was therefore to (i) include NDWI among the physical factors used for determining heat exposure, (ii) to produce a heat vulnerability map with spatial resolution greater than the resolution of socio-demographic vulnerability factors and (iii) use remote sensing physical variables obtained from the improved Landsat 8 optical and thermal data to map heat vulnerability of the highly heterogeneous Harare Metropolitan City during the hot season.

4.2 Methodology

4.2.1 Pre-processing of remote sensing datasets

A cloud free 170/72 path/row 30 m Landsat 8 image covering the entire study area acquired on 30 October 2014 was downloaded from the USGS-EROS Centre archive (www.earthexplorer.usgs.gov). The image was geo-rectified using a 1:5000 topographic map and 20 ground control points collected using a GPS at the intersection of major roads in the city. The Landsat image was corrected for atmospheric effects using the FLAASH module in ENVI.

4.2.2 Processing of vulnerability factors

Socio-demographic and bio-physical vulnerability factors were considered. The socio-economic factors were obtained from the 2012 population census data at ward resolution (ZIMSTAT, 2012) as well as close consultation with the Zimbabwe National Statistics Agency (ZIMSTAT). The socio-demographic factors included population density, extreme age population (below 5 and above 65 years of age), unemployed economically active population

and average household income. Each socio-demographic vulnerability factor was scaled between 0 and 1 with values increasing as vulnerability increased (Buscail, et al., 2012). The scaled socio-demographic factors were combined into a single social vulnerability layer using weighted sum by assigning equal importance to all the variables (Tomlinson, et al., 2011; Buscail, et al., 2012). The resultant composite social vulnerability layer was converted from a vector to raster layer (Ho et al., 2015), resampled to the same properties as the 30 m bio-physical properties described below and scaled between 0 and 1 for further analysis (Tomlison et al., 2011).

Surface bio-physical exposure factors included density of buildings/imperviousness, bareness extent, vegetation abundance, and health as well as surface water content. The bio-physical factors were derived from remotely sensed 30 m NDVI, NDBI and NDWI. NDVI was used as a proxy for vegetation abundance and health, NDBI as a proxy for built-up/imperviousness/bareness extent and NDWI as a proxy for surface water content. The use of these indices was motivated by their high quantitative performance in discriminating surface properties, as well as ease of computation (Chen, et al., 2006; Gottshe & Olesen, 2001; Amiri, et al., 2009; Ma et al., 2010; Pu et al., 2006). These properties were selected due to their high correlation with land surface temperature which is well documented (Zhang, et al., 2009; Chen, et al., 2006; Pu, et al., 2006; Ma, et al., 2010; Song & Wu, 2015; Kerchove, et al., 2013; Essa, et al., 2013; Xu, et al., 2013). Studies have shown strong negative correlation between NDVI and NDWI with temperature (Steeneveld, et al., 2014; Chun & Guldmann, 2014). On the other hand, temperatures have been shown to increase with increasing density of buildings and imperviousness/bareness, thus high where NDBI is high (Srivanit et al., 2012; Yuan & Bauer, 2007; Essa, et al., 2013; Song & Wu, 2015; Chun & Guldmann, 2014). For example, Chen et al. (2006) observed that temperatures are high in areas of high building density. Combining NDVI and elevation has been reported to predict temperature better than each of the indices separately (Chen, et al., 2006; Maeda, 2015; Sobrino, et al., 2012). Therefore, combining these surface properties has the potential for adequately mapping risk of extreme surface temperatures. The land surface properties and digital to radiance conversion were obtained using the equations in Table 4.1 (Abegunde & Adedeji, 2015; Chen, et al., 2006; Xu, et al., 2013).

Reducing vegetation fraction increases exposure of an area to high temperature except over water, while surface dryness and low altitude increases exposure of an area to high temperature. An increase in the proportion of bare and built-up areas increases exposure of an area to high temperature (Chen et al., 2012). Temperature also decreases with surface wetness during the day (Steeneveld, et al., 2014; Chen, et al., 2006; Weng & Lu, 2008), therefore a low value of NDWI would increase vulnerability to high temperatures. Several studies have reported a decrease in temperature with increasing NDVI for values between -0.1 and 1, while temperature decreases as NDVI becomes more negative as it approaches -1 from -0.1 (Srivanit, et al., 2012; Cao, et al., 2008; Song & Wu, 2015). Water bodies have very low (negative) NDVI values and low daytime temperatures hence vulnerability was set to zero in these areas. Therefore, in this study, vulnerability to high temperatures was set to decrease as NDVI increased from -0.1 to 1, as well as when it decreased to become more negative, from -0.1 to -1. Each bio-physical vulnerability factor was scaled between 0 and 1 with values increasing as vulnerability increased.

Table 4.1: Selected vegetation indices

Function	Equation	References
Normalized difference built-up index	$NDBI = \frac{dBand6 - dBand5}{dBand6 + dBand5}$	(Zha et al., 2003)
Normalized difference bareness index	$NDBaI = \frac{dBand6 - dBand10}{dBand6 + dBand10}$	(Zhao & Chen, 2005)
Digital number (DN) to radiance conversion	$\rho Bandn = M_L dBandn + A_L$	(USGS, 2016)
Normalized difference vegetation index	$NDVI = \frac{\rho Band5 - \rho Band4}{\rho Band5 + \rho Band4}$	(Tucker, 1979)
Normalized difference water/wetness index	$NDWI = \frac{\rho Band5 - \rho Band6}{\rho Band5 + \rho Band6}$	(McFeeters, 1996)

dBandn represents 16 bit digital numbers of the n^{th} band of Landsat 8, *ρBandn* are the radiance values, ρBandn*(max)* is the maximum radiance, *ρBandn(min)* is the minimum radiance and *dBandn(max)* is the maximum digital number (65535) for the n^{th} band of Landsat 8. For each band M_L and A_L for the conversion of DN to radiance are obtained from the metadata.

4.2.3 Vulnerability mapping

In vulnerability analysis, the variables are combined using overlay functions which include weighted sum and weighted average (Tomlinson, et al., 2011; Buscail, et al., 2012; Johnson, et al., 2014). However, the use of different weights based on relative importance of factors results in subjectivity of the vulnerability map produced, thus making the maps open to manipulation (Tomlinson et al., 2011). Therefore, the three scaled bio-physical vulnerability factors and the scaled composite social vulnerability layer were combined using weighted sum with all the factors assigned equal importance to produce the heat vulnerability. Tomlinson et al. (2011) and Buscail et al. (2012) also assigned equal importance to heat vulnerability to all considered factors. The weighted sum overlay function in ArcMap10.2 version was used to assign each of the four vulnerability factors a weight of 25%. The resultant heat vulnerability index layer was scaled between 0 and 1 and categorized using quantiles for presentation purpose. Similar to the categorization of heat vulnerability by Buscail et al. (2012), the lower 20% quantile was categorized as "Very low" vulnerability, the three intermediate quantiles as "Low", "Moderate" and "High" while the upper 20% quantile was categorized as "Very high" vulnerability.

4.2.4 Derivation of LST from thermal radiances

The Landsat 8 data contains two thermal bands, which enabled computation of temperature using the split window algorithm (Yang, Lin, et al., 2014; Qin, et al., 2001; McMillin, 1975; Rozenstein, et al., 2014). The digital numbers of thermal data, Band 10 and Band 11 of Landsat 8, were converted to thermal radiance as described in Table 4.1. Brightness temperature (T_{10} and T_{11}) were computed using Equation 4.1 with radiances derived from Bands 10 and 11 as input thermal layer.

$$\boldsymbol{T_N = \frac{K_2}{In\left(\frac{K_1}{L_N}+1\right)}} \qquad \text{Equation 4.1}$$

Where T_N is the brightness temperature computed using thermal band N (10 or 11). Thermal conversion coefficients, K_2 and K_1, are constants obtained in the metadata file which accompanies the Landsat 8 images. Brightness temperature layers obtained were used in the split window algorithm land surface temperature derivation parameters in a procedure described in Qin et al. (2001) and Rozenstein et al. (2014). The general split-window algorithm for generating surface temperature (T_s) using two thermal bands takes the form:

$$\boldsymbol{T_S = A_O + A_{10}T_{10} + A_2T_{11}} \qquad \text{Equation 4.2}$$

Parameters A_0, A_1 and A_2 are obtained using algorithms that combine atmospheric transmissivity with other parameters also provided and described by Rozenstein et al. (2014).

Atmospheric transmissivity was derived from water vapour using an algorithm obtained from Qin et al (2001) and water vapour data at the time of image acquisition obtained from Aerosol Robotic Network (AERONET). The AERONET sun photometer data were previously recommended as a good source of water vapour data especially for daytime observations on cloud-free days (Yang, Lin, et al., 2014; Rozenstein, et al., 2014). Besides atmospheric transmittance, the algorithm for retrieving land surface temperature from two thermal bands of Landsat 8 developed by Rozenstein et al. (2014) also require land surface emissivity for each thermal band. Therefore, we retrieved pixel based spectral land surface emissivity for each thermal band using spectral radiance and blackbody radiance as developed by Yang et al. (2004). Blackbody radiance was retrieved using Equation 4.3

$$\boldsymbol{\rho Bandn(BB) = \rho Bandn(min) + \frac{[\rho Bandn(max) - \rho Bandn(\min)][dBandn(mean) - dBandn(\min)]}{65535}}$$

Equation 4.3

Yang, et al. (2004) obtained better blackbody emissivity values using dBandn(mean) than using 65535 hence the choice for use in this study. Land surface emissivity for each thermal band was computed using Equation 4.4

$$\boldsymbol{LSE = \frac{dBandn}{dBandn(BB)}}$$

Equation 4.4

Where dBandn(mean) is the average of the maximum digital number for scene and 65535 while the other variables are defined in Table 1. Land surface emissivity maps were used in Equation together with other parameters described above to retrieve land surface temperature. Land surface temperature was calculated using the brightness temperature layers using Equation 2. Furthermore, we performed a spatial correlation between the mapped heat vulnerability and observed distribution of land surface temperatures.

4.3 Results

4.3.1 Variability of selected image based indices during the hot season in Harare

Figure 4.2 shows how vegetation abundance (NDVI), built up density (NDBI) and surface wetness (NDWI) and socio-economic factors varied spatially in their contribution to heat vulnerability during the hot season in the study area. The central and western parts of Harare were marked by the convergence of high social vulnerability and high bio-physical vulnerability. In this region, the density of buildings was high (Figure 4.1a) while surface wetness (Figure 4.1b) and vegetation fraction were low (Figure 4.1c), as indicated by values close to 1 for all the vulnerability factors. However, all the vulnerability factors largely indicated values close to zero in the northern half of the country. Overall, the combination of

high vegetation abundance (NDVI > 0.6), low density of buildings (NDBI close to 0), high surface wetness (NDWI > 0.6) and low socio-demographic vulnerability observed in the northern half reduced heat vulnerability to the north.

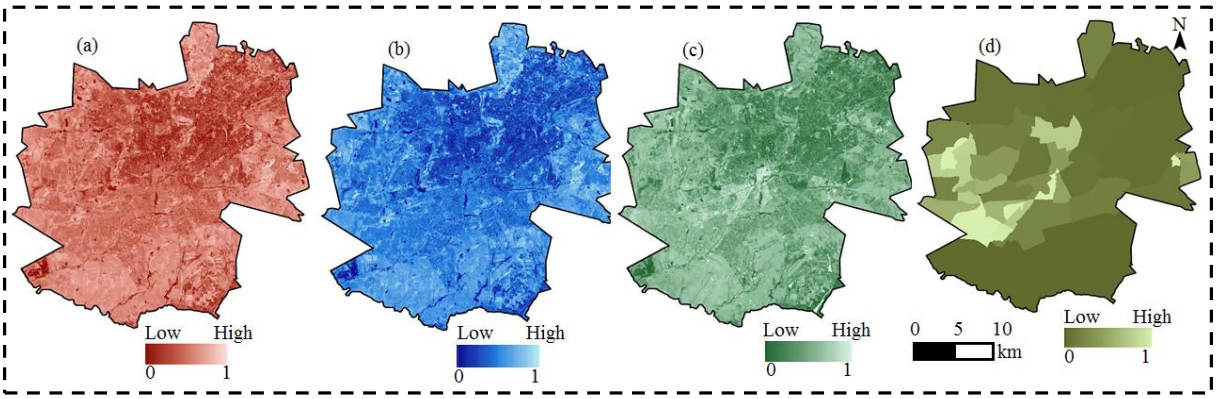

Figure 4.1: Distribution of heat vulnerability as a function of (a) built-up/bareness extent, (b) surface water content, (c) vegetation abundance and health and (d) socio-economic pressure in Harare. (a) to (d) are vulnerability factors scaled between 0 and 1

4.3.2 The vulnerability of the city of Harare to extreme surface temperature

Figure 4.2 shows the heat vulnerability of the city during the hot season as predicted by the factors derived from bio-physical indices obtained from Landsat 8 and socio-demographic variables. Heat vulnerability was found to be very high (index values ranged from 0.49 to 1) in the city core and south western areas. Heat vulnerability was also in the moderate to high (index value range from 0.41 to 0.49) category over most of the southern areas making the southern half of the city more vulnerable than the northern areas. The land use and land cover (LULC) map (Figure 4.2b) was obtained from another study at an overall accuracy of 87.59% and kappa statistic of 0.82 (Mushore et al., 2016). The LULC map shows that the southern half of the city is mostly occupied by high density residential areas and industrial sites. The north-eastern half of the city had heat vulnerability index values below 0.41, which implied very low to low vulnerability categories. The northeastern half of the city is mostly covered by low-medium density residential areas. Furthermore, medium density residential areas were found to have higher heat vulnerability values than low density residential areas. Heat vulnerability was in the low to moderate range (0.34 – 0.45) over medium density residential areas while it was largely in the very low to low range (below 0.41) over low density residential areas. Low heat vulnerability values were also noted in wetlands and their surroundings as well as in urban parks.

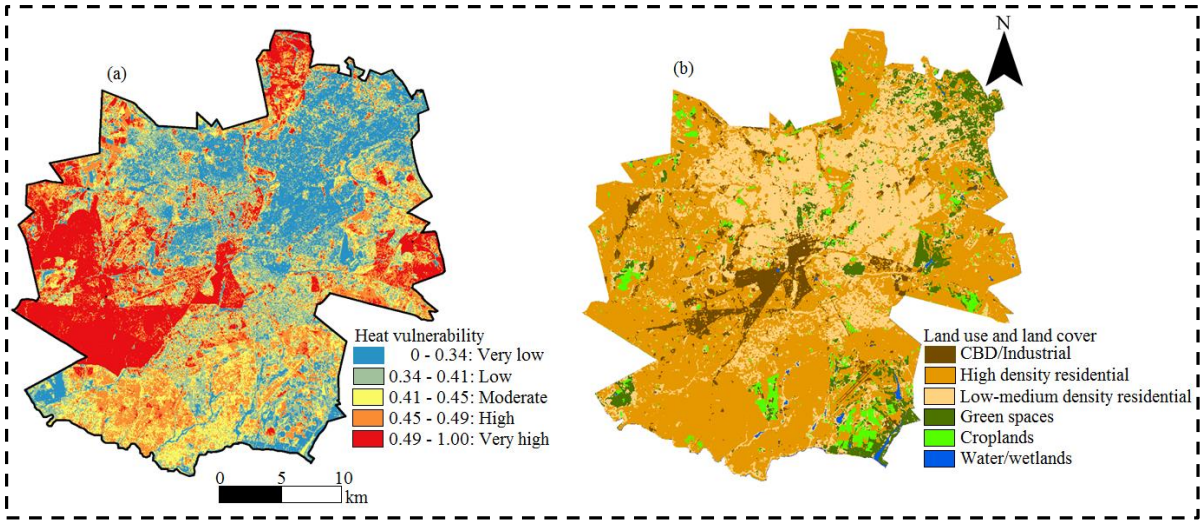

Figure 4.2: Distribution of (a) Heat vulnerability and (b) land use and land cover (LULC) types in Harare.

Table 4.2 shows that due to urbanization and socio-demographic pressures, heat vulnerability was high to very high over more than 40% of the metropolitan city of Harare during the hot season.

Table 4.2: Coverage of mapped vulnerability to high surface temperatures and its link to observed surface temperatures.

Vulnerability	Observed mean temperature (°C)	Area covered (km^2)	Proportion covered (%)
Very Low	28.1	165.7	19.4
Low	32.4	168.4	19.7
Moderate	35.3	162.2	18.9
High	38.6	183.5	21.5
Very high	40.2	174.9	20.5

4.3.3 Spatial correlation between estimated vulnerability and remotely sensed temperature

Figure 4.3 shows that areas where heat vulnerability was high are also at high risk, as high surface temperatures were also recorded in these areas. The spatial correlation between heat vulnerability and temperatures during the hot season was high (α=0.61). High temperatures (greater than 35°C) were observed in the southern and western parts where heat vulnerability was moderate to very high. Temperatures were observed to be low in the north eastern half of the city with values mostly ranging from 17-25°C observed, heat vulnerability was also mapped to be low. Low temperatures and vulnerability were also observed in the extreme south eastern areas where large water bodies are located.

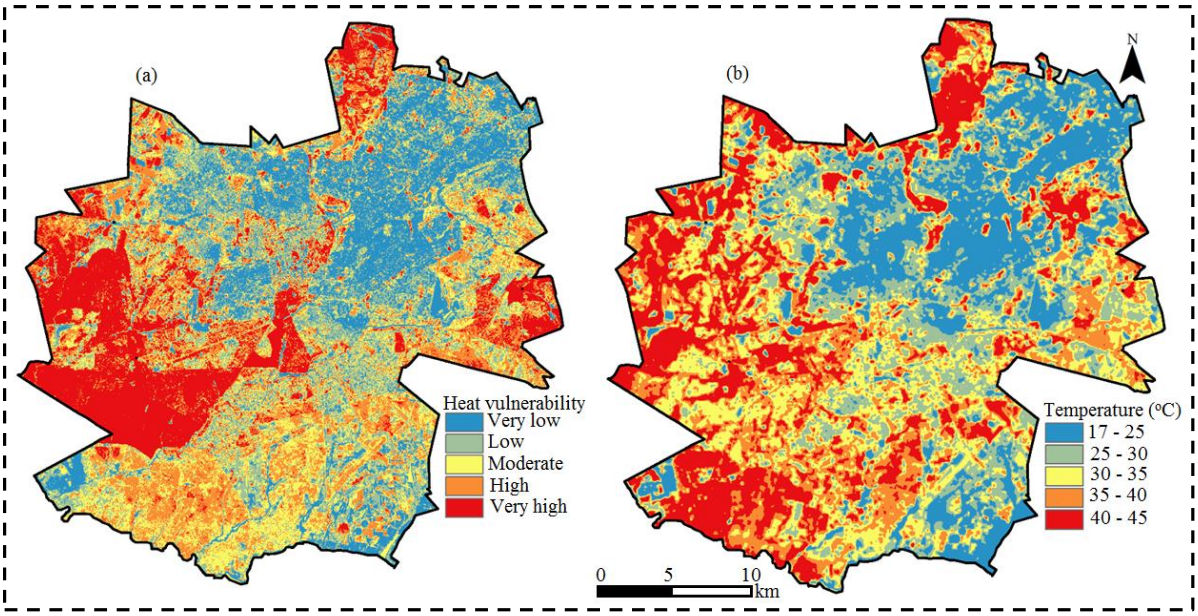

Figure 4.3: Mapped vulnerability of Harare to high surface temperatures (a) and its link to Surface temperature observed on 30 October 2015 (b).

There was a convincing agreement between the distribution of vulnerability and temperature. The average temperature was low (32.2^{o}C) where vulnerability was very low compared to very high average temperature (42.2^{o}C) where vulnerability was very high (Table 4.2).

4.4 Discussion

Urbanization causes surface temperatures to increase due to replacement of surfaces that favor evaporation with those that absorb energy during the day. Such surfaces trap energy and release large amounts of heat during both day and night. Surface physical properties such as density of buildings and vegetation fraction are highly correlated with land surface temperatures such that increases in land surface temperatures also increase environmental temperatures. This affects human comfort, especially those under socio-economic stress, such as low income strata, when it results in excessive temperatures that may cause heat related diseases and increase energy and water demands. The study hypothesized that land surface properties derived quantitatively using vegetation indices; vegetation abundance (NDVI), surface wetness (NDWI), built-up extent and bareness (NDBI) derived from recently launched Landsat 8 data, together with socio-demographic factors, combine to reduce or increase vulnerability of an area to high surface temperatures. In order to inform response and mitigation strategies, there is a need to assess vulnerability of an urban area to high surface temperatures. Therefore, compared to previous studies such as by Johnson, et al. (2012) which produced heat vulnerability maps at census blocks level, this study mapped vulnerability at 30 m resolution that characterize Landsat 8 imagery. This provided detailed heat vulnerability distribution information which,

according to Wilhelmi and Hayden (2010) and Dewan and Corner (2012) ensures effective implementation of localized adaptation and mitigation strategies. Congruently, Johnson, et al. (2009) pointed out that supplementing socio-demographic data with remotely sensed bio-physical data improves delineation of intra-urban variations in risk from extreme heat events although they mapped vulnerability at census block level.

Heat vulnerability to high surface temperatures was found to be high in the southern areas characterized by a combination of low vegetation fraction, dry surfaces and highly built-up areas occupied by low income residents. Observations along a southwest to northeast direction showed that heat vulnerability was high where high NDBI, low NDVI, low NDWI and high social vulnerability co-existed. This aligns with previous studies which showed that surface temperatures increase with increasing density of buildings, and decrease with increasing surface wetness and vegetation cover (Yuan & Bauer, 2007; Maeda, 2015; Spronken-Smith & Oke, 1998). In Greater Dhaka, Bangladesh, Dewan and Yamaguchi (2009) also noted that clearing of vegetation resulted in a wide range of environmental impacts including reduction in habitat quality. This study observed that the biophysical properties combine additively to give a measure of vulnerability to high surface temperatures. As such, Maeda (2015) observed that the correlation between surface temperature with a combination of NDVI and elevation was higher than with each of the factors alone. Southern areas of Harare, where heat vulnerability is very high, are mainly occupied by high density residential areas with a low income demographic, thus compromised capacity to cope with heat related pressures during the hot season (Mushore et al., 2016, Kamusoko et al., 2013). According to Brenkert and Malone (2005), the Indian state of Orissa recorded very high vulnerability level due to significant poverty, low level of industrialization and low human development. This is consistent with previous studies which showed that low household income increases heat vulnerability by reducing capacity to adapt (Harlan, et al., 2013; Aubrecht & Özceylan, 2013; Uejio, et al., 2011; Coates et al., 2014). Harlan et al (2013) observed that deaths from heat exposure in Maricopa County, Arizona were high among people who lack access to cool environments and air conditioning facilities. Coates, et al. (2014) observed that, in Australia, most vulnerable groups live in houses that are poorly adapted to extreme heat.

Differences in levels of heat vulnerability were observed between high density residential areas in the southwest and those in the south. Besides low household income, southwestern suburbs

have larger populations aged below 15 and above 65 years. This is in tandem which earlier studies that recorded a huge impact of heat stress on the elderly and very young ages (Klein Rosenthal et al., 2014; Scherer et al., 2013). For example, Rosenthal et al. (2014) observed that heat related mortality was high in places where the ratio of people aged above 65 years to the total population was high. The buildings are also more densely packed and older in the southwestern suburbs than elsewhere, hence the very high vulnerability. The old buildings may not be designed to enable effective heat removal by natural ventilation in view of changes in climate since their period of construction and low household income levels. The wide disparity in quality of residential areas between the northern and the southern areas can be linked to the colonial past (Potts, 2011). According to Potts (2011), the southern suburbs have small plots that were meant to host an influx of poor people moving to the city as a labour force. In agreement with Dewan and Corner (2012), packed buildings in the high density residential areas absorb large amounts of heat as indicated by large surface temperatures thus requiring indoor air-conditioning. In Australia, the most vulnerable groups were also found to live in low quality housing units (Coates, et al., 2014). In London, thermo-insulation of homes and high population density were also observed to increase vulnerability (Wolf & McGregor, 2013). In agreement of our finding, lack of wealth was also found to reduce the capacity of a society to access markets, technology and other resources that can be used to adapt to climate change (Brenkert & Malone, 2005). In urban Georgia, low income was also found to combine with physical exposure to increase heat vulnerability in low quality residents (Maier et al., 2014).

In this study, low vegetation cover (NDVI<0.5) and low surface wetness (NDWI<0.5) in the southern suburbs can be linked to resource constraints that prohibit high density residential dwellers from watering and maintaining urban greenery as well as from affording spacious settlements with abundant greenery. Surface wetness and greenery favor evapo-transpiration rather than absorption of heat. Such cooling effect is thus retarded in the southern areas. This agrees with Spronken-Smith and Oke (1998) who observed that during the day, there is a negative correlation between NDWI and surface temperature. Water has high heat capacity such that a lot of energy is required to raise its temperature compared to other surfaces during the day. Open water and high surface wetness favor latent heat transfer thereby lowering surface radiant heat, while surface wetness provides moisture for latent heat transfer thereby reducing amount absorbed by surfaces, thus lowering surface temperatures (Weng & Lu, 2008). Fanham et al. (2015) observed that daytime temperatures of a city can be reduced using a mist

fan, which blows moisture on to surfaces, thereby increasing their wetness. Therefore, low level of cooling by latent heat transfer together with limited resources for air conditioning increased heat vulnerability in high density residential areas. Although it was moderate to very high in all high density residential areas, vulnerability was not uniform. Similar to our findings, previous studies also observed that buildings were older while population density, socio-economic pressure and density of buildings were higher in high density areas to the southwest than to the south in Harare (Mlambo, 2008; Zinyama et al., 1993; Wania, et al., 2014). This combination of old buildings and inadequate resources to cope with extreme heat was also labeled as increasing vulnerability in another study (Tomlinson, et al., 2011).

There was a strong spatial correlation between the spatial distribution of vulnerability to extreme temperature and observed surface temperatures (α=0.61). High surface temperatures (40 – 45^{o}C) were observed where vulnerability was in the high to very high categories in southern residential areas. The agreement between observed surface temperature and extent of vulnerability indicate the success of vegetation indices derived from Landsat 8 to accurately measure surface bio-physical properties which in turn strongly correlate with temperature. Generally, land surface temperature was high where vulnerability was high and vice versa. It has been observed that combining two or more surface properties improves the prediction of surface temperatures by increasing correlation (Maeda, 2015). Maeda (2015) observed that during daytime, the correlation between temperature and elevation alone was 0.68 (R^2) but increased to 0.94 when NDVI was included. Therefore, in this study, combining NDVI, NDWI, and NDBI improved vulnerability mapping as evidenced by strong agreement between the mapped vulnerability and observed surface temperatures. The daytime land surface temperature distribution can thus be used to indicate areas where heat vulnerability is high. Harlan et al (2013) also demonstrated that surface temperature might also be used to indicate heat vulnerability in Maricopa County, Arizona (Xu, et al., 2013). In the western areas of Arizona, high heat vulnerability and high surface temperature were also found to coincide due to physical exposure (Chow, et al., 2012). However, this alone is not sufficient as vulnerability was moderate in some of the southern areas of Harare where temperature was high.

Vulnerability was found to be in the high to very high category in 42% of the total areas of the Metropolitan City of Harare. The large proportion of areas with high vulnerability to extreme surface temperature is due to the extent of built up areas, especially high density dwellings for

low income groups, that has increased over the years (Kamusoko et al., 2013). This agrees with previous studies that have shown that as a result of urbanization, most of the areas in a city experience high surface temperatures especially when compared with surrounding rural areas where the density of buildings is low (Qiao, et al., 2013). Zhang et al. (2008) also asserted that urbanized surfaces modify the energy and water balance and influence dynamics of air movement, making urbanized areas warmer than the surroundings. It was also observed that population growth and residential developments result in increased temperatures of emerging cities (Zhang, Qi, et al., 2013). Increased density and spatial extent of buildings due to city growth results in elevated temperatures, increased thermal risk and energy consumption through air conditioning (Polydoros & Cartalis, 2014). However, in agreement with Souza, et al. (2009) this makes the low income strata highly vulnerable by raising energy requirements and related costs beyond their reach. Furthermore, Batih and Sorapipatana (2016) observed that the ratio of heat intensity to household income is a strong indicator of vulnerability.

In this study, vulnerability to high surface temperatures in the hot season was observed to be decreasing northwards due to increasing vegetation abundance and reduction in socio-demographic pressures. Except for water bodies which have both low vegetation fraction and low vulnerability, very low to moderate vulnerability were observed north of the CBD where vegetation fraction was greater than 40% and NDVI was between 0.5 and 1. This agrees with Chen et al. (2006) that there is an inverse relation between surface temperature and vegetation abundance represented by high NDVI values. Even in areas where there are buildings, vegetation cover lowers temperature due to latent heat transfer by increasing the surface-air vapour gradient (Chun & Guldmann, 2014). High NDBI values in the CBD implied that the density of buildings was high thus reducing extent of cooling by evaporation as there were few spaces available for vegetation cover and water bodies (Chen, et al., 2006; Yuan & Bauer, 2007). Vegetation lowers surface radiant temperatures as most of the energy received from the sun is used to evaporate water from vegetation surfaces instead of heating the ground and the surrounding (Amiri, et al., 2009; Gottshe & Olesen, 2001; Zhang, et al., 2009). A study by Amiri et al. (2009) showed that human surface alterations can create cool green edges by irrigated plantations due to high thermal capacity and increased latent heat transfer. Zhang et al. (2009) also revealed that urban greenery plays a role in mitigating the heat island effect. Therefore, a combination of generally high income which increases capacity to adapt and vegetation abundance which enhances coping with extreme temperatures reduces heat

vulnerability in the northern areas. Abundance of green space was found to reduce heat vulnerability by reducing ambient temperature and providing shelter in Michigan, USA (Gronlund et al., 2015). Vegetation within the urban fabric, such as trees, lowers temperatures and visiting green areas is a good coping strategy during periods of heat stress (Depietri, et al., 2013).

Low to medium density residential areas which occupy the north and eastern parts of the city had moderate vulnerability to extreme surface heating. In these areas, buildings are spaced out, allowing for urban greenery as indicated by vegetation fraction between 40% and 60%, thus higher surface wetness. A study in the same area also revealed that the northern parts of the city are largely occupied by high income strata (Wania, et al., 2014). Therefore, residents of low to medium density residential areas in Harare largely afford to sufficiently maintain urban greenery such as lawns and orchards as indicated by high NDWI and high NDVI compared to the southern suburbs. Increased surface wetness increases heat capacity, increasing latent heat transfer and suppresses temperature of a surface (Cao, et al., 2008; Steeneveld, et al., 2014). Therefore, surface wetness and greenery reduces vulnerability which supports observations that NDWI and NDVI have an inverse relationship with surface temperature (Chen, et al., 2006). Similarly, Chow, et al. (2012); (Batih & Sorapipatana, 2016) observed that eastern areas of Phoenix had low heat vulnerability due to high income of residents and increased surface greenness due to landscape modification. The significant value of urban greenery in mitigating against extreme surface temperatures was also observed in a recent study (Odindi, et al., 2015). Odindi et al., (2015) observed that in all seasons, dense vegetation lowers surface temperatures and there was a strong correlation between NDVI and land surface temperature (R^2=0.7653).

Surface properties were observed to expose the central business district and industrial areas of the city to high risk of extreme temperatures. In these areas, there was a combination of low NDVI, low NDWI and high NDBI. The NDVI and NDWI ranged between 0.1 and 0.4 while NDBI was generally above 0.5. Thus high vulnerability to extreme temperatures results from high NDBI values, low NDVI and low NDWI, which agrees with several previous works which showed that daytime temperatures are bound to be high where NDBI is high, vegetation fraction is low and the surface is dry (Chen, et al., 2006; Farnham et al., 2015; Spronken-Smith & Oke, 1998; Chun-ye & Wei-ping, 2011; Steeneveld, et al., 2014). Among densely built areas, high vulnerability was also observed in the CBD and industrial areas. This is due to high

imperviousness (low NDVI, low NDWI and high NDBI) as well as effects of high rise buildings which characterize the CBD. These buildings increase temperatures by reducing sky view factor, reducing heat removal by wind and by storing large amounts of energy absorbed by the walls of the buildings (Chun & Guldmann, 2014). This agrees with Aubrecht and Ozceylan (2013) who obtained higher levels of heat vulnerability in urbanized areas than in non-urbanized surroundings in the USA. Consistent with our findings, concentration of high rise buildings was also identified as a heterogeneous indicator of potential heat exposure (Rinner et al., 2010). The vulnerability in industrial areas is consistent with Harlan et al (2013) who stressed that people who are physically active in hot environments are highly likely to suffer from heat distress, especially in non- air-conditioned settings.

4.5 Conclusion

This study assessed the potential vulnerability of Harare residents to extreme heat based on a heat vulnerability index which used normalized indices of physical exposure to heat (NDVI, NDBI and NDWI) and socio-demographic factors. Together with NDBI and NDVI which were employed for vulnerability mapping by previous studies, we further included the NDWI for surface water content and exhaustive vegetation health quantification. The indices were retrieved using data from the recently launched Landsat 8 mission taking advantage of improvements such as in radiometric and spectral resolution compared to earlier Landsat missions. We demonstrated that vulnerability varied significantly over space in a manner which cannot be adequately displayed at census block spatial scale. Therefore, a heat vulnerability map produced at the 30m resolution of derived indices improved spatial detail and is thus important for area specific interventions within the city of Harare. Based on findings of this study, we concluded that heat vulnerability was high in the densely built-up and highly impervious areas of Harare which included the CBD and high density residential areas. The major contributions to heat vulnerability in the CBD and industrial areas were physical exposure (high heat absorption and impeded heat removal by wind due to compact buildings) and population density. High heat vulnerability in the high density residential areas mostly in the southern areas of the city was due to physical exposure (such as low vegetation cover fraction) and compromised capacity to adapt to and mitigate against extreme heat due to poverty. In addition, very high heat vulnerability in the southern areas was due to low income as residents largely occupy low quality housing and cannot afford air conditioning and related costs. Population of the vulnerable groups below 15 and above 65 years of age was also higher in the high density residential areas which also contributed to the high heat vulnerability. On

the contrary, the northern areas had low heat vulnerability due to low physical exposure evidenced by high NDVI and NDWI, low population density and high income. In these areas we concluded that abundance of healthy vegetation has high heat mitigation value. Overall, the heat vulnerability map produced provides a strong basis to guide policy formulation and interventions especially in order enhance the capacity of the urban poor to combat heat extremes.

4.6 Link between Chapter 4 with other chapters

Chapter mapped the spatial distribution of heat vulnerability of Harare using remote sensing and socio-demographic data. The study went on to link the heat vulnerability with the spatial distribution of LULC mapped in Chapter 3. LULC in this study was mapped using multi-spectral reflective data since Chapter 3 showed that classification based on these also results in high accuracy of urban mapping. Indices (NDVI, NDWI, NDBaI and NDBI) and thermal infrared data were not used for LULC mapping because they were used among the inputs to the heat vulnerability map which was to be related to LULC in Harare. The study also showed the association between heat vulnerability and land surface temperature intensities of the hot season. However, the study only mapped land surface temperature for the hot season making way for Chapter 5 to analyze seasonal patterns of heat intensity in the lower atmosphere.

CHAPTER 5: IMPLICATIONS OF LAND USE AND LAND COVER DISTRIBUTION ON SPATIO-SEASONAL VARIATIONS IN URBAN OUTDOOR THERMAL DISCOMFORT

This chapter is based on:

Mushore T. D., Odindi J., Dube T., Mutanga O. (**accepted - in press**). Outdoor thermal discomfort analysis in Harare, Zimbabwe in Southern Africa. *South African Geographical Journal*, http://dx.doi.org/10.1080/03736245.2017.1339630

5.0 Abstract

This study investigated the impact of seasonal land cover changes on human thermal outdoor comfort in Harare, Zimbabwe. A method was developed for estimating seasonal outdoor thermal discomfort using moderate resolution thermal data from Landsat 8. Multi-temporal thermal infrared and in situ air temperature data were used to develop simple linear regression model for retrieving air temperature from land surface temperature (r^2=0.6897). Season specific simple linear regression models for deriving relative humidity from land surface temperature were also developed (r^2 greater than 0.78). The developed models were tested for computation of Discomfort Index (DI) as a function of land surface temperature (LST) only. When tested against in situ observations, the LST based approach retrieved DI with high accuracy for each sub-season (mean percentage error less than 20%). The models were further used to map seasonal variations in outdoor thermal conditions. The findings showed that vegetation fraction was higher (0.60) in the most comfortable post rainy season than in the most thermally uncomfortable season (0.43), hot season. Outdoor thermal discomfort was high in hot season (mean DI of 31^{o}C) while the post rainy season was the most thermally comfortable (mean DI of 19.9^{o}C). During the hot season, thermal discomfort was higher in densely built-up areas (DI greater than 27^{o}C) than in the northern areas where low density residential areas, forests and most well maintained parks are located (DI less than 27^{o}C). It was concluded that Landsat 8 data detects seasonal land use/cover and thermal discomfort changes with high accuracy. It was also concluded that that reduction in vegetation fraction and surface wetness coupled with increase in density of buildings/impervious areas reduces outdoor thermal comfort especially during the hot periods. Overall, outdoor thermal discomfort can be mapped parsimoniously with high accuracy using Landsat thermal infrared data.

Keywords: Surface temperature, vegetation fraction, discomfort index, heat island, Landsat 8, land cover classification, remote sensing

5.1 Introduction

Understanding thermal comfort patterns is important for solving related health, global warming and wasted energy problems (Goshayeshi, et al., 2013b). Thermal discomfort is when 80 to 90% express dissatisfaction with prevailing temperature at a given instant and location (Yilmaz, 2007). Heterogeneity in urban surface properties exposes citizens to spatially variable levels of thermal comfort as it is mainly affected by surface conditions (Zhang, et al., 2009). Thermal discomfort causes fatigue, malaise, reduced ability to perform intellectual activities, health problems and even death (Buscail, et al., 2012; de-Azevedo et al., 2015; Roelofsen, 2015; Haruna et al., 2014). Studies have revealed that thermal discomfort affects physical and psychological performance. For example attention and performance in the classroom are compromised by thermal discomfort (Mazon, 2013). Furthermore, the usage of a location for activities is affected by thermal discomfort while urban citizens enjoy leisure in thermally comfortable outdoor locations such as parks and lakes (Setaih et al., 2014; Goshayeshi, et al., 2013b). Outdoor thermal discomfort also affects thermal conditions indoors; in developed countries people spend 10% of time outdoor during hot season and less than 5% in winter (Setaih, et al., 2014). Therefore, there is need for mapping the seasonal and spatial distribution of thermal comfort in order to assist citizen in making informed decisions in selecting places with thermal comforts within their preferred ranges for various activities across seasons.

Indices such at the Physiological Equivalent Temperature (PET) and Discomfort Index (DI) have been preferred by recent studies due to simplicity and parsimony compared to empirical methods such as Predicted Mean Vote (PMV) which involve significant parameterization (Mohan, et al., 2014; Roelofsen, 2015; Shastry, et al., 2016). PET requires temperature, humidity and wind speed only and DI requires air temperature and humidity, compared to more variables including human metabolism and insulation provided by clothing required in the computation of PMV (Goshayeshi, et al., 2013b). Also while other studies utilize point meteorological data to measure outdoor thermal discomfort (Yousif & Tahir, 2013; Cheng, et al., 2010; Abdel-Ghany, et al., 2014; Tulandi, et al., 2012), remote sensing enables synoptic measurement of intensity and spatial distribution of thermal discomfort for the whole city (Sobrino, et al., 2004). While low resolution National Oceanic and Atmospheric Administration's Advanced Very High Resolution Radiometer (NOAA AVHRR) and Multi-functional transport Satellite (MTSAT) data have been used in thermal discomfort studies (Polydoros & Cartalis, 2014; Okamura, et al., 2014), the spatial resolution is not adequate in monitoring urban climates as vast changes are observed within short distances. Although

resolution greater than 50m was recommended for urban thermal analysis (Sobrino, et al., 2004), data in this range is not readily available. There is thus need to utilize freely available medium resolution datasets such as from Landsat to understand thermal comfort patterns especially in urban areas in developing countries.

Landsat series offers freely available data for urban studies such as 30m resolution for VIS/IR bands and 100m thermal data from recently launched Landsat 8. Previously, Landsat TM and ETM have been used in thermal discomfort analysis (Wei-wu et al., 2004). However, the improved Landsat 8 have not yet been used in outdoor thermal comfort studies despite high sensitivity, improved signal to noise ratio and improved spectral range (Jia, et al., 2014; Dube & Mutanga, 2015a). Landsat 8 data was found to improve land cover mapping, heat island analysis, monitoring of active volcanoes and identification of hydro-chemical rock alterations (Dube & Mutanga, 2015a; Jia, et al., 2014; Banskota, et al., 2014; Oumar, 2015; Kharat & Musande, 2015; Blackett, 2014; Han & Nelson, 2015). This study thus hypothesizes that Landsat 8's multi-spectral and multi-temporal data should effectively and parsimoniously detect and map seasonal variations in thermal discomfort in a complex urban environment. Outdoor thermal discomfort should vary with seasons as well as between locations due to spatial and temporal variations of land cover in urban areas. Land surface temperature retrieved using remote sensing is highly correlated with air temperature, enabling estimation of air temperature from space-borne remote sensing observations of surface temperature (Widyasamratri et al., 2013; Cheng & Ng, 2006; Polydoros & Cartalis, 2014). This relationship could be useful in retrieving seasonal urban outdoor thermal discomfort using medium resolution Landsat data for the first time. Previous studies by Okamura, et al. (2014) and (Polydoros & Cartalis, 2014) used coarse spatial resolution which is not sufficient, given the heterogeneity of urban landscapes. Medium resolution data have been successfully used to link land surface temperature with land use and land cover despite their complex configuration in urban areas (Amiri, et al., 2009; Connors, et al., 2012; Chen, et al., 2006). However, adoption of medium resolution data such as Landsat data for outdoor thermal discomfort analysis has remained limited only to a study by Wei-wu, et al. (2004). Given the success of medium resolution dataset in mapping urban thermal variations, there is need to further test their potential in mapping spatial and seasonal patterns in outdoor thermal discomfort.

As aforementioned, a detailed understanding of spatial and seasonal thermal discomfort patterns is important for identifying spatial variations in thermal risk levels within an urban

area. Wei-wu, et al. (2004) measured outdoor thermal discomfort using air temperature derived from land surface temperature and relative humidity derived from Normalized Difference Vegetation Index (NDVI). Their procedure was tedious as it required land surface temperature and NDVI obtained using Landsat 5 multi-spectral data. In this study, it is hypothesized that data requirements for retrieval of DI can be reduced by developing models for obtaining both relative humidity and air temperature from land surface temperature. Fortunately, there is also a strong inverse correlation between air temperature and relative humidity (de-Azevedo, et al., 2015) and this may also be useful in reducing data requirements for discomfort analysis using the Discomfort Index (DI). Therefore, there is need to retrieved relative humidity as a function of land surface temperature derived from medium resolution such as the recently launched and improved Landsat 8 multi-spectral data. As a result, outdoor thermal discomfort can be modelled as a function of air temperature and relative humidity both derived from surface temperatures retrieved from thermal bands of Landsat 8. This will reduce data requirement by making land surface temperature the only input in DI computation, important in data scarce cities such as Harare, Zimbabwe. This has potential to effectively map spatial variations of DI and promote thermal discomfort assessments in urban areas of developing countries where scarcity of in-situ observations may hinder such analysis. This is important for deriving area and season specific heat mitigation policies and strategies especially in cities of developing countries such as Harare city where the poorest are usually the most vulnerable (Mushore, Mutanga, et al., 2017a). Therefore, this study will develop analysis techniques which aid urban areas plan and develop sustainably.

The objective of this study was thus to use air temperature retrieved from Landsat 8's thermal data for mapping seasonal variations in thermal discomfort in Harare, Zimbabwe as well as to investigate how the relationship between relative humidity and air temperature can be useful in reducing data requirements for thermal discomfort mapping using DI. The link between outdoor thermal discomfort and land cover types across four sub-seasons in Harare, Zimbabwe was also investigated. The aim was mainly to understand extent to which distribution of buildings and vegetation influences thermal discomfort across sub-seasons in Harare. This was important for the identification of potentially uncomfortable places for temperature related disaster management purposes as no similar study has been previously done. This was also necessary for identification of comfortable places in different sub-seasons to inform temperature sensitive outdoor activities as well as city planning and management. The hypothesis was that seasonal changes in land cover patterns could trigger significant

differences in intensity and spatial distribution of outdoor thermal discomfort between seasons in Harare. The study was mainly driven by the paucity in literature on use of medium resolution satellite data such as from Landsat series for outdoor thermal discomfort analysis and the need for such assessment in Zimbabwe in view of the observed and expected climatic changes. The study also aimed at expressing the potential of freely available Landsat datasets for use in thermal discomfort analysis in cities of resource constrained developing countries in view of the common in-situ observation network inadequacy.

5.2 Methodology

5.2.1 Description of the study area

The study was done in Harare, the Capital City of Zimbabwe found in Southern Africa (Figure 5.1). The city experience two major seasons (summer from mid-September to mid-March and winter from mid-March to mid-September). The seasons are further subdivided into 4 sub-seasons which are the rainy (mid-November to mid-March), post rainy (mid-March to mid-May), cool (mid-May to mid-September) and hot sub-seasons (mid-September to mid-November) (Unganai, 1996; Manatsa, 2012; Torrance, 1981; Mushore, 2013a). Generally summers are warmer and wetter than winters, thus vegetation abundance should also be seasonal.

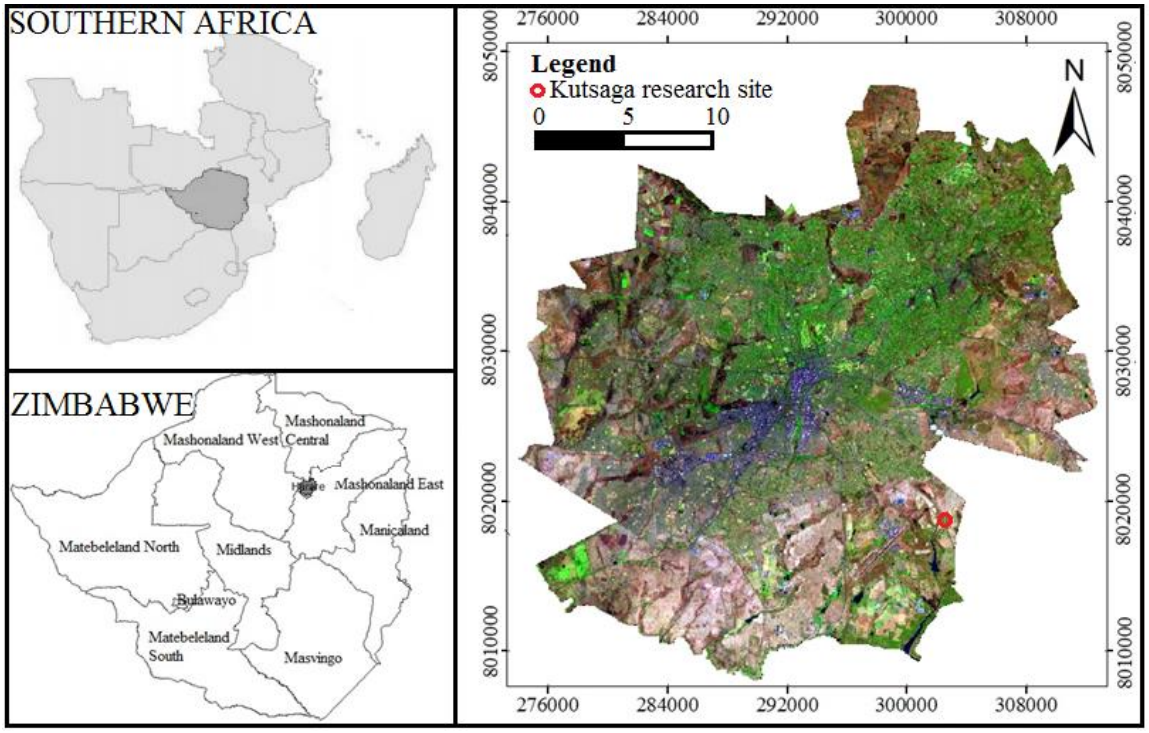

Figure 5.1: Location of the study area.

5.2.2 Meteorological data collection and processing

Meteorological field data were obtained from Kutsaga Research Station located near Harare International Airport in the southeast of the city (Figure 5.1). These were relative humidity and dry bulb temperature collected at hourly resolution using an automatic weather station for the period from 1 January 2013 to 31 December 2015. The data period was selected in order to capture the variations between and within sub-seasons while at the same enabling obtaining of data coinciding with cloud free Landsat images. In the computation of thermal discomfort using Discomfort Index (DI) relative humidity data are required (Yilmaz, 2007; de-Azevedo, et al., 2015; Abdel-Ghany, et al., 2014; Polydoros & Cartalis, 2014; Tulandi, et al., 2012). Humidity varies in space within a city such that Meteorological field measurements from a single site are not sufficient. There was need to upscale relative humidity measurements from point observation in order to obtain representative and accurate spatially variable relative humidity measurements. Regression analysis was, therefore, used to model the relationship between air temperature and relative humidity for each sub-season. The regression models were validated by comparing observed with modelled relative humidity for each of the four sub-seasons.

5.2.3 Remote sensing data collection and pre-processing

The properties and functions of the 11 bands of Landsat 8 have been extensively described in several recent studies (Dube & Mutanga, 2015a; Jia, et al., 2014; Banskota, et al., 2014; Oumar, 2015; Kharat & Musande, 2015; Blackett, 2014; Han & Nelson, 2015). Cloud free daytime Landsat data acquired on dates corresponding to the four sub-seasons (Table 5.1) and covering the entire study area were freely downloaded from the USGS earth explorer website. It is difficult to obtain cloud-free images during the December to February period as this coincides with the peak of rainfall in Zimbabwe

Table 5.1: Landsat data (Path/row 170/72) used in this study

Image date	Season	Image date	Season
24 March 2015	Rainy season	6 June 2013	Cool season
19 April 2013	Post rainy season	25 August 2013	Cool season
25 April 2015	Post rainy season	25 June 2014	Cool season
11 May 2015	Post rainy season	11 July 2014	Cool season
26 September 2013	Hot season	27 July 2014	Cool season
28 October 2013	Hot season	12 August 2014	Cool season
13 November 2013	Hot season	28 August 2014	Cool season
31 October 2014	Hot season	13 September 2014	Cool season

Coordinates on an image must agree with those on the ground in order to accurately relate remote sensing retrievals with ground reality. The process of geo-referencing makes use of

ground control points whose coordinates to correct the coordinates on an image. The images were geo-referenced using 30 ground control points obtained at intersection of major roads. The points were collected from 30 different and far-spaced locations in Harare where major roads were meeting. Intersections of major roads were sampled because they are easy to identify on an image when locating ground control points during geo-referencing. Atmospheric correction was done using the FLAASH module in the ENVI Version 4.7 software (Dube & Mutanga, 2015a). Emissivity correction is necessary in the conversion from at-satellite brightness temperature to surface temperature (Wu, et al., 2014). For each season, the reflectance of near infrared and Red bands were used to retrieve the normalized difference vegetation index, vegetation fraction and surface emissivity as describe by Wu et al., (2014). The thermals band 10 for each date was used to compute the brightness temperature which was then converted to surface temperature through emissivity correction. Since each sub-season spans for about 3 months, there was need to cater for intra-season variability in surface property. Therefore, instead of using a single date as representative for each season, average temperature was derived from the available data for further analysis.

5.2.4 Relative humidity retrieval from satellite and field observation

Relative humidity was determined using a linear regression model relating relative humidity with air temperature obtained using data from Kutsaga Research Station. Another linear regression model was developed for obtaining air temperature from land surface temperature derived from Landsat 8 for each sub-season. In order to obtain relative humidity map for each sub-season, we applied the relationship between air temperature and relative humidity obtained from field observations to the air temperatures retrieved from thermal data. A two-step approach was thus taken involving i) estimation of air temperature from land surface temperature and ii) further estimating spatial distribution of relative humidity using linear regression models aforementioned.

5.2.5 Retrieval of seasonal thermal discomfort patterns

Discomfort indices are commonly used due to parsimony while derivation of comfort indices such as by PMV using the Rayman, ENVI-MET or other models requires parameterization (Mohan, et al., 2014; Roelofsen, 2015; Shastry, et al., 2016). Furthermore, thermal indices are simple to compute; for example the ET only requires outdoor temperature to compute indoor thermal comfort and the Discomfort Index (DI [^{o}C]) requires temperature (^{o}C) and humidity (%) data only. For this reason the Discomfort Index was used in this study for analyzing

outdoor thermal discomfort and was computed using mean air temperature (T_a [ºC]) and mean relative humidity (*RH* [%]) derived from land surface temperature as described above. The equation for computing DI from air temperature and relative humidity (Equation 5.1) and the criteria for categorizing discomfort were obtained from Polydoros and Catalis (2014).

$$\boldsymbol{DI}(℃) = \boldsymbol{T_a} - \mathbf{0.55}(\mathbf{1} - \mathbf{0.01}\boldsymbol{RH})(\boldsymbol{T_a} - \mathbf{14.5}) \quad \text{Equation 5.1}$$

In this study equation one was further adjusted using regression models so that discomfort was computed as a function of air temperature only for each of the four sub-seasons. This thus further reduced the data requirements for the computation of thermal discomfort.

5.2.6 Linkage between land cover fraction and thermal discomfort patterns

The link between spatial distribution of thermal discomfort and land cover types as well as land cover fractions per sub season was investigated. Land cover fraction provides a quantitative analysis of distribution of surface covers while land cover classification provides qualitative classes. The vegetation fraction was used to represent land cover fraction with high values (close to 1) representing abundant vegetation cover while low values (close to zero) representing impervious, bare and built-up areas. Vegetation fraction (F_c) was retrieved from NDVI map for each sub-season according to dimidiate pixel model using Equation 5.2 (Cao, et al., 2008).

$$\boldsymbol{F_c} = \frac{\boldsymbol{NDVI - NDVI_{soil}}}{\boldsymbol{NDVI_{veg} - NDVI_{soil}}} \quad \text{Equation 5.2}$$

Where $NDVI_{soil}$ is NDVI for a pure soil pixel and $NDVI_{veg}$ is for a pure vegetation pixel. In this study NDVIsoil of 0.05 and NDVIveg of 0.7 (Hu & Jia, 2010) were used.

For qualitative land cover classification, the Support Vector Machine (SVM) algorithm (Petropoulos, et al., 2012; Adelabu, et al., 2013; Jia, et al., 2014; Yang, Lin, et al., 2014; Forkuor & Cofie, 2011) was used in supervised classification to map Harare into seven classes described in Table 5.2. The advantages of the Support Vector Algorithm and high performance in land cover mapping are explained by Yu et al., (2014) and Forkuor and Cofie (2011). A cloud free image obtained on 13 September 2013 was used together with 100 ground control points per class obtained from locations evenly distributed across cover type and study area to capture variability within and between classes. The points were split into 70% for training/classification and 30% for accuracy assessment as recommended by Adelabu, et al. (2013). The 30m resolution visible/infrared bands, except for the cirrus clouds band (band 9) and sea coastal water monitoring band (band 1) and the 15m resolution panchromatic band

(band 8) were used for land cover classification. Thermal infra-red bands (Band 10 and 11) were not included for image classification due to their relative low resolution (100m) which may not effectively map heterogeneous urban landscapes. The accuracy of the classification was assessed using independent ground control points for each land cover type obtained in field survey described already in Chapter 3. In order to increase number of control points per LULC type, the points were superimposed on an RGB composite image of the study area and polygons were digitized around them creating regions of interest (ROI) in ENVI software. ROI instead of points were then used for both classification and accuracy assessment. This was following recommendation that use of ROI instead of direct (Global Position System) GPS based points from field survey increases classification accuracy (Acharya, et al., 2015). A confusion matrix was obtained by cross validating the classified map with field observations. Further, accuracy was quantified using Producer's accuracy (PA), User's accuracy (UA), Overall accuracy (OA) and kappa. Several studies on image classification explain the extraction of classification accuracy indicators from the confusion matrix (Southworth, 2004; Panah, et al., 2001; Witt, et al., 2007; Sun & Schulz, 2015; Liu et al., 2003).

Table 5.2: Description of the major land cover classes considered for this study

Class	**Description**
Densely built (DB)	Very high built density (CBD and industrial areas)
Low-medium density residential (LMR)	Low and medium density residential areas with higher vegetation fraction than high density residential
High density residential (HDR)	Built-up with higher density of building and lower vegetation cover than low-medium residential
Forested Areas (Fr)	moderate to dense forest cover
Development (Dv)	High density residential under development; mixture of bare and building with very low vegetation cover
Grasslands (Gr)	Grass covered areas with little or no trees
Water (Wt)	Water bodies

We further investigated the link between thermal discomfort and land cover quantitatively and qualitatively. Quantitatively, we analysed the responses of average temperature and discomfort to average land cover fraction (vegetation fraction) across the four sub-seasons. Qualitatively, we analysed the link between the spatial distribution of thermal discomfort and land cover themes in Harare per sub-season.

5.3 Results

5.3.1 Relationship between air temperature and land surface temperature

Figure 5.2 shows that there was a positive correlation between air temperature obtained from a meteorological station at a height of 2m and land surface temperature retrieved from thermal infra-red data of Landsat 8. The R^2 value was 0.69 implying an acceptable correlation.

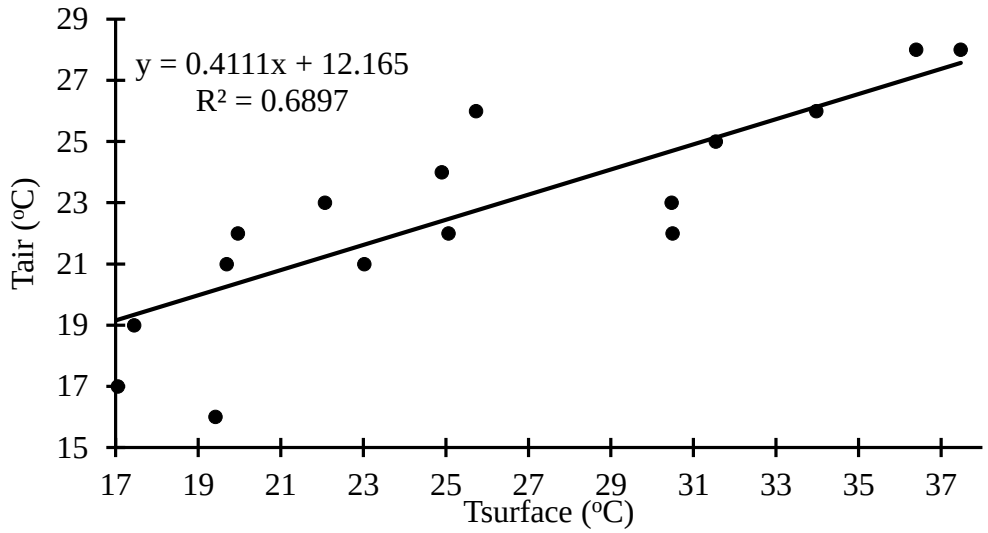

Figure 5.2: Relationship between land surface temperature and air temperature

5.3.2 Relationship between relative humidity and air temperature for different sub-seasons in Harare

Table 5.3 shows that there was a [negative] correlation between relative humidity and air temperature. However, the correlation was weak (R^2= [-]0.328) when all sub-seasons were considered in a single regression analysis. However, strong correlations were observed when regression analysis was done for each sub-season separately (R^2>0.79). Of the four sub-seasons, the correlation between relative humidity and air temperature was strongest in the post rainy sub-season (0.8731) and weakest in the hot sub-season (0.7947).

Table 5.3: Relationship between relative humidity and air temperature across seasons

Season	Regression model	R-squared	Percentage Error (%)
All seasons	$RH = [-]2.29T_a + 102$	0.3278	28.1
Rainy	$RH = [-]5.65T_a + 189.75$	0.8292	9.3
Post rainy	$RH = [-]4.35T_a + 138.25$	0.8731	16.7
Cool	$RH = [-]2.98T_a + 94.71$	0.8694	10.4
Hot	$RH = [-]3.09T_a + 122.15$	0.7947	15.2

5.3.3 Performance of the regression models

The validity of the regression models using independent field observations on a randomly selected day in each season was tested. Figure 5.3 and Table 5.3 show that there was a strong agreement between observed and modelled relative humidity patterns evidenced by percentage errors below 20% for all sub-seasons. Table 1 shows that regression model for the rainy season had the highest accuracy (90.7%), while the model for the post rainy season had the least accuracy (83.3%).

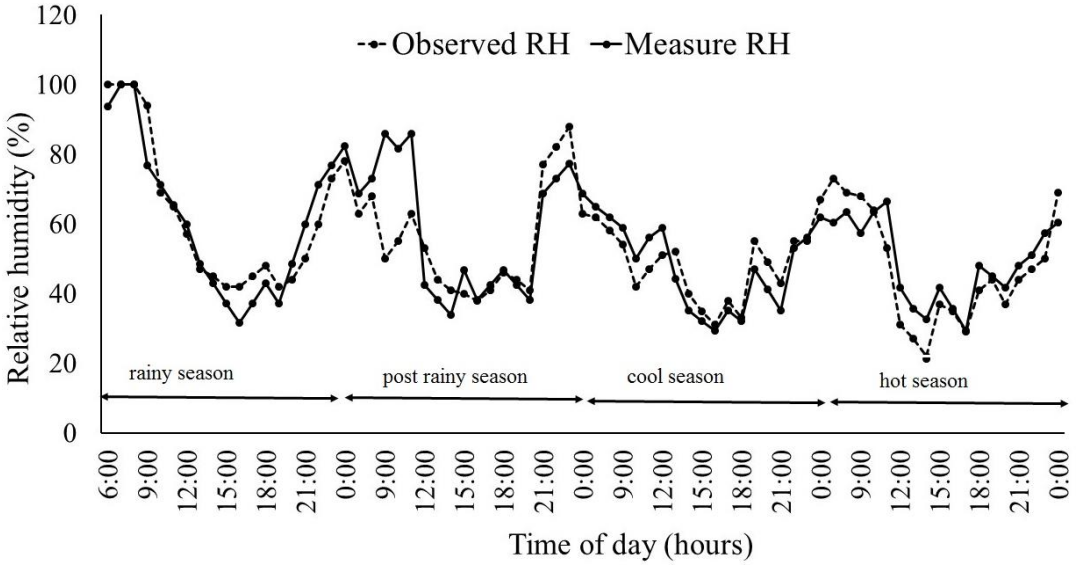

Figure 5.3: Verification of regression models for seasonal relative humidity

Figure 5.3 shows that the models closely resembled the trend that was obtained using field observations in all sub-seasons.

5.3.4 Spatial and temporal patterns of thermal discomfort in Harare

Based on discomfort index analysis, the proportion of the study area where less than 50% of the subjects would feel uncomfortable was largest during the post rainy sub-season (59%) and smallest in the hot sub-season (2.1%). Coverage of areas where everyone would feel thermally uncomfortable was largest during the hot sub-season (49.9%) and smallest in the cool and post rainy sub-seasons, where the proportion was 0%.

Table 5.4: Areal coverage of thermal discomfort conditions per sub-season

	Coverage of discomfort category per season (% of total area)			
	Rainy	Post rainy	Cool	Hot
No discomfort	3.0	59.0	53.1	2.1
<50% feel discomfort	19.3	40.1	46.2	13.1
50% feel discomfort	29.0	0.6	0.5	15.2
Most feel discomfort	29.6	0.3	0.1	19.7
Everyone feels discomfort	19.1	0	0	49.9

State of emergency	0	0	0	0

Although the post rainy sub-season had more areas, where less than 50% would feel discomfort than the cool sub-season, the coverage was not very different (Table 5.4). Both sub-seasons were almost equally very comfortable evidenced by small coverage of areas were most or all people would feel uncomfortable. Although discomfort is felt in more than 70% of the city during the hot and in 50% of the city during the rainy sub-season, a significant proportion was thermally comfortable (more than 30% of the city).

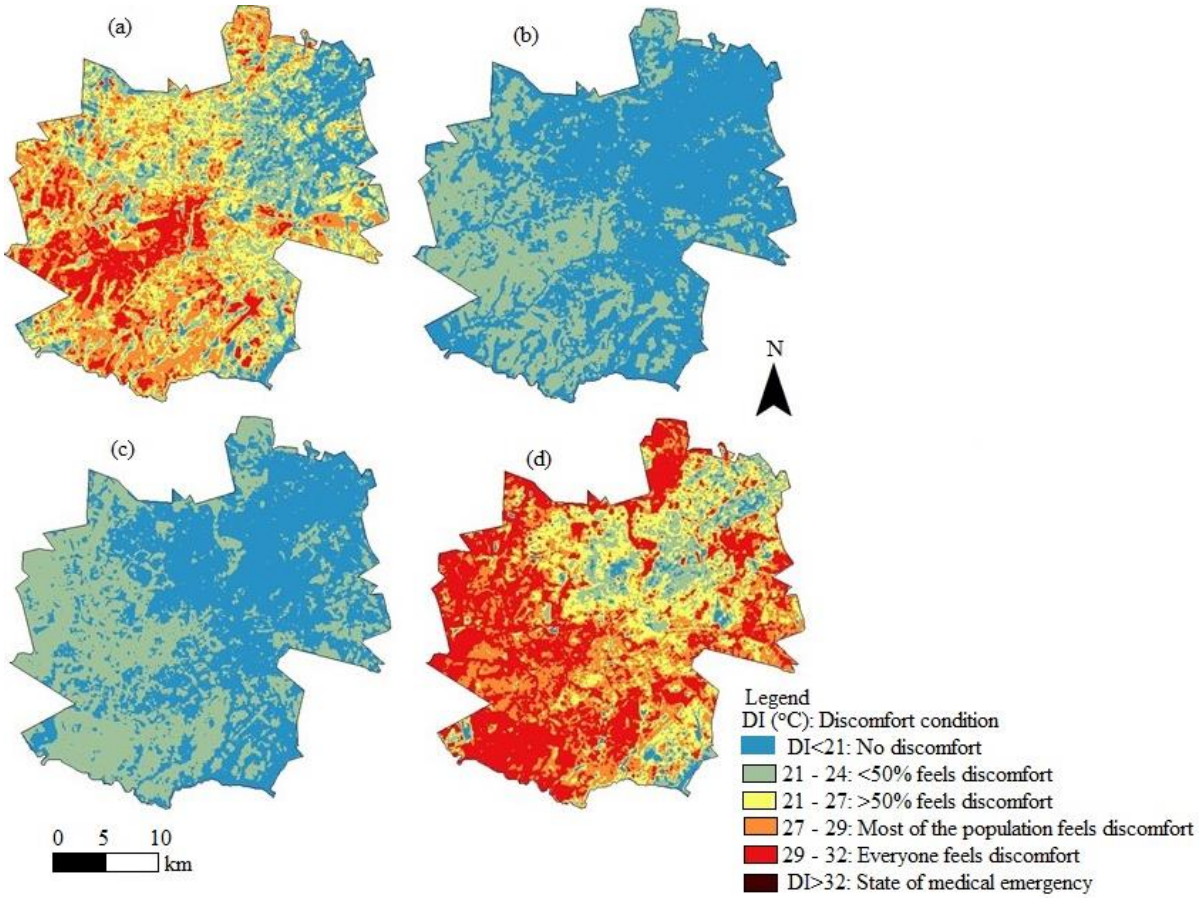

Figure 5.4: Seasonal and spatial variations in outdoor thermal discomfort in Harare in (a) rainy, (b) post rainy, (c) cool and (d) hot sub-seasons

Figure 5.4 shows that thermal discomfort is not uniform across the urban area and that the intensities as well as their spatial distributions vary seasonally. Discomfort indices below 24^{o}C are experienced across the country in the cool (Figure 5.4c) and post rainy sub-seasons (Figure 5.4b). During these sub-seasons, very low discomfort indices (below 21^{o}C) were observed in the northern and eastern areas. During the hot sub-season (Figure 5.4d) the Discomfort Indices took values greater than 24^{o}C in much of the country. However, values were generally higher in the southern and western parts (DI was greater than 27^{o}C) than in the northern and eastern parts of the city (DI was less than 27^{o}C).

5.4 Urban land cover classification and link with observed thermal discomfort

5.4.1 Distribution of land use/cover types in Harare

We also performed a qualitative land cover classification using the SVM algorithm. Results are presented in Figure 5.5 and Table 5.5. Figure 5.5 shows that high density residential areas and areas under development occupy the southern parts of the study area. The northern areas are occupied mostly by low-medium residential areas.

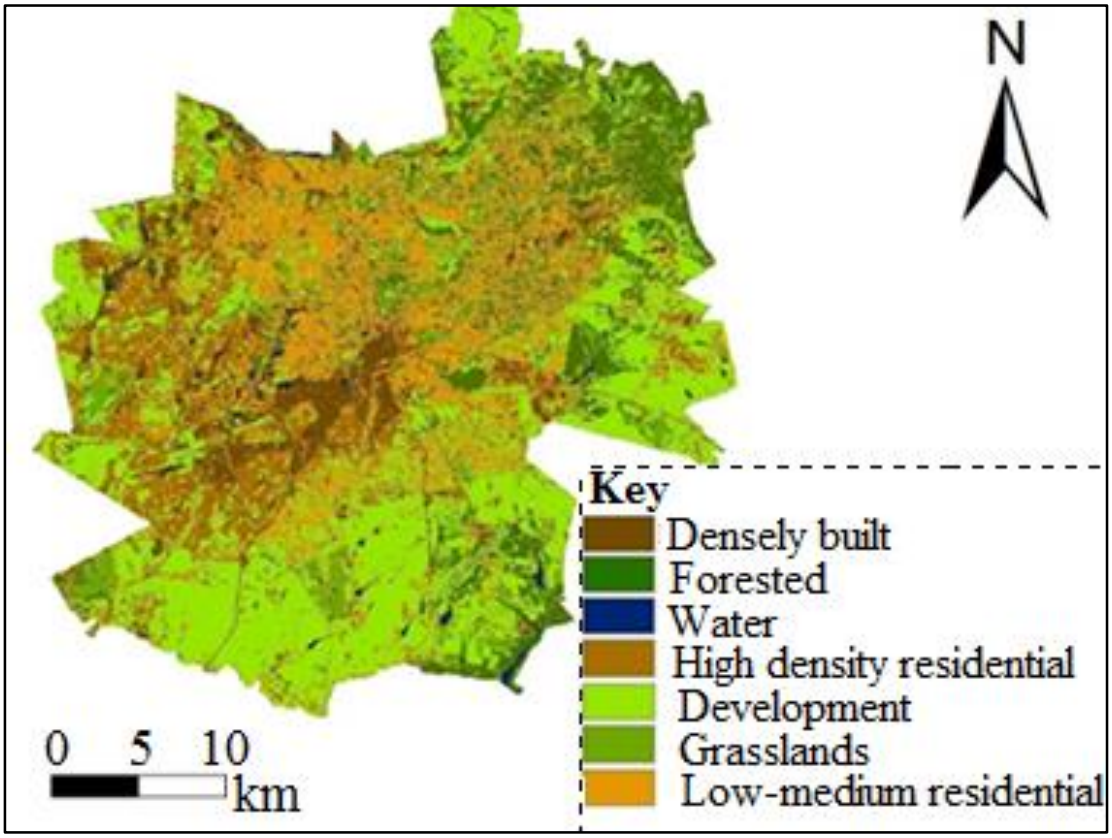

Figure 5.5: Distribution of land use/cover types in Harare, Zimbabwe in Southern Africa

Table 5.5: Accuracy assessment of the land use/cover classification

	Ground truth						
Classified	DB	LMR	HDR	Fr	Cr	Gr	Wr
Densely built-up (DB)	956	0	5	10	91	0	0
Low-medium density (LMR)	0	755	14	0	37	20	29
High Density residential (HDR)	13	0	1181	0	2	1	5
Forests (Fr)	83	5	0	667	119	40	4
Cropland (Cr)	9	7	2	123	1667	104	49
Grasslands (Gr)	22	7	14	7	26	840	45
Water (Wt)	0	4	0	0	183	11	621
Producer's Accuracy (PA)	83.8	88.5	81.4	95.0	73.5	88.3	92.9
User's Accuracy (UA)	77.9	88.0	72.5	87.7	89.3	74.0	99.8

Overall accuracy (OA)=84.3% Kappa=0.81

The User's accuracy was high ranging, from 73% to 99.8%. User's accuracy was highest for the water class (99.8%) and lowest for the high density residential class (72.5%). Producer's

accuracy was also high for all classes (ranged from 74% to 93%); highest for the water bodies class and lowest for the croplands class. Besides the croplands class, producer's accuracy was greater than 80% for the other classes. Overall accuracy was 84.3% and kappa statistic was 0.81, hence significantly high accuracy of classification in an urban landscape.

5.4.2 Link between LULC types in seasonal thermal discomfort patterns in Harare

Figure 5.4 shows that in all seasons the northern areas, which in Figure 5.5 are occupied mostly by parks and low density residential areas thermal discomfort was generally lower than in the southern areas. For example, in the hot sub-season, almost all occupants feel thermally uncomfortable (DI greater than 27^{o}C) in the bulk of the southern areas while more than 50% would feel comfortable (DI less 27^{o}C) in most of the areas in the north. The densely built up areas, which correspond to the central business district and industrial areas have all occupants in discomfort (DI between 29 ^{o}C and 32^{o}C) during the rainy and the hot sub-seasons. In all sub-seasons, the state of medical emergence thermal discomfort category (DI above 32^{o}C) was not recorded.

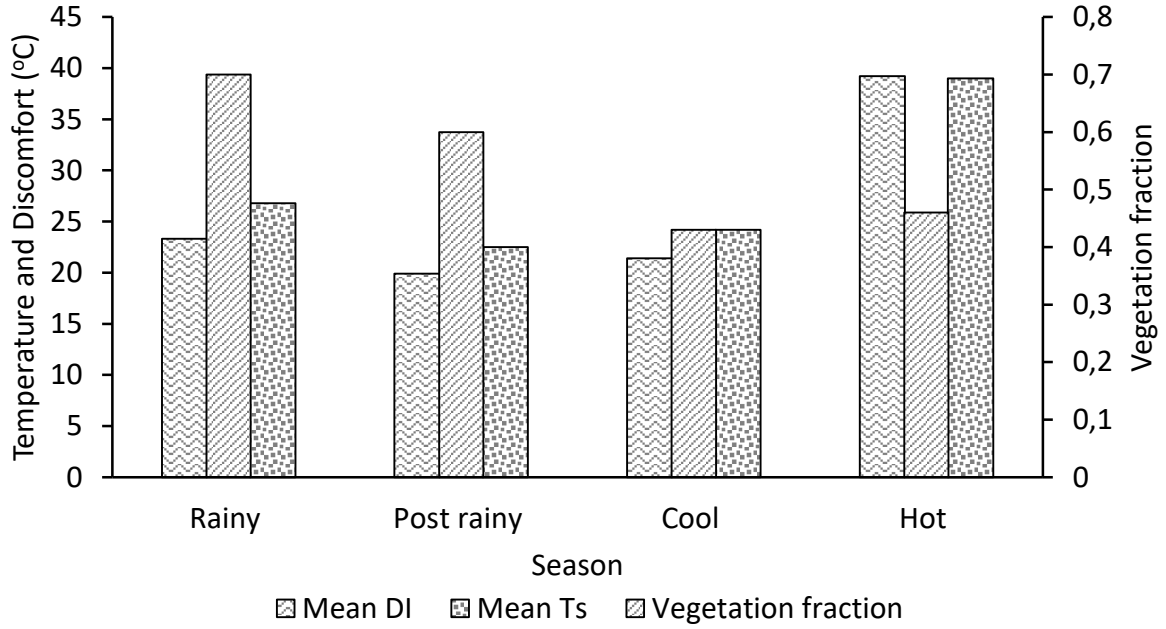

Figure 5.6: Seasonal variations in mean thermal discomfort and vegetation fraction

Figure 5.6 shows that the average discomfort was very high in the hot sub-season (DI=31^{o}C) while it was low in the cool sub-season (20^{o}C) and even lower in the post rainy sub-season (20^{o}C). There was higher vegetation fraction and lower mean discomfort in the post rainy (0.6) than the cool (0.43) season. The hot season was characterized by low vegetation fraction (0.46)

and high thermal discomfort (average of 30^{o}C). Therefore, there was a general negative relationship between thermal discomfort and vegetation fraction.

5.5 Discussion

The potential of recently launched Landsat 8 and improved relative humidity observations in improving thermal discomfort mapping was tested. Thermal discomfort was computed for four sub-seasons using air temperature retrieved from Landsat 8. In addition, regression analysis resulted in strong correlation between relative humidity and air temperature. The correlation was stronger when seasons were considered separately (R^2 greater 0.79) than when a single model was used for all sub-seasons (R^2=0.33). The regression models were also verified using independent observations and their accuracy was high (relative errors below 20%) for all sub-seasons. The correlation between air temperature and relative humidity is known to be strongly negative (de-Azevedo et al., 2015). A strong correlation between air temperature and land surface temperatures (R^2=0.69) was also observed. The relationship between temperature and humidity was used to retrieve relative humidity such that discomfort index was computed as a function of air temperature only, thus reducing the data requirement.

The hot and the rainy sub-seasons were observed to be more thermally uncomfortable (mean discomfort index was 31^{o}C) than the post rainy and the cool seasons (mean DI was less than 24^{o}C). This was because the hot and post rainy sub-seasons comprise the summer season when generally a lot of insolation is received compared to winter season (post rainy and cool sub-seasons). Further, vegetation abundance and surface wetness had a significant cooling effect on the rainy and post rainy sub-seasons. Similarly, the cool sub-season was on average more thermally uncomfortable (DI of 21.4^{o}C) than the post rainy sub-season (mean DI of 19.9^{o}C), although the latter receives more insolation (not quantified in this study) due to low vegetation fraction and low surface wetness. Vegetation is mostly dry in the cool sub-season while some trees even shed their leaves during the period in Harare. Vegetation cover reduces radiant heat transfer by increasing latent heat transfer thereby increased cooling effect as vegetation fraction increases between hot and the rainy sub-seasons (Odindi, et al., 2015; Cao, et al., 2008; Zhang, et al., 2012). Plants convert a lot of energy from the sun to potential energy weakening heating effect of solar energy (Klok, et al., 2012)

In order to link the distribution of land cover types to the seasonality of thermal discomfort, a supervised classification of Landsat 8's visible/infrared bands was performed. Seven classes were observed at an overall accuracy of 84.5% and kappa of 0.81. The user's and producer's

accuracy were higher than 73% for all the land use/cover types implying strong agreement between the mapped classes and field observations. The accuracy was higher than previously achieved, when Harare was classified into built and non-built using high resolution SPOT image (Wania, et al., 2014). Wania et al., (2014) obtained an overall accuracy of 83.5 and kappa of 0.64. The high accuracy of LULC mapping was attributed to the support vector machine algorithm as well as quality of Landsat 8 data, which improve land surface property retrievals; the quality attributes include improvements in radiometric resolution, spectral range and noise to signal ratio which has been found to improve land use/cover mapping (Jia, et al., 2014; Mwaniki, et al., 2015; Ke, et al., 2015). Landsat 8 has outperformed earlier Landsat versions as well as moderate resolution datasets such as MODIS in mapping land surface characteristics, especially in heterogeneous urban landscapes (Mwaniki, et al., 2015; Ke, et al., 2015; Yu, et al., 2013; Jia, et al., 2014).

During the post rainy sub-season, most of the city including all residential areas had no discomfort (DI less than 21^{o}C) except for the densely built-up areas (CBD and industrial areas) where less than 50% of subjects would feel uncomfortable (DI between 21^{o}C and 24^{o}C). The slight thermal discomfort (DI between 21^{o}C and 24^{o}C) observed in the CBD in the post rainy and cool sub-seasons when other areas were more comfortable can be supported by findings that inner cities are exposed to increased health risk and intense temperatures (Tomlinson, et al., 2011). The high density of buildings here impedes wind movement hence removal of heat (Qiao, et al., 2013). The large size of the thermally comfortable proportion (59% of the city) was because during the post rainy sub-season, the ground will be relatively wet while vegetation fraction be will high (including intra-urban farming) hence high evapo-transpiration. Further, compared to the rainy sub-season, the sun will be on its northward transition making way for the cool sub-season, thereby reducing intensity of radiation received during this period. However, the densely built-up areas, although not very uncomfortable thermally, were slightly more uncomfortable (DI between 21^{o}C and 24^{o}C) than the bulk of the city during the same period. This was due to high absorption of radiation as well as presence of surfaces which store and release heat, thus increasing temperatures during the day (Srivanit, et al., 2012). This agrees with the observation that built-up areas have large heat storage fraction due to changes in characteristics of the ground by lowering vegetation cover and surface reflectance (Setaih, et al., 2014).

In the hot, rainy and cool sub-seasons the southern and western areas are thermally more uncomfortable than the northern and eastern areas. For example in the southern and western areas, during the hot season, DI ranged from 27^{o}C to 32^{o}C while it was mostly less than 27^{o}C in the rest of the city. The southern and south eastern areas are mostly occupied by high density residential areas and areas under residential development. Increased density of buildings results in high absorption and storage heat resulting in high surface temperatures, especially in the hot season (Qiao, et al., 2013; Chun & Guldmann, 2014). Due to large coverage of impervious surfaces, buildings and bare areas, evidenced also by small coverage of grasslands and forests in the southern areas, heat loss by evapo-transpiration is reduced during the hot season. Densely built-up and bare areas show similar thermal characteristics during the hot sub-season hence almost equal and high discomfort in high-density residential, densely built-up area and areas under development.

Even in the hot sub-season, fewer people would feel uncomfortable in the low-medium density residential areas (DI mostly below 27^{o}C) than in the CBD and high density residential areas (DI mostly greater than 27^{o}C). In these areas, vegetation fraction is high while density of buildings is low due to spacious settlement hence space for greenery. In all sub-seasons, greenery is generally healthy in the low-medium residential because even during the dry seasons, the citizens here afford to manage and irrigate the green spaces due to high income. Furthermore large park and vast grasslands are also found in the north of the city thus contributing to low thermal discomfort across all sub-seasons in Harare. Even in areas where there are buildings, vegetation reduces temperatures and hence increases thermal comfort of an area. Residential areas with high vegetation cover have low irradiance during the day (Lo, et al., 1997; Lo & Choi, 2004; Weng, et al., 2004).

In all seasons there was no thermal discomfort at daytime in water covered areas (DI less than 21^{o}C). The large water body in the extreme southeast is characterized by low discomfort index values in all seasons. Water has high heat capacity thus takes long to heat up during the day resulting in low skin temperatures (Wang & Zhu, 2011; Amiri, et al., 2009). Spraying surfaces with water mist was also found to significantly reduce temperatures and discomfort during daytime in summer (Farnham, et al., 2015). Covering a surface with water also reducing daytime temperature of an area by increasing heat loss by evaporation thus reduced daytime temperatures towards water bodies (Steeneveld et al., 2013). Surface irradiance was found, in another study, to be least in water, followed by vegetation while higher than this in residential

areas where there was mixture of vegetation and buildings (Lo, et al., 1997; Steeneveld, et al., 2013).

5.5 Conclusion

The following conclusions were drawn from this study

- there is a negative correlation between air temperature and humidity which is stronger when different sub-seasons are considered separately
- Landsat 8 produces land cover and thermal discomfort maps of high accuracy in heterogeneous and complex urban landscapes
- The post rainy sub-season is the most thermally comfortable in Harare due to reduction in incoming radiation when approaching winter and high vegetation fraction.
- In all sub-seasons, the low-medium density residential areas are more comfortable than the high density residential areas.
- Intra-urban farming contributes in reducing thermal discomfort especially in high density residential and development areas during the rainy and post rainy sub-seasons.

5.6 Link between Chapter 5 and other chapters

Chapter 4 showed the spatial structure of heat vulnerability in Harare. The chapter also mapped the spatial structure of land surface temperature intensities but only for the hot season. The chapter demonstrated that heat vulnerability was high in the southern and south western areas occupied mainly by the low-income strata. Due to temporal variations in the in incoming radiation, need remained to establish the link between LULC mapped in Chapter 3 with land surface temperature intensities across seasons. Therefore, Chapter 5 established the link between LULC and heat island intensities in four sub-seasons experienced in Harare (cool, hot, rainy and post rain sub-seasons). Since Chapter 5 investigated LULC-LST relationship at seasonal time scales, Chapter 6 will look at a longer time scale (1984 to 2015).

CHAPTER 6: RESPONSES OF URBAN LAND SURFACE TEMPERATURES TO LONG TERM CHANGES IN LAND USE AND LAND COVER SPATIAL STRUCTURE

This chapter is based on:

Mushore T. D., Mutanga O., Odindi J., Dube T. (**2017**). Linking major shifts in land surface temperatures to long term land use and land cover changes in Harare, Zimbabwe. *Urban Climate*, 20, 120–134, http://dx.doi.org/10.1016/j.uclim.2017.04.005

6.0 Abstract

Rapid urban development is known to increase a landscape's thermal values, exposing residents to among others adverse heat related health impacts, discomfort as well as energy and water demand. Therefore, there is need to determine the implication of the transforming urban landscapes on urban micro-climate to optimise urban land uses and to effectively mitigate adverse impacts. In this study, we aimed at assessing dynamics of micro-climate caused by Land Use and Land Cover **(**LULC) changes in the heterogeneous Harare Metropolitan City, Zimbabwe, between 1984 and 2015. To achieve this objective, the transformation of major LULCs within the city was determined and relative brightness temperature used to assess long-term thermal changes in the city. Results show that coverage of high density residential areas increased by 92% between 1984 and 2016 at the expense of cooler green-spaces, which decreased by 75.5%. This translated to a 0.98^{o}C and 1.98^{o}C temperature increase, attributed to LULC changes alone and to all factors that include greenhouse effect and ozone depletion respectively. Results also show that converting bare areas to water bodies reduced surface temperatures by 4.5^{o}C, while the construction of low-to-medium density residential areas reduced bare surface temperatures by 3.78^{o}C. Conversion of green-spaces to low-medium residential areas increased temperatures by 0.16^{o}C. Overall, conversion of LULC types contributed more than 0.5^{o}C thermal elevation within the city, largely attributed to increases in built-up areas and reduction in heat mitigating green-spaces. These findings offer insight into landscape surface energy balance changes arising from urbanization, critical for urban planning, environmental governance as well and climate change management in cities.

Keywords: climate change, urbanization, land-use-land-cover, urban heat island, temperature increases, green-spaces, remote sensing

6.1 Introduction

Rising temperature and climate change have become a concern in the recent decades (Nayak & Mandal, 2012; Simone et al., 2011; Zvigadza et al., 2010; Hartmann et al., 2013; Chagutah, 2010). Rising temperatures lead to heat stress and increase in vector-borne diseases such as malaria and cholera, which may cause morbidity and mortality to vulnerable persons in society (Cuculeanu et al., 2002; Newland, 2011; McMichael & Confalonieri, 2012; Tanser et al., 2003; Simone, et al., 2011). Furthermore, an increase in urban temperatures causes accumulation of smog and deterioration of air quality, increases discomfort, affect work performance as well as outdoor and indoor activities and increase energy and water demands (Simone, et al., 2011; Goshayeshi, et al., 2013b; Yilmaz, 2007; Mazon, 2013; Mohan, et al., 2014; de-Azevedo, et al., 2015; Akbari, 2005). Therefore, understanding the implication of urban transformation on urban thermal change is necessary for mitigation of adverse impacts, urban planning, policy formulation and sustainable urban growth.

The observed and projected temperature intensity in Urban Heat Islands (UHI) can be attributed to natural phenomena that include the 60 year solar and thermohaline circulation. Such intensity can also be attributed to anthropogenic activities that include rise in atmospheric greenhouse gases and landscape transformations (Loehle, 2011; Hartmann, et al., 2013). Urbanization alters energy and water balance, resulting in higher temperatures at the city core and lower temperatures towards the urban fringe and rural areas (Nayak & Mandal, 2012; Ward et al., 2014; Dirmeyer et al., 2010; Sertel et al., 2011). Hence, there is need to determine the implication of urban growth on urban temperatures, particularly in developing countries where resources for adaptation and mitigation are largely limited. Whereas in situ observations offer accurate data for analysis of temperature trends, they have limited spatial coverage, making it expensive to achieve desired coverage especially in developing countries. These countries often have low station density, inadequate for interpolation to map thermal distribution in heterogeneous urban landscapes (Barrett et al., 2007). Conversely, remote sensing offers low cost archival data at relevant spatial resolution valuable for understanding the relationship between LULC and their respective thermal characteristics (Sithole & Odindi, 2015; Owen, et al., 1998). Landsat imagery data series for instance offers thermal and optical data dating back to 1972 free of charge (Gusso, et al., 2014; Tao, et al., 2013). However, despite availability of such datasets, their adoption in understanding the nexus between urbanization and climate change, particularly in African cities remains limited. Consequently, urban thermal elevation has mainly been associated with greenhouse gases and ozone depletion. Optical and thermal

remotely sensed data therefore provide a unique opportunity for understanding the implication of LULC transformation on urban thermal characteristics.

Generally, previous studies that have analysed the relationship between long term changes in surface UHI and land cover changes have mostly used the difference between rural and urban temperature as a measure of UHI effect (Feng et al., 2014; Ogashawara & Bastos, 2012; Zhang, et al., 2012). However, literature shows that comparing land surface temperature between rural and urban areas is not an effective method of quantifying UHI effect as rural areas around urban areas keep changing (Weng et al., 2007). Furthermore, long-term determination of rural/urban temperature differentiation for instance, considers combined thermal values for the entire urban landscape, dis-regarding the contribution of the changing LULC matrix and their thermal contribution to the UHI.

Feng (2014) recently suggested the use of different UHI indicators in determining long term effect of urban LULC transformation. As such, the relative brightness temperature has been proposed as an effective measure of UHI intensity, useful for monitoring shift in average temperature due to urbanization (Xu et al., 2013). The approach has numerous advantages which include computational simplicity and efficiency, as it is applied on brightness temperatures without emissivity correction. Hence this approach has been useful in determining the implication of LULC types on heat island intensities as well as their variations between season (Wu et al., 2012; Zhang, et al., 2012). Zhang, et al., (2012) for instance applied this approach to show the link between Normalized Difference Vegetation Index (NDVI) and urban heat island based on single date imagery in Wuhan city, China. The unique potential and strength of the of the relative brightness temperature has also been demonstrated by Xu et al (2013) who determined the responses of heat island intensity to seasonal changes in land surface properties derived from vegetation indices in Beijing, China. Despite the successful application of the relative brightness temperature approach in understanding multi-temporal relationship surface UHI and land cover changes, its link with long terms changes is necessary for urban landscape management needs to be further explored. Specifically, this will provide insight on the significance of urban LULC modification and how it combines with other factors such as increases in greenhouse gas concentrations to alter climate over time, useful for improving future climate prediction (Dirmeyer, et al., 2010; Ward, et al., 2014)

This study thus hypothesizes that changes in relative brightness temperature intensities can be reliably used to determine the impacts of urban LULC transformation on urban heat patterns

over a 30 year period (i.e. from 1984 to 2015). Differences in the distribution of relative heat island intensities between images obtained in different decades may be valuable in quantifying shift in temperature as the city grows between the periods. Hence the study sought to quantify long term changes in temperature due to urban growth using changes in the relative brightness temperature as an indicator of changes in the UHI intensity and distribution. Since urban temperature changes can be attributed to myriad factors, the study also attempted to isolate the impact LULC conversion on urban thermal values from other causes like rise in greenhouse, ozone depletion and solar cycles.

6.2 Materials and methods

6.2.1 Description of the study area

This study was conducted in Harare, the capital city of Zimbabwe (Figure 6.1). The city is experiencing growth as evidenced by increase in population and built up area (Kamusoko et al., 2013; ZIMSTAT, 2012). The urban core and industries are found at the centre while major roads radiate from the city centre. Settlements are more spacious in the north where mostly low and medium density residential suburbs are found (Wania, et al., 2014). The month of October is the hottest and driest while the summer season is noted to be warming and experiencing prolonged hot spells (Manatsa et al., 2013), hence the selection of the period.

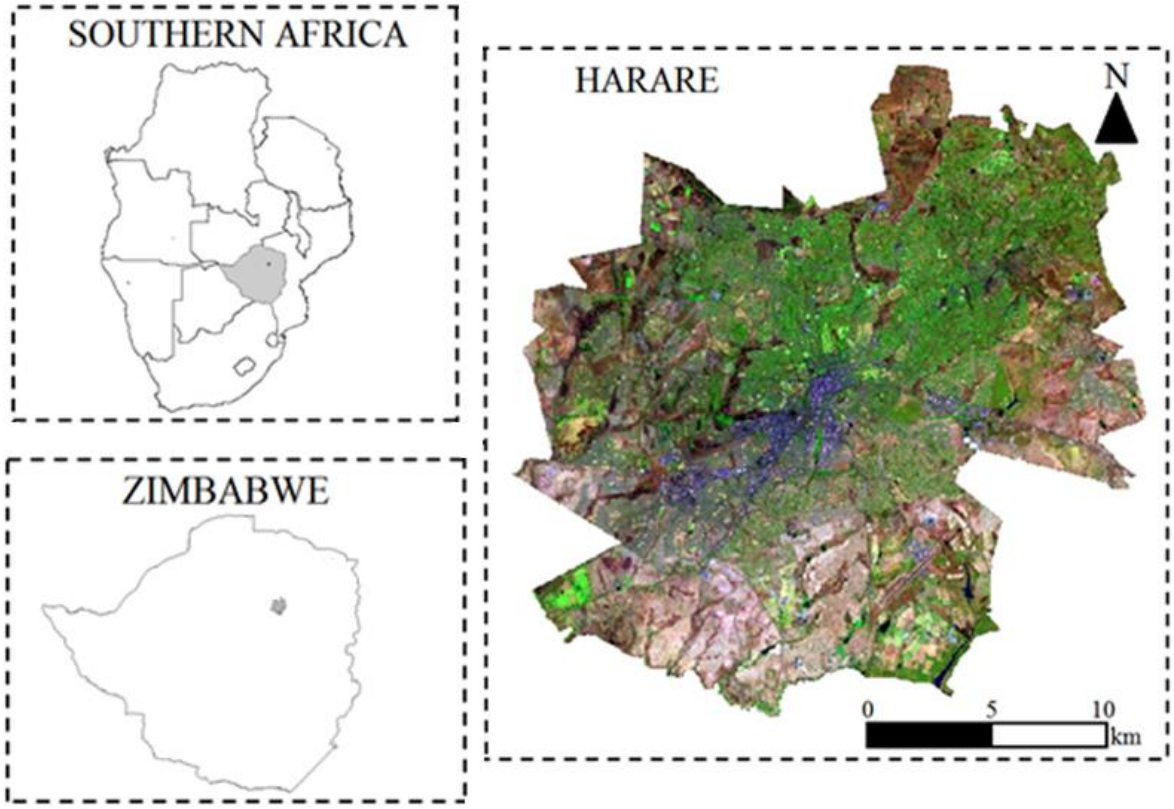

Figure 6.1: Location of the study area and general variations in spectral properties of land-cover regimes.

6.2.2 Pre-processing of remotely sensed data

Landsat Thematic Mapper TM 5, Landsat ETM+7 and Landsat 8 OLI and TIRS images with Path/Row of 170/72 were acquired from the United States Global Survey Earth Resources Observation System (USGS-EROS) website. Landsat data were selected due to adequate archival data, ease of access and previous performance in land cover classification and temperature analysis (Odindi et al., 2015). The 30 year time-span was selected in line with World Meteorological Organization's recommended length for climate change analysis (World Meteorological Organization, 2000, 2007). The image reflective bands were corrected for atmospheric effects using the Fast Line-of-sight Atmospheric Analysis of Spectral Hypercubes (FLAASH) module in the ENVI software (Dube & Mutanga, 2015a; Mushore, et al., 2016). The images were geometrically corrected using a 1:50 000 topo-sheet and 30 ground control points collected at intersection of major roads and invariant features recognisable on satellite images. The Landsat imagery used, as well as the meteorological condition at Harare Airport Meteorological Office during the time of Landsat acquisition are shown in Table 6.1.

Table 6.1: Landsat path/row 170/72 images used for temperature analysis in this study. Meteorological conditions at Harare Airport Meteorological Station are also presented.

Image	Date	Temperature (^{o}C)	Humidity (%)
Landsat 5	17 October 1984	28.4	37.0
Landsat 5	21 October 1993	28.7	33.0
Landsat 7	19 October 2001	28.6	36.3
Landsat 8	18 October 2015	29.0	42.0

6.2.3 Land use and cover classification, accuracy assessment and change detection

Land use land cover maps for the year 1984, 1993, 2001 and 2015 were derived using the 30m reflective bands of Landsat 5, 7 and 8 images. Ground truth data per LULC type for classification and accuracy assessment were obtained during a field survey as already described in Chapter 3. In order to improve accuracy classes with spectral similarities were merged following a separability test before classification using the Transformed Divergence Separability Index (TDSI) (Chemura & Mutanga, 2017; Matongera et al., 2017). According to Matongera, et al. (2017), the closer the TDSI to 2 the higher the separability of two LULC classes from each other using a specific remote sensing dataset. Value less than 1 implies that two LULC types are difficult to separate such that trying to do so will reduce classification accuracy. Separability test was thus done because high accurate classification is obtained when LULC classes are adequately separable for a given spatial resolution of remote sensing data.

This also enabled merging of classes that have similar spectral properties. As a result, contrary to Chapter 3 where seven general classes were used, in this Chapter the LULC were reduced to six major classes described in Table 6.2 after separability test. Supervised classification using the Support Vector Machine (SVM) algorithm was implemented to generate LULC maps for each of the years under investigation. The SVM algorithm places no assumption to the probability distribution of the data and has low training data requirements. The classifier was found in previous studies to be better than commonly used algorithms like Maximum Likelihood Classifier (MLC), Parallelepiped, Minimum Distance, Mahalanobis Distance and the Artificial Neural Network classifiers (Omran, 2012; Adelabu, et al., 2013).

Table 6.2: Description of LULC classes observed in Harare during field survey

LULC class	**Description**
CBD/Industrial (CBDI)	Areas with very high density of buildings and a very high proportion of impervious surface that include central business district and industrial areas.
High density residential (HDR)	High density residential areas and areas under residential development (bare or impervious) with low vegetation fraction.
Low-medium density residential (LMR)	Established low and medium density residential areas with high vegetation fraction.
Croplands (Cr)	Areas where intra-urban agriculture is practised including research sites which could be bare in the dry season
Green spaces (Gr)	Areas covered by grasslands and clusters of tree characterised by high vegetation fraction even during the dry season.
Water (Wt)	Areas covered by water bodies or wetlands.

Supervised classification requires field observation for training and accuracy assessment, therefore, 120 points per class were obtained from a field survey using a GPS between the 1st and 30th of April 2015. The points were split into training (80%) and validation (20%) based on recommendation by Adelabu et al. (2013). Regions of interest (polygons created around ground truth points) were used instead of points to increase the number of sample points upon which to base classification and validation. Acharya et al., (2015) showed that higher accuracy is achieved using regions of interest than points. Accuracy was assessed using the kappa coefficient by comparing mapped LULC classes with field observations, expert knowledge and auxiliary LULC data from topo-sheets and aerial photographs. LULC changes were analysed using visual inspection and calculation of changes in spatial coverage.

6.2.4 Derivation of thermal characteristics

We adopted stages of retrieving temperature from Landsat data series which include the conversion of digital numbers of thermal bands to thermal radiances, calculation of brightness temperature and emissivity correction (Sobrino, et al., 2004). We used thermal Band 6 of Landsat 5 for 1984 and 1993, Band 6 of Landsat 7 for 2001 and Band 10 of Landsat 8 for 2015 for analysis. The surface emissivity maps used to compute surface temperature from brightness temperature were derived using Normalized Difference Vegetation Index (NDVI) for each period (Jiang & Tian, 2010). The land surface temperatures were used to derive the relative radiative temperature with respect to the average of 1984 using equation 1 (Zhang, et al., 2012; Xu, et al., 2013).

$$\boldsymbol{T_{R,n}} = \frac{\boldsymbol{T_n - T_{mean,1984}}}{\boldsymbol{T_{mean,1984}}} \qquad \text{Equation 6.1}$$

Where T_n is the temperature at a point year n, $T_{R,n}$ is the relative temperature in year n and n is the year for example 2015. The average temperature of 1984 was used as a reference when LULC distribution had not been significantly modified by urbanization. In order to compare heat island distribution of a year with that of 1984, we computed the spatial distribution of relative radiative temperatures for four periods in different decades. For ease of comparison, the relative temperatures were further classified into categories described in Table 6.3 as recommended by Zhang, et al., (2012).

Table 6.3: Description of relative temperature level

UHI level	Description
Less than 0	Green Island
0 – 0.005	Weak heat island
0.005 – 0.010	Strong heat island
0.010 – 0.015	Stronger heat island
0.015 – 0.020	Strongest heat island
Greater than 0.020	Violent heat island

6.2.5 Responses of temperature to LULC changes

We calculated average temperature of each class for each year collected from points evenly distributed across the study area to capture all possible inter- and intra-class variations. We further calculated the difference between the average temperature in 1984 and 2015 for each land cover. The differences were attributed to other anthropogenic factors than land cover changes. In order to determine the change in average temperature, due to change from LULC changes, we used the normalized difference in temperature to correct for influence of other

anthropogenic factors. This was computed using the equations adapted from Zhou & Wang (2010) and expressed as;

$$\boldsymbol{dT_{ij} = T_{j2015} - T_{i1984}} \quad \text{Equation 6.2}$$

$$\boldsymbol{\Delta T_i = T_{i2015} - T_{i1984}} \quad \text{Equation 6.3}$$

$$\boldsymbol{dT_n = dT_{ij} - \Delta T_i} \quad \text{Equation 6.4}$$

Where dT_n is the change in temperature cause by replacement of i by land cover j, ΔT_i is the change due to other anthropogenic factors than LULC change and dT_{ij} is the change in temperature before normalization.

6.2.6 Changes in the contribution of land cover to the thermal environment in the city

The proportional contribution of land covers to the thermal characteristics was expressed using the contribution index (CI) based on Equation 6.5 (Odindi, et al., 2015; Chen, et al., 2006).

$$\boldsymbol{CI = D_t \times S} \quad \text{Equation 6.5}$$

Where D_t is the difference between the average temperature of the entire study area and the average of the LULC class type. Variable S is the proportional area of the LULC type, which is the ratio of the area covered by the class to the total area of the study. Positive values of CI indicate how much the LULC type contributes to raising the surface temperatures of an area while negative values indicate heat mitigation value. The CI was computed from the year 1984 to 2015 using the same value of D_t but varying for each land cover. The assumption was that the changes in the contribution of LULC were not due to changes in average temperatures, but as a result of changes in proportional areas covered. The assumption was made in order to eliminate the contribution of other external factors, such as ozone depletion and greenhouse gas concentrations.

6.2.7 Normalized change in average temperature due to land cover changes

We proposed a technique to derive changes in average temperature solely due to LULC changes that excludes changes in other contributing factors to surface temperature rises. In this technique, we assumed that contribution of LULC changes was due to changes in proportional area covered between the year 1986 and 2015. The proposed normalized average temperature of the study area was computed using the Equation 6.6 (Feng, et al., 2014).

$$\boldsymbol{LST_{average,k} = \frac{\sum_i S_{i,k} \times T_{i,j}}{\sum_i S_{i,k}}} \quad \text{Equation 6.6}$$

Where $LST_{average,k}$ is the average temperature of the study area in year *k*. $T_{i,j}$ is the average temperature of the land cover type *i* in year *j* before land cover changes took place and $S_{i,k}$ is the proportional area of land cover type *i* in year *k*. We compared the change in temperature of the study area from the year 1984 to 2015 with and without normalization. This provided both a measure of how LULC alone and how a composite of contributing factors changed the average temperature of the study area.

6.3 Results and discussion

6.3.1 Changes in LULC distribution between 1984 and 2015

The city's LULC maps for 1984, 1993, 2001 and 2015 were produced at high accuracy using the SVM algorithm (Figure 6.2). Validation showed an overall accuracy of 88.55%, while the kappa was 0.85 for the year 1984 image. Table 6.4 shows the accuracy of remote sensing based urban LULC mapping in 1993, 2001 and 2015 classifications, respectively. The overall LULC classification accuracies for all the years under study were higher than the recommended 80% threshold (Omran, 2012). High LULC classification accuracy can be attributed to the superior performance of the SVM classifier, in comparison to other existing methods like the Maximum Likelihood, Artificial Neural Network and Parallelepiped classier (Adelabu, et al., 2013; Omran, 2012). The high accuracy can further be attributed to use of regions of interest for training the classification, an approach known to increase mapping accuracy (Acharya, et al., 2015).

Table 6.4: Accuracy of multi-temporal remote sensing based land use/cover classification

Year	Overall Accuracy (%)	Kappa coefficient
1984	88.55	0.85
1993	87.70	0.83
2001	90.86	0.87
2015	87.59	0.82

Producer accuracies were greater than 75%, except for the croplands class, which had producer accuracies less than 50% in 1993, 2001 and 2015. User accuracies were greater than 80% for most LULC classes except in the year 1993 and 2001, when croplands had overall accuracies of 69.13% and 72.66%, respectively. These accuracies are comparable with the 85 and 95% achieved by Kamusoko et al (2014) in classifying the city's built-up and non-built areas. Their slightly higher classification accuracy can be attributed to a two class LULC generation. Harare has seen expansion of built-up areas at the expense of water/wetlands, green-spaces and croplands. In this study we also managed to separate built-up areas into densely built

(CBD/Industrial), high density residential and low-medium density residential. Visual inspection of the LULC maps showed a decline in green spaces and expansion of residential areas in the study area between 1984 and 2015. Most of the areas which were occupied by croplands and green spaces in the year 1984 had been converted to residential developments.

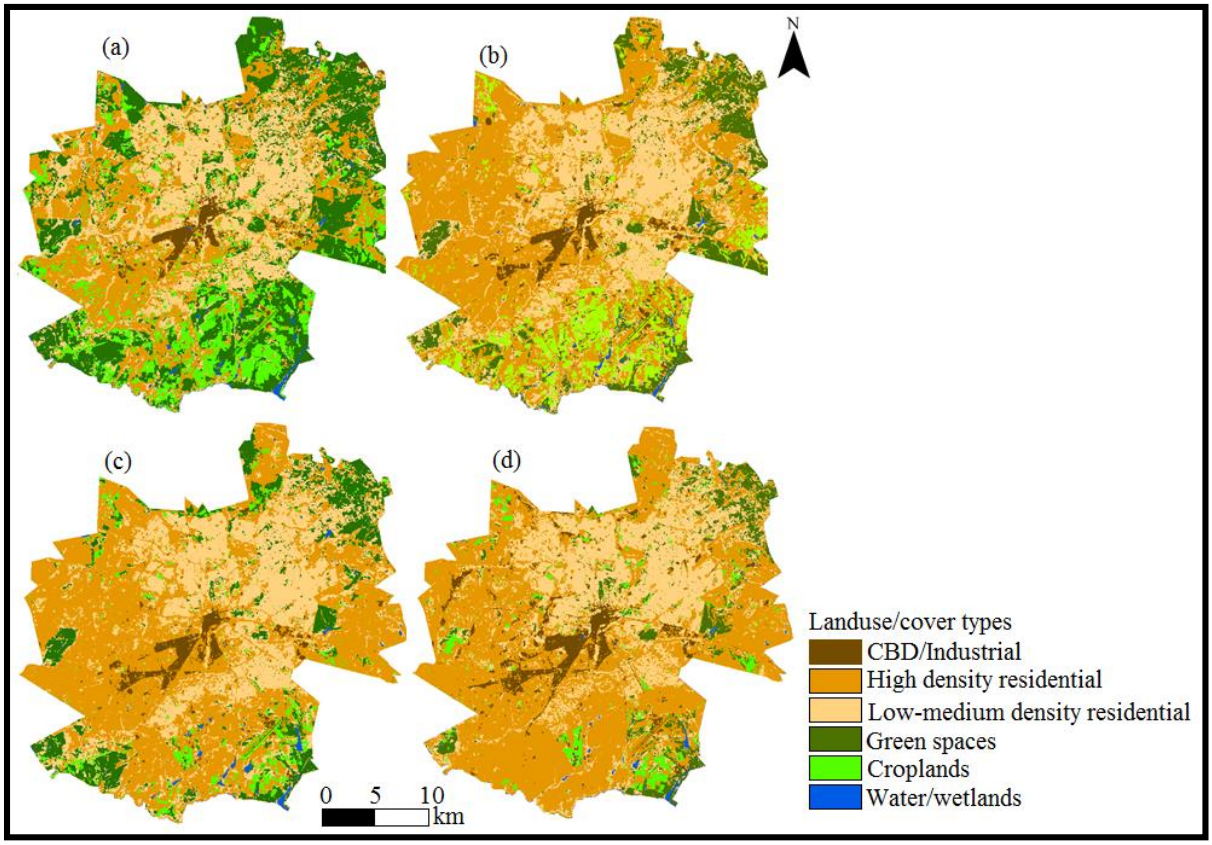

Figure 6.2: The distribution of LULC types in the year (a) 1984, (b) 1993, (c) 2001 and (d) 2015 in Harare, Zimbabwe.

Table 6.5 shows that built up areas increased in coverage, while the proportion of land area occupied by croplands, green-spaces and water decreased during the study. For example, between 1984 and 1993, high density residential areas increased from 385.48 to 244.24km^2, while green-spaces decreased from 234.38 to 105.09km^2. Cropland decreased from 110.54 to 30.27km^2 between the same periods. The observed growth is consistent with Wania et al., (2014) and Kamusoko et al., (2013) who noted that the built up proportion has increased in Harare since independence. The LULC maps are also consistent with Kamusoko et al (2014) who note that low density residential areas mostly cover the northern while high density residential southern parts of the city. Water bodies decreased from 6.98 to 4.15km^2 during the same time while impervious surfaces under commercial use (CBD/Industrial areas) grew from 23 to 48.92km^2 over the thirty year period. The decrease in coverage of the water class may

signify intrusion into wetlands by built-up and impervious areas as the city continues to grow. The decrease in the water class coverage may also be due to water contamination by among others algal bloom, common in urban areas that changes spectral properties on water bodies, thus reducing proportion of water pixels (Dube, et al., 2014).

Table 6.5: Changes in proportion of LULC types between 1984 and 2015.

	Coverage (km^2)			
UHI level	**1984**	**1993**	**2001**	**2015**
CBD/Industrial	23.00	25.64	24.74	48.92
High density residential	244.24	385.48	441.84	470.02
Low-medium density residential	235.68	253.52	255.11	244.05
Green-spaces	234.38	105.09	94.73	57.42
Croplands	110.54	80.92	33.17	30.27
Water	6.98	4.18	5.24	4.15

6.3.2 Changes in Land surface temperatures between 1984 and 2015

Table 6.6 shows that surface temperatures increased between 1984 and 2015, with larger increases observed over built up areas than in areas covered by vegetation and water. Land surface temperature increased by 3.29^{o}C in the CBD/Industrial areas and 1.51^{o}C over green-spaces during the study period. Lowest increases in temperature were observed over water surfaces (0.74^{o}C) croplands (0.86^{o}C) and green spaces (1.51^{o}C). Magnitude of temperature rises also differed between residential types, with high and low density residential areas experiencing a rise by 2.55^{o}C and 1.7^{o}C respectively. Temperature changes were also found to be faster in built-up than in other areas (Ogrin & Krevs, 2015). Built-up and impervious areas have high Bowen's ratio (close to I), thus favouring sensible heat transfer and absorption of high proportion of incident radiation (Gusso, et al., 2014).

High temperatures were observed in the CBD and industrial areas compared to other LULC types in 1984 (38.19^{o}C) and 2015 (41.48^{o}C). As aforementioned, areas with a higher density of buildings have high Bowen's ratio (above 1) implying high radiant heat transfer, due to very low latent heat transfer (Zhou & Wang, 2011a; Jalan & Sharma, 2014; Owen, et al., 1998). Furthermore, tall buildings increase surface roughness and reduce ventilation thereby reducing heat removal by advection and radiative cooling, thus increasing temperature (Tursilowati, 2007; Sithole & Odindi, 2015; Cinar, 2015).

Low temperatures were observed on areas covered by water (32.54 in 1984 and 33.28 2015) and over green spaces (33.47^{o}C in 1984 and 34.93^{o}C in 2015). Green-spaces tend to be porous

and assimilate heat, hence act as heat sinks (Odindi, et al., 2015; Sithole & Odindi, 2015). In this study, thermal difference between water and green-spaces was smaller than other LULCs. This finding concurs with other studies which observed small differences in temperature between dense vegetation and wetlands (Adebowale & Kayode, 2015). Both have cooling effect as they promote heat removal by latent heat transfer, thus reducing sensible and ground heat flux (Adebowale & Kayode, 2015). The evaporation cooling effect was also observed in low density residential areas as they have higher vegetation fraction than densely built-up areas (Mushore, et al., 2016). During the hot season, croplands are largely bare resulting in high temperatures compared to vegetation surfaces. This is because their surface temperature increases, approaching that of bare areas due to reduced vegetation (Xiao, et al., 2007).

Table 6.6: Observed increases in land surface temperature between the year 1984 and 2015.

	Temperature (ºC)		Temperature
Landuse and land cover	**1984**	**2015**	**change (ºC)**
CBD/Industrial	38.19	41.48	3.29
High density residential	37.09	39.64	2.55
Low-medium density residential	34.31	36.01	1.70
Croplands	37.34	38.20	0.86
Green-spaces	33.47	34.98	1.51
Water	32.54	33.28	0.74

6.3.3 Changes in distribution of relative temperatures (surface heat island intensities) between the year 1984 and 2015

The heat island effect became more intense in 2001 and 2015 than 1984 and 1993 as indicated by the relative temperature in Figure 6.3. Figure 6.3(a) shows a larger spatial extent covered by green islands (relative temperatures below 0), than in Figure 6.3(b). There were fewer violent heat islands (relative brightness temperature above 0.02) in 1984 (Figure 6.3(a)), 1993 (Figure 6.3(b)), 2001 (Figure 6.3(c)) than in 2015 (Figure 6.3(d)). In 2015, the heat islands became high (at least 0.01), stretching from the core to the south-western part of the city. However, the northern half of the city generally had more green islands extents than the rest of the city, especially in 2001 and 2015. Generally, in 1984, the relative radiant temperatures were generally higher in the south-western areas (mostly between 0.005 and 0.015), than in the northern areas (below mostly 0.05). The northern areas are mostly occupied by middle and high income earners (Kamusoko, et al., 2013) who can afford to protect and maintain greenery, thus benefiting from its cooling effect. A study by (Cai, et al., 2011) observed high urban heat island intensities in areas of high building density and other impervious surfaces and low heat intensities on grasslands, trees and water bodies.

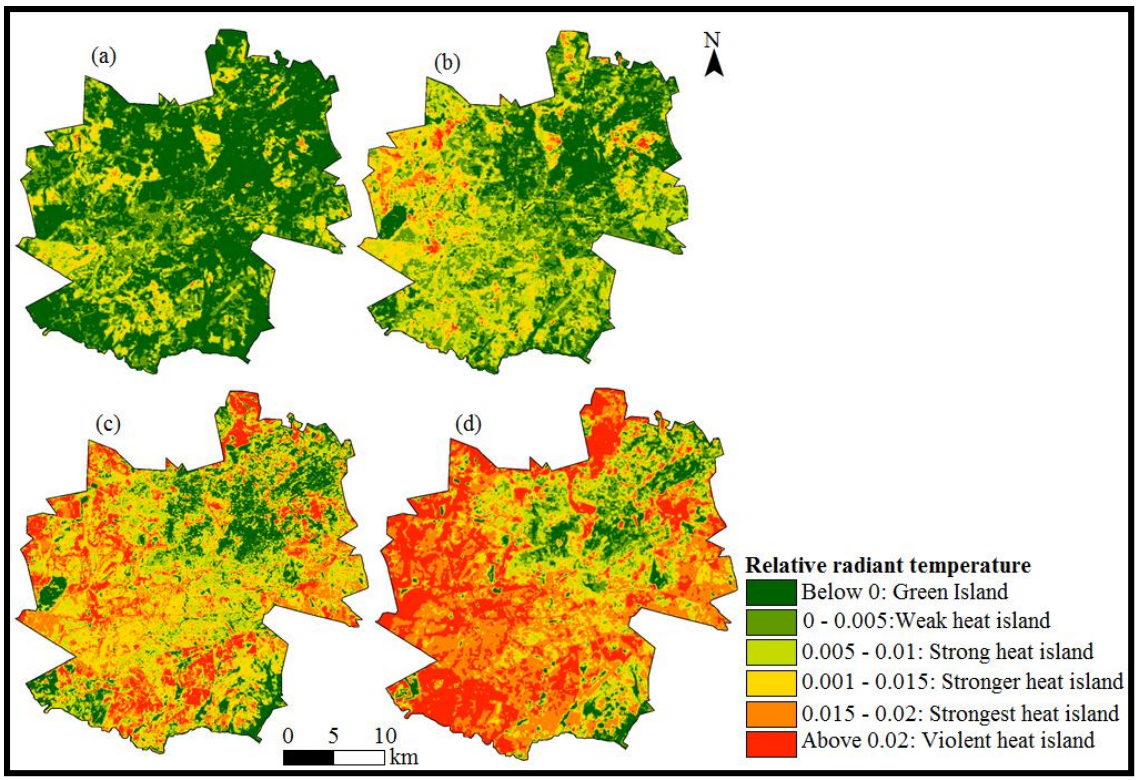

Figure 6.3: Distribution of relative heat intensities in the year (a) 1984, (b) 1993, (c) 2001 and (d) 2015.

The green island proportion decreased from 54.95 to 5.57%, while the violent level of UHI (relative radiant temperature above 0.02) increased from 0.01% to 26.18% from 1984 to 2015 (Table 6.7). In 1984 and 1993, green and weak heat islands (relative radiant temperatures below 0.005) covered more than 50% of the total area while stronger to violent heat islands occupied less than 20%. Strong to violent UHI levels increased in coverage from below 20% in 1984 to above 70% of the total area in the year 2015, implying that a significant proportion of Harare warmed significantly between 1984 and 2015. This finding is in agreement with the known increase in heating island coverage due to effect of impervious surfaces as urbanized area expands (Li et al., 2012; Zhang, Qi, et al., 2013). Expansion of surface urban heat island as the city expands is also in tandem with observation in the expanding Lahore District, Pakistan between 2000 and 2011 (Sha & Ghauri, 2015).

Table 6.7: Proportion covered by UHI levels in 1984 and 2015 in Harare.

	Proportion (%)			
UHI level	**1984**	**1993**	**2001**	**2015**
Green Island	54.95	23.94	13.41	5.57
Weak	24.82	29.05	7.84	8.13
Strong	12.48	26.18	19.39	11.58
Stronger	7.31	16.49	28.90	15.31
Strongest	0.44	3.44	18.74	33.23

Violent	0.01	0.90	11.72	26.18

6.3.4 Changes in the contribution of LULC types to thermal characteristics of Harare

The major contribution to warming in the city comes from high density residential areas, due to their larger coverage, than CBD/industrial areas (Figure 6.4). The warming is explained for example by the contribution index for high density residential areas which increased from 0.457 in 1984 to 0.879 in 2015. In 1984, green-spaces had the largest cooling effect which has been replaced by residential areas. The cooling contribution of green-spaces in the city has reduced from -0.553 in 1984 to -0.133 in 2015 (Figure 6.4). On the contrary, the cooling contribution of low-medium density residential areas increased slightly between the periods as evidenced by a negative contribution index of -0.324 in 1984 to -0.337 in 2015. During the hot season, surrounding croplands are mostly left bare, warming the city as indicated by positive CI values in 1984, 1993, 2001 and 2015. Most of the croplands have been converted to built-up areas, mainly high density residential areas, resulting in a reduction of the contribution to summer warming from CI value of 0.239 in 1984 to 0.066 in 2015. The contribution of water/wetlands to cooling was more in 1984 (-0.242) than in 1993 (-0.144), 2001 (-0.167) and 2015 (-0.145). Consistent with previous studies, CI was negative in vegetation and water covered areas and positive in areas with high building density (Xu, et al., 2013). However, CI was also negative in low-medium density residential areas, due to cooling effect of vegetation as these areas have high vegetation fraction (Mushore, et al., 2016). This observation agrees with decreases in the cooling effect of vegetation as their coverage was reduced by replacement with buildings between 1984 and 2015.

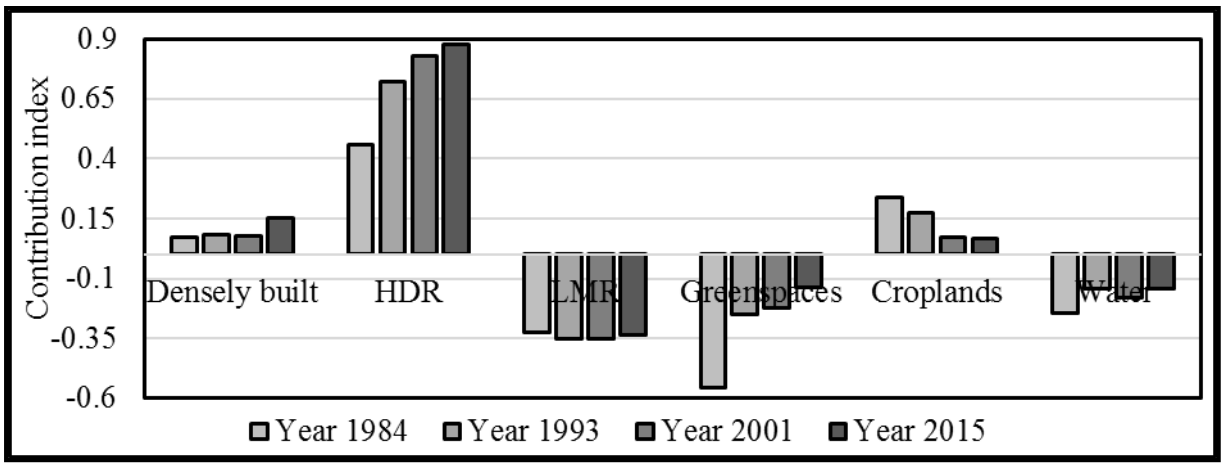

Figure 6.4: Contribution of LULC types and their changes to heating in Harare. *HDR: high density residential areas and *LMR: low-medium density residential areas

6.3.5 Normalized effect of land cover transformation on temperature of a location

Results in Table 6.8 show that changing from cropland to low-medium density residential reduces temperature of the converted area by 4.03^{o}C while conversions of low-medium to high density residential areas raise temperature by 3.78^{o}C. The constructions of CBD/Industrial areas within low-medium density residential areas raise temperature of the area by 2.88^{o}C. A very large reduction of 4.88^{o}C would be experienced by converting a high density residential area portion to a water body. On the contrary, very small changes in temperature occur when industries are constructed in high density residential areas (0.90^{o}C) as well as when green-spaces are converted to low-medium density residential areas (-0.16^{o}C). The small change is consistent with Adebowale and Kayode (2015) who observed that the thermal characteristics of high vegetation density closely resemble those of water bodies. Similarly, conversion of bare to industrial areas also resulted in small change in temperature (0.90^{o}C) during the hot season. Bare areas, which include land cleared for construction, are often dry during the hot season, resulting in high radiant heat transfer which almost equates that of areas with high building density. Rasul et al., (2015) observed that bare areas are as warm as built up areas with low vegetation cover. Other studies (Grossman-Clarke et al., 2010; Weng et al., 2007) also observed large changes in temperature when natural surfaces were replaced with buildings and impervious material. For example, Grossman-Clarke et al. (2010) observed that conversion of vegetated areas to built-up and impervious surfaces increases daytime temperatures by 2-4^{o}C.

Table 6.8: The matrix for normalised changes in average temperature per LULC conversion scenario.

Converted to	**Initial land use and land cover class**					
	CBD/ Industrial	High density	Low-medium	Croplands	Green-spaces	Water
CDB/Industrial	0	-0.9	2.88	-1.15	2.72	3.65
High density	0.9	0	3.78	-0.25	3.62	4.55
Low-medium	-2.88	-3.78	0	-4.03	-0.16	0.77
Croplands	1.15	0.25	4.03	0	3.87	4.80
Green-spaces	-2.72	-3.62	0.16	-3.87	0	0.93
Water	-3.65	-4.55	-0.77	-4.80	-0.93	0

*Low-medium: low-medium density residential areas *High density: High density residential areas

6.3.6 Normalized change in average temperature of Harare in response to LULC changes

Results in Figure 6.5 show that in absence of other anthropogenic and natural effects, LULC would still have increased the average land surface temperature of Harare by 0.98^{o}C. However,

due to a combination of LULC changes and other factors, the temperature increased by close to 1.9^{o}C during the entire study period. It should however be noted that the implication of other factors were not measured in this study, which made it difficult to further isolate natural effects from other anthropogenic effects, such as changes in greenhouse gas concentrations. The temperature increase due to LULC conversion is consistent with literature, for instance Grossman-Clarke, et al. (2010) noted that urbanization can raise daytime surface temperatures by 2 to 4^{o}C. Sweden for instance experienced a 1.6^{o}C increase in temperature between 1951 and 2000, while Turkey experienced a rise of 0.5-1.5^{o}C between 1975 and 2005 due to population growth, urbanization and LULC changes (Elmhagen et al., 2015; Sertel, et al., 2011). Similarly, eastern Australia recorded summer warming of 0.4-2^{o}C from 1951 to 2003 (Mcalpine et al., 2007). Findings in this study are also consistent with existing literature which suggest that anthropogenic influences account for a larger proportion (above 90%) of causes of temperature rises than natural causes (Loehle, 2011; Hartmann, et al., 2013).

When all climate forcing factors are considered, the temperature increased by approximately 1.9^{o}C between 1984 and 2015. In consistency with Ahmed et al., (2013) and Zhou & Wang, (2011), temperature changes were observed even in areas with no LULC conversion, implying that modification of urban land surface is not the only cause of temperature increase. However, modification of surface characteristics may enhance the background effect of global warming. This is based on the notion that anthropogenic heat emissions increase with built extent and that heat island raises temperature and induces global warming (Blake, Curitiba, et al., 2011). Our findings concur with the view that LULC changes significantly modify temperature of an area and also magnify warming due to increases in long wave radiation in the lower atmosphere (Nayak & Mandal, 2012).

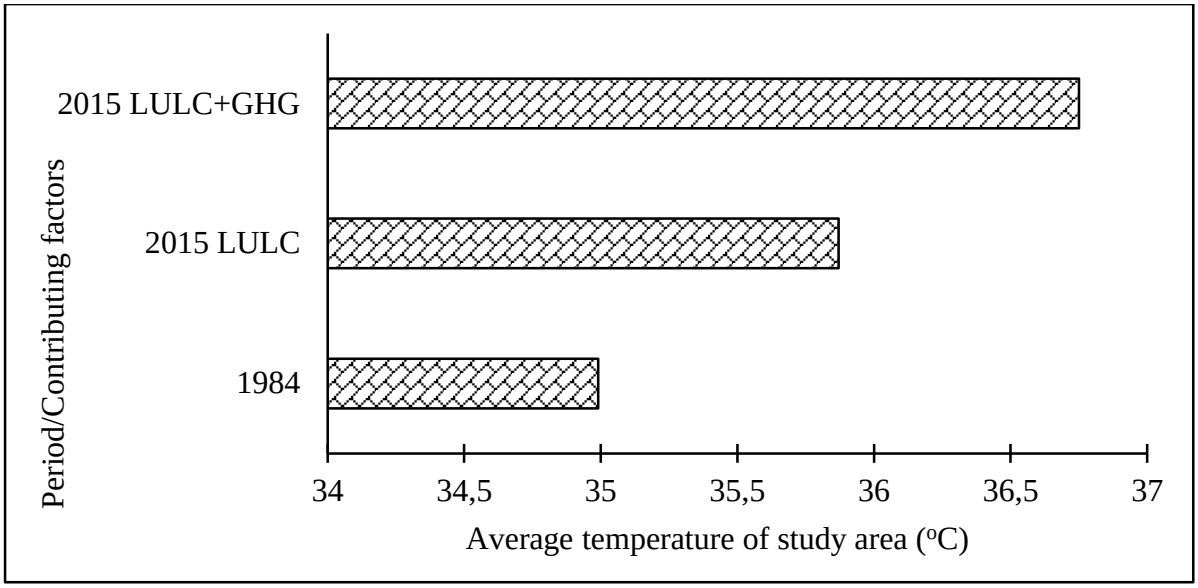

Figure 6.5: Normalized link between LULC changes and changes in temperature.

Overall, increase in proportion of an urban area occupied by buildings, dry bare areas and impervious surfaces caused and increase in temperature within Harare. Urban LULC changes in the form of expansion of built-up and impervious area significantly changes the temperature of a city. This influence exchange of energy and modifies the transfer of energy and moisture between the land surface and the atmosphere (Nayak & Mandal, 2012). The transformation also exposes the area to further rises in temperature. Moisture and surface wetness play significant role in reducing temperature. The overall value of green-spaces and wetlands to mitigate temperature rises depends on the proportion of the city which they occupy (Rasul, et al., 2015).

6.4 Conclusions

Utilizing the benefit of archival Landsat series data, the following conclusions can be drawn from the study;

1. Land cover conversion accounts for a significant proportion of changes in temperature due to urban growth,
2. The observed intra-class increases in temperature are indicative of the influence of the effect of other factors, than LULC conversion, such as ozone depletion,
3. Larger rises in temperature over a thirty-year period were observed in built than in non-built environments, and
4. Residential built densification influenced temperature changes i.e. larger changes were observed in high density than low-medium density residential areas.

6.5 Link between Chapter 6 and other chapters

Chapter 5 established the responses heat island intensities to seasonal LULC changes in Harare and obtained that other seasons have tolerable heat island intensities than the hot season. This is in the background of long term rising temperatures hence the need to investigate impact of global warming on heat island intensities. Chapter 6 thus investigated the long term implications of historical changes in LULC on land surface temperatures. The findings showed that urban growth results in expansion of areas which experience high land surface temperatures in the hot season. Growth of high density residential areas with high built-up proportion has resulted in intense heat islands in these areas which are also expanding with time. The study paved way for the need to understand the potential socio-economic implications leading to Chapter 7 which assessed the potential effect of these changes on air conditioning energy demand.

CHAPTER 7: ASSESSMENT OF IMPACT OF URBAN LAND SURFACE TEMPERATURE CHANGES ON INDOOR AIR-CONDITIONING ENERGY DEMAND IN A RESOURCE

This chapter is based on:

Mushore T. D., Odindi J., Dube T., Mutanga O. (**2017**). Understanding the relationship between urban outdoor temperatures and indoor air-conditioning energy demand in Zimbabwe. *Sustainable Cities and Society Journal*, 34, 97-108, http://dx.doi.org/10.1016/j.scs.2017.06.007

7.0 Abstract

Urbanization causes thermal elevation which increase household energy consumption through air conditioning to reduce human heat stress. The objective of this study was thus to quantify the long term changes in potential energy requirements for indoor space warming and cooling in the built environment of Harare using remotely sensed satellite data. Landsat and in-situ temperature data were used to determine land use and land cover distribution, as well as to estimate trends in air conditioning energy requirements between 1984 and 2015. Daytime Heating Degree Days (HDD) and the Cooling Degree Days (CDD) derived from Landsat thermal data and in situ temperature measurements were used as a measure of indoor heating and cooling energy in the cool and hot season, respectively. Due to surface alterations from urban growth between 1984 and 2015, surface temperature increased on average by 2.26^{o}C and by 4.10^{o}C in the cool and hot season, respectively. This decreased potential indoor heating energy needed in the cool season by 1 degree day and increased indoor cooling energy during the hot season by 3 degree days. In-situ observations revealed that energy consumption in residential areas of Harare increases with temperature in summer and the opposite in winter. Findings in this are important for implementation of mechanisms to rationalize power supply based on spatial differences in levels of need for air conditioning. The findings are also relevant for authorities to devise measures to capacitate the most vulnerable societies, such as by subsidizing electricity for the urban poor, and ensure that they are protected from stress due to low or high temperature.

Keywords: Urbanization, heat island, climate change, thermal, heating degree day, cooling degree days

7.1 Introduction

Urbanization-induced land use and land cover (LULC) distribution and change alter the energy and water balances, causing thermal elevation as natural covers are replaced by impervious surfaces (Nayak & Mandal, 2012). Built up areas absorb and radiate high amounts of heat energy while green-spaces act as heat sinks as they are porous and assimilate local heat (Sithole & Odindi, 2015). Furthermore, preferential heating of the city, in comparison to the surrounding creates convectional currents which further trap heat (Tursilowati, 2007). Generally, elevated temperatures increase resident's thermal discomfort as well as heat related diseases and mortality (Guhathakurta & Gober, 2007; McDonald et al., 2011a; Hallegatte & Corfee-Morlot, 2010). Urbanization also increases economic strain, particularly in developing countries, as necessary interventions are required to cope with thermal change related impacts (Brown., et al., 2012). Depending on the season, urban thermal characteristics influence energy demand for indoor heating and cooling to ensure human comfort. Thermal elevation arising from urbanization may therefore alter energy requirements due to increased built-up density. Increased energy requirements to mitigate household thermal elevation like air-conditioning have been associated with rise in greenhouse gas concentration which further raised temperature and household cooling energy demand. Hence there is need to monitor responses of energy demand to localized warming for sustainable urban growth and management of risks associated with indoor thermal discomfort.

Several studies have attempted to estimate the impact of urbanization on energy consumption for heating and cooling, however, each approach has its own limitation. Among others, studies have utilized household electricity bills to determine impact of urban growth on energy consumption through air conditioning (Hirano, et al., 2009; Souza, et al., 2009; Shahmohamadi, et al., 2010; Arifwidodo & Chandrasiri, 2015). Shahmohamadi et al. (2010) for instance established that energy consumption in the United Kingdom, United States of America and Sri Lanka household energy consumption increased with land surface temperature and intensification of urban heat island (UHI). However, the major limitation of this approach is that household electricity usage is not restricted to air conditioning but include other usage like refrigeration, lighting and cooking (Ewing & Rong, 2008). Degree Days derived from temperature have also been as a proxy for energy requirement for indoor cooling or heating (Vardoulakis, et al., 2013; Arifwidodo & Chandrasiri, 2015; Ewing & Rong, 2008). Degree Days are based on a base temperature below or above which human discomfort is triggered, thus a direct measure of need for space heating and cooling (Bolattürk, 2008). Cooling Degree

Days (CDD) provide a measure for energy for space cooling while Heating Degree Days (HDD) infer energy for household warming (Christenson, et al., 2006). Degree Days strongly relate with energy consumptions. (Balaras, et al., 2005) for instance found a strong positive correlation between CDD and energy in European cities. However, a major limitation in the adoption of Degree Days in previous studies is the use of in-situ measurements of temperature, characterized by limited spatial coverage (Stathopoulou, et al., 2006). (Stathopoulou, et al., 2006) for instance, noted that even in developed countries multiple meteorological stations within $1km^2$ are rare. Hence in-situ observations are commonly unrepresentative and unable to capture temperature variation, especially in urban landscapes characterized by heterogeneous land-use-land-cover types with high thermal variability (Ogrin & Krevs, 2015). This limitation is even worse in most developing countries, especially in Africa, often characterized by limited meteorological stations coverage, in-adequate to effectively depict urban landscape heterogeneity (Owen, et al., 1998; Shahmohamadi, et al., 2010; Tao, et al., 2013; Zhou & Wang, 2011a).

The emergence of thermal space-borne remotely sensed data offer great potential in determining intra-urban thermal characteristics, hence spatial characterization of space heating requirements. Furthermore remotely sensed data offer a cost effective means for spatio-temporal analysis and a rich archival data, spanning over 30 years, valuable for climate change analysis (Senanayake, et al., 2013; Tao, et al., 2013; Owen, et al., 1998). However, despite the proliferation of remotely sensed data, its spatial coverage and improvements in data quality such as in radiometric resolution, its adoption to estimate trends in cooling and heating energy has remained limited. To the best of our knowledge, only a single study (Stathopoulou, et al., 2006) has used satellite data to estimate energy consumption in space cooling using Degree Days. In their study, Stathopoulou, et al. (2006) used National Oceanic and Atmospheric Administration's (NOAA) Advanced Very High Resolution Radiometer (AVHRR) thermal data and estimated Cooling Degree Days (CDD) with an error of 2.2 degree cooling days when compared to retrievals from in-situ temperature data. Furthermore, they obtained a strong correlation (R^2=0.78) between estimated and observed CDD for a base temperature of 25 ^oC. However, NOAA AVHRR has low spatial resolution of 1.1 km, which may cause errors due to an assumption of uniform temperature over a relatively large and heterogeneous area that often, characterize urban landscapes. Therefore, medium resolution Landsat series data offer great potential to improve estimation of energy requirements for indoor cooling and heating.

Although not yet used to estimate Degree Days, Landsat data has been instrumental in the estimation of spatial and temporal variations of temperature even in complex urban environments. Landsat has long history of freely-downloadable archival data dating back to 1972, making the series suitable for temperature estimation at single day, seasonal and long term temporal scales (Gusso, et al., 2014; Tao, et al., 2013). In comparison to in-situ observations, surface temperatures estimated from Landsat are on cloud-free days enabling estimation of extreme energy consumption levels. The spatial resolution of the thermal data enables mapping of variations in energy demands between built-up regimes. This is important for identifying the most vulnerable strata and communities, power supply rationalization and in designing of future housing. Furthermore, at the spatial resolution of thermal data from Landsat missions, temperature is estimated over comparatively smaller units than using NOAA AVHRR thus capable of improving accuracy of measurement of Degree Days satellites in urban areas. This is made possible by the capability of Landsat data to produce detailed maps of both LULC and potential thermal stress. At the spatial resolution of multi-spectral data from Landsat, it is possible not only to extract built-up areas but also to further zone them based on characteristics such as density of buildings and vegetation cover fraction. This is important in accurately mapping the complex urban thermal characteristics as well as their impacts which vary within short space. We therefore hypothesize that Landsat data with lower spatial resolution can quantify Degree Days and air-conditioning energy demand in complex urban settings better than in-situ observations.

The objective of this study was thus to quantify the impact of urbanization on energy consumption for indoor heating and cooling energy in Harare, an emerging African city, using remotely sensed data. Specifically, the study adopts LULC changes between 1984 and 2015 to quantify the city's growth and monitors subsequent response of energy consumption. The study achieves this by quantifying differences in heating and cooling energy requirements based on built-up categories, i.e. Central Business District, high, medium and low density residential areas. The study thus presents a novel approach of estimating Heating and Cooling Degree Days as well as their link with actual energy consumption using medium resolution space-borne satellite remote sensing datasets.

7.2 Materials and methods

7.2.1 Description of the study area

The study was conducted in Harare, the capital city of Zimbabwe (Figure 7.1). Settlement regimes in the city are closely linked with income and the northern half of the city is mainly occupied by moderate to high income earners (Wania, et al., 2014). The city has a humid sub-tropical climate with an average temperature of 18^{o}C and mean rainfall of 850mm (Iied, 2011). It experiences four sub-seasons namely, the rainy season, post-rainy season, cool season and the hot season (Torrance, 1981). The city experiences temperature extremes i.e. lowest during cool season and highest during summer.

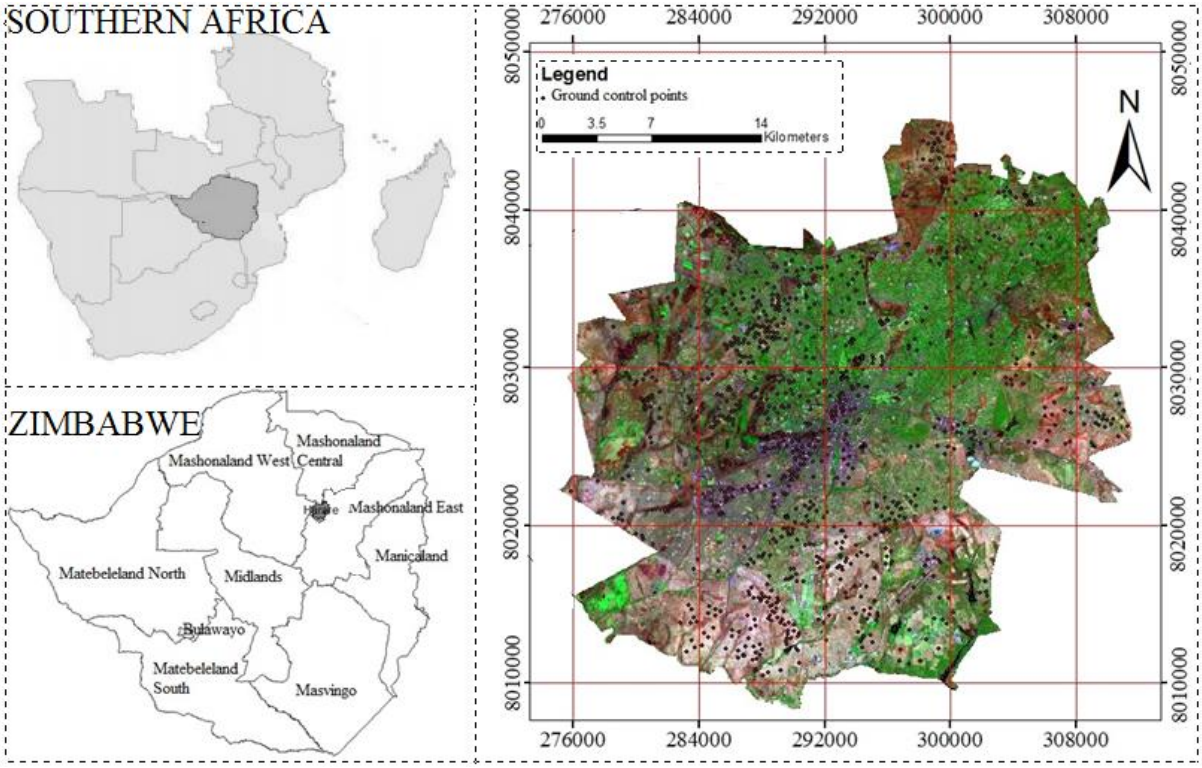

Figure 7.1: Location of the study

7.3 Remote sensing data processing

7.3.1 Acquisition and pre-processing

For the purpose of analyzing trends in Degree Days between 1984 and 2015, cloud-free summer and winter Landsat images acquired described in Table 7.1 were used. An independent set of cloud free images obtained between 1 January and 31 December 2015 was used to build and assess a model for estimating air temperature from Land surface temperature. We used Level-1 images corrected for geometric and radiometric distortion, currently available on the United States Geological Survey website (www.earthexplorer.usgs.gov). However, we further verified and corrected the images for positional errors using 30 control points obtained in the

field using a GPS as well as from auxiliary data points from easily identifiable features on the satellite images such as intersection of major roads. There were no cloud-free images for the month of June in 2001, hence the use of the 2002 image, assuming negligible differences. The same month was used in all years and each season to eliminate monthly differences in temperature.

Table 7.1: Medium resolution Landsat data utilized in this study for long term analysis

1984 (Landsat 5)	1993 (Landsat 5)	2001 (Landsat 7)	2015 (Landsat 8)
11 May*	30 May*	26 April*	27 May*
27 May*	2 August*	16 August*	12 June*
4 September*	3 September*	1 September*	14 July*
20 September#	19 September#	17 September#	16 September#
6 October#	5 October#	19 October#	2 October#
22 October#	21 October#	4 November#	18 October#

*Cool season, #Hot season

7.3.2 In-situ meteorological data

In-situ minimum and maximum temperature data at monthly resolution were obtained from the Meteorological Services Department of Zimbabwe as well as from Kutsaga Research Station. Monthly maximum and minimum temperature data covering period from 1950 to 2010 were obtained the Meteorological Services Department of Zimbabwe's Belvedere Weather Station in Harare (Latitude -17.83 and Longitude 31.02). Other datasets included temperature data for time and dates corresponding to cloud-free Landsat 8 images between 1 January and 31 December 2015 were obtained from Kutsaga Research Station (Latitude -17.92 and Longitude 31.13) and Harare Airport Meteorological Office (Latitude -17.93 and Longitude 31.01). The three are the only collection sites for weather data in Harare hence the station density is sparse.

7.3.3 Energy consumption data

Historical energy consumption data was obtained from the Zimbabwe Electricity Transmission and Distribution Company covering a period from 2009 to 2016 at monthly resolution. In order to obtain the data, the researcher negotiated with the Tariffs Department of the organization who facilitated the requested and later provided that data. The data was in two categories namely residential and industrial thus generalized and could not provide a picture of the differences in energy consumption between residential types. In order to obtain information about consumption for different residential types, we conducted a field survey for acquiring the information from household energy bills. However, using this technique, we only managed to get average monthly household consumption for high density, medium density and low

density residential areas for recent months. Due to recording keeping constraints, residents could not provide historical data hence seasonal and long term analysis could not be done at residential type.

7.3.4 Urban growth detection between 1984 and 2015

To determine the city's LULC classes, field identification and collection of representative GPS points were done from 1 to 30 of April 2015. Six major classes (described in Table 7.2) were identified. To capture intra- and inter-class variability, well distributed 120 GPS points per class collected across the city were captured (Mushore, et al., 2016). Using Support Vector Machines (SVM) algorithm, a supervised classification was done to map LULC distribution in 1984, 1993, 2001 and 2015. The SVM algorithm was selected due to its superior classification accuracy, in comparison to other commonly used schemes like Maximum Likelihood Classifier and Artificial Neural Networks and low ground truth data requirement for training (Adelabu, et al., 2013). Field generated points, auxiliary data and expert knowledge of LULC classes were used to create ground truth polygons (Regions of Interest - ROI) for training the classification and accuracy assessment in the ENVI Version 4.7 software. Classification using ROIs has been found to yield higher accuracy than points (Acharya, et al., 2015). Accuracy assessment was done using the kappa index, Overall Accuracy (OA), User Accuracy (UA) and Producer Accuracy (PA) for each year. LULC maps were used to determine the area covered by each LULC type in 1984, 1993, 2001 and 2015. The city growth was determined as the difference between the areas covered by each LULC class over the study period.

Table 7.2: Description of general land use and land cover types identified in Harare

LULC class	**Description**
Central Business District (CBD)	Areas with very high density of buildings and a very high proportion of impervious surface that include central business district and industrial areas.
High density residential (HDR)	High density of buildings and also including low vegetation cover fraction.
Medium density residential (MDR)	Moderate to high income residential areas with moderately spaced out buildings and high vegetation cover fraction.
Low density residential (LDR)	High income residential areas with spaced out buildings and high vegetation cover fraction.
Croplands (Cr)	Areas where intra-urban agriculture is practised including research sites which could be bare in the dry season
Green-spaces (Gr)	Areas covered by grasslands and clusters of tree characterised by high vegetation fraction even during the dry season.
Water (Wt)	Areas covered by water bodies or wetlands.

7.3.5 Link between LULC and seasonal LST changes

Land surface temperatures for summer and winter were computed using corresponding thermal infra-red bands for 1984, 1993, 2001 and 2015 obtained from Landsat missions on dates presented in Table 7.1. In order to minimize effect of randomness due to variations in weather conditions associated with single date analysis, at least three cloud free thermal images were used per season for each year. Therefore, for each seasonal analysis an average land surface temperature was retrieved from multi-date thermal data. A number of studies including Sobrino, et al. (2004) have describe the method for retrieval of land surface temperature from a single thermal infra-red channel of Landsat, which was also followed in this study. The procedure involves the use of raw digital numbers (DN) of thermal bands to derive thermal spectral radiances (L_λ) for each season which are further utilized to compute brightness temperature (T_b). Band 6 of Landsat 5, high gain Band 6 of Landsat 7 and Band 10 of Landsat 8 were used for this retrieval of land surface temperature (Jalan & Sharma, 2014; Chen, et al., 2006; Abutaleb, et al., 2015). Initially, spectral radiances were derived from each thermal band using Equation 7.1 where Gain and Offset are supplied with the data and differ for Landsat 5, 7 and 8

$$\boldsymbol{L_\lambda = Gain * DN + Offset} \qquad \text{Equation 7.1}$$

The thermal radiances were used to calculate brightness temperature by implementing Equation 7.2

$$\boldsymbol{T_b = \frac{K_2}{\ln\left(\frac{K_1}{L_\lambda}+1\right)}} \qquad \text{Equation 7.2}$$

The calibration coefficients, K_1 and K_2 were obtained from metadata files as they vary for different Landsat missions. Brightness temperature assumes uniform emissivity and that all landscapes are blackbodies, hence the need for emissivity correction (Wang, et al., 2010). For each season and year, land surface emissivity (ε) was derived from Normalized Difference Vegetation Index (NDVI) in each year as described in Sobrino and Raissouni (2000). Land surface temperature was derived by correcting brightness temperature layers of surface emissivity differences using Equation 7.3:

$$\boldsymbol{T_s = \frac{T_b}{\left\{1+\left(\frac{\lambda T_b}{\rho}\ln\varepsilon\right)\right\}}} \qquad \text{Equation 7.3}$$

Where λ represents the wavelength of the emitted radiance while $\rho=1.438X10^{-2}m$ (Stathopoulou et al., 2004; Sobrino & Raissouni, 2000; Sobrino, et al., 2004). The temperatures were re-classified into similar classes for each season and coverage of corresponding classes tabulated against each other for comparison of values in different years. The changes in the

coverage of temperature classes were used to indicate the extent and direction of the cool and hot season temperatures between 1985 and 2015. The changes were also used to compare the extent of temperature changes between the cool and hot seasons. In order to test for statistical significance of the land surface temperature changes, the Shapiro Wilk test showed that temperature distributions were non-parametric ($p>0.05$). Therefore, we log-transformed the temperature data and performed repeated measures Analysis of Variance (ANOVA) with initial hypothesis, H_o: $\mu_1= \mu_2= \mu_3= \mu_4$ and alternative, H_1: the mean temperatures for 1984, 1993, 2001 and 2015 are not equal.

7.3.6 Estimation of impact of urbanization on energy consumption in buildings

We proposed and utilized a method of assessing the impact of urbanization induced changes in temperature on energy demand for air conditioning using Landsat imagery. We used the daytime Degree Days to estimate the impact of temperature changes on energy consumption. Computation of Degree Days requires outdoor air temperature measurements which are usually obtained from in-situ observations. However, in-situ observations have limited spatial coverage thus inadequate to represent temperature variations in an urban landscape. Therefore, in order to improve the spatial representation of temperature distribution, we estimated air temperature from Landsat's mean daytime land surface temperature retrievals for each year. This estimation requires a regression model which accurately transfers from remotely sensed surface temperature to a map of air temperature at the same resolution as thermal imagery of Landsat. Linear regression model can be used to estimate air temperature (T_{air}) from land surface temperature (T_s) where measurements coincided in time if the correlation is strong. For example, in order to calculate Degree Days from NOAA AVHRR satellite data, Stathopoulou, et al. (2006) developed a model to retrieve air temperature from midday land surface temperature. We therefore used in-situ observations coinciding with surface temperature measurements during overpass times of Landsat 8 obtained between 1 January and 31 December 2015 (cloud free only) to develop and test a simple linear regression function in order to estimate air temperature at the time of Landsat's overpass.

The retrieved estimates of a temperature were used to derive Degree Days using Eq. (3) and (4). The trends in energy consumption for space heating were estimated using the mean daytime Heating Degree Days (HDD) retrieved from surface temperatures of the cool season in 1984, 1993, 2002 and 2015. The mean daytime HDD were calculated by subtracting the mean daytime temperature from a base temperature of 18^{o}C, widely proposed in literature

(Santamouris, et al., 2001; Sivak, 2009; Bolattürk, 2008; Sailor & Pavlova, 2003; Guerra Santin, et al., 2009). Mean daytime HDD for the cool season for each year was retrieved using Equation 7.4:

$$\boldsymbol{HDD = N(T_{base} - T_{air})} \quad \text{Equation 7.4}$$

N is the number of days and the term in brackets is a daily average difference between base and air temperature. In this study we focused on an average cloud-free day in the cool and hot season, therefore *N* was 1 day. We also estimated trends for energy demand for space cooling in the hot seasons using the mean daytime Cooling Degree Days (CDD) on cloud-free days in 1984, 1993, 2001 and 2015. The CDD was computed relative to a base temperature (T_{base}) of 18^{o}C (65^{o}F) using Equation 7.5:

$$\boldsymbol{CDD = N(T_{air} - T_{base})} \quad \text{Equation 7.5}$$

The base temperature was defined as the outdoor temperature above which ambient cooling is required and below which space heating is required (Eto, 1988). Whereas the choice of base temperature has been widely varied, as studies have used values ranging from 8 to 26^{o}C (Bolattürk, 2008; Christenson, et al., 2006; Büyükalaca, et al., 2001; Durmayaz, et al., 2000; Sarak, 2003; Dombaycı, 2009; Satman & Yalcinkaya, 1999; Papakostas & Kyriakis, 2005). The 18^{o}C was selected in this study due to its apparent popularity in literature (Santamouris et al., 2001; Sivak, 2009; Bolattürk, 2008; Sailor & Pavlova, 2003; Guerra Santin et al., 2009). According to Bolattürk (2008) the use of a base temperature of 18^{o}C makes an analysis standard and comparable to other studies globally by assuming that the temperature where energy is demanded for heating and cooling is the same everywhere. For this reason, a base temperature of 18^{o}C was chosen in this study.

7.3.7 Estimation of mean CDD and HDD using in-situ temperature observations

Average minimum temperature was used to estimate the average HDD for the cool season with a base temperature 18^{o}C. The average maximum temperature in the hot season of each year and the same base temperature were used to estimate CDD for the entire period. Typically, hourly and daily average dry bulb temperature is used, however, use of maximum and minimum temperature has grown in popularity e.g. (Dombaycı, 2009) used maximum and minimum to determine degree days for 79 city centers in Turkey. Time series for HDD and CDD were plotted in order to determine their trend and significance assessed using the p-value at 95% significance level. The temporal patterns in HDD and CDD from in-situ observations were compared with respective remotely sensed distributions.

7.3.8 Accuracy assessment of degree days' estimation

Cloud-free Landsat 8 data obtained in the period between January and December 2015 were used to assess accuracy of degree days estimated from Landsat series. The period was chosen due to availability of in-situ observations at overpass time. For coincident observations, CDD was computed using both in-situ and satellite temperature observations. The same procedure and base temperature as described above were used. Therefore, in-situ observations produced Observed CDD while Estimated CDD was obtained from satellite thermal data. Accuracy of Estimated CDD against Observed CDD was measured using Mean Absolute Error and Percentage Error.

7.4 Results and discussion

7.4.1 Urban growth and LULC changes between 1984 and 2015

Figure 7.2 shows changes in land use and land cover distribution in Harare between 1984 and 2015 (overall accuracy>80% and kappa>0.75 for all classifications). The overall classification accuracy were higher in 2015 (84.4%) and 2001 (89.4%) than in 1993 (83.9%) and 1984 (82.6). All the classification accuracies were above the 80% threshold recommended by Omran (2012).

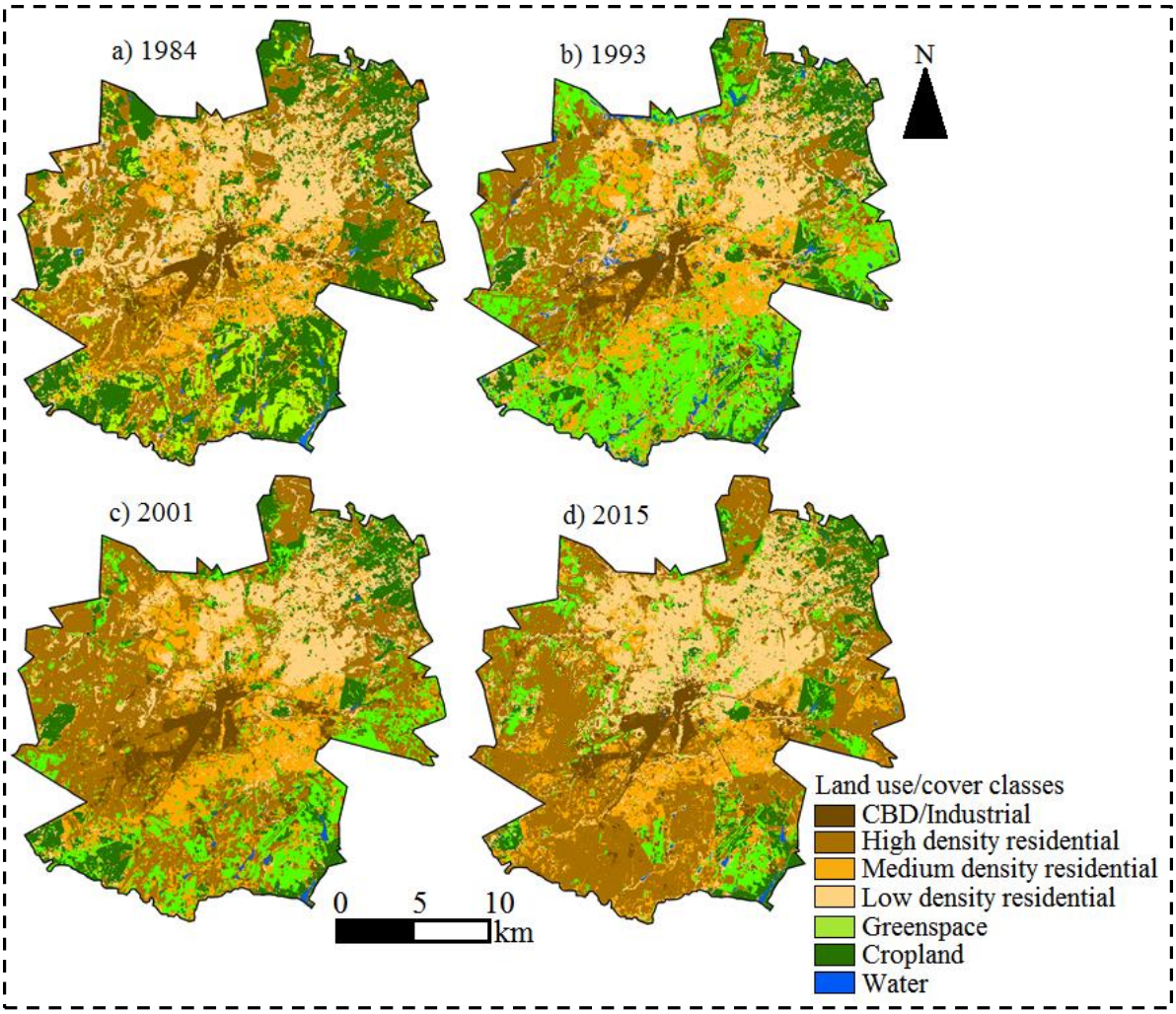

Figure 7.2: Land use and land cover maps for Harare in 1984 and 2015.

The Producer and User Accuracies (PA and UA) were greater than 70% for all the LULC classifications performed (Table 7.3). Furthermore, high PA and UA for all classes indicate that Landsat could be effectively used to distinguish between complex urban LULC classes, categorizing areas according to built-up densification. As such, four built-up density categories found in Harare were easily separated using the 30 m multi-spectral Landsat data. Based on visual inspection of Figure 7.2 the area covered by green-spaces and croplands decreased between 1984 and 2015. These were replaced by built-up areas, mostly the high density residential areas which increased in coverage between the periods.

Table 7.3: Classification accuracies per LULC class for different years

LULC	1984		1993		2001		2015	
	OA	UA	OA	UA	OA	UA	OA	UA
DB	86.06	93.70	88.37	97.67	84.12	94.25	87.96	91.65
HDR	83.14	75.66	94.28	79.79	94.50	86.22	94.49	81.97

MDR	84.88	82.54	78.60	99.76	82.49	90.02	75.55	73.21
LDR	88.10	80.91	87.30	83.67	94.75	89.62	88.25	80.96
GR	93.45	86.98	92.80	91.94	96.65	96.15	94.66	89.90
CR	79.74	73.28	37.67	65.53	70.75	73.57	77.64	82.93
Wt	96.54	99.13	70.74	82.61	97.96	100.00	97.48	99.79

High density residential areas increased in coverage from 234.15 km^2 to 334.50 km^2 while the CBD class also increased from 29.49km^2 to 53.21 km^2. Significant decreases were noted in green spaces which reduced in coverage from 216.45 km^2 in 1984 to 72.53 km^2 in 2015. Expansion of built up areas has also led to a reduction in remnant cropland within the city from 193.53 to 81.91 km^2 between 1991 and 2015. The area covered by low-medium density built-up category increased from 257.57 km^2 to 310.70 km^2 during the same period, a finding consistent with Kamusoko, et al. (2013) who showed an increasing built up trend within the city. Kamusoko et al. (2013) also showed that settlements are more spacious in the northern than the southern and southwestern suburbs.

7.4.2 LST changes between 1984 and 2015

Visual inspection of Figure 7.3 shows an upward temperature shift within the city, indicating warming of the cool season. The coverage of warm temperature categories (22-30^{o}C) increased in the southern and western parts of the city. Figure 7 shows that the northern and eastern areas were dominated by lower (12-20^{o}C) temperatures. However, in 2015, most of these areas had shifted to the 18-22^{o}C temperature range in winter. The high temperature (24-30^{o}C) category was prevalent within the city's CBD in 2015. Other winter temperature hotspots were observed in the southwestern area, where highest density of residential areas and in the southeastern area around the city's major airport. Generally northern and eastern areas have remained cooler over time with daytime surface temperatures mostly below 22^{o}C.

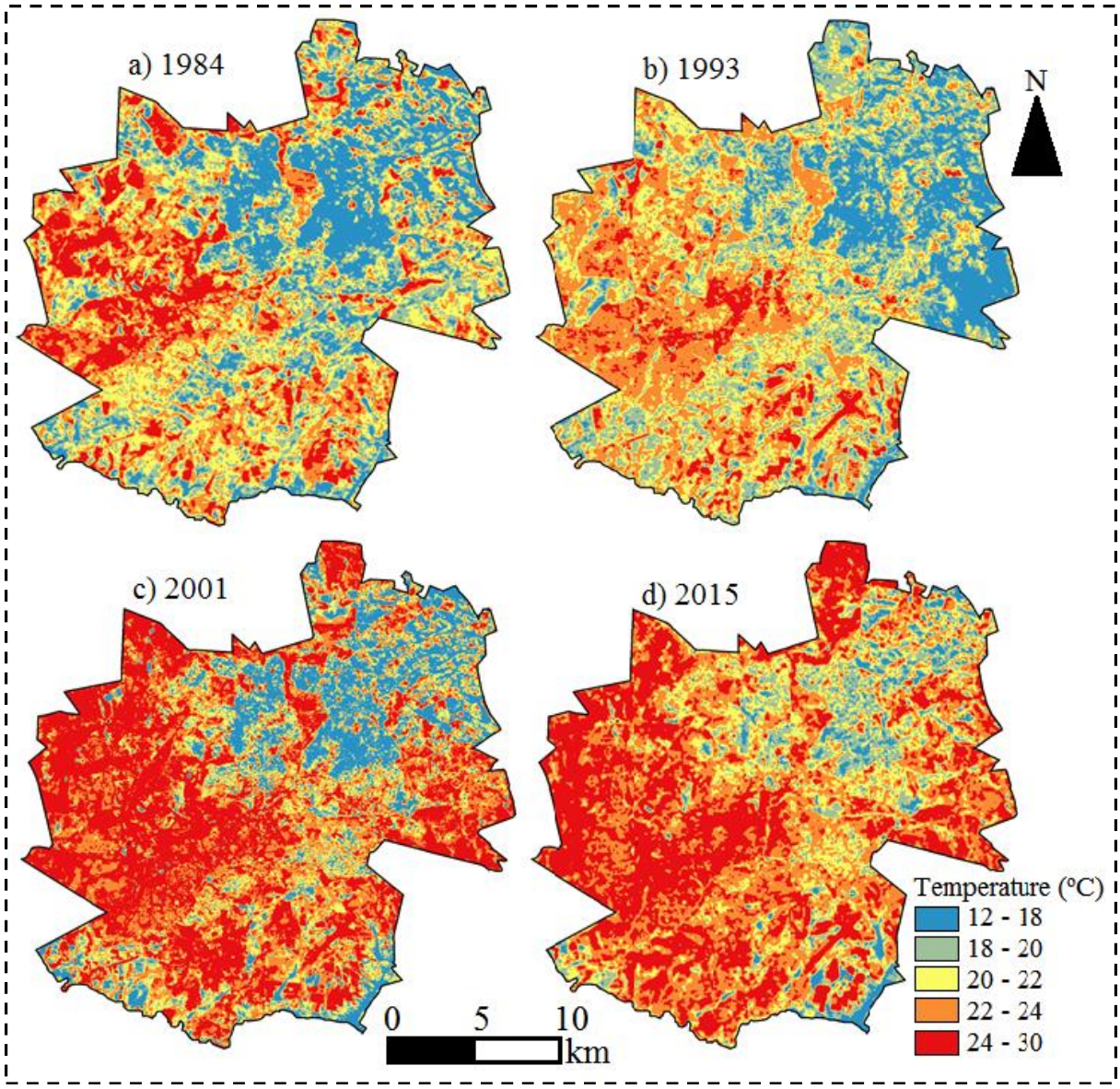

Figure 7.3: Long term changes in cool season land surface temperature distribution in Harare

There was decrease in areal coverage of the 12 to 22°C category and increase in the 22 to 30°C category in the cool season between 1984 and 2015. For example, the 22 to 30°C temperature range covered less than 330km^2 in 1984, which increased to more than 600 km^2 in 2015. Daytime surface temperature in the 12 to 18°C range occupied 157.47 km^2 in 1984 but declined to 30.50 km^2 in 2015.

Daytime temperatures also shifted towards high temperature ranges between 1984 and 2015 in summer (Figure 7.4). Temperature values greater than 36°C were not common in 1984 while they were covering a significant proportion of the city in 2015. Although land surface

temperature increased in all areas, greater warming was observed in the southwestern parts than in the northern areas.

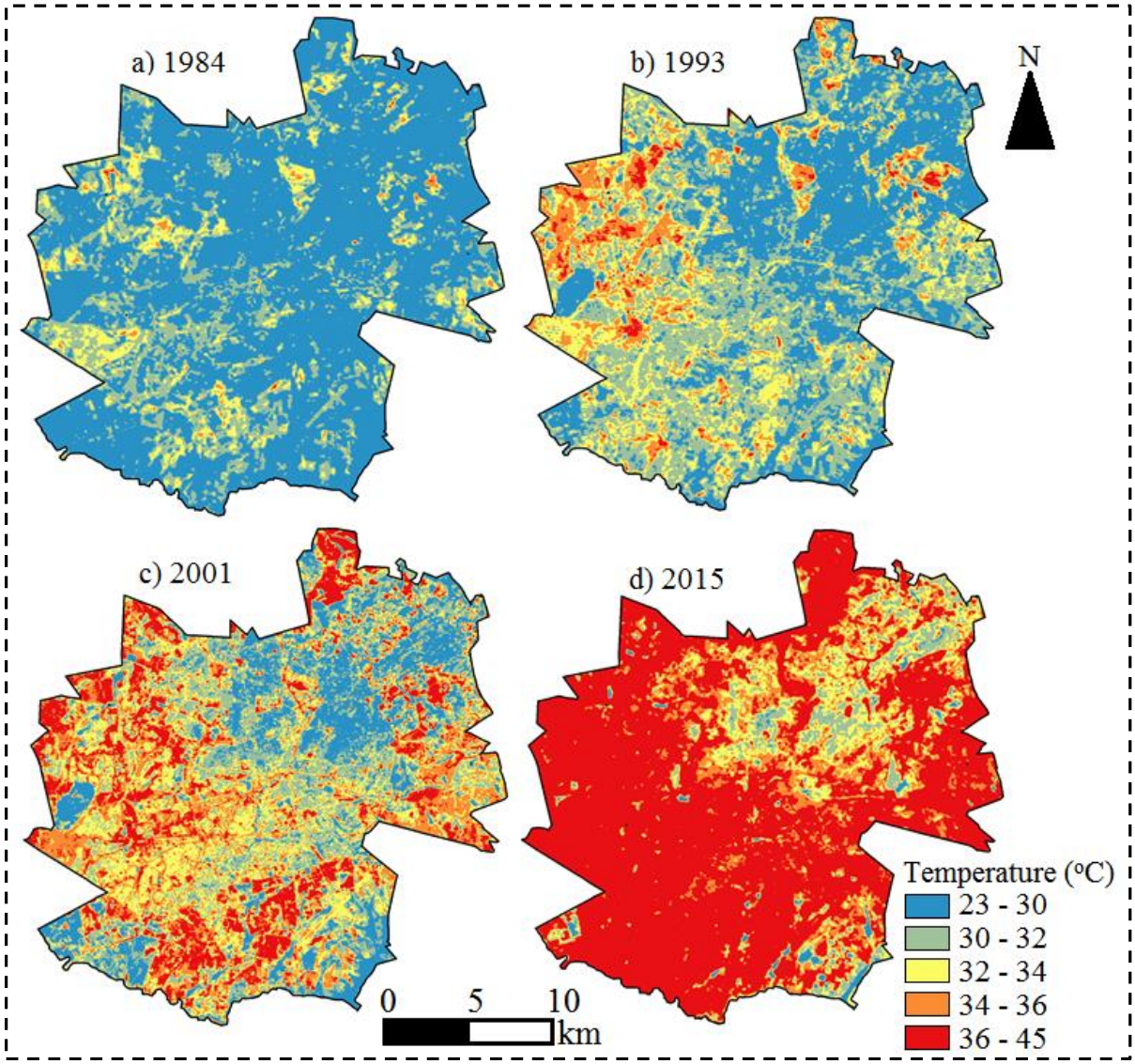

Figure 7.4: Long term changes in summer-time land surface temperature distribution in Harare

Temperatures in the 23-32°C category were experienced in more than 600 km^2 of the area in 1984, which decreased to 7.89 km^2 in 2015. This implies that more areas were experiencing high daytime surface temperature (greater 36°C) during in the hot season in 2015 than in 1984. For example, the coverage of places experiencing temperatures greater than 36°C increased from 0.27 km^2 to over 580 km^2. Daytime summer warming was more pronounced in the central, southern and western parts than the rest of the city. Therefore, in response to increases in the coverage of built-up and impervious areas, daytime temperature increased, making the hot season even hotter on an average cloud-free day.

The observed increase in temperature over time due to urbanization is in agreement with existing literature (Adebowale & Kayode, 2015; Cinar, 2015; Grossman-Clarke, et al., 2010). For example, Grossman-Clarke et al. (2010) noted an increase in daytime temperatures between 2-4^{o}C from 1973 to 2005 in Phoenix Metropolitan Area. Such increases are mainly caused by reduction in evaporation and increase in sensible and ground heat flux due to conversion from natural to impervious surfaces (Weng, et al., 2007; Jalan & Sharma, 2014; Zhou & Wang, 2011a). Furthermore, human activities increase with city growth, resulting in increased pollution and enhanced warming due to release of anthropogenic heat (Flanner, 2009). Flanner (2009), for instance noted that anthropogenic activities have potential to increase temperatures by 0.4 to 0.9^{o}C. Temperature and warming were greater in summer than in winter between 1984 and 2015, which is attributed to differences in insolation received between the two seasons as a large amount is received during the hot season. The ANOVA showed that the changes in surface temperature of the cool and hot seasons between 1984 and 2015 were statistically significant ($p<0.05$).

7.4.3 Link between LULC and seasonal changes in LST between 1984 and 2015

Built-up areas showed generally higher values and increases in winter temperature than non-built LULC types in all the periods between 1984 and 2015. As indicated on Table 7.4, the effect of high built-up density in all the years was characterized by comparatively higher temperature in CBD and high density residential areas. The high temperatures in the CBD can be attributed to large coverage of impervious surfaces, which absorb heat reduced sky view that impedes radiation loss and heat removal by wind (Blake, Curitiba, et al., 2011). However, differences in temperature between the built-up areas were not significantly pronounced during the cool season. For example, in 2015, the average temperature for the CBD was 24.17^{o}C while it was 23.96^{o}C in medium density residential areas. This is consistent with (Gusso, et al., 2014) who noted that the amount of heat absorbed by buildings increases with amount of radiation received in the lower atmosphere. On average, the daytime surface temperatures for the cool season increased by 2.26^{o}C as the city grew between 1984 and 2015.

Table 7.4: Average long-term changes in winter surface temperature due to urbanisation

LULC	Average temperature (^{o}C)

	1984	1993	2001	2015	Change
CBD/Industrial	21.50	21.42	22.39	24.17	2.67
High density	21.30	21.39	22.59	23.96	2.66
Medium density	20.87	20.34	21.08	23.19	2.32
Low density	19.93	19.41	19.65	22.13	2.20
Green space	19.80	19.90	19.97	22.01	2.21
Cropland	20.70	21.22	22.41	24.11	3.41
Water	18.48	20.08	19.26	18.16	0.32
Average	20.37	20.53	21.05	21.40	2.26

Although temperature of the hot season increased in all areas within the city, lower values and increases in temperature were recorded in green-spaces and wetlands (Table 7.5). This finding is in agreement with Zhou and Wang (2011a) who detected lower changes in temperature in wetlands (-0.7^{o}C) and in areas covered by vegetation (1.3^{o}C). Temperature was also low in low-medium density residential areas where vegetation fraction is generally high. However, temperature increased with an increase in built-up density (Table 8). Generally, vegetation within built-up areas and surface moisture offers mitigation against extreme temperature elevation by reducing temperatures through latent heat transfer (Rasul, et al., 2015; Tao, et al., 2013). The findings are consistent with other studies (Sertel, et al., 2011) who attributed a 0.5 to 1.5^{o}C increase to urbanization in Marmara Region, Turkey between 1975 and 2005 and a 0.4 to 2^{o}C in eastern Australia attributed to LULC change (Mcalpine, et al., 2007). Similarly, the dependence of temperature change on LULC type agrees with Zhou and Wang (2011a) who observed changes as large as 5.1^{o}C in agricultural areas while forests recorded a temperature change of 1.3^{o}C. Besides the changes in temperature which occurred due to conversion from one LULC to another, the average temperature for each LULC type also increased between 1984 and 2015. This agrees with other studies which suggested that, globally, there is a background warming due to factors such as increase in greenhouse gas concentration, ozone depletion induced increase in long-wave radiation in the lower atmosphere and heat intensification due to solar cycles (Nayak & Mandal, 2012; Manatsa, et al., 2013). Therefore, urbanization-induced warming is superimposed on already rising temperature thus intensifying heat related extremes as well as elevating demand for adaptation and mitigation efforts in cities.

Table 7.5: Average changes in summer surface temperature for different LULC types in Harare

LULC	Average temperature (^{o}C)				
	1984	1993	2001	2015	Change

CBD/Industrial	30.98	32.86	34.21	37.04	6.06
High density	30.83	30.91	32.98	35.76	4.93
Medium density	30.18	30.33	31.29	33.87	3.69
Low density	28.83	29.09	29.23	31.79	2.96
Green space	28.64	29.57	30.12	31.10	2.46
Cropland	29.37	31.52	33.23	35.81	6.44
Water	21.03	22.15	22.94	23.20	2.17
Average	28.55	29.49	30.57	32.65	4.10

7.4.4 Relationship between in-situ and remotely sensed observation of mean Cooling Degree Days

We developed a simple linear regression model for estimating air temperature from land surface temperature derived from Landsat thermal data (r-squared=0.68). The agreement between Degree Days modelled from Landsat thermal data with those from in-situ data at the time of overpass is displayed in Figure 7.5. The Degree Days estimated based on model closely compared with in-situ data based computation with relatively high accuracy as indicated by a mean percentage error of 21.2 % and Mean Absolute Error of 1.06 degree days. This was higher than accuracy attained in Athens, Greece using NOAA AVHRR land surface temperature with a base temperature of 25^{o}C (Stathopoulou, et al., 2006). Stathopoulou, et al. (2006) obtained a Mean Absolute Error of 2.2^{o}C, which could be due to generalization of temperature caused by the low spatial resolution of NOAH AVHRR compared to Landsat data.

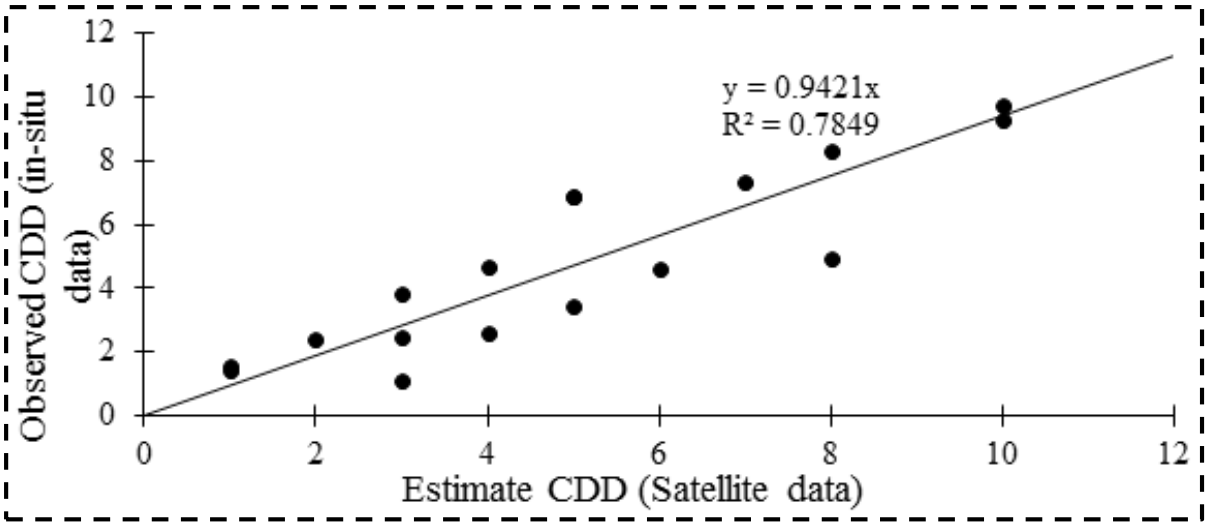

Figure 7.5: Scatter-plot of Observed against CDD estimated from Landsat data

7.4.5 Effect of urban heat island on energy demand in Harare

Figure 7.6 shows that mean energy consumption in residential areas of Harare increased as minimum and maximum temperature decreased during the winter season (May to September). During the summer season (October to March of the next year) energy consumption increased

as temperatures rose. Highest energy consumption in residential areas in the summer season (above $1.05X10^6$KWh) corresponded with highest maximum temperature in October and in January. However, energy consumption was higher in winter than in summer. This suggests that during the winter season consumption is increased due to use of heaters as well as warm water for bathing in all residential areas. Even the urban poor who mostly characterize the high density residential areas who do not afford air conditioning facilities can warm water for bathing. The slightly lower energy consumption during the summer season suggests that some parts of the season are comfortable or residents especially in low income residential areas use natural ventilation to remove heat. This may also imply that, although maximum temperatures will cause discomfort, a large proportion of the residents do not afford air conditioning facilities and hence are vulnerable. This concurs with Mushore, et al. (2017a) who observed that heat vulnerability in Harare is high in high density residential areas due to factors which included low household income levels, high population density and physical exposure. Energy consumption in industrial areas was also higher in winter than in summer although responses to maximum temperature in summer were not as pronounced as in residential areas.

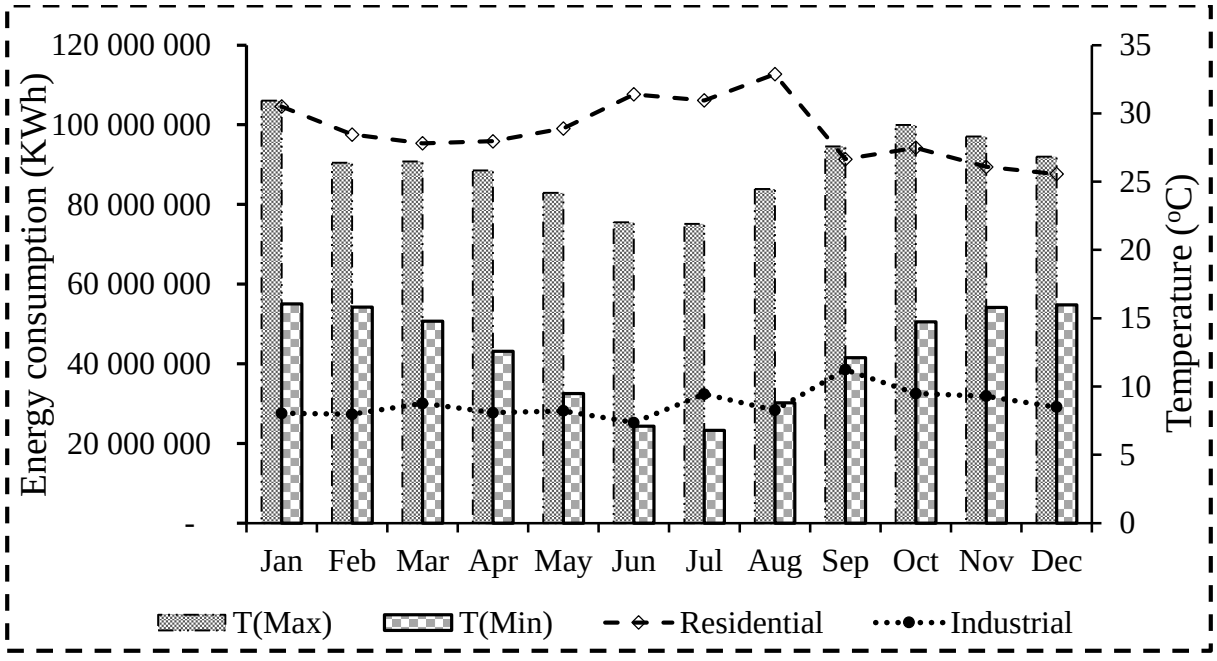

Figure 7.6: Response of energy consumption to monthly temperature changes in Harare

The mean daytime HDD values for the cool season were decreasing with time regardless of built-up density between 1984 and 2015. The decline in heat requirements for space heating increased with built-up density; largest in the CBD and high density residential areas where there was a decrease by 1 degree day and smallest in the low density residential areas where the decrease was about 0.5 degree days (Table 7.6). The general decrease in winter heating energy requirement concurs with observation of reduction in the number of cold days in

Zimbabwe (Chagutah, 2010). Mean HDD values were higher in low and medium density residential areas than in high density residential areas and the CBD in all years. This was because low and medium density residential areas have lower temperatures than other residential with higher built-up density. According to Kamusoko, et al. (2013), low density high income residential areas are characterized by high vegetation cover fraction. The vegetation which includes trees and lawns reduce the temperatures in these areas by evaporation cooling (Odindi, et al., 2015). Furthermore, the buildings are also spaced out, allowing cooling by advection due to low resistance to wind flow. Therefore, the low temperatures result in higher requirement of energy for indoor heating in the low density than other built-up areas during the cool season.

On the contrary, energy demand for cooling during daytime in summer increased between 1984 and 2015 as indicated by rising CDD in all residential types. For example, CDD increased from 7.71 to 9.43 degree days in the CBD and industrial areas while it increased from 5.73 to 9.28 in the low density residential areas. This was in tandem with (Blake, Curitiba, et al., 2011) who showed an increase in temperature since 1978 based on in-situ observations in the city. In consistence with Vardoulakis, et al. (2013) we also found that elevation of temperatures resulted in increases in CDD values hence leading to a rising trend in energy requirement for indoor cooling in the hot season. Throughout summer, daytime cooling energy requirements were larger in the CBD and high density residential areas than in the low-medium density residential areas. For example, in 2015, the CDD was 8.90 degree days in high density residential areas while it was 7.27 degree days in low density residential areas. This was because of the UHI effect which causes higher temperatures in areas within the CBD and high density of buildings (Guan, 2011; Salvati, 2015). Salvati (2015) noted that increases in temperature leads to increase in energy demand, which vary with urban density. Hirano, et al. (2009) also reported that energy consumption increased with total floor area such that it was high in densely built up areas, with buildings with more than two floors, hence very high daytime HDD in the CBD. Consistent with UHI spatial distribution, low-medium density residential areas have larger heating and lower cooling energy requirements. Mushore, et al. (2016) and Kamusoko, et al. (2013) established a high vegetation fraction, which increase cooling by latent heat transfer in these areas. The range of CDD values was consistent with mean midday CDD obtained using data from NOAA Advanced Very High Resolution Radiometer (AVHRR) in Athens, Greece (Stathopoulou, et al., 2006).

Table 7.6: Changes in energy requirement for air conditioning

	Energy (KWh)	Average daytime HDD				Average daytime CDD			
		1984	1993	2001	2015	1986	1993	2001	2015
CBD/Industrial	-	-3.04	-3.01	-3.40	-4.14	6.94	7.71	8.26	9.43
High density	480	-2.97	-2.99	-3.49	-4.05	6.87	6.91	7.76	8.90
Medium density	768	-2.79	-2.56	-2.87	-3.73	6.61	6.67	7.06	8.12
Low density	1440	-2.39	-2.18	-2.18	-3.30	6.05	6.16	6.26	7.27

*Energy=current mean monthly energy consumption per residential type

However, although the CDD values showed that higher cooling energy requirements were in the high density residential than in the low-medium density residential areas, household income seemed to influence actual energy consumption differences. For example, Table 7.6 shows that mean energy consumption per household was inversely related to population density. As such low density residential areas had the highest mean monthly energy usage (1440KWh) while the lowest was in high density residential areas (480KWh). This is in tandem with Arifwidodo and Chandrasiri (2015) who observed a strong positive correlation between income, number of air-conditioning units in a house and energy consumption in Bangkok. Therefore, in Harare, the CDD can also be linked to heat health risks because heating requirement is high in the high density residential areas where the majority of residents are low-income earners (Wania, et al., 2014). Similarly, in Indonesia the ratio of electricity need to income was a measure of vulnerability to temperature extremes (Batih & Sorapipatana, 2016). Therefore, residents in low CDD low-medium density residential areas have the potential to utilize larger amounts of energy in air conditioning due to high income. Although this was not determined as it fell outside the scope of the study, houses in low-medium density residential areas are generally more spacious and have wealthier occupants than in the high density residential areas. The high consumption of energy by residents with large houses and high income was associated with the capacity to own sophisticated air conditioning facilities (Ewing & Rong, 2008; Batih & Sorapipatana, 2016).

Figure 7.7 shows that warming has reduced daytime requirements for space heating in the cool season and increased heat requirements for space cooling in buildings. Therefore, relative to the 18^{o}C threshold for human comfort, urban warming has increased household requirement of energy for cooling in summer in Harare. The increase in requirement for space heating was larger than the decrease in energy requirement for space cooling, implying a net increase in energy requirement for air conditioning. The summer CDD trends are in agreement with projections that household energy consumption in Zimbabwe would increase from 133221TJ

in 1994 to 147190TJ in 2010 and further increase to 313045 in 2050 (Ministry of mines environment and tourism., 1998). In Rome and Barcelona, temperature elevation increased energy demand from 10 to 33% (Salvati, 2015).

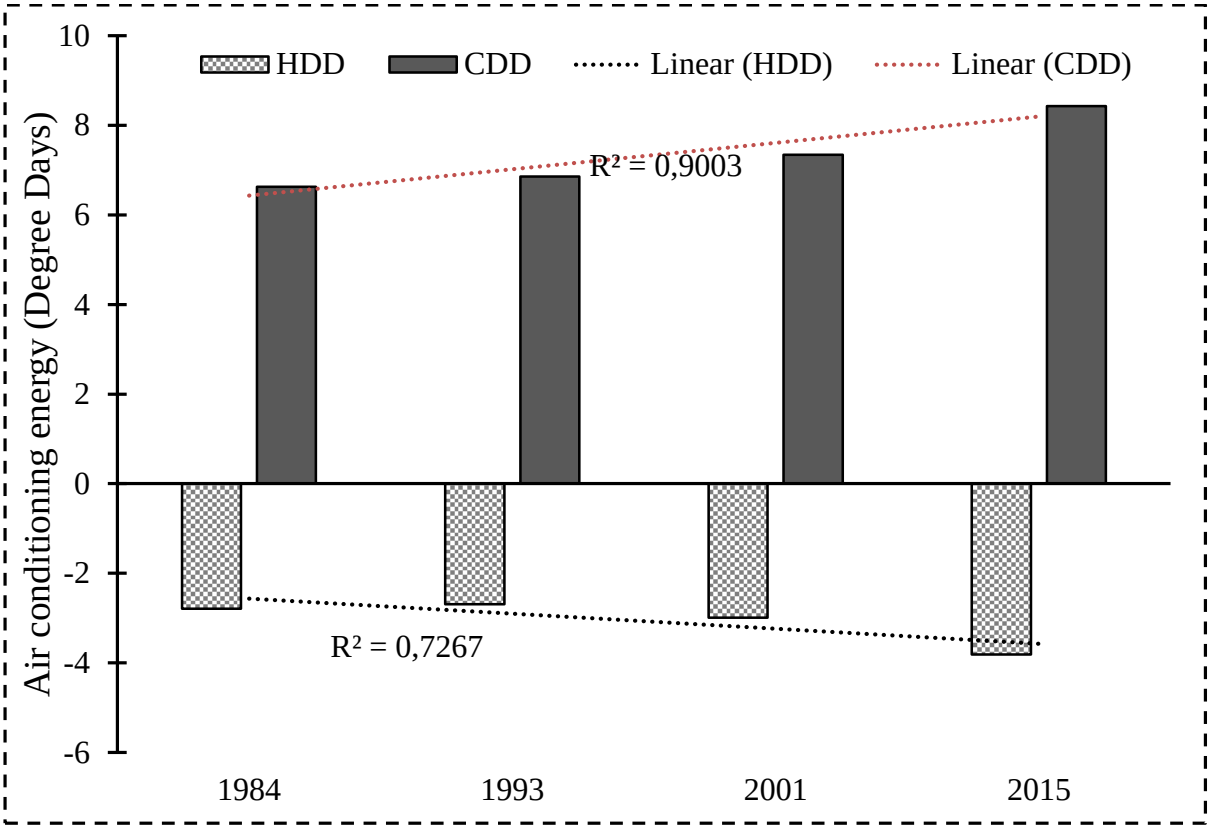

Figure 7.7: Estimated impact of urban warming on daytime household energy consumption

7.4.6 In-situ observed long-term changes in space cooling and heating requirements

In agreement with estimations from remotely sensed data, the city is warming as indicated by significant decrease in HDD derived from mean annual minimum temperature since 1950 ($p<0.05$ at 95% confidence interval). The mean HDD are decreasing at an average rate of 0.02^{o}C per annum (Figure 7.8). The HDD values were positive; close to 3 degree days in the 1950s, decreasing over time and approaching zero over time. Implying a trend towards reduction in indoor discomfort associated with low temperatures in the area over time. Both in-situ based and remotely sensed HDD retrievals showed a trend of declining values indicating that indoor heating requirements are decreasing with time in Harare.

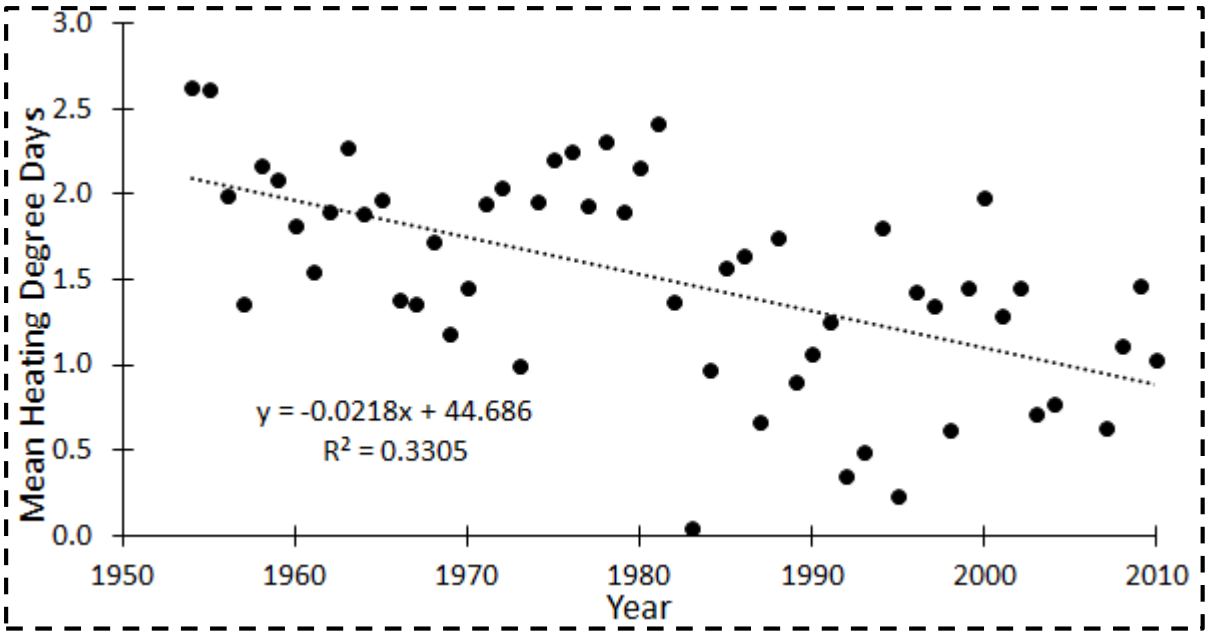

Figure 7.8: Changes in mean early morning space heating energy requirement in Harare

Analysis of in-situ data between 1950 and 2010 also showed that mean annual maximum temperatures have also increased, leading to significant increase in daytime CDD ($p<0.05$). The CDD are rising at a rate of 0.02 degree days per annum as displayed in Figure 7.9. The values of CDD ranged between 6.5 and 10 degree days and increased by close to four between 1950 and 2010, which is closely comparable to changes observed using Landsat thermal data. However, contrary to remote sensing retrievals, the CDD from in-situ temperature data showed variations with time. The difference is attributed to the fact that, contrary to remote sensing retrievals, in-situ average temperature includes observations on days that are not cloud-free.

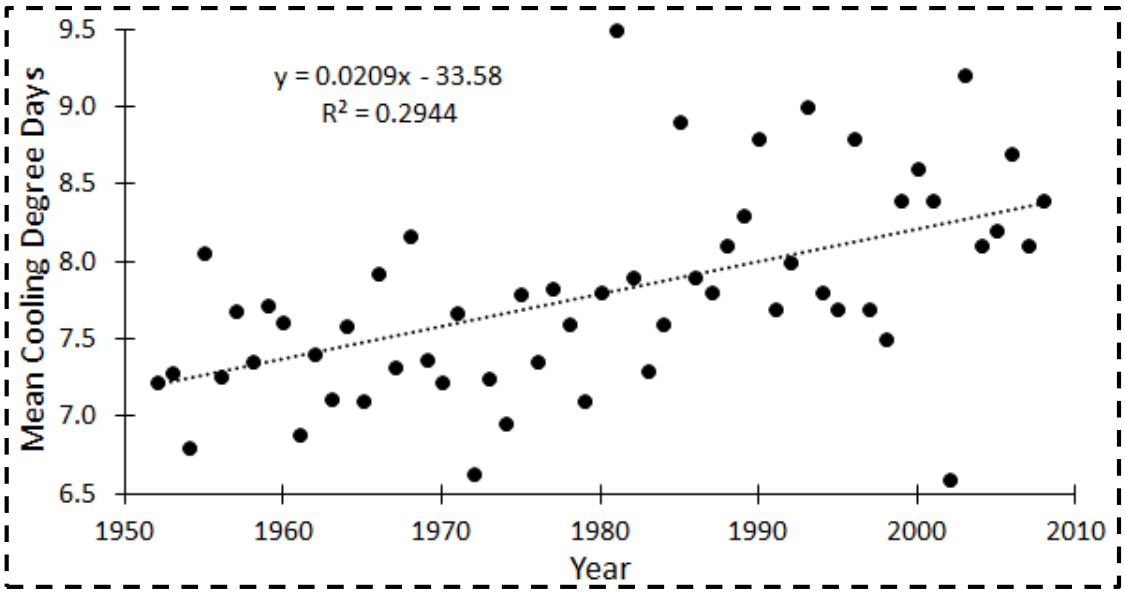

Figure 7.9: Changes in mean daytime space heating energy requirement in Harare

7.5 Conclusion

Climate change induced by urbanization such as raising local temperature has potential to increase energy demand for space heating during the hot season. In the absence of air-conditioning and other indoor heat removal technologies, urban communities are exposed to heat related distress. We investigated variations in indoor heating and cooling needs between residential types in a complex urban setting utilizing medium resolution Landsat thermal data. Previous studies relied mostly on in-situ meteorological data which are limited in spatial coverage especially in resource constrained developing countries such as in Africa. We used Cooling Degree Days (CDD) and Heating Degree Days (HDD) as proxy for air-conditioning energy for indoor cooling and heating, respectively. We investigated over a period from 1984 to 2015 in Harare and drew the following;

- Energy consumption in residential areas increased as maximum temperature rose in summer and as minimum temperature decreased in winter. Therefore, Degree Days derived from minimum and maximum temperature are a good indicator of responses of energy consumption to temperature changes in Harare.
- Medium resolution Landsat thermal data estimates daytime HDD and CDD and their variations across residential types in a complex urban setting with high accuracy
- Due to warming induced by urban growth, energy requirements for space heating in the cool season in Harare are decreasing
- Cloud-free days in the hot season are becoming increasingly uncomfortable, raising energy demand for space cooling especially in low-income high density residential areas
- The heat mitigation value of urban greenery remains significant as indicated by low CDD in low-medium density residential areas where buildings are spaced out and vegetation cover fraction is high.

During the hot season, actual energy consumption was low in low-income residential areas despite high air-conditioning energy needs. This indicated that low-income residents lack air-conditioning facilities hence are vulnerable to heat extremes.

7.6 Link between Chapter 7 and other chapters

Surface temperature modulates ambient outdoor temperatures. This also elevates indoor temperatures with potential to increase air conditioning energy demand. Since LULC was shown to affect surface temperature distribution in Chapters 4 to 6 this may also influence air-conditioning needs in different residential areas. Chapter 6 showed that long term LULC changes elevate land surface temperature. This together with background warming has potential to increase indoor temperatures. Chapter 7 established the possible link between urban growth, surface temperature changes and potential air-conditioning energy consumption. Urban growth closely associated with observed rising trends in energy consumption as well as potential air conditioning energy demand. Demand was found to be high in densely built-up areas which, as was established in Chapter 4, are occupied by low income strata indicating increasing vulnerability. All previous chapters looked at historical LULC and LST patterns as well as their socio-economic implications. Based on these historical patterns, Chapter 8 predicts the state of LULC and LST spatial patterns.

CHAPTER 8: REMOTE SENSING BASED PREDICTION OF URBAN GROWTH AND IMPACT ON LAND SURFACE TEMPERATURE PATTERNS

This chapter is based on:

Mushore T. D. Odindi J., Dube T., Mutanga O. (**2017**). Prediction of future urban surface temperatures using medium resolution satellite data in Harare Metropolitan City, Zimbabwe. *Building and Environment*, 122, 397-410, http://dx.doi.org/doi.org/10.1016/j.buildenv.2017.06.033

8.0 Abstract

The objective of the study was to determine the impact of urban growth on future micro-climate of Harare by predicting future distribution of land use and land cover (LULC), as well as land surface temperature using. Landsat series data was used to map Land Use and Land Cover and land surface temperature distribution during the month of October for the year 1984, 1993, 2001 and 2015. The Cellular Automata Markov Chain analysis was used to determine long term landscape transformation at 10-year time steps from 2015 to 2045. We further tested the potential of a variety of vegetation and non-vegetation indices to predict land surface temperature. Results show that the Urban Index (UI), a non-vegetation index was the best predictor of surface temperature, since it had the highest correlation with retrieved surface temperature (r=0.9831). When tested against temperature derived from thermal band in October 2015, the mean absolute percentage error of the UI derived temperature was 5.27%. Based on changes which occurred between 1984 and 2015, the Cellular Automata Markov Chain analysis predicted that high density built-up areas will increase monotonically from 470.02 in 2015 to 490.36km^2 in 2045. Green spaces were predicted as decreasing from 57.42 to 27.85km^2, while croplands also decrease from 30.27 to 16.93km^2 between 2015 and 2040. Using UI as predictor of land surface temperature, we predicted that the 18-28^{o}C class will decrease in coverage between 2015 and 2040, while the 36-45^{o}C category will increase in proportion covered from 42.5 to 58% of city. We concluded that continued urban growth will increase warming and result in high future temperatures unless mitigation efforts are strengthened. The findings of this study are important in informing future development of cities to consider growth implications on future temperatures and thermal comfort of urban residents.

Keywords: Land surface temperature, Cellular Automata Markov, Markov Chain analysis, urban growth, urban growth, vegetation indices, Harare

8.1 Introduction

Urban growth, which is characterised by replacement of natural surfaces with heat absorbing impervious surfaces (artificial structures such as pavements covered by asphalt, concrete, brick, stone and roof tops) and buildings, results in elevated surface temperatures in cities compared to surrounding rural areas (Rao, 1972). Typically, high thermal values are obtained where density of buildings is high, proportion of impervious surfaces is high, as well as in areas where heat removal by advection and radiation loss is retarded, such as at city core with tall buildings (Hu & Jia, 2010; Zhang, Schaaf, et al., 2013; Amiri, et al., 2009). Such increase in temperature may have adverse socio-economic and environmental impacts on urban residents that include increased water use, energy cost for air conditioning and health risk, due to pollution (McCarthy, et al., 2010; Tonnang et al., 2010; McDonald, et al., 2011a; Hung, et al., 2006; Guhathakurta & Gober, 2007). Furthermore, the influence of urban growth on urban micro-climate is projected to continue increasing as urban population continue to rise globally (McCarthy, et al., 2010; Seto, et al., 2012; Zhang, Schaaf, et al., 2013; Valsson & Bharat, 2009). Natural landscapes, particularly vegetation and wetlands favour latent heat transfer and play a significant role in mitigating against urban heat (Odindi, et al., 2015). However, their coverage and mitigation is reduced, due to replacement by impervious surfaces and buildings as cities grow. For the purpose of sustainable urban growth and planning, the link between Land Use and Land Cover (LULC) transitions and future climate projections need to be understood. Specifically, there is need to predict the implication of long term localized LULC transformation on surface temperatures in order to enhance area specific adaptation, mitigation, as well as policy formulation and implementation.

A number of studies have analysed the relationship between urban LULC patterns and land surface temperatures, using remotely sensed imagery without making future projections (Larsen & Gunnarsson-Östling, 2009; Yuan & Bauer, 2007; Xu, et al., 2013; Wilson & Brandes, 1979; Hu & Jia, 2010). These studies have shown that impervious surfaces within urban areas are characterised by high temperatures, due to a combination of high heat absorption rate, low thermal emissivity and low latent heat transfer. Conversely, natural landscapes like wetlands and vegetated areas have also been characterised by low temperatures (Jiang & Tian, 2010; Sung, 2013; Mushore, et al., 2016). Several studies also explored seasonal and long term historical changes in temperature with urban growth (Yuan & Bauer, 2007; Hu & Jia, 2010; Valsson & Bharat, 2009; Odindi, et al., 2015). Other studies have used urban and vegetation indices to show the quantitative relationship between LULC and temperatures but

placing little focus on future temperature patterns (Weng, et al., 2004; Chen, et al., 2006; Yuan & Bauer, 2007; Tran, et al., 2006; Xiao, et al., 2007; Wilson & Brandes, 1979; Yang Zhang et al., 2012; Senanayake, et al., 2013; Hung, et al., 2006). For example, Chen et al. (2006) showed that temperatures decrease with normalized difference vegetation index, normalized difference bareness index and normalized difference wetness index while increasing with normalized difference built up index. The relationship between land surface temperature and a variety of land cover indices are known to be strong. Therefore, trends in land cover indices such as vegetation fraction (FVG) and normalized difference built-up index (NDBI) have potential to accurately project future temperature. However, there is paucity of literature on the use of land cover indices to project localized future distribution of urban LULC and temperature patterns.

Despite their strength to forecast urban growth patterns, only a single study used land cover indices to predict future distribution of land surface temperature (Ahmed, et al., 2013). Whereas Ahmed et al. (2013) used Normalised Difference Vegetation Index (NDVI) to project remnant urban natural landscape and future land surface temperature values, NDVI is known to saturate at high vegetation fraction, thus offering a limited temperature range. Studies have also shown that NDVI is a weaker predictor of land surface temperature than other indices like the Normalised Difference Built Index (NDBI), vegetation fraction and the percentage Impervious Surface Area (ISA) (Li & Liu, 2008; Chen, et al., 2006; Yuan & Bauer, 2007; Deng & Wu, 2013); Chen et al 2006). Furthermore, Ahmed et al. (2013) used single date images to compute NDVI to represent entire season; a method which is subject to randomness given that land cover may vary significantly with a season. There is thus need to improve the approach such as by using seasonal averages of land cover indices. In another study, Hasanlou & Mostofi, (2015) estimated LST based on a linear function of a combination of indices which included NDVI, NDBI, Normalized Difference Bareness Index (NDBaI), Normalized Difference Water Index (NDWI), Soil Adjusted Vegetation Index (SAVI), Enhanced Built-up and Bareness Index (EBBI), Urban Index (UI), and Built Up Index (BUI) (Hasanlou & Mostofi, 2015). However, Ahmed et al. (2013) notes that when several factors are used in a linear regression model, accuracy of retrieved dependent variable may be compromised, due to noise caused by collinearity between the factors. Climate forecasts are as useful as they are accurate thus there is need to identify indices that best predict LST accurately without errors due to collinearity.

The Markov Chain Model has been widely used among others to predict LULC changes and urban expansion (Ahmed & Ahmed, 2012; Fan, et al., 2008; Hashem & Balakrishnan, 2015; Araya & Cabral, 2010). For example, Hashem and Balakrishnan (2015) used Markov Chain analysis and predicted a 20% increase of built-up areas for Doha, Qatar in 2020. Fan, et al. (2008) predicted farmland loss due to urban expansion between 2003 and 2013 in Pearl river delta using Cellular Automata Markov Chain analysis. However, there is paucity in literature on extending the adoption of Markov Chain analysis to further determine effect of LULC transformation on urban surface temperature change. Temperature predictions have widely been done using global and regional models which usually exclude urban trends and consider their impact as negligible (McCarthy, et al., 2010; Saitoh, et al., 1996; Unganai, 1996). Such models are often at coarse resolution, require further downscaling and therefore not very suitable for understanding localized phenomena (Hoffmann, et al., 2012; Smith & Roebber, 2011). Furthermore, global and regional models commonly emphasize on greenhouse induced temperature changes, disregarding the implication of LULC transformation on temperature change, particularly in urban areas. Analysis based on Markov Chain offer an opportunity for projecting landscape transformation, providing insight into future surface thermal characteristics, due to landscape change (Ahmed et al 2013). The analysis is suitable for predicting temperature changes at the same spatial and temporal resolution with LULC changes, thus capable of mapping localized phenomena such as urban surface dynamics. Due to previous successes in mapping LULC changes related impacts, accessibility, simplicity and parsimony, the Markov Chain model offers great potential to predict future temperature, hence needs to be further explored. The analysis is important for providing guidance and impression about how future urban thermal environment may be affected if historical urban growth patterns persist.

Despite the growing evidence from other parts of the world that urban growth leads to surface temperature changes, there is still a paucity of literature on the subject in Zimbabwe. Climate studies in the country have largely used in situ meteorological data and large scale climate models, concentrated on rainfall and mostly focused on impacts on agriculture (Manatsa et al., 2017; Mushore, Manatsa, et al., 2017; Mazvimavi, 2010; Moyo et al., 2012; Charles et al., 2014). Remote sensing based analysis of climate, especially at much localized scale such as the urban microclimate has remained scarce in the country. On the other hand, remote sensing based assessments of urban growth have only focussed on quantifying long term historical

LULC changes (Wania, et al., 2014; Kamusoko, et al., 2013). For example, Wania, et al. (2014) used high resolution SPOT data to map expansion of built-up areas in Harare between 2004 and 2010 without providing further insight into the expected future patterns and impacts. Similarly, using medium resolution Landsat multi-spectral data, Kamusoko, et al. (2013) delimited expansion of built-up areas in Harare between 1984 and 2013 but did not extend focus to implications on observed and future land surface temperature patterns. Recently, Mushore, Mutanga, et al. (2017b) linked urban growth to historical land surface temperature trends using multi-spectral Landsat datasets but did not predict future trends as well as their implication on micro-climate of Harare. Attempts to predict future urban growth patterns and their implications on surface temperature using remote sensing in Zimbabwe have thus not yet been made, to the best of our knowledge. Therefore, there is need to predict future urban growth and implications on the thermal environment of Zimbabwean cities with high level of detail using medium resolution remote sensing datasets. This has potential to enhance local level adaptation practices, improve temperature related decision making and encourage sustainable urban growth which incorporates future implications of LULC conversions on micro-climates.

This study sought to identify optimal land cover indices derived from medium resolution Landsat data that best represents a correlation between urban surface temperature and LULC changes in Harare, Zimbabwe. The study further sought to adopt the selected indices to predict future distribution of LULC and surface temperatures using the coupled Cellular Automata and Markov Chain analysis. The study also aims at quantitatively using seasonally averaged land cover indices rather than single date states used in previous studies to represent land cover patterns of a season as input in the Cellular Automata Markov model.

8.2 Methods

8.2.1 Description of the study area

This study was conducted in Harare, the largest and capital city of Zimbabwe located in Southern Africa (Figure 8.1). The city is located between 17º40’ and 18º00’ south and between 30º55’ and 31º15’ east, lies approximately 1500m above mean sea level occupies approximately 94 000ha (Kamusoko, et al., 2013; Wania, et al., 2014). According to Kamusoko, et al. (2013), the geology to the north is dominated by gabbro and dolerite, the centre by an intrusion of metagreywacke and phylite while granites are popular to the east and south. The city has experienced rapid population growth, hence built-up densification since independence in 1980 (Kamusoko, et al., 2013; Wania, et al., 2014; ZIMSTAT, 2012).

Kamusoko, et al. (2013) outlined that the population of Harare increased from 642191 (1982) to 1435784 (2012). High density built-up areas dominate the south-western half of the city, which include the CBD, industrial areas and high density settlements, while low and medium density built-up areas dominate the north-eastern low and medium density residential suburbs (Wania, et al., 2014; Mushore, et al., 2016). According to Wania, et al. (2014), high income strata mainly occupy 'leafy' suburbs in the north while low income strata are concentrated in the high density residential areas in the south. Generally, the climate of Harare is humid with an average temperature of 18^{o}C and mean annual rainfall of 850mm (Iied, 2011; Torrance, 1981). The city experiences rainy (mid-November to mid-March), post rainy (mid-March to mid-May), cool (mid-May to mid-September) and hot (mid-September to mid-November) sub-seasons (Torrance, 1981). The hot season (mid-September to mid-November) was chosen because it is the warmest, hence ideal for understanding extreme seasonal thermal elevation during the year (Manatsa, et al., 2013). The peak temperature of the hot sub-season is recorded in October with an average of 28^{o}C. During the hot sub-season, grasslands are mainly dry while croplands are bare due to field preparation ahead of rainy sub-season thus worsening warming in lower atmosphere. Therefore, it is important to understand how urban growth will impact on temperature of the hot season as this has potential to adversely affect the thermal comfort of the growing population of Harare.

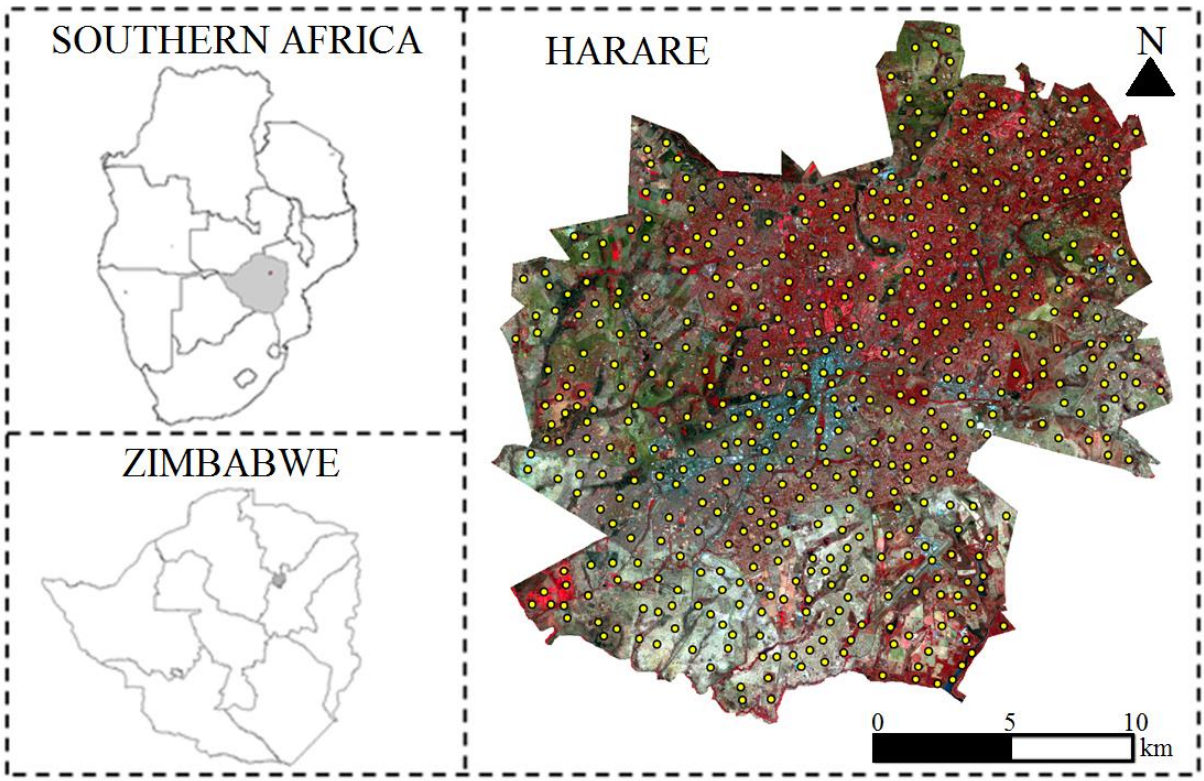

Figure 8.1: Location of the study area showing distribution of points used in modelling the relationship between indices and temperature.

8.2.2 Radiometric and geometric correction of remote sensing data

Landsat Thematic Mapper TM 5, Landsat ETM+7 and Landsat 8 OLI and TIRS images with Path/Row of 170/72 were acquired from the United States Global Survey Earth Resources Observation System (USGS-EROS) website (https://eros.usgs.gov/). Landsat data were selected due to adequate archival data, ease of access and performance in land cover classification and temperature analysis demonstrated in previous studies. Cloud-free images detailed in Table 8.1 and Table 8.2 were used for the study. The reflective bands were corrected for atmospheric effects using the Fast Line-of-sight Atmospheric Analysis of Spectral Hypercubes (FLAASH) module in the ENVI software. The images were then geometrically corrected using aerial photos, a 1:50 000 topo-sheet and 30 ground control points collected at intersection of major roads and invariant features recognisable on satellite images. In order to ensure independence between datasets, images in Table 8.1 were used to build the model and assess its performance for predicting land surface changes while data in Table 8.2 were used for making actual future predictions.

Table 8.1: Landsat path/row 170/72 images used for land use/cover classification and training of model to predict temperature.

Image	Date	Air temperature (^{o}C)	Relative humidity (%)
Landsat 5	22 October 1984	28.4	37.0
Landsat 7	19 October 2001	28.6	36.3
Landsat 8	18 October 2015	29.0	42.0

Table 8.2 shows an independent set of images obtained on cloud free days during the hot seasons (mid-September to mid-November) in 1984, 1993, 2001 and 2015. Three images were used per year in order to enable computation of average temperature and land cover indices for the prediction of future land cover and land surface temperature distribution. The use of seasonal averages was done for the purpose of eliminating the influence of randomness associated with single date images on predictions.

Table 8.2: Landsat images obtained in the hot season used for historical analysis and future prediction of land surface temperature

1984 (Landsat 5)	**1993 (Landsat 5)**	**2001 (Landsat 7)**	**2015 (Landsat 8)**

20 September	19 September	17 September	16 September
6 October	5 October	3 October	2 October
7 November	6 November	4 November	3 November

8.2.3 Qualitative LULC mapping and accuracy assessment

Land use and land cover maps for the year 1984, 1993, 2001 and 2015 were derived from 30m reflective bands of Landsat 5, 7 and 8 images using a supervised Support Vector Machine (SVM) algorithm. Each of the images was classified into the six major classes; i.e. CBD/industrial, high density residential, low-medium density residential, green spaces, croplands and water/wetlands (see Table 8.3). The SVM algorithm was chosen because it places no assumption to the probability distribution of the data and has low training data requirements. Furthermore the SVM classifier has demonstrated high performance in LULC classification than other classifiers like Maximum Likelihood Classifier (MLC), Parallelepiped, Minimum Distance, Mahalanobis Distance and the Artificial Neural Network classifiers (Omran, 2012; Adelabu, et al., 2013).

Table 8.3: Description of LULC classes observed in Harare during field survey

LULC class	**Description**
CBD/Industrial	Areas with very high density of buildings and a very high proportion of impervious surface that include central business district and industrial areas.
High density residential	High density residential areas and areas under residential development (bare or impervious) with low vegetation fraction.
Low-medium density residential	Established low and medium density residential areas with high vegetation fraction.
Croplands	Areas where intra-urban agriculture is practised including research sites which could be bare in the dry season
Green-spaces	Areas covered by grasslands and clusters of tree characterised by high vegetation fraction even during the dry season.
Water	Areas covered by water bodies or wetlands.

Since supervised classification requires field observation for training and accuracy assessment, 120 representative GPS points per class were obtained from a field survey between the 1st and 30th of April 2015. The points were split into training (80%) and validation (20%) based on recommendation by Adelabu et al. (2013). Regions of interest were used instead of points to

increase the number of sample points upon which to base classification and validation. Acharya et al., (2015) showed that higher accuracy is obtained using regions of interest than points. For 1984, 1993 and 2001 expert knowledge and auxiliary LULC data from topo-sheets and aerial photographs were used to create ground truth regions of interest for classification and accuracy assessment. The overall accuracy and the kappa coefficient were used to assess accuracy of the LULC classifications. Post classification (Yu, et al., 2013; Jensen, 1983) derived changes in area per land cover class between 1984 and 2015 were used quantify urban growth patterns in Harare.

8.2.4 Computation of urban and vegetation indices

Table 8.4 shows the description of indices whose potential to predict future land surface temperature was tested. The table consists of urban indices which were computed using digital numbers of indicated bands and vegetation indices which were computed using reflectance of indicated bands as described by Hasanlou & Mostofi (2015). As aforementioned, several indices were tested in order to compare the differences in the strengths of relationships with surface temperature and to identify indices with strongest capability to predict urban surface temperature.

Table 8.4: Derivation of urban and vegetation indices from Landsat data

Index	Computation	Reference
1. Normalized Difference Bareness Index (NDBaI)	$NDBaI = \frac{SWIR1-TIRS1}{SWIR1+TIRS1}$	(Zhao & Chen, 2005)
2. Normalized Difference Built-up Index (NDBI)	$NDBI = \frac{SWIR1-NIR}{SWIR+NIR}$	(Zha, et al., 2003)
3. Bare Soil Index (BI)	$BI = \frac{(SWIR1+RED)-(NIR+BLUE)}{(SWIR+RED)+(NIR+BLUE)}$	(Chen et al., 2004)
4. Urban Index (UI)	$UI = \frac{SWIR2-NIR}{SWIR2+NIR}$	(Kawamura et al., 1996)
5. Index-based Built-up Index (IBI)	$IBI = \frac{\frac{2\times SWIR1}{SWIR1+NIR} - \frac{NIR}{NIR+RED} - \frac{GREEN}{GREEN+SWIR1}}{\frac{2\times SWIR1}{SWIR1+NIR} + \frac{NIR}{NIR+RED} + \frac{GREEN}{GREEN+SWIR1}}$	(Xu, 2008)
6. Enhanced Built-up and Bareness Index (EBBI)	$EBBI = \frac{SWIR1-NIR}{10\times\sqrt{(SWIR1+TIRS1)}}$	(As-syakur et al., 2012)
7. Normalized Built Index (NBI)	$NBI = \frac{RED\times SWIR1}{NIR}$	(Chen, et al., 2006)

8. Normalized Difference Vegetation Index (NDVI)	$NDVI = \frac{NIR-RED}{NIR+RED}$	(Tucker, 1979)
9. Enhanced Vegetation Index (EVI)	$EVI = \frac{NIR-RED}{NIR+6\times RED-7.5\times BLUE+1}$	(Liu & Huete, 1995)
10. Soil Adjusted Vegetation Index (SAVI)	$SAVI = \frac{(NIR-RED)}{NIR+RED+L} \times (L+1)$, 0<L<1	(Huete, 1988)
11. Normalized Difference Water Index (NDWI)	$NDWI = \frac{NIR-SWIR1}{NIR+SWIR1}$	(McFeeters, 1996)
12. Modified Normalized Difference Water Index (MNDWI)	$MNDWI = \frac{GREEN-NIR}{GREEN+NIR}$	(Xu, 2006)
13. Vegetation fraction (FVG)	$FVG = \frac{NDVI-NDVI_{Soil}}{NDVI_{Veg}-NDVI_{Soil}}$	(Gutman & Ignatov, 1998)

*1 to 7 are urban indices computed from digital numbers of indicated images while 8-13 are vegetation indices computed using radiances of indicated Landsat bands (Hasanlou & Mostofi, 2015).

8.2.5 Derivation of land surface temperature

Land surface temperatures for each year were derived from thermal bands of Landsat 5 (Band 6), Landsat 7 (Band 6) and Landsat 8 (Band 10) acquired on dates indicated in Table 8.1 and Table 8.2. In order to avoid the effect of seasonality, images obtained in the month of October were used. Although Landsat 8 has two thermal bands (Bands 10 and Band 11) retrievals from Band 10 were used as they have been found to be less affected by atmospheric carbon dioxide and therefore more accurate than from Band 11 (Yang, Lin, et al., 2014; Reddy et al., 2014). Retrieval of land surface temperature involved conversion of digital numbers to radiances, computation of brightness temperatures from radiance and emissivity correction to obtain surface temperatures from brightness temperature maps (Sobrino, et al., 2004; Xiao, et al., 2007; Avdan & Jovanovska, 2016). Conversion of digital numbers (DN) to radiances (L_λ) was done using the Reflectance Toolbox an extension added to ArcMap 10. The tool extracts parameters from metadata files and applies them together with corresponding thermal data. Brightness temperature (T_b) was derived from thermal radiance using Equation 8.1 which is the single channel Landsat specific estimate of Planck's blackbody temperature (Srivanit, et al., 2012; Stathopoulou, et al., 2006; Chen, et al., 2006).

$$\boldsymbol{T_b = \frac{K_2}{\ln\left(\frac{K_1}{L_\lambda}+1\right)}}$$ Equation 8.1

In this study Landsat 5, 7 and 8 thermal data were used to retrieve land surface temperature in 1986, 1993, 2001 and 2015. Therefore, values of K_1 and K_2 for each Landsat mission are shown in Table 8.5 (Srivanit, et al., 2012; Weng & Lu, 2008; Weng, et al., 2007).

Table 8.5: K_1 and K_2 coefficient values for Landsat 5, 7 and 8 thermal data

Mission	**K_1 [W/(m^2 srμm)]**	**K_2 [W/(m^2 srμm)]**
Landsat 5	607.76	1260.56
Landsat 7	666.09	1282.71
Landsat 8	774.89	1321.08

For each thermal band, we retrieved pixel-based land surface emissivity map (ε) from spectral radiance and blackbody as developed and described by Yang, et al. (2004) and also applied recently by (Mushore, et al., 2017a). Finally, actual land surface temperature was obtained after applying emissivity correction on brightness temperature using Equation 8.2 (Weng, et al., 2007).

$$\boldsymbol{T_S = \frac{T_B}{1+\left(\frac{\lambda T_B}{\rho}\right)\ln \varepsilon}}$$ Equation 8.2

The symbol λ represents the wavelength of emitted thermal radiance (11.5μm) while ρ is equal to 1.438x10^{-2}mK. This procedure was used to retrieve land surface temperature (LST) for all the date corresponding to images described in Tables 8.1 and 8.2 above. The LST were used to explain long term changes in temperature for the hot season as well as in training model to predict future temperatures as will be described in sections to follow. Using thermal data for the dates shown in Table 8.2, the average land surface temperature for 1984, 1993, 2001 and 2015 was computed. This was done in order to check if the land surface temperatures were indeed changing in response to urban growth and ascertain if it was necessary to predict future changes.

8.2.6 Variable selection for the prediction of temperature

Estimation of surface temperatures using several variables requires that correlation between the predictor variables and surface temperature should be high, with no collinearity between the variables. The indices described in Table 3 were tested for strength of correlation with land surface temperature, as well as with each other. The indices with highest correlation with land surface temperature were selected for use in linear regression model to predict future land surface temperatures. Correlation between these indices was also assessed to avoid use of highly correlated predictors which can cause errors due to collinearity. Therefore, a multi-

variate linear model was developed using indices which are weakly correlated with each other but strongly correlated with land surface temperature. In order to assess the performance of the model, we used it to predict the known land surface temperature of 2015 and accuracy was quantified using Mean Absolute Percentage error [MAPE] -Equation 8.3- (Lam et al., 2001).

$$\boldsymbol{MAPE}\ (\%) = \frac{\mathbf{1}}{\boldsymbol{N}} \sum_{\boldsymbol{i=1}}^{\boldsymbol{N}} \left(\left| \frac{\boldsymbol{T_{predicted} - T_{observed}}}{\boldsymbol{T_{observed}}} \right| \right)_{\boldsymbol{i}} \boldsymbol{X100} \qquad \text{Equation 8.3}$$

Where $T_{predicted}$ is the modeled surface temperature and $T_{observed}$ is the actual land surface temperature recorded from Landsat data for the *ith* pixel. The mean absolute percentage is a measure of prediction accuracy which expresses error as a percentage. Accuracy of the model in predicting temperature was also assessed using Nash Sutcliff efficiency, Root Mean Square Error, Mean Bias Error and Index of Agreement. After accuracy assessment, the model was then used to predict land surface temperature distribution for the period from 2025 to 2045 at 10 year intervals. The 10 year intervals were chosen given that historical analysis had shown significant changes at similar time steps.

8.2.7 Prediction of future LULC and LST using Markov and Cellular Automata analysis

The flowchart in Figure 8.2 summarizes the procedure from remote sensing data collection to prediction of future LULC and LST distribution using Cellular Automata Markov Chain analysis. Araya and Cabral (2010) compared results of simulation for 2006 with a real map for 2006. In this study the simulation of the 2015 state was done for validation purposes so that the predicted would be compared with the actual land surface temperature distribution. The details of the summarized steps are elaborated in section 8.2.8 and 8.2.9.

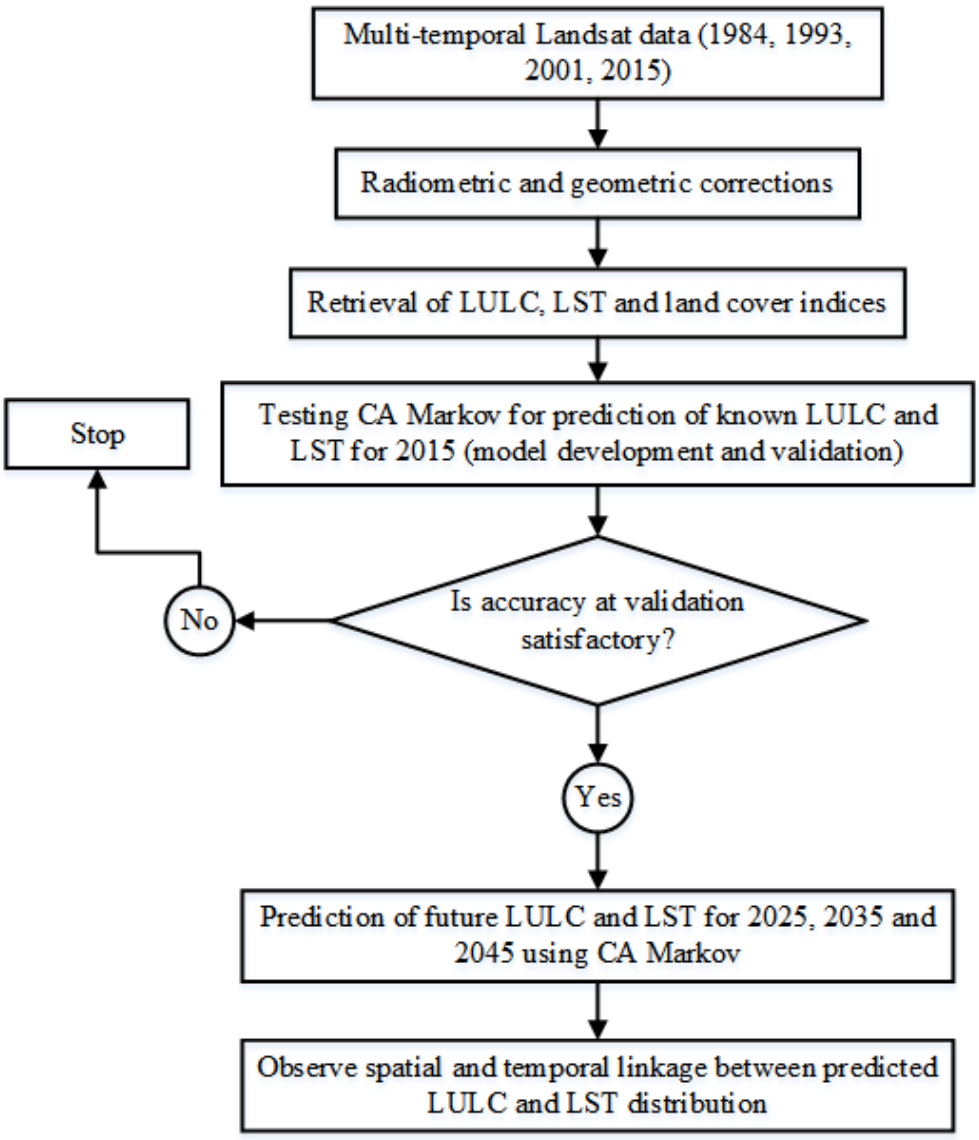

Figure 8.2: Summary of procedure up to prediction of future LULC and LST

8.2.8 Prediction of urban growth in Harare using CA Markov analysis

IDRISI is an integrated Geographical Information and image processing licensed software providing close to 300 modules for analysis and display of digital spatial information (Eastman, 2012b). Environmental monitoring, decision support, risk analysis, modeling and surface characterization tools are found in the software. Among the modules in IDRISI is the Markov Chain analysis which is a non-deterministic method for determining land use changes between periods using a series of values the next of which depends on the current (Aaviksoo 1995; Elsner et al 2003; Bayes Ahmed 2012; Araya and Cabal 2010). The Markov model gives the probability that the system develops from initial state *i* to a state *j* over a time interval *T* (Aaviksoo, 1995). Markov Chain produces (i) transition matrix which indicates the number of pixels that are expected to change from one state to another, (ii) transition probability matrix

showing probability that each land use category will change to every other and (iii) conditional probability maps which display the probability that each land use type might be found at each pixel (Hashem & Balakrishnan, 2015). For an extended description of prediction of future LULC using Markov Chain see Araya & Cabral (2010) and Ahmed et al (2013). The Markov Chain model was chosen due to its proven capabilities in predicting LULC changes in time as well as its simplicity of implementation (Araya & Cabral, 2010; García-Frapolli, et al., 2007). Furthermore, Markov Chain is effective in predicting changes of a complex system (Li, et al., 2011), hence the need to test its capability for estimating changes in heterogeneous urban systems. However, the Markov Chain model only derives changes over time but does not map their spatial distribution. In order to produce a map of the future states, the Markov Chain model is coupled with other models such as the Stochastic Choice, Multi-Layer prediction system and Cellular Automata (Eastman, 2012b). Therefore, the outputs of the Markov Chain model are used as input in other models to produce maps of future land use distribution. In this study the Cellular Automata (CA) was selected to map the spatial distribution of projected urban growth and impact on land surface temperature due to its simplicity and parsimony (García-Frapolli, et al., 2007). The CA allows the transition of several classes of pixels using a Markov transition matrix, suitability map and a neighborhood filter (Araya & Cabral, 2010). According to Fan, et al. (2008), the CA can be used to simulate complex dynamic spatial patterns through a set of simple rules. In CA the state of pixel at the next time step is computed based on the states of all cells in its neighborhood at the current time. The suitability of a pixel for a given transition is determined by pixel values within a defined kernel. The more the pixels of the same category of land cover in the neighborhood the more the suitability of that particular type increases, else the pixel remain unchanged (Ahmed & Ahmed, 2012).

Prediction of LULC distribution for 2015, 2025, 2035 and 2045 was done using the coupled Markov Chain and the Cellular Automata models (also called Cellular Automata Markov Chain Analysis) in IDRISI software. In summary, the transition probability matrices obtained from Markov Chain analysis were used as input to the Cellular Automata model which produces maps of predicted LULC distributions. Therefore, combining Markov Chain with Cellular Automata produced spatial and temporal changes in LULC. Before we employed the Cellular Automata Markov Chain analysis in actual prediction, we tested its potential to predict future LULC patterns in a complex urban setting. In order to achieve this, we used LULC transitions that occurred between 1986 and 2001 to predict LULC distribution for 2015. The predicted

LULC were compared with the pattern obtained using SVM classification in 2015. The accuracy of the prediction for 2015 was assessed using the Kappa Index of Agreement (KIA) which tests the level of agreement between two maps of the same event (Sayemuzzaman & Jha, 2014; Eastman, 2012a). According to Sayemuzzaman and Jha (2014), KIA compares two maps to statistically check for the agreement between the classes. An overall KIA as well as KIA per class are obtained with values ranging between 0 and 1 (the closer to 1 the values, the higher the agreement between the spatial distribution of classes on compared maps). Therefore, the KIA was thus used to assess performance of CA Markov in predicting LULC changes by comparing the LULC map form supervised SVM classification with the modeled map for 2015. After assessing model accuracy, we used LULC patterns of 1986 and 2015 in Cellular Automata Markov Chain analysis to predict future distribution of landscapes for 2025, 2035 and 2045.

8.2.9 Prediction of land surface temperature distribution in Harare using land cover indices in CA Markov analysis

The Urban Index (UI) was selected as described in section 8.2.6 as the best predictor variable of land surface temperature distribution in the Cellular Automata Markov Chain analysis. Details of performance of different land cover indices in predicting land surface temperature leading to the selection of UI are explained in Table 8.8 under section 8.3.3 below. In order to avoid the limitation of randomness associated with single date images, in each of 1984, 2001 and 2015 an average UI for the hot season was calculated using images obtained in September, October and November as described in Table 8.2. The average UI for 1984 and 2001 were input into the Markov Chain model to generate transition probability matrices which were used to map future state of the index for 2015 in the CA model. Similarly, the average UI for 1984 and 2015 was used to in CA Markov analysis to predict the state of the UI in 2025, 2035 and 2045. A simple linear regression function (see section 8.3.4) was used to convert UI predictions into land surface temperature distributions for 2015, 2025, 2035 and 2045. Since Cellular Automata Markov Chain analysis predicts classes, the maps UI maps were reclassified before input into model so that they could predict 18-28^{o}C, 28-32^{o}C, 32-36^{o}C and 36-45^{o}C surface temperature classes. The categories were chosen solely to enable comparison of land surface temperature distributions in different years since the same ranges were used to map surface temperature classes observed both in 1984 and 2015. Therefore, the major outcomes of this step were land surface temperature predictions for Harare for 2025, 2035 and 2045.

8.2.10 Statistical significance of the forecast urban growth and land surface temperature

We tested the statistical significance of the predicted changes in LULC and temperature distribution between 2015 and 2045. We applied the test on coded LULC and temperature class values extracted from 522 points. The temperature categories for each period were coded 1 to 5 while LULC classes were coded 1 to 6 based on requirements and output of Markov analysis. Initially, we used the Shapiro-Wilk statistic to test for normality (Shapiro & Wilk, 1965). The changes in LULC and temperature were tested for significance using the Mann Whitney statistic (Mann & Whitney, 1947; Birnbaum, 1956) following normality test of the data ($p>0.05$). We tested the hypothesis Ho: that spatial distributions of LULC and land surface temperature were different versus the alternative hypothesis Ha: the LULC and land surface temperature pairs were not the same in 2015 and 2045.

8.3 Results

8.3.1 Observed LULC and transitions from 1986 to 2015

Table 8.6 shows changes in land use and land cover distribution between 1984 and 2015 obtained at high accuracy using the Support Vector Machines Algorithm. Overall accuracy and kappa were 88.55% and 0.85, 87.70% and 0.83, 90.86% and 0.87 and 87.59% and 0.82 for the years 1984, 1993, 2001 and 2015, respectively. Table 4 displays LULC transitions that were observed between 1984 and 2015 as the city was growing. Built-up areas increased at the expense of green-spaces and croplands from 1984 to 2015 in Harare (Table 8.6). For example, high density residential areas increased in coverage from 244.24km^2 in 1984 to 470.02km^2 in 2015 while green-spaces, such as grasslands and forests decreased from 234.38km^2 to 57.42km^2.

Table 8.6: Changes in proportion of LULC types between 1984 and 2015

	Coverage (km^2) and percentage (%) of total area is in brackets			
UHI level	**1984**	**1993**	**2001**	**2015**
CBD/Industrial	23.00 (2.7)	25.64 (3.0)	24.74 (2.9)	48.92 (5.7)
High density res	244.24 (28.6)	385.48 (45.0)	441.84 (51.7)	470.02 (55.0)
Low density res	235.68 (27.6)	253.52 (29.7)	255.11 (29.8)	244.05 (28.6)
Green-spaces	234.38 (27.4)	105.09 (12.3)	94.73 (11.1)	57.42 (6.7)
Croplands	110.54 (12.9)	80.92 (9.5)	33.17 (3.9)	30.27 (3.5)
Water	6.98 (0.8)	4.18 (0.5)	5.24 (0.6)	4.15 (0.5)

*res: residential areas

8.3.2 Observed satellite based temperature transitions from 1984 to 2015

Land surface temperatures have increased in response to urban growth in Harare metropolitan city between 1984 and 2015. Visual inspection of Figure 8.3 shows that in 1984, the area was

dominantly covered by temperatures in the 18 to 28ºC category, compared to other later periods. In 2015, the 36 to 45ºC category became dominant although lower surface temperature categories still remained in some areas to the northeast. Larger rises in temperature were observed in the southwestern half with high density built-up areas than in the northeastern areas with spaced out buildings. Although, land surface temperatures are markedly warming over time, temperatures below 30ºC are still common in the northern half where 'leafy' low and medium density residential areas are found. However, even in cooler periods, such as 1984 and 1993, higher surface temperatures were observed in the central business district and industrial areas than in other areas. Of great concern is that temperatures have shifted to the 36-45ºC range in the southern half which may cause heat transfers in the lower atmosphere causing elevation of temperatures where the vulnerable low income strata reside.

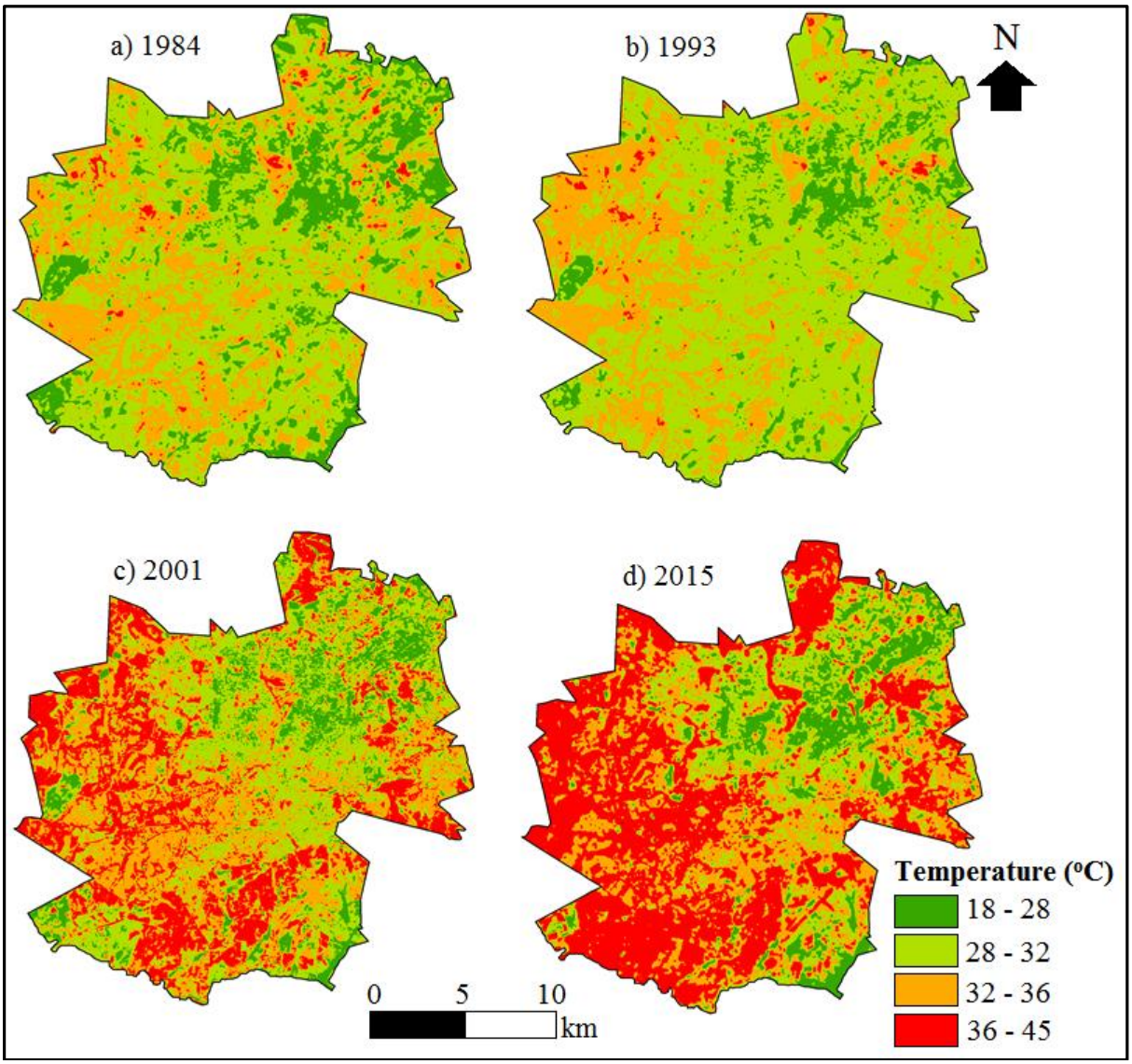

Figure 8.3: Observed changes in the distribution of mean surface temperatures during the hot season in a) 1984, b) 1993, c) 2001 and d) 2015.

Table 8.7 provides a detailed analysis of changes in land surface temperature observed in Harare between 1984 and 2015. As the city grew between the periods the proportion of land surface experiencing temperature in the 18-28^{o}C categories decreased by about 7%. During the same period the coverage of high land surface temperatures (36-45^{o}C) in the hot sub-season increased by at least 40% indicating a strong land surface warming bias in Harare.

Table 8.7: Average land surface temperature responses to urban growth in Harare

	Coverage (km^2) and percentage (%) of total area is in brackets			
Temperature (^{o}C)	**1984**	**1993**	**2001**	**2015**
18 – 28	151.69 (17.7)	84.38 (9.9)	85.68 (10.0)	86.23 (10.1)
28 – 32	444.25 (51.9)	520.99 (60.9)	264.68 (30.9)	166.26 (19.4)
32 – 36	248.06 (29.0)	242.02 (28.2)	288.90 (33.8)	239.56 (28.0)
36 – 45	11.83 (1.4)	8.44 (1.0)	216.57 (25.3)	363.78 (42.5)

8.3.3 Variable selection: correlation between urban indices and temperature

Table 8.8 shows that there was strong correlation between surface temperature and BI, EBBI, FVG, IBI, NDBI, SAVI and UI indicated by magnitudes of correlation coefficients greater than 0.5. The other indices displayed weaker correlation with temperature; for example, the EVI had the weakest correlation with surface temperature (correlation coefficient was less than 0.001). Although BI, EBBI, IBI, NDBI and SAVI had strong correlation with land surface temperature, they were also strongly correlated with each other and with FVG. However, FVG had a stronger correlation with temperature (0.8836) than BI, EBBI, IBI, NDBI and SAVI. UI had the strongest correlation with temperature (r=0.9381) and also had a strong negative correlation with FVG (r=-0.9089). UI was found to be the best predictor of urban surface temperature in comparison to other indices due to highest correlation with land surface temperature. This is why UI was used to predict future surface temperature patterns as described in Section 8.2.9 above.

Table 8.8: Correlation between temperature and urban as well as vegetation indices

	BI	EBBI	EVI	FVG	IBI	MNDWI	NBI	NDBaI	NDBI	SAVI	UI	TS
BI	1.0000	0.9804	0.0009	-0.8876	0.9742	0.4408	0.9089	0.6576	0.9749	-0.5895	0.9548	0.7783
EBBI	0.9804	1.0000	0.0008	-0.8485	0.9924	0.3188	0.8634	0.6101	0.9902	-0.5958	0.9584	0.7639
EVI	0.0009	0.0008	1.0000	-0.0001	0.0010	-0.0008	0.0002	-0.0000	0.0010	-0.0001	-0.0008	0.0033
%GF	-0.8876	-0.8485	-0.0001	1.0000	-0.8572	-0.3758	-0.8186	-0.4186	-0.8522	0.7600	-0.9089	-0.8836
IBI	0.9742	0.9924	0.0010	-0.8572	1.0000	0.2599	0.8215	0.5491	0.9976	-0.4247	0.9650	0.5015
MNDWI	0.4408	0.3188	-0.0008	-0.3758	0.2599	1.0000	0.6542	0.7754	0.2632	0.0436	0.2710	-0.0797
NBI	0.9089	0.8634	0.0002	-0.8186	0.8215	0.6542	1.000	0.8035	-0.4037	0.8302	0.8399	0.4550
NDBaI	0.6576	0.6101	-0.0000	-0.4186	0.5491	0.7754	0.8035	1.0000	0.5541	-0.0867	0.4866	0.0634
NDBI	0.9749	0.9902	0.0010	-0.8522	0.9976	0.2632	-0.4037	0.5541	1.0000	-0.6232	0.9683	0.8357
SAVI	-0.5895	-0.5958	-0.0001	0.7600	-0.4247	0.0436	0.8302	-0.0867	-0.6232	1.0000	-0.7089	-0.6062
UI	0.9548	0.9584	-0.0008	-0.9089	0.9650	0.2710	0.8399	0.4866	0.9683	-0.7089	1.0000	0.9381
TS	0.7783	0.7639	0.0033	-0.8836	0.5015	-0.0797	0.4550	0.0634	0.8357	-0.6062	0.9381	1.0000

8.3.4 Retrieval of surface temperature from the urban index

Figure 8.4 shows the regression model for predicting surface temperature based on UI. Land surface temperature increase as UI increased and the relationship between the two was strong (R^2 = 0.88) and significant at 95% significant level ($p<0.05$). The relationship did not suffer from saturation which affects indices such as NDVI as UI continued to increase with temperature unbound.

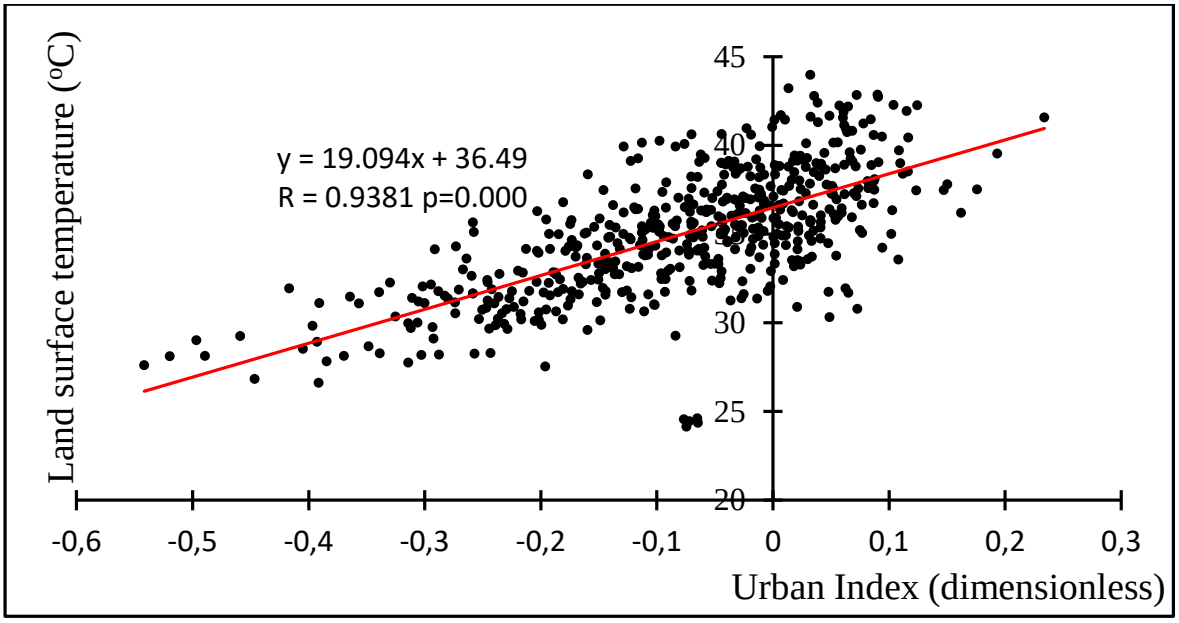

Figure 8.4: Linear model for the prediction of surface temperature from UI.

8.3.5 Accuracy of temperature retrievals using the urban index

The regression model was tested on an independent Landsat data obtained in October 2015 and the model closely resembled the observed temperature trends (Figure 8.5). Temperature retrieved from UI was compared with that retrieved directly from thermal infrared data (Band 10) of Landsat 8. Based on 200 points sampled across the study area (indicated in Figure 8.1), the UI predicted surface temperature with high accuracy (mean relative percentage error=5.27%, Nash Sutcliff efficiency=0.74, root mean square error=1.26°C, mean bias error=-0.0002°C and index of agreement=0.80).

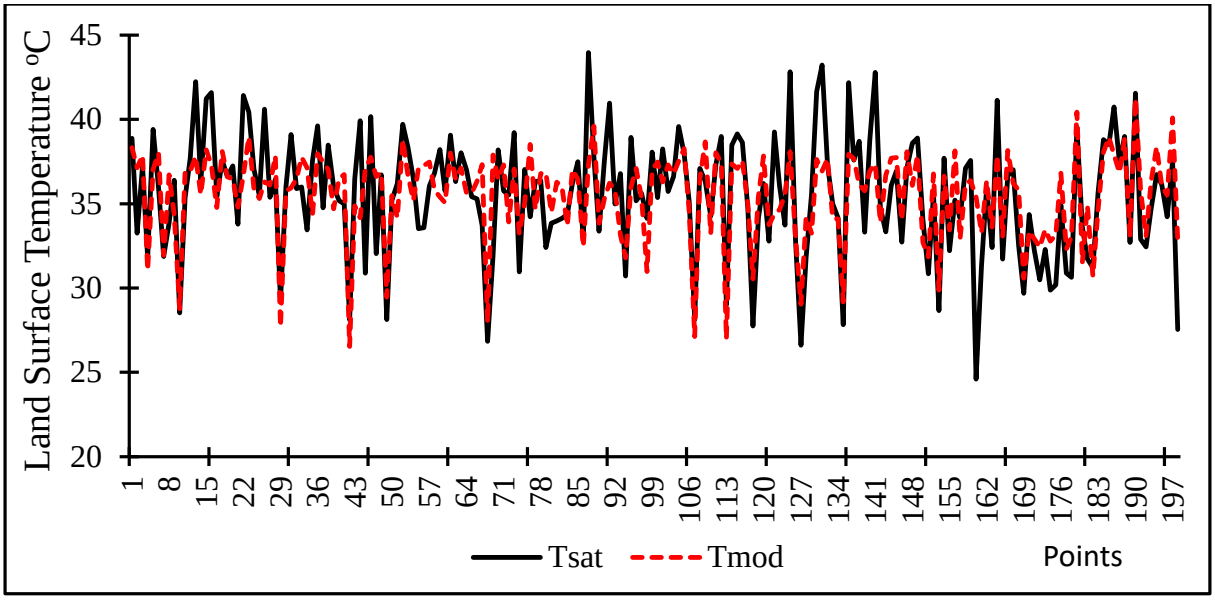

Figure 8.5: Comparison of surface temperature derived from thermal band with surface temperature derived from the UI.

8.4 Future LULC and LST for 2025, 2035 and 2045

8.4.1 Accuracy assessment of Cellular Automata Markov Chain LULC prediction

Visual inspection showed agreement between LULC distribution mapped from supervised image classification using the Support Vector Machine classifier and LULC distribution for 2015 predicted using the Cellular Automata Markov Chain analysis (Figure 8.6). The model managed to closely mimic the spatial distribution of LULC types as classified by the SVM guided by in-situ observations.

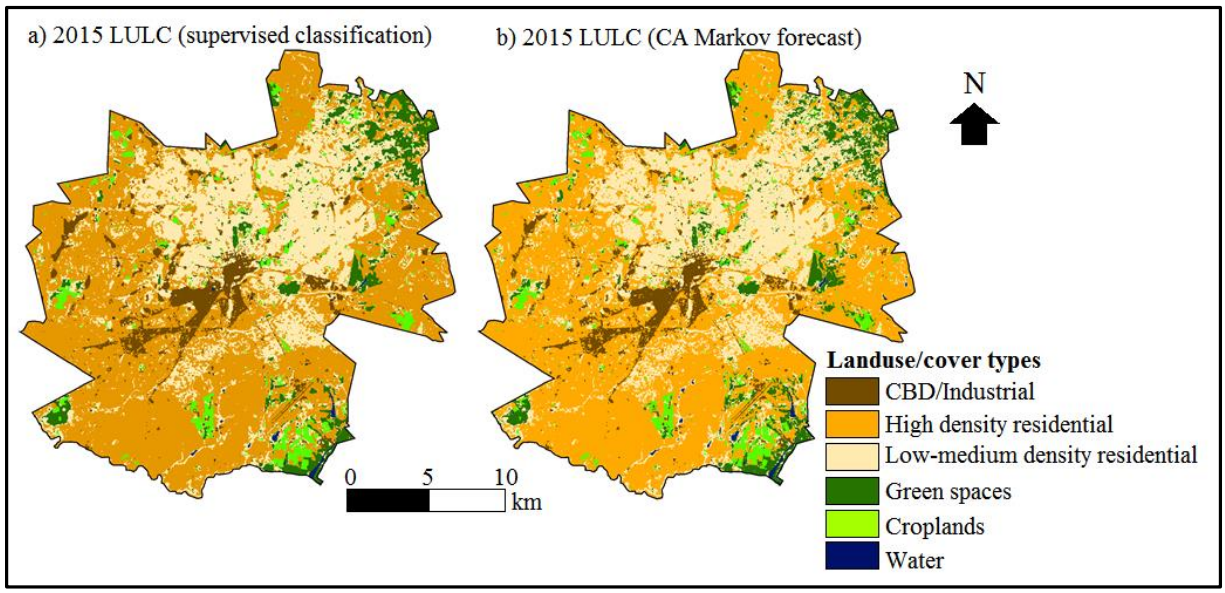

Figure 8.6: LULC distribution for 2015 mapped using a) supervised classification and b) Cellular Automata Markov Chain analysis prediction.

The overall Kappa Index of Agreement (KIA) between the LULC predicted using Cellular Automata Markov and the distribution mapped using SVM classifier was 0.91 (Table 8.9). The agreement was strongest (KIA=0.88) between the CBD/Industrial and weakest (KIA=0.63) between the green-space classes in the two maps. The maps matched with an overall high accuracy of 89.29% using the SVM supervised classification LULC map for 2015 as a reference.

Table 8.9: Statistical measurement of agreement between supervised classification and Cellular Automata Markov Chain based prediction for 2015.

LULC class	**Kappa Index of Agreement**
CBD/Industrial	0.88
High density residential areas	0.86
Low-medium density residential areas	0.86
Green-spaces	0.63
Croplands	0.65
Water/wetlands	0.77

8.4.2 Future LULC distribution in Harare

Figure 8.7 shows that the coupled Cellular Automata Markov Chain model predicted growth of low-medium and high density residential areas at the expense of green-spaces and wetlands in 2025, 2035 and 2045. Furthermore, the model predicted that if patterns observed between 1984 and 2015 would persist built-up areas may encroach into parks.

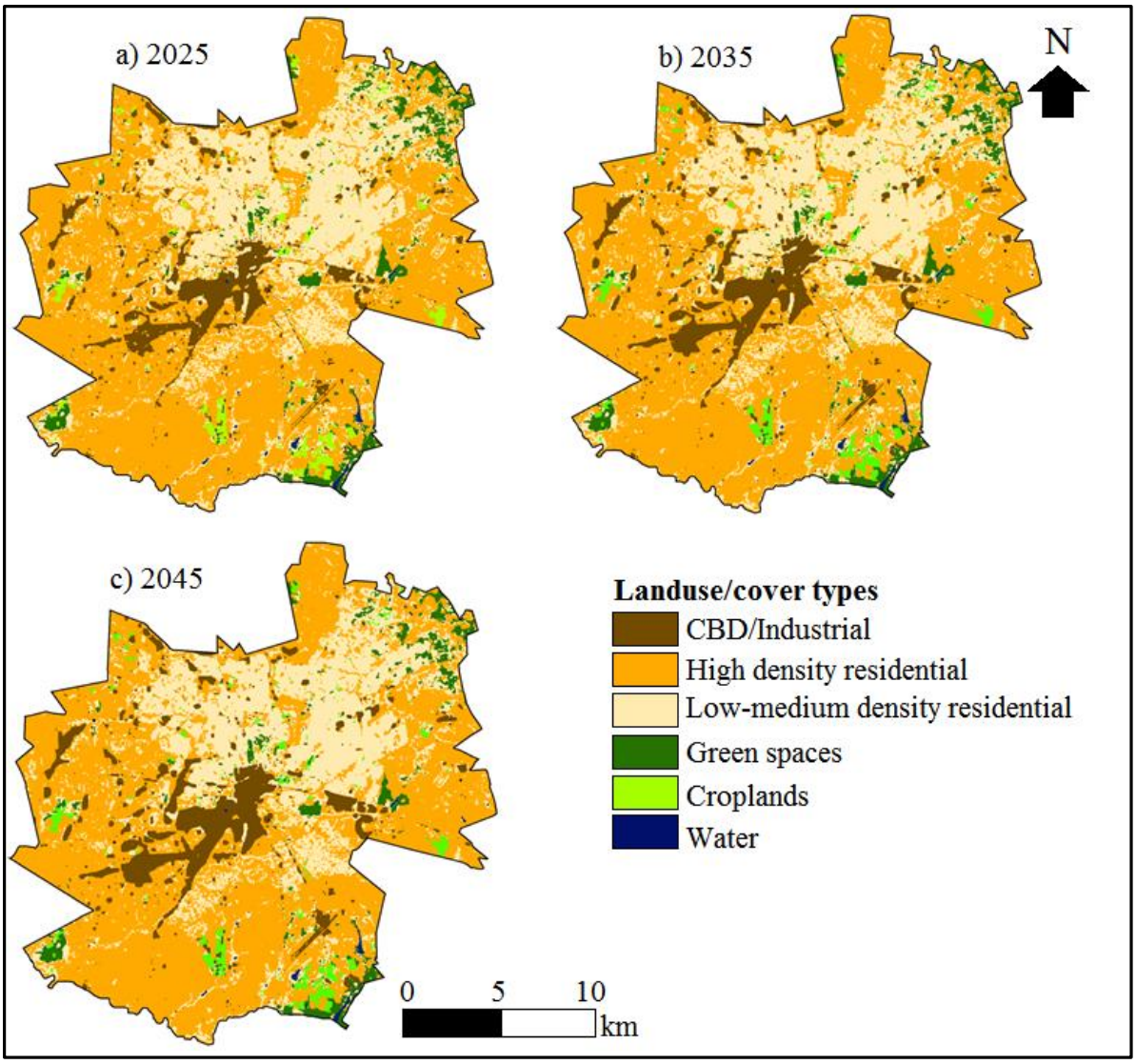

Figure 8.7: Predicted distribution of LULC in a) 2025, b) 2035, and c) 2045

Built up areas are predicted to continue increasing from their current extent through to 2045 as indicated by Table 8.10. For example CBD and industrial areas are predicted to grow from 48.92 to 79.32km^2 between 2025 and 2045. High density residential areas are predicted to increase in coverage from 470.02 to 490.36km^2. As the city grows, green-spaces would be expected to decrease in area from 57.42 to 27.85km^2 while croplands would to decrease from 30.27 to 16.93km^2 during the same time interval. Low-medium density residential areas are predicted to slightly decrease in coverage from 244.05 to 237.08km^2 during the same period. Therefore, based on model predictions and assumptions, future growth may be characterized mainly by expansion of densely built-up areas at the expense of wetlands, croplands and green spaces.

Table 8.10: Markov and Stochastic chain based future coverage of LULC classes in Harare

	Coverage (km^2) and percentage (%) of total area is in brackets			
LULC type	**2015**	**2025**	**2035**	**2045**
CBD/Industrial	48.92 (5.7)	66.32 (7.75)	73.43 (8.58)	79.32 (9.27)
High density res	470.02 (54.9)	476.23 (55.7)	482.09 (56.3)	490.36 (57.3)
Low density res	244.05 (28.5)	237.10 (27.7)	236.73 (27.7)	237.08 (27.7)
Green space	57.42 (6.7)	43.39 (5.1)	38.33 (4.5)	27.85 (3.3)
Croplands	30.27 (3.5)	28.04 (3.3)	20.76 (2.4)	16.93 (2.0)
Water/wetlands	4.15 (0.5)	3.73 (0.4)	3.48 (0.4)	2.70 (0.3)

*res: residential areas

8.4.3 Predicted temperature distribution in Harare up to year 2045

The rising temperature trends observed between 1984 and 2015 may continue through to 2045 (Figure 8.8). The coverage of high temperature category (greater than 38^{o}C) was predicted to increase at the expense of low temperature categories. However, in all the predictions i.e. 2025, 2035 and 2045 north-eastern areas where low density residential areas are located were relatively cooler than southern-western areas where high density residential areas are found. Predictions show that land surface temperatures below 32^{o}C will potentially remain common in the northern half where low and medium density residential areas are located. Furthermore, assuming that growth patterns observed between 1984 and 2015 persist, expansion of high density built-up areas would result in high surface temperatures (above 40^{o}C) is southern areas such as in high density residential areas.

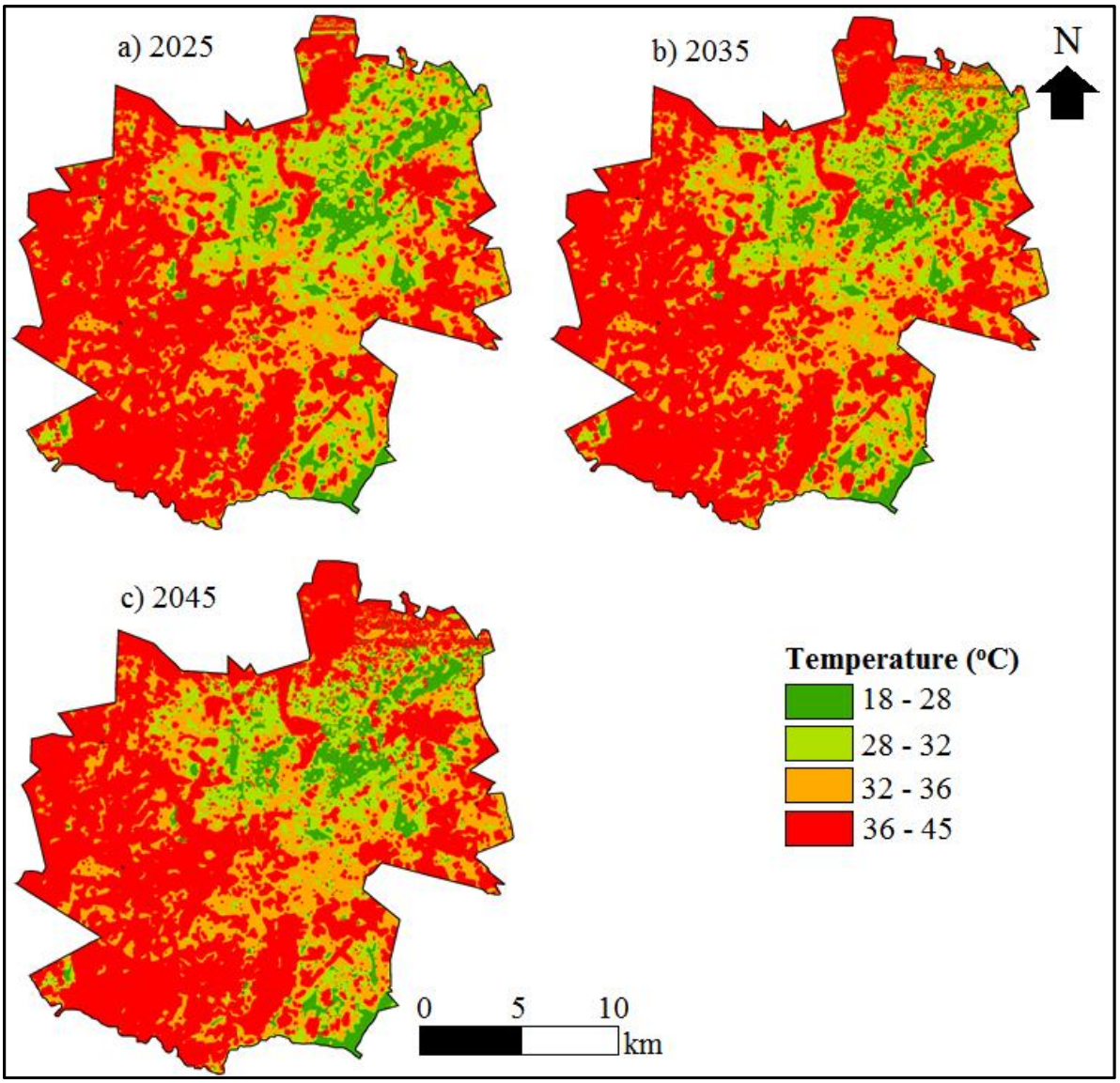

Figure 8.8: Predicted temperature distribution for Harare in a) 2025, b) 2035, and c) 2045.

Table 8.11 shows that coverage of low temperature classes (18-28ºC and 28-32ºC) may decrease while most areas, especially in the south, could shift towards high temperature (greater than 36ºC). The model predicted that the 18-28ºC temperature range could decrease in coverage from 86.23km^2 to 55.97km^2 while the 36-45ºC category is expected to increase from 363.78 to 498.45km^2 between 2015 and 2045. Spatial distributions land surface temperature classes significantly changed between 2015 and 2045 ($p<0.05$).

Table 8.11: Projected changes in surface temperature due to urban growth

	Coverage in each (km^2 and % of total area)			
Temperature (ºC)	**2015**	**2025**	**2035**	**2045**
18 - 28	86.23 (10.1)	65.43 (7.7)	60.08 (7.0)	55.97 (6.3)
28 - 32	166.26 (19.4)	122.64 (14.3)	115.22 (13.5)	107.68 (12.7)
32 - 36	239.56 (28.0)	209.34 (26.5)	203.10 (23.7)	197.74 (23.1)
36 - 45	363.78 (42.5)	458.43 (53.6)	477.43 (55.8)	498.45 (58.0)

8.5 Discussion

Urban growth is expected to continue across the globe hence the need to understand its implications on urban landscapes and climate. In this study, we used the coupled Markov Chain and Cellular Automata models to predict future LULC and surface temperature distribution in Harare. In order to predict the responses of temperature to urban transformation, we tested the potential of a variety of land cover indices to predict changes in the spatial distribution of temperature. The UI was found to be the best index for predicting future land surface temperature distribution when compared to a variety of other indices such as NDVI, FVG and NDBI. Therefore, a simple linear regression model was preferred and used to forecast urban growth as well as associated changes in temperature distribution. The use of a simple linear regression model is supported by Ahmed et al (2013) who observed that utilization of multivariate regression is only suitable where predictor variables are not strongly correlated with each other. In this study, all predictors of strength were collinear hence the selection of UI which had the strongest correlation with temperature to avoid errors.

Therefore, we used the UI as a proxy for urban growth and its future spatial distribution to map future distribution of land surface temperature categories. Comparison of LST derived from thermal band with that derived from linear model using UI showed that the model predicted temperature with a mean absolute error of 1.85ºC. The high performance of UI in predicting urban growth induced warming can be explained by previous studies which showed that it is strongly correlated with a variety of indicators of urban growth (Kawamura et al., 1997; Katayama et al., 2000). For example, Katayama et al. (2000) observed that UI increases with density of buildings and decreases with NDVI in Tokyo Bay. Although the correlation between UI and temperature was not tested in previous studies, the high predictive power observed in this study is because areas with high density of buildings and low vegetation fraction are known to have high temperatures (Senanayake, et al., 2013; Zuvela-aloise et al., 2015). Kawamura et al. (1997) also observed that UI was high in areas where residential energy and water consumption were high in Colombo, Sri Lanka. Studies have also shown that domestic energy

and water consumption increases with urban heat intensity, hence the high correlation between UI and temperature (Rawal & Shukla, 2014; Wang, Chen, et al., 2010). The UI was also found to be high in bare areas thus enhances its potential to predict temperature since bare and built-up areas are comparatively hot during the day (Srivanit, et al., 2012; Pu, et al., 2006). Therefore, the comparative strength of the relationship between UI and land cover properties enhanced its potential to map urban growth and corresponding responses of temperature.

The SVM is a classifier of repute hence high classification accuracies obtained both in 1984 and 2015 despite the complexity of urban LULC distribution. This is consistent with previous studies such as by Adelabu et al (2013) which showed that SVM classifier results in high accuracy maps. The high quality of maps is also linked to the use of digitized regions of interest instead of points as ground-truth data for classification hence accuracies above the 80% requirement (Omran, 2012). The derived LULC maps showed that built up areas increased while wetlands and vegetation cover decreased between 1984 and 2015 which agrees with previous studies in the same area (Wania, et al., 2014; Kamusoko, et al., 2013). The Cellular Automata Markov Chain analysis reliably predicts LULC patterns as indicated by strong agreement between the predicted 2015 map and the one derived from supervised classification. The KIA was close to 1, implying close similarity and strong agreement between the modeled and observed LULC distribution for 2015. Due to high accuracy and strong agreement with the known LULC distribution for 2015, the Cellular Automata Markov Chain model was deemed reliable for future predictions. Based on LULC changes between 1984 and 2015, the Cellular Automata Markov Chain model projected that unless other interventions are employed and similar patterns persist, coverage of built up area will continue increasing at the expense of natural covers through to 2040. This finding is consistent with global predictions that urban population will continue to rise resulting in expansion of built-up areas at the expense of green-space (Araya & Cabral, 2010; Ahmed & Ahmed, 2012; Seto, et al., 2012; McCarthy, et al., 2010; Nayak & Mandal, 2012).

Based on Cellular Automata Markov model, temperatures may increase due to urban growth between 2015 and 2040, which agrees with already observed warming trends in Zimbabwe (Dube & Phiri, 2013; Chagutah, 2010; Unganai, 1996; Zvigadza, et al., 2010; Mushore, 2013a; Brown., et al., 2012). In this study, area covered by 18-28, 28-32 and 32-34 ^{o}C temperature categories are projected to decrease while area covered by warmer categories such as the 40-

46^{o}C are expected increase. The warming patterns are in response to LULC distribution changes which will see built up areas increase in coverage at the expense of wetlands and green-spaces. The future rises in temperature due to urban growth induced LULC changes are also consistent with other previous studies (McCarthy, et al., 2010; Larsen & Gunnarsson-Östling, 2009; Omran, 2012; Sithole & Odindi, 2015; Odindi, et al., 2015; Nayak & Mandal, 2012; Zhang, Qi, et al., 2013; Hung, et al., 2006; Amiri, et al., 2009). For example, Hung et al (2006) and Senanayake, et al., (2013 observed that as urban population increases, urban growth increase, commensurate with the urban heat island effect.

Wetlands and green-spaces have high thermal capacity enabling them to serve as heat sinks, hence replacing them with impervious surface will raise temperature of an area (Sithole & Odindi, 2015; Zemba, 2010). This is why northern areas with low density residential areas and characterized by high vegetation fraction are projected to potentially remain cooler than high density residential areas. Buildings absorb heat, furthermore high building density areas like the CBD impede heat removal by wind, further elevating temperatures (Sertel, et al., 2011; Pielke, et al., 2011; Zhou & Wang, 2011a; Blake, Grimm, et al., 2011). The removal of vegetation and emission of waste heat also leads to accumulation of heat energy (Owen, et al., 1998; Senanayake, et al., 2013; Blake, Grimm, et al., 2011). According to Owen et al (1998), this increases sensible heat flux at the expense latent heat flux, hence high urban surface temperatures.

The projected rises in temperature between 2015 and 2040 is consistent with predictions from regional and global models (Ahmed, et al., 2013; McCarthy, et al., 2010; Unganai, 1996; Simone, et al., 2011; Brown., et al., 2012; Newland, 2011; Blake, Grimm, et al., 2011). Blake et al (2011) projected that urban population will grow to 70% by 2050, causing surface alterations and anthropogenic heat emissions that will increase temperatures while Newland (2011) estimated that by 2050, 200 million people will be displaced by warming. According to Brown et al (2012) such increase will result in degradation of air quality and increased energy demand for cooling. Using an urban land surface model in the HadAM3 Global Circulation Model, high population growth was found to coincide with high heat island areas. These findings are also consistent with predictions for cities in other countries for example Bahrain, Tokyo in Japan and Dhaka in Bangladesh (Hassan Radhi et al., 2013; Saitoh, et al., 1996; Ahmed, et al., 2013).

Findings in this study show that temperature may increase even in areas where LULC types may remain unchanged. The rise in temperature is due to a combination of factors including change in surface characteristics and background of already warming temperatures global temperatures as a result of greenhouse effect and global warming. The increase can be attributed to background global warming, which will affect all areas even in the absence of increased urban growth (Argueso et al., 2014; Terando et al., 2014; Kahn, 2009; Dereczynski et al., 2013; Grimmond, 2007). This concurs with Terando et al (2014) who note that temperature rises due to urban growth are superimposed on rising global temperatures. Lauwet at al. (2015) also observed that due to increases in greenhouse gas concentrations, there is an increase in incoming long wave radiation towards the lower atmosphere. However, although low-medium density residential areas and other vegetated areas are expected to warm, their extent is smaller than in high density residential areas in the southwest. This is because the vegetation cover around the buildings mitigates the impact of global warming (Weng, et al., 2004; Hu & Jia, 2010; Zhou & Wang, 2011b; Amiri, et al., 2009; Dousset & Gourmelon, 2003; Smith & Roebber, 2011; Odindi, et al., 2015; Senanayake, et al., 2013). Hence, maintenance of urban greenery remains a significant mitigation measure against extreme temperature elevation, even when greenhouse gas emissions and ozone depletion continue uncontrolled.

The predicted possible increases in temperature due to increased continued urban growth could concur with a variety of global and regional models which predict continuation of 'business as usual' approach to urban growth (Dholakia et al., 2015; Pilli-Sihvola et al., 2010; Isaac & van Vuuren, 2009; Flanner, 2009; Satterthwaite, 2008). This is primarily a consequence of high energy demands caused by increase in the middle income class as cities grow, as well as a result of economic and political reasons which make it difficult to implement policies to reduce emissions or manage urban growth. For example Kahn (2008) and Flanner (2009) observe that anthropogenic heat emissions and greenhouse gas concentration will increase in response to urban growth as the population of the middle class will increase. Middle level income earners raise the consumption of electricity from use of gadgets such as heaters, air conditioners, cooking stoves and fridges (Kahn, 2009). Satterthwaite (2008) observed that urban areas are important political and economic hubs as they also provide over 50% of national GDPs even in mostly rural nations thus difficult to implement strict emission reduction policies. Although

difficult to implement effectively, McMichael et al (2006) stressed that forecasts will strengthen policies and guide priorities for planned adaptation strategies.

8.6 Conclusion

The study aimed at assessing and comparing the potential of a variety of land cover indices to predict future distribution of land surface temperatures in Harare using the Cellular Automata Markov Chain analysis. Based on findings, we conclude that implementing the support vector machines algorithm on multispectral Landsat data classified urban areas with very high overall accuracies above 80%. The Urban Index (UI) was found to predict land surface temperature better than other land cover indices (spatial correlation of 0.9381). The Cellular Automata Markov Chain analysis predicted urban growth with high accuracy (kappa index of agreement was 0.88 between the predicted and SVM classification for 2015). Based on CA Markov, urban growth predicted to continue with CBD/industrial areas potentially increasing in proportion by 4% while high density residential areas may increase in proportion by 3% between 2015 and 2045. Growth will be accompanied by surface temperature increases especially in the southern half of Harare. The 36-45^{o}C temperature class which dominates the southern half may increase in proportion from 42.5% to cover 58% of the city between 2015 and 2045. However, the model is limited by not accounting for the effects of other factors than urban growth on temperature changes. Other factors such as effective mitigation strategies and changes in city growth policies have potential to influence surface temperature patterns. Overall, the findings of this study underscore the importance of medium resolution satellite data in predicting future surface temperatures in urban settings. There is however, need for future studies to explore the feasibility of these methods and techniques at national or regional spatial scales.

8.7 Link between Chapter 8 and other chapters

Chapter 6 showed that Harare is growing evidenced by expansion of built-up areas modifying the spatial structure of temperatures in the lower atmosphere. Chapter 7 showed that energy demand was also increasing especially in the hot season over the years since 1984. Chapter 7 also showed that the need for air conditioning was higher in areas occupied by low income residents indicating increasing risk. Globally, urban growth is expected to continue which triggered the need to investigate possible implications of urban expansion on temperature in Harare. This was fulfilled in Chapter 8 where LULC and LST changes between 1984 and 2017 obtained in Chapter 7 where used to predict future urban growth and LST spatial structure up to year 2045. Throughout the study classification methods developed in Chapter 3 were used

to map LULC as well as urban growth whose links with the indoor and outdoor thermal environment were evaluated.

Finally, all procedures and results from Chapter 3 to 8 are summarized in Chapter 9.

CHAPTER 9: REMOTE SENSING OF THE RESPONSES OF INDOOR AND OUTDOOR THERMAL CONDITIONS TO URBAN GROWTH: A SYNTHESIS

9.1 Introduction

According to the IPCC (2007), mean temperatures are rising while the frequency and intensity of heat waves are also increasing. Recently, there has been an improved understanding of the nexus between the rising temperatures and climate change. However, existing global models stress on the impact of greenhouse gases and largely ignore the contribution of land covers, clouds, water vapor and ocean circulations (Loehle, 2011; IPCC, 2007). Specifically, the irreversible nature of urbanization implies that related changes in temperature could be a major contributor to long term changes in temperature at local, regional and global scales (Owen, et al., 1998). According to Cinar (2015) land cover changes may result in a 4^{o}C temperature increase by 2100. In urban areas, this can be attributed to among others replacement of natural with impervious surfaces, changes in radiative transfer due to complex buildings and streets geometry and increase anthropogenic heating (Rasul, et al., 2015; Dousset & Gourmelon, 2003; Xiao, et al., 2007). Studies have indicated that this may cause extreme temperatures which significantly reduce indoor and outdoor comfort while at the same time compromising productivity by reducing performance at work and increasing morbidity and mortality (Tanabe, et al., 2015; Humphreys, 2015; Lin, et al., 2016). Therefore, sustainable development requires in-depth understanding of impact of urban growth patterns on temperature, hence the need to review previous studies to identify strength and gaps in the subject area.

Urbanization is characterized by surface alterations which mostly entail increase in area covered by surfaces which absorb heat (Zhang, et al., 2009; Sobrino, et al., 2012; Amiri, et al., 2009). For example, vegetated areas are replaced with impervious surfaces and buildings, resulting in elevated surface temperatures, much higher than the surrounding rural and undisturbed areas (Johnson, et al., 2014; Steeneveld, et al., 2014; Tomlinson, et al., 2011; Hua, et al., 2013; Song & Wu, 2015; Sobrino, et al., 2012). Furthermore, surface temperatures are closely linked to near surface air temperatures, which affects human comfort inside and outside buildings (Guan, 2011). According to Xian and Crane (2005), urbanization alters air temperature of the atmospheric boundary and is a key component of the surface energy balance. Generally, the impact of elevated temperatures within cities differs from place to place due to differences in physical exposure, landscape characteristics and socio-demographic factors

(Johnson, et al., 2014). Moreover, literature has revealed that increase in surface temperatures have the potential to expose residents to heat related stress, especially the urban poor without air conditioning facilities (Parsons, 2014; Hsiang, 2010; Dokladny, et al., 2006). Additionally previous studies have also indicated that extreme temperatures significantly reduce indoor and outdoor comfort while at the same time compromising productivity by reducing performance at work and increasing morbidity and mortality (Tanabe, et al., 2015; Humphreys, 2015; Lin, et al., 2016).

Thermal analysis and forecasting enables assessment and prediction of impacts of heat island on temperature sensitive organisms, processes and activities useful for planning, policy formulation as well as for identifying adaptation and mitigation priorities. For example, Brune (2016) used temperature predictions and projected that a variety of urban tree species within built up areas may not tolerate the urban heat projected in 2050. In Japan heat island projection was used to project energy demand for air conditioning (Hirano, et al., 2009). In Australia thermal forecasts are used to influence heat adaptation and mitigation strategies such as use of green infrastructure to reduce greenhouse gas emissions (Block et al., 2012). In Kunming China understanding of the influence of urban growth on thermal characteristics of a city led to a decade of grass recovery to mitigate the heat (Zhou & Wang, 2011a). In Chicago Illinois thermal forecasts were used to model the impact of green roof on urban heating by simulating under variable roof types important for climate change adaptation (Smith & Roebber, 2011). Using future projections of temperature enabled assessment of value of external shading which was found to be significantly valuable in mitigating future overheating risks (McLeod et al., 2013). The benefits also include reduction in energy wastage and pollution, thermal comfort in buildings and outdoor as well as sustainable growth of urban areas. This is important especially for growing cities in developing countries where vulnerability to climate change is already high while resources for adaptation and mitigation to further changes in climate may not be adequate in future.

In situ meteorological data is useful in quantifying the responses of near surface temperature to changes in land use and land cover. Studies have used in-situ air temperature data to monitor seasonal and long term climatic changes, to assess human thermal discomfort as well as to quantify the effect of temperature changes on household air conditioning energy consumption. However, in-situ observations are limited in spatial coverage thus inadequate to for monitoring

spatial variations in temperature such as in heterogeneous and complex urban landscapes. This inadequacy is pronounced in developing countries where financial constraints make it difficult to establish a high weather station density. Further, even in well-resourced developed nations, it is economically impractical to establish a desired network of meteorological stations. On the other hand, space-borne remote sensing has capability to simultaneously monitor both land use land cover changes and responses of the thermal environment. Using medium resolution space-borne multi-spectral data allow mapping of complex landscapes such as urban areas as well as the complex spatial structure of surface temperature. Due to exchange of heat between the land surface and the lower atmosphere, there is a strong link between land surface temperatures and near-surface air temperatures. This linkage enables spatial up scaling of thermal analysis by combining or replacing in-situ observations of air temperature with land surface temperature maps retrieved from remote sensing dataset. Therefore, combining in situ meteorological data with multi-spectral medium resolution remote sensing data has potential to improve understanding of the implications of urban growth on the thermal environment especially in data scarce countries.

In view of urban growth and potential implications on the thermal environment, inadequacy of situ data, availability and ease of access of medium resolution space-borne multispectral data and paucity of literature especially in the study area, the objectives of the study were;

1. To assess the potential of merging thermal data and vegetation indices with multi-spectral medium resolution remote sensing data in improving urban land use/cover mapping
2. To determine extreme heat vulnerability of Harare metropolitan city using multi-spectral remote sensing and socio-economic data
3. To assess seasonal and spatial daytime outdoor thermal comfort variations using recently launched and improved Landsat 8 data
4. To link major dynamics in urban near-surface temperatures to long term changes in land use/cover
5. To understand the link between built-up density and indoor air-conditioning energy demand in Harare using degree days derived from remote sensing and in-situ data
6. To predict future land use/cover distribution and implications on near-surface temperatures in Harare using land cover indices retrieved from remote sensing data in CA-Markov modelling

9.2 Chapter 3: Potential of merging thermal data and vegetation indices with multi-spectral medium resolution remote sensing data in improving urban land use/cover mapping

Accurate land use and land cover (LULC) mapping is important for planning and urban growth monitoring. In land surface temperatures analysis, land use and land cover maps can also be used for assigning emissivity values in order to enable conversion of blackbody to actual and accurate land surface temperatures. Due to heterogeneity, urban mapping requires high spatial resolution remote sensing data to minimize the effect of mixed pixels on classification accuracy. However, high resolution space-borne remote sensing data is usually expensive to acquire, especially for non-funded projects in resource constrained countries. Fortunately, medium resolution datasets such as Landsat series have proven capabilities for urban LULC classification. In this study the potential to further improve accuracy of urban LULC mapping using medium resolution multi-spectral Landsat data was tested. The study also took advantage of the recently launched Landsat 8's datasets given the improved radiometric resolution, signal to noise ratio and spectral range. In order to identify the best method for improving classification accuracy, land use and land cover maps for Harare Metropolitan city were produced using i) traditional reflective (visible/infrared) bands alone, ii) vegetation indices (NDBI, NDVI, NDBaI and NDWI) alone, iii) thermal infra-red bands, iv) combined reflective and thermal data, v) combined thermal infrared data and vegetation indices, vi) combined reflective bands and indices vii) combined reflective bands, thermal data and vegetation indices. The accuracies of other methods were compared with the traditional method of classification using multi-spectral reflective bands alone based on the overall accuracies and kappa indices. The statistical significance of the differences in accuracy between the methods was tested using the McNemar Z score. Results showed that higher accuracy was achieved by combining all the datasets (i.e. reflective bands, thermal infrared data and vegetation indices) than when using each dataset as standalone. For example, the overall accuracy was 89.33% (kappa=0.86) when all datasets were combined in one classification compared to 82.65% (kappa=0.81) when traditional reflective bands are used. Lowest accuracy of 53.4% was attained when thermal infrared data was used as standalone in classification attributed to their low spatial resolution (100m). However, the contribution of thermal data is better when they are combined with indices (overall accuracy of 83.97 and kappa=0.82) or with reflective bands (overall accuracy of 84.03 and kappa=0.81). The McNemar Z scores greater than zero showed that the differences in accuracy between the tested methods and the traditional method were

statistically significant. Except using thermal bands as standalone, other classifications managed to extract land use and land cover classes in the complex urban landscapes of Harare with high User's and Producer's accuracies per class (mostly above 75%).

9.3 Chapter 4: Determining extreme heat vulnerability of Harare metropolitan city using multi-spectral remote sensing and socio-economic data

Land surface alterations due to replacement of natural covers such as vegetation and wetlands with buildings and impervious surfaces change thermal characteristics of urban areas. This may result in thermal elevations in areas where materials with high heat absorption are concentrated such as in densely built-up areas. Chapter three provided methods for accurate land use and land cover classification, which also help in mapping the built-up areas where urban residents live and work. This chapter related the distribution of land use and land cover types to heat vulnerability in Harare. The study was driven by the need for detailed extreme heat vulnerability maps given that temperatures are increasing due to background global warming. Partitioning of atmospheric energy is affected by differences in energy balance between land covers within the city. Previous studies mapped heat vulnerability at course resolution such as census block level while variations may exist even within each block. Although indices such as NDVI and NDBI were incorporated in heat vulnerability mapping, the maps produced were not at the resolution of remote sensing data. In this study heat vulnerability was mapped by combining NDVI, NDBI and NDWI retrieved from Landsat 8 with socio-demographic data from the 2012 Zimbabwe national census data. Inclusion of NDWI was found to significantly aid vulnerability mapping since the index relates both to surface water content and combine with NDVI to indicate vegetation health both of which strongly relate with surface and near-surface temperature. The input vulnerability factors were normalized based on how each related with temperature and a composite vulnerability map was produced using equal-weighted sum. The heat vulnerability map was scaled between 0 and 1 and reclassified using quantiles such that the lower 20% was classified as "Very low vulnerability", the three intermediate quantiles as "Low", "Moderate" and "High" while the upper 20% quantile was categorized as "Very high" vulnerability. This was based on an adopted reclassification of heat vulnerability approach of using quantiles (Buscail, et al., 2012). Due to physical exposure and socio-demographic pressures, results showed that heat vulnerability was high to very high in more than 40% of the metropolitan city during the hot season. Extreme heat vulnerability was found to be very high in the densely built-up city core and south western areas (index values ranged from 0.49 to 1). The southern half of the city which is characterized by high density of

population and buildings, very low vegetation fraction as well as low income residents had heat vulnerability in the moderate to high (index value range from 0.41 to 0.49). The northern parts where vegetation is abundant, density of buildings is low and the moderate to high income strata reside had low heat vulnerability level (index values below 0.41). Results also indicated a high spatial correlation (r=0.61) between land surface temperature and extreme heat vulnerability in Harare. This implied that medium resolution land surface temperature derived from Landsat thermal data is a good indicator of heat vulnerability in Harare. Overall, the heat vulnerability map produced was more detailed than could be produced using census blocks.

9.4 Chapter 5: Assessment of seasonal and spatial daytime outdoor thermal comfort variations using recently launched and improved Landsat 8 data

Chapter four showed the spatial distribution of heat vulnerability in case extreme temperature affect Harare, especially during the hot season, in view of projected continued global temperature rises. The chapter also found that heat vulnerability is closely related to land surface temperature which also depend on land use and land cover spatial structure. However, effect of temporal LULC changes such as seasonal variations which may also affect heat distribution were not considered in Chapter four. In this chapter, changes in the spatial distribution of outdoor thermal discomfort in response to seasonal LULC changes were investigated. The Thom's Discomfort Index (DI) was used, using air temperature and relative humidity retrieved from land surface temperature using simple linear regression models. Thermal discomfort patterns were investigated in four sub-seasons namely the rainy-, post rainy-, cool- and hot sub-seasons. Landsat 8's data and meteorological observations of temperature and humidity were used i) to develop models for estimating temperature and humidity from land surface temperature and ii) to produce seasonal maps of outdoor thermal discomfort for Harare and iii) to relate thermal discomfort with land use and land cover spatial patterns. Results showed that there was strong correlation (R-squared=0.69) between land surface temperature and air temperature. Season specific linear models were developed for retrieving relative humidity from land surface temperature. When compared with in-situ relative humidity, the model retrievals were at high accuracy (percentage errors less than 20% in all seasons). Results also showed that due to variations in humidity ranges between seasons, using a single model in all seasons would result in less accurate retrievals (percentage error of 28.1%) than when seasons are analysed separately. The proportion of the study area where less than 50% of the subjects would feel uncomfortable was largest during the post rainy sub-season (59%) and smallest in the hot sub-season (2.1%). DI values 24^{o}C were recorded indicating

comfortable thermal conditions across the country in the cool (Figure 5.4c) and post rainy sub-seasons (Figure 5.4b). During these comfortable sub-seasons, very low discomfort indices (below 21^{o}C) were also observed in the northern and eastern areas. The city was thermally uncomfortable outdoors during the hot sub-season (Figure 5.4d) when DI values greater than 24^{o}C were recorded with high values of DI (above 27^{o}C) in the southern and western than the rest of the city. Figure 5.4 and Figure 5.5 showed that in all sub-seasons, outdoor thermal discomfort was less in northern areas occupied by parks and low density residential areas than in densely built-up central and southern areas. For example, results showed that during hot sub-season, almost all occupants feel thermally uncomfortable (DI greater than 27^{o}C) in the bulk of the southern areas while more than 50% would feel comfortable (DI less 27^{o}C) in most of the areas in the north. Thermal discomfort for all occupants (DI between 29^{o}C and 32^{o}C) was recorded in densely built up areas, which correspond to the central business district and industrial areas during the rainy and the hot sub-seasons. Figure 5.6 showed outdoor thermal discomfort was strongly affected by vegetation as low DI values were recorded in seasons with high vegetation cover fraction. As such the average discomfort was very high in the hot sub-season (DI=31^{o}C), which was characterized by low vegetation fraction (0.46) and high thermal discomfort (average of 30^{o}C). Therefore, there was a general inverse relationship between thermal discomfort and vegetation fraction.

9.4 Chapter 6: To link major dynamics in urban near-surface temperatures to long term changes in land use/cover

It was observed in Chapter 5 that seasonal changes in land use and land cover affect outdoor thermal comfort. Findings of the chapter also showed that the hot sub-season (mid-September to mid-November) is the most thermally uncomfortable in Harare. However, the impacts of long-term land use and land cover changes, which characterize urban growth also need to be quantified. Therefore, Chapter 6 further aimed at establishing the link between long-term changes in land use and land cover distribution and dynamics of the spatial configuration of land surface temperatures. LULC and land surface temperature patterns for 1984, 1993, 2001 and 2015 were retrieved from Landsat multi-spectral data. Urban surface temperatures are not only affected by surface properties but also by intensity of incoming radiation received. Therefore, the study also aimed at separating effects of LULC changes from the contribution of background warming. In order to achieve this, a temperature difference normalization approach which assumes that intra-class changes in average temperature are due to background warming was used. Average land surface temperatures were considered to only change

significantly when there is a change from one land cover to another, else they would remain almost the same when no conversion occurs. Changes in the contribution of individual LULC to the heating in Harare were assessed using the Contribution Index (CI). On the other hand, changes in the spatial structure of land surface temperature were analysed using the relative radiant temperature. The relative radiant temperature was chosen to indicate changes in urban heat island as it eliminates subjective procedure of selecting a representative rural pixel associated with other methods. The quality of LULC maps produced was high as indicated by overall accuracies greater than 80% for all the periods. Findings of this chapter showed that Harare experienced growth evidenced by increase in extent of built-up area between 1984 and 2015. For example, the coverage of high density residential areas increased by 92% at the expense of cooler green-spaces which decreased by 75.5% between 1984 and 2016 (Figure 6.2). Average land surface temperature for the whole area as well as per LULC type increased during the studied period. During the period, average land surface temperature in the CBD/Industrial areas increased by 3.29^{o}C and by 1.51^{o}C over green-spaces during the study period. Lowest increases in temperature were observed over water surfaces (0.74^{o}C) croplands (0.86^{o}C) and green spaces (1.51^{o}C). Surface temperature rises were found to be in higher density residential areas when an increase by 2.55^{o}C was recorded than in "leafy" low density residential areas which experienced a rise by 1.7^{o}C. The normalized temperatures differencing procedure yielded that LULC changes alone caused an increase in surface temperatures of 0.98^{o}C while combined with background warming the surface temperatures rose by 1.98^{o}C. The trend in CI displayed on Figure 6.4 indicated that warming was contributed by increase in warming contribution due to expansion of densely built-up areas. Conversely, the cooling contribution of vegetation and wetlands decreased as their proportional coverage decreased between 1984 and 2015. Overall, effect of growth induced long-term changes in LULC distribution was significant as this contributed more than 0.5^{o}C thermal elevation within the city.

9.5 Chapter 7: Understanding the link between built-up density and indoor air-conditioning energy demand in Harare using degree days derived from remote sensing and in-situ data

In Chapter 5 and Chapter 6, it was shown how seasonal and long-term changes in LULC spatial structure affect distribution of land surface temperature and thermal discomfort. It was shown that thermal discomfort is immense during the hot season and the intensity and spatial coverage of extreme surface temperatures were increasing as the city of Harare was growing. Chapter 7

analysed the potential responses of air-conditioning energy demand to the seasonal and long term changes in LULC and land surface temperature. Cloud-free Landsat images acquired in the cool and hot sub-seasons on dates indicated on Table 7.1 in 1984, 1993, 2001 and 2015 were used. In-situ temperature data for the period from 1950 to 2010 were obtained from the Meteorological Services Department of Zimbabwe. Energy consumption data covering period from 2009 to 2016 were obtained from Zimbabwe Electricity Transmission and Distribution Company (ZETDC). Household energy consumption data in different residential types where retrieved from samples of electricity bills since data obtained from ZETDC was not resolved to the scale of residential types found in the area. Cooling and Heating Degree Days (CDD and HDD) are used as a proxy for energy requirement for indoor space cooling and heating. The Degree Days have most widely been computed using in-situ measurements of temperature but no attempt has been made to employ medium resolution thermal data for this purpose. In this study a simple linear model developed in Chapter 5 was used to estimate the spatial distribution of near surface air temperature from land surface temperature. The retrieved air temperatures were used to compute trends in the spatial distribution of CDD and HDD from 1984 to 2015. In order to verify the trends CDD and HDD were also computed using in-situ observations maximum and minimum temperatures, respectively. CDD were used to detect potential trends in cooling energy during the hot sub-season while HDD were used to determine potential space heating energy demand in the cool season. The link between actual energy consumption and CDD/HDD patterns was also investigated. LULC maps derived in Chapter 6 were used to establish the link between residential types/built-up spatial structure and energy demand as well as actual energy consumption in Harare. Results in Figure 7.3 and 7.4 showed that land surface temperature rises between 1984 and 2015 were more pronounced for the hot than the cool sub-season. Between 1984 and 2015, there was decrease in the proportion of the city experiencing on average the 12 to 22^{o}C category and increase in those affected by the 22 to 30^{o}C category during the cool season. As such, the 22 to 30^{o}C temperature range covered less than 330km^2 in 1984 but this increased to cover more than 600 km^2 in 2015. During the hot season, average land surface temperature values greater than 36^{o}C were not common in 1984 (0.27km^2) but were covering a significant proportion of the city (above 580km^2) in 2015. Land surface temperature based Degree Days closely compared with retrievals based on in-situ temperature data as indicated by a mean percentage error of 21.2 % and Mean Absolute Error of 1.06 degree days. Results in Figure 7.6 showed that mean household energy consumption increased as minimum temperatures decreased and as maximum temperatures increased in the cool and wet season, respectively. Highest energy consumption in residential areas in the summer season (above

$1.05X10^6$KWh) corresponded with highest maximum temperature in October and in January. In the hot season, daytime cooling energy requirements were larger in densely built-up areas than in the low-medium density residential areas. As such, in 2015, the CDD was 8.90 degree days in high density residential areas while it was 7.27 degree days in low density residential areas. The results also revealed a mismatch between cooling energy demand (CDD) and actual mean household energy consumption. Although low density residential areas had lowest CDD values, they had the highest mean monthly energy usage (1440KWh). Similarly, actual energy consumption was the lowest in high density residential areas (480KWh) where demand based on temperatures should be high. Since Chapter 3 showed that high density residential areas are occupied by low-income strata, results indicated that household income seemed to influence actual energy consumption differences. The disparity between cooling energy requirement and actual energy consumption also confirms why residential areas in the southern half of the city were categorized as highly vulnerable to heat extremes in Chapter 2.

9.6 Chapter 8: To predict future land use/cover distribution and implications on near-surface temperatures in Harare using land cover indices retrieved from remote sensing data in CA-Markov modelling

Previous chapters focused on current, short-term as well as long term historical patterns of LULC and land surface temperature spatial structure in Harare. Chapter 2 revealed that there is paucity of remote sensing based predictive studies while urban growth and its impacts are expected to continue. Therefore, the objective of Chapter 8 was to use historical patterns observed between 1984 and 2015 to predict future LULC and land surface temperature trends. Since Chapter 5 showed that extreme heat events are prevalent during the hot, sub-season, focus was placed on forecast for this period. Table 8.2 and 8.3 show the Landsat images used in the study to analyse temperature patterns for the hot season in 1984, 2001 and 2015. The LULC maps obtained in Chapter 6 were also used to link urban growth with surface temperature trends for the hot season. In this chapter the Cellular Automata Markov Chain analysis was used to predict future urban growth and surface temperature. Initially, LULC changes between 1984 and 2001 were used to predict LULC for 2015. This was done to test the performance of the model in predicting future growth before its use in further predictions. After assessing the accuracy of the model, the CA Markov was then used to predict LULC for 2025, 2035 and 2045 based on transition matrix, transition probabilities and transitions areas generated based on changes between 1984 and 2015. Secondly, the potential of a variety of land cover and vegetation indices shown on Tables 8.4 in predicting future land surface temperature was tested. Correlation analysis was performed in order to find an index with the

highest spatial correlation with land surface temperature. The selected predictor index was computed for 1984 and 2015 and used to generate transition areas, transition probabilities and transition matrix for 2025, 2035 and 2045 in Markov Chain Analysis. The future states of the predictor index were mapped using the Cellular Automata module in IDRISI and reclassified into future land surface temperature maps based on the model in Figure 8.4. Due to highest spatial correlation with land surface temperature (r=0.9381), Urban Index (UI) was found to be the best predictor of urban surface temperature in comparison to other indices. Based on Figure 8.5, UI was also found to predict land surface temperature with high accuracy (mean relative percentage error=5.27%, Nash Sutcliff efficiency=0.74, root mean square error=1.26^{o}C, mean bias error=-0.0002^{o}C and index of agreement=0.80). Based on CA Markov analysis, the rising temperature trends observed between 1984 and 2015 may continue through to 2045 (Figure 8.8). In Figure 8.6, the CA Markov model was found reliable in predicting future LULC distribution due to strong agreement between the predicted and the SVM classification based map for 2015 (overall Kappa Index of Agreement was 0.91). Figure 8.7 showed that the model predicted built-up areas at the expense of green-spaces and wetlands in 2025, 2035 and 2045. High density residential areas are predicted to expand from 470.02 to 490.36km^2 between 2015 and 2045. As the city grows, green-spaces would be expected to decrease in area from 57.42 to 27.85km^2 during the same time interval. The proportion of the study area to experience the high temperature category (greater than 38^{o}C) was predicted to increase as the city will continue to grow. The model predictions in Table 8.11 that the 18-28^{o}C temperature range could decrease in coverage from 86.23km^2 to 55.97km^2 while the 36-45^{o}C category is expected to increase from 363.78 to 498.45km^2 between 2015 and 2045.

9.7 Objectives revisited

The potential of integrated Landsat data and derived indices in mapping urban landscapes was successfully tested when it was obtained that combining reflective bands with thermal infrared data and indices results in higher accuracy than using reflective bands alone. Remotely sensed vegetation indices were also successfully combined with socio-demographic data to map heat vulnerability in Harare. The study managed to accurately map urban growth and its implications on the spatial structure of surface temperatures between 1984 and 2015. Spatial and temporal analyses of surface temperatures using medium resolution remote sensing datasets were done successfully. As such the link between thermal discomfort and LULC distribution was mapped in four sub-seasons. In this analysis, the study managed to show that the hot sub-season is the most thermally uncomfortable with higher stress levels in densely

built than other areas. Temporal analysis also convincingly showed that surface temperatures are increasing due to expansion of urban fabric as the city of Harare is growing.

The study also met the objective to link urban growth with potential indoor energy consumption using CDD and HDD as a measure. Using actual energy consumption data the study observed that household energy use is increasing in Harare which also agreed with findings based on CDD and HDD. Actual energy consumption was also found to be high in leafy areas occupied by middle and high income strata where temperatures and heat stress are generally low. This agreed with Chapter 2 which showed that heat vulnerability is high in southern areas occupied by low income strata. Low energy use may signify that the occupants do not afford air-conditioning facilities hence subjected to high heat stress levels during hot periods. Since the city of Harare is still growing, based on historical patterns the study predicted future growth and implications on the thermal environment of Harare using multi-spectral and multi-temporal Landsat data. Therefore, the objectives of the study were largely met although cognisant of limitations which are highlighted below.

9.8 Limitations

In this study, limitations were encountered some of which need to be addressed in future studies. The following limitations were identified;

- Landsat thermal infrared data were the most easily accessible but not at the most desired spatial and temporal resolution. Due to low temporal resolution of Landsat data (16 days), the study could not analyse the diurnal cycles of land surface temperature per LULC type. This also limited the extent to which remote sensing retrievals of LST could be matched with in-situ observations of temperature for correlation analysis. This also affected seasonal analysis as only a few imageries could be found per season
- The cloud-free imagery requirement for space-borne visible and infrared remote sensing based land surface analysis was limited due to small number of such imageries during the rainy and post-rain sub-seasons.
- The study depended on only three weather stations in Harare which had different observation times and instrumentation. Harare Airport Meteorological Office (HAMO) and Kutsaga Research Stations are automated such that hourly data could be obtained. The station at Belvedere is operated manually with observations taken at synoptic times based on World Meteorology Organization (WMO) recommendations. Access to the data was also not uniform during the study period. As a result, earlier analyses were

done using data only from Kutsaga Research Station. Furthermore, besides being few the observation points were also not adequately representative to capture variability in temperature due to LULC spatial patterns in Harare.

- No attempt was made to merge Landsat data with sensors such as Meteosat to improve temporal resolution. Although such sensors have very low spatial resolution, there was need to test if merging could create a new dataset with medium spatial resolution and high temporal resolution.
- LULC classifications produced schemes which may not be easily related to climate. The classes produced are named into region specific schemes whose interpretation may differ from one part of the world to another. The study did not classify Harare into standard Local Climate Zones (LCZ) which are of easy global communication and comparison. If so done, the study would have directly contributed to the WUDAPT project's effort of creating a global database of urban LCZs.
- Household energy consumption data could not separate contribution of air-condition from other uses such as cooking and lighting. This made it difficult to single out the effect of urban growth on indoor cooling and heating energy

In order to address these limitations, recommendations and suggestions for future studies are highlighted in the next section

9.9 Recommendations and suggestions for future studies

This study has displayed the unique value of multi-spectral remote sensing data in analyzing the link between urban growth and the thermal environment. The study showed that thermal data from space-borne sensors can replace or combine with in-situ air temperature data to provide detailed spatial and temporal analysis not viable with in-situ data alone. However, the challenge of inadequate spatial and temporal resolutions associated with medium resolution sensors such as Landsat remains a major setback. For example, although high accuracy of urban LULC mapping is achieved using Landsat data, the mixed pixel problem still needs to be minimized. Furthermore, the spatial resolution of space-borne thermal infrared sensors has not yet matched the resolution higher than 50m for urban thermal analysis as recommended by Sobrino, et al. (2004). There is thus a mismatch in spatial resolution between thermal data and that of LULC maps and land cover indices derived from visible and infrared data. For example, the thermal data of Landsat 8 are at a spatial resolution of 100m while the optical bands are at 30m resolution. The challenge of spatial resolution is further worsened given that current high resolution space-borne sensors such as SPOT have no thermal infrared data. The other

limitation of using medium resolution datasets such as Landsat is that of low temporal resolution which, for example, is 16 days for Landsat series. Desired temporal resolution is obtained with geo-stationary satellites but characterized by very low spatial resolution. However, the medium resolution datasets remain valued especially in non-funded projects and resource constrained regions where access to high resolution data such as air-borne sensors is rare. In order to improve monitoring of urban growth and its impacts on land- and near-surface temperature, future studies should consider the following recommendations;

- There is need to develop algorithms for temporal up scaling of medium resolution space-borne remote sensing data. For, example, blending low temporal resolution with geostationary sensors' datasets has potential to create datasets with acceptable spatial and temporal resolution. This will improve both spatial and temporal details of urban growth and temperature analysis.
- Recently, the European Space Agent (ESA) launched Sentinel-2 satellite providing as high spatial resolution as 10 and 20m for visible and short wave infrared data. Application of this data has potential to improve urban LULC and growth monitoring. There is need to compare Sentinel-2 with widely used sensors such as Landsat and ASTER to assess if there are significant differences in mapping accuracy. Other datasets such as the high resolution German TerraSAR-X need to be tested for mapping urban areas in developing countries especially in Africa.
- Engineers should develop high resolution low earth orbiting space-borne sensors. This will improve characterization of urban land surface temperatures given the complex landscapes and heterogeneity in urban areas. This will also improve spatial correlation between land surface temperature and LULC maps as well as land cover indices derived from visible and infrared data from medium and high resolution sensors
- Clouds block solar radiation from reaching the earth's surface. Due to this, land surface temperatures are only determined on cloud-free days while in-situ measurements of air temperature are done under all conditions. However, thermal comfort assessments need to be done for both the hot and cold extremes while the readily available in-situ data have limited spatial coverage. There is thus need to develop algorithms for retrieving land surface temperatures even under a cloud. Studies should thus analyze the relationship between cloud properties (e.g. amount and thickness) and land surface temperatures for different LULC type in an urban setting.

- Access to urban climate research products by policy makers must be increased such as by creating global and local portals for sharing information. As such, scientists in developing countries need to contribute to the already existing efforts such as the WUDAPT. Clauses on urban climate need to be included in climate policies of many developing countries which currently place much emphasis on agriculture.
- Urban development has potential to elevate temperature in urban areas. Urban planners should spearhead sustainable development with climate implications in mind.
- There is great need to increase the weather station network in developing countries through government support and partnerships. In Harare, the study would not have been possible if there were no space-borne remote sensing datasets. The spatial variations in urban temperatures cannot be adequately mapped using few stations due to heterogeneity and complexity of landscape. Increasing station density will improve capability to relate remote sensing with observed temperature.
- Future studies should develop methods of separating energy use due to air-conditioning from other household uses. This will make it easier to relate heat island intensities with air-conditioning energy demand over time.

9.10 Conclusion

The responses of land surface temperature and related socio-economic impacts to spatial and temporal land use and land cover (LULC) dynamics were investigated in Harare, Zimbabwe. In view of meteorological observational network which does not match complex urban structure, Landsat multi-spectral were used. A method was developed to improve accuracy of urban LULC classification by combining the full spectral range of Landsat with vegetation indices (NDVI, NDWI, NDBaI and NDBI) in a single classification. The link between the LULC types and extreme heat vulnerability was also investigated. Extreme heat vulnerability index map was derived by combining NDBI, NDVI and NDWI with socio-demographic factors extracted from the latest census data in Harare. The responses of outdoor thermal discomfort to seasonal variations in LULC were also assessed. The Discomfort Index (DI) was retrieved based on simple linear models developed to replace relative humidity and air temperature with land surface temperature derived from Landsat thermal infrared data. In this study, the long term impact of urban growth (1986 to 2015) on land surface temperature was quantified and separated from effect of other factors using normalized temperature difference approach. The implications of long-term LULC and surface temperature changes on potential indoor air-conditioning demand for human comfort assurance was also analyzed. Heating and Cooling Degree Days were used as a proxy for air-conditioning energy in the cool and hot season, respectively. The Degree Days were derived from Landsat thermal infrared data based on linear models developed and linked with i) growth patterns, ii) Degree Days from in-situ meteorological data and iii) actual energy consumption. In order to inform future growth LULC and land surface temperature were predicted up to year 2045 using the Cellular Automata Markov Chain analysis. Based on findings of the study in Harare, the following conclusions were drawn;

- Urban LULC mapping using medium resolution remote sensing datasets is improved significantly by merging reflective bands, thermal data and derived vegetation indices in a single classification.
- Extreme heat vulnerability was high in densely built-up areas where there was a combination of low-income strata, high population density, large population in the extreme age ranges (0-15 and above 65) and physical exposure due to highly heat absorbing LULC types.
- Outdoor thermal discomfort has its peak in the hot sub-season due to high incoming radiation, low surface temperature and sparse or dry vegetation cover. Outdoor thermal discomfort was higher in densely built-up than other LULC types all year round

- Although background warming is also causing surface temperatures to increase, long term LULC changes due to urban growth had a significant contribution
- LULC change induced warming is reducing energy consumption for indoor warming during the cool season and increase space heating energy demand during the hot season in Harare especially in densely built-up areas. There was a mismatch between energy requirement for space cooling and actual household energy consumption due to affordability. Low income strata in high density residential areas required more energy and cooling facility than they afford thus rendering them vulnerable.
- Assuming growth patterns experienced between 1984 and 2015 would continue through to 2045 with no heat mitigation strategies implemented, urban surface temperatures will continue to shift towards extreme values especially as densely built-up areas expand.

Overall, remote sensing offers great capabilities to accurately monitor urban growth and its impacts on the thermal environment essential in data scarce regions. Removal of green spaces and wetland replacing them with buildings and impervious areas significantly alters the thermal characteristics of the lower atmosphere in urban areas. At the spatial resolution of Landsat thermal data, in-situ air temperature data can be replaced in a variety of analysis to map the spatial and temporal temperature patterns.

REFERENCES

Aaviksoo, K. (1995). Simulating vegetation dynamics and land use in a mire landscape using a Markov model. *Landscape and Urban Planning, 31*(1-3), 129-142.

Abdel-Ghany, A. M., Al-HELAL, I. M., & Shady, M. R. (2014). Evaluation of human thermal comfort and heat stress in an outdoor urban setting in summer under arid climatic conditions. *Environment Protection Engineering, 40*(3).

Abegunde, L., & Adedeji, O. (2015). Impact of Landuse Change on Surface Temperature in Ibadan, Nigeria. *International Journal of Environmental, Ecological, Geological and Geophysical Engineering, 9*(3), 235-241.

Abutaleb, K., Ngie, A., Darwish, A., Ahmed, M., Arafat, S., & Ahmed, F. (2015). Assessment of Urban Heat Island Using Remotely Sensed Imagery over Greater Cairo, Egypt. *Advances in Remote Sensing, 2015*(4), 34-47.

Acharya, T. D., Parajuli, J., Poudel, D., & Yang, I. (2015). Extraction and Modelling of Spatio-Temporal Urban Change in Kathmandu Valley. *International Journal of IT, Engineering and Applied Sciences Research, 4*, 1-11.

Adebowale, B. I., & Kayode, S. E. (2015). Geospatial Assessment of Urban Expansion and Land Surface Temperature in Akure , Nigeria. On *ICUC9 - 9th International Conference on Urban Climate jointly with 12th Symposium on the Urban Environment*.

Adelabu, S., Mutanga, O., Adam, E., & Cho, M. A. (2013). Exploiting machine learning algorithms for tree species classification in a semiarid woodland using RapidEye image. *Journal of Applied Remote Sensing, 7*(1), 073480-073480.

Ahmed, B., & Ahmed, R. (2012). Modeling Urban Land Cover Growth Dynamics Using Multi‐Temporal Satellite Images: A Case Study of Dhaka, Bangladesh. *ISPRS International Journal of Geo-Information, 1*, 3-31.

Ahmed, B., Kamruzzaman, M., Zhu, X., Rahman, M., & Choi, K. (2013). Simulating Land Cover Changes and Their Impacts on Land Surface Temperature in Dhaka, Bangladesh. *Remote Sensing, 5*(11), 5969-5998.

Akbari, H. (2005). Energy Saving Potentials and Air Quality Benefits of Urban Heat Island mitigation. *Lawrence Berkeley National Laboratory*.

Almutairi, M. K. (2015). Derivation of Urban Heat Island for Landsat-8 TIRS Riyadh City (KSA). *Journal of Geoscience and Environment Protection, 3*, 18-23.

Amiri, R., Weng, Q., Alimohammadi, A., & Alavipanah, S. K. (2009). Spatial-temporal dynamics of land surface temperature in relation to fractional vegetation cover and land use/cover in the Tabriz urban area, Iran. *Remote Sensing of Environment, 113*(12), 2606-2617.

Aplin, P. (2003). Comparison of simulated IKONOS and SPOT HRV imagery for classifying urban areas. *Remotely sensed cities*, 23-45.

Araya, Y. H., & Cabral, P. (2010). Analysis and modeling of urban land cover change in Set??bal and Sesimbra, Portugal. *Remote Sensing, 2*, 1549-1563.

Argueso, D., Evans, J. P., Fita, L. s., & Bormann, K. J. (2014). Temperature response to future urbanization and climate change. *Climate Dynamics, 42*, 2183-2199.

Arifwidodo, S., & Chandrasiri, O. (2015). Urban Heat Island and Household Energy Consumption in Bangkok, Thailand. *Energy Procedia, 79*, 189-194.

As-syakur, A. R., Adnyana, I. W. S., Arthana, I. W., & Nuarsa, I. W. (2012). Enhanced built-up and bareness index (EBBI) for mapping built-up and bare land in an urban area. *Remote Sensing, 4*, 2957-2970.

Aubrecht, C., & Özceylan, D. (2013). Identification of heat risk patterns in the U.S. National Capital Region by integrating heat stress and related vulnerability. *Environment International, 56*, 65-77.

Avdan, U., & Jovanovska, G. (2016). Algorithm for Automated Mapping of Land Surface Temperature Using LANDSAT 8 Satellite Data. *Hindawi, Journal of Sensors, 2016*.

Balaras, C. A., Droutsa, K., Dascalaki, E., & Kontoyiannidis, S. (2005). Heating energy consumption and resulting environmental impact of European apartment buildings. *Energy and Buildings, 37*, 429-442.

Banskota, A., Nilam Kayastha , Falkowski, M. J., Wulder, M. A., Froese, R. E., & White, J. C. (2014). Forest monitoring using Landsat time-series data- A review. *Canadian Journal of Remote Sensing, 40*(5), 362-384.

Barrett, C. B., Barnett, B. J., Carter, M. R., Chantarat, S., Hansen, J. W., Mude, A. G., Osgood, D., Skees, J. R., Turvey, C. G., & Ward, M. N. (2007). Poverty traps and climate risk: limitations and opportunities of index-based risk financing.

Batih, H., & Sorapipatana, C. (2016). Characteristics of urban households' electrical energy consumption in Indonesia and its saving potentials. *Renewable and Sustainable Energy Reviews, 57*, 1160-1173.

Bechtel, B., Alexander, P. J., Böhner, J., Ching, J., Conrad, O., Feddema, J., Mills, G., See, L., & Stewart, I. (2015). Mapping local climate zones for a worldwide database of the form and function of cities. *ISPRS International Journal of Geo-Information, 4*(1), 199-219.

Bhattacharjee, S., & Ghosh, S. K. (2015). Spatio-Temporal Change Modeling of Lulc: A Semantic Kriging Approach. *ISPRS Annals of Photogrammetry, Remote Sensing and Spatial Information Sciences, II-4/W2*, 177-184.

Birnbaum, Z. (1956). *On a use of the Mann-Whitney statistic.* Paper presented at the Proceedings of the third Berkeley symposium on mathematical statistics and probability.

Blackett, M. (2014). Early Analysis of Landsat-8 Thermal Infrared Sensor Imagery of Volcanic Activity. *Remote Sensing, 6*, 2282-2295.

Blake, R., A. , Grimm, T., Ichinose, R., Horton, S., Gaffi n, S., Jiong, D., & Bader, L. D. (2011). Urban climate: Processes, trends and projections. *Climate Change and Cities: First Assessment Report of the Urban Climate Change Research Network, C. Rosenzweig, W. D. Solecki, S. A. Hammer, S. Mehrotra, Eds., Cambridge University Press, Cambridge, UK*, 43-81.

Blake, R., Curitiba, A. G., Toshiaki, I., & Horton, R. (2011). Urban climate: Processes, trends and projections. *First Assessment Report of the Urban Climate Change Research Network*, 43-81.

Block, A. H., Livesley, S. J., & Williams, N. S. (2012). Responding to the urban heat island: a review of the potential of green infrastructure. *Melbourne: Victorian Centre for Climate Change Adaptation (VCCCAR)*.

Bolattürk, A. (2008). Optimum insulation thicknesses for building walls with respect to cooling and heating degree-hours in the warmest zone of Turkey. *Building and Environment, 43*(6), 1055-1064.

Brenkert, A. L., & Malone, E. L. (2005). Modeling vulnerability and resilience to climate change: A case study of India and Indian states. *Climate Change, 72*, 57-102.

Brousse, O., Martilli, A., Foley, M., Mills, G., & Bechtel, B. (2016). WUDAPT, an efficient land use producing data tool for mesoscale models? Integration of urban LCZ in WRF over Madrid. *Urban Climate, 17*, 116-134.

Brown., D., Chanakira., R. R., Chatiza., K., Dhliwayo., M., Dodman., D., Masiiwa., M., Muchadenyika., D., Mugabe., P., & Zviga.., S. (2012). Climate change impacts, vulnerability and adaptation in Zimbabwe. *iied*.

Buscail, C., Upegui, E., & Viel, J. F. (2012). Mapping heatwave health risk at the community level for public health action. *Int J Health Geogr, 11*, 38-47.

Büyükalaca, O., Bulut, H., & Yılmaz, T. (2001). Analysis of variable-base heating and cooling degree-days for Turkey. *Applied Energy, 69*(4), 269-283.

Byomkesh, T., Nakagoshi, N., & Dewan, A. M. (2012). Urbanization and green space dynamics in Greater Dhaka, Bangladesh. *Landscape and Ecological Engineering, 8*, 45-58.

Cai, G., Du, M., & Xue, Y. (2011). Monitoring of urban heat island effect in Beijing combining ASTER and TM data. *International Journal of Remote Sensing, 32*(5), 1213-1232.

Cai, M., Ren, C., Xu, Y., Dai, W., & Wang, X. M. (2016). Local Climate Zone Study for Sustainable Megacities Development by Using Improved WUDAPT Methodology–A Case Study in Guangzhou. *Procedia Environmental Sciences, 36*, 82-89.

Cao, L., Li, P., Zhang, L., & Chen, T. (2008). Remote sensing image-based analysis of the relationship between urban heat island and vegetation fraction. *The International Archives of the Photogammetry. Remote Sensing and Spatial Information Sciences, XXXVII*.

Chagutah, T. (2010). Climate Change Vulnerability and Adaptation Preparedness in Southern Africa. *Heinrich Boll Stiftung Southern Africa*.

Charles, K. E. (2003). *Fanger ' s Thermal Comfort and Draught Models Fanger ' s Thermal Comfort and Draught Models IRC Research Report RR-162.* Paper presented at the National Research Council Canada.

Charles, N., Reneth, M., Shakespear, M., & Virginia, M. (2014). Climate change adaptation for rural communities dependent on agriculture and tourism in marginal farming areas of the Hwange District, Zimbabwe. *African Journal of Agricultural Research, 9*(26), 2045-2054.

Chemura, A., & Mutanga, O. (2017). Developing detailed age-specific thematic maps for coffee (Coffea arabica L.) in heterogeneous agricultural landscapes using random forests applied on Landsat 8 multispectral sensor. *Geocarto International, 32*(7), 759-776.

Chen, S.-S., Chen, X.-Z., Chen, W.-Q., Su, Y.-X., & Li, D. (2011). A simple retrieval method of land surface temperature from AMSR-E passive microwave data – a case study over Southern China during the strong snow disaster of 2008. *International Journal of Applied Earth Observations and Geoinformation, 13*, 140–151.

Chen, W., Liu, L., Zhang, C., Wang, J., Wang, J., & Pan, Y. (2004). *Monitoring the seasonal bare soil areas in Beijing using multitemporal TM images.* Paper presented at the Geoscience and Remote Sensing Symposium, 2004. IGARSS'04. Proceedings. 2004 IEEE International.

Chen, X.-L., Zhao, H.-M., Li, P.-X., & Yin, Z.-Y. (2006). Remote sensing image-based analysis of the relationship between urban heat island and land use/cover changes. *Remote Sensing of Environment, 104*(2), 133-146.

Chen, Z., Gong, C., Wu, J., & Yu, S. (2012). The influence of socioeconomic and topographic factors on nocturnal urban heat islands: a case study in Shenzhen, China. *International Journal of Remote Sensing, 33*(12), 3834–3849.

Cheng, V., & Ng, E. (2006). Thermal Comfort in Urban Open Spaces for Hong Kong. *Architectural Science Review, 49*(3), 236-242.

Cheng, V., Ng, E., & Givoni, B. (2010). Outdoor thermal comfort in sub-tropical climate: A longitudinal study based in Hong Kong. *International journal of biometeorology 56*(1), 43-56.

Chow, W. T. L., Chuang, W.-C., & Gober, P. (2012). Vulnerability to extreme heat in metropolitan Phoenix: spatial, temporal, and demographic dimensions. *The Professional Geographer, 64*, 286-302.

Christenson, M., Manz, H., & Gyalistras, D. (2006). Climate warming impact on degree-days and building energy demand in Switzerland. *Energy Conversion and Management, 47*(6), 671-686.

Chun-ye, W., & Wei-ping, Z. H. U. (2011). Analysis of the Impact of Urban Wetland on Urban Temperature Based on Remote Sensing Technology. On *2011 3rd International Conference on Environmental Science and Information Application Technology (ESIAT 2011)*.

Chun, B., & Guldmann, J. (2014). Spatial statistical analysis and simulation of the urban heat island in high-density central cities. *Landscape and Urban Planning, 125*, 76-88.

Cinar, İ. (2015). Assessing the Correlation between Land Cover Conversion and Temporal Climate Change—A Pilot Study in Coastal Mediterranean City, Fethiye, Turkey. *Atmosphere, 6*(8), 1102-1118.

Coates, L., Haynes, K., O'Brien, J., McAneney, J., & De Oliveira, F. D. (2014). Exploring 167 years of vulnerability: An examination of extreme heat events in Australia 1844-2010. *Environmental Science and Policy, 42*, 33-44.

Collatz, G. J., Bounoua, L., Los, S., Randall, D., Fung, I., & Sellers, P. (2000). A mechanism for the influence of vegetation on the response of the diurnal temperature range to changing climate. *Geophysical Research Letters, 27*(20), 3381-3384.

Connors, J. P., Galletti, C. S., & Chow, W. T. L. (2012). Landscape configuration and urban heat island effects: assessing the relationship between landscape characteristics and land surface temperature in Phoenix, Arizona. *Landscape Ecology, 28*(2), 271-283.

Crow, T. J., Deakin, J. F., & Longden, A. (1975). Proceedings: Do anti-psychotic drugs act by dopamine receptor blockade in the nucleus accumbens. *Br J Pharmacol, 55*(2), 295P.

Cuculeanu, V., Tuinea, P., & Bălteanu, D. (2002). Climate change impacts in Romania: Vulnerability and adaptation options. *GeoJournal, 57*(3), 203-209.

Cutter, S. L. (2009). *Measuring and Mapping Social Vulnerability*. Paper presented at the Cities at Risk.

Cutter, S. L., Boruff, B. J., & Shirley, L. W. (2003). Social Vulnerability to Environmental Hazards. *Social Science Quarterly, 84*(2).

Dash, J., Mathur, A., Foody, G. M., & Curran, P. J. (2007). Land cover classification using multi temporal MERIS vegetation indices. *International Journal of Remote Sensing, 28*, 1137-1159.

de-Azevedo, P. V., Bezerra, P. T. d. C., Leitão, M. d. M. V. B. R., & Santos, C. A. C. d. (2015). Characterization of human thermal comfort in urban areas of Brazilian semiarid. *Revista Brasileira de Meteorologia, 30*(4), 371-380.

De-Simone, G., Janeiro, R. D., Toronto, T. D., Jack, D., York, N., Toronto, J. P., & Rahman, M. (2011). Climate change and human health in cities Coordinating Lead Authors : Lead Authors :. *Cities And Climate Change - First Assessment Report of the Urban Climate Change Research Network*, 179-213.

De Fries, R. S., Hansen, M., Townshend, J. R. G., & Sohlberg, R. (1998). Global land cover classifications at 8 km spatial resolution: the use of training data derived from Landsat imagery in decision tree classifiers. *International Journal of Remote Sensing, 19*(16), 3141-3168.

Deng, C., & Wu, C. (2013). Examining the impacts of urban biophysical compositions on surface urban heat island: A spectral unmixing and thermal mixing approach. *Elsevier, Remote Sensing of Environment 131* 262-274.

Depietri, Y., Welle, T., & Renaud, F. G. (2013). Social vulnerability assessment of the Cologne urban area (Germany) to heat waves: Links to ecosystem services. *International Journal of Disaster Risk Reduction, 6*, 98-117.

Dereczynski, C., Silva, W. L., & Marengo, J. (2013). Detection and Projections of Climate Change in Rio de Janeiro, Brazil. *American Journal of Climate Change, 02*(01), 25-33.

Dewan, A. M., & Corner, R. J. (2012). The impact of land use and land cover changes on land surface temperature in a rapidly urbanizing megacity. *IGARSS*, 6337-6339.

Dewan, A. M., & Yamaguchi, Y. (2009). Land use and land cover change in Greater Dhaka, Bangladesh: Using remote sensing to promote sustainable urbanization. *Applied Geography, 29*, 390–401.

Dholakia, H. H., Mishra, V., & Garg, A. (2015). Predicted increases in heat related mortality under climate change in urban India. *Indian Institute of Management*, 1-31.

Dirmeyer, P. A., Niyogi, D., de Noblet-Ducoudré, N., Dickinson, R. E., & Snyder, P. K. (2010). Impacts of land use change on climate. *International Journal of Climatology, 30*(13), 1905-1907.

Dokladny, K., Moseley, P. L., & Ma, T. Y. (2006). Physiologically relevant increase in temperature causes an increase in intestinal epithelial tight junction permeability. *American Journal of Physiology-Gastrointestinal and Liver Physiology, 290*(2), G204-G212.

Dombaycı, Ö. A. (2009). Degree-days maps of Turkey for various base temperatures. *Energy, 34*(11), 1807-1812.
Dominguez, A., Kleissl, J., Luvall, J. C., & Rickman, D. L. (2011). High- resolution urban thermal sharpener (HUTS). *Remote Sensing of Environment, 115*, 1772–1780.
Dousset, B., & Gourmelon, F. (2003). Satellite multi-sensor data analysis of urban surface temperatures and landcover. *ISPRS Journal of Photogrammetry and Remote Sensing, 58*(1-2), 43-54.
Dube, T., Gumindoga, W., & Chawira, M. (2014). Detection of land cover changes around Lake Mutirikwi , Zimbabwe , based on traditional remote sensing image classification techniques Detection of land cover changes around Lake Mutirikwi , Zimbabwe , based on tradition. *African Journal of Aquatic Science, 39*, 89-95.
Dube, T., & Mutanga, O. (2015a). Evaluating the utility of the medium-spatial resolution Landsat 8 multispectral sensor in quantifying aboveground biomass in uMgeni catchment, South Africa. *ISPRS Journal of Photogrammetry and Remote Sensing, 101*, 36-46.
Dube, T., & Mutanga, O. (2015b). Investigating the robustness of the new Landsat-8 Operational Land Imager derived texture metrics in estimating plantation forest aboveground biomass in resource constrained areas. *ISPRS Journal of Photogrammetry and Remote Sensing, 108*, 12-32.
Dube, T., & Mutanga, O. (2015c). Quantifying the variability and allocation patterns of aboveground carbon stocks across plantation forest types, structural attributes and age in sub-tropical coastal region of KwaZulu Natal, South Africa using remote sensing. *Applied Geography, 64*, 55-65.
Dube, T., Mutanga, O., & Ismail, R. (2016). Quantifying aboveground biomass in African environments: A review of the trade-offs between sensor estimation accuracy and costs. *Tropical Ecology 57*(3), 393-405.
Dube, T., & Phiri, K. (2013). Rural livelihoods under stress: the impact of climate change on livelihoods in south western Zimbabwe. *American International Journal of Contemporary Research, 3*, 11-25.
Durmayaz, A., Kadoğlu, M., & En, Z. (2000). An application of the degree-hours method to estimate the residential heating energy requirement and fuel consumption in Istanbul. *Energy, 25*, 1245-1256.
Eastman, J. R. (2012a). IDRISI Selva Tutorial. *Idrisi Production, Clark Labs-Clark University, 45*, 51-63.
Eastman, R. J. (2012b). IDRISI Selva Manual. *IDRISI Production. Clarke University, Manual Version 17*.
Elmhagen, B., Destouni, G., Angerbjörn, A., Borgström, S., Boyd, E., Cousins, S. A. O., Dalén, L., Ehrlén, J., Ermold, M., Hambäck, P. A., Hedlund, J., et al. (2015). Interacting effects of change in climate, human population, land use, and water use on biodiversity and ecosystem services. *Ecology and Society, 20*(1).
Elsner, J. B., Niu, X., & Jagger, T. H. (2004). Detecting Shifts in Hurricane Rates Using a Markov Chain Monte Carlo Approach. *Journal of Climate, 17*(13), 2652-2666.
Esch, T., Marconcini, M., Felbier, A., Roth, A., Heldens, W., Huber, M., Schwinger, M., Taubenböck, H., Müller, A., & Dech, S. (2013). Urban footprint processor—Fully automated processing chain generating settlement masks from global data of the TanDEM-X mission. *IEEE Geoscience and Remote Sensing Letters, 10*(6), 1617-1621.
Essa, W., Kwast, J. V. D., Verbeiren, B., & Batelaan, O. (2013). Downscaling of thermal images over urban areas using the land surface temperature – impervious percentage

relationship. *International Journal of Applied Earth Observation and Geoinformation, 23*, 95-108.
Eto, J. H. (1988). On using degree-days to account for the effects of weather on annual energy use in office buildings. *Energy and Buildings, 12*(2), 113-127.
Ewing, R., & Rong, F. (2008). The impact of urban form on U.S. residential energy use. *Housing Policy Debate, 19*(1), 1-30.
Fan, F., Wang, Y., & Wang, Z. (2008). Temporal and spatial change detecting (1998-2003) and predicting of land use and land cover in core corridor of Pearl River Delta (China) by using TM and ETM+ images. *Environ Monit Assess, 137*(1-3), 127-147.
Farnham, C., Emura, K., & Mizuno, T. (2015). Evaluation of cooling effects : outdoor water mist fan. *Building Research and Information, 43*, 334-345.
Feng, H., Zhao, X., Chen, F., & Wu, L. (2014). Using land use change trajectories to quantify the effects of urbanization on urban heat island. *Advances in Space Research, 53*(3), 463-473.
Flamenco-Sandoval, A., Martínez Ramos, M., & Masera, O. R. (2007). Assessing implications of land-use and land-cover change dynamics for conservation of a highly diverse tropical rain forest. *Biological Conservation, 138*(1-2), 131-145.
Flanner, M. G. (2009). Integrating anthropogenic heat flux with global climate models. *Geophysical Research Letters, 36*(2).
Foody, G. M. (1996). Approaches for the production and evaluation of fuzzy land cover classifications from remotely-sensed data. *International Journal of Remote Sensing, 17*(7), 1317-1340.
Forkuor, G., & Cofie, O. (2011). Dynamics of land-use and land-cover change in Freetown , Sierra Leone and its effects on urban and peri-urban agriculture – a remote sensing approach. *International Journal of Remote Sensing, 32*, 1017-1037.
Franco, S., Mandla, V. R., Rao, K. R. M., Kumar, M. P., & Anand, P. C. (2015). Study of Temperature Profile on Various Land Use and Land Cover for Emerging Heat Island. *Journal of Urban and Environmental Engineering, 9*, 32-37.
Gallo, K. P., & Owen, T. W. (1998). Assessment of urban heat Islands: A multi-sensor perspective for the Dallas-Ft. worth, USA region. *Geocarto International, 13*(4), 35-41.
Ganopolski, A., Kubatzki, C., Claussen, M., Brovkin, V., & Petoukhov, V. (1998). The influence of vegetation-atmosphere-ocean interaction on climate during the mid-Holocene. *Science, 280*(5371), 1916-1919.
García-Frapolli, E., Ayala-Orozco, B., Bonilla-Moheno, M., Espadas-Manrique, C., & Ramos-Fernández, G. (2007). Biodiversity conservation, traditional agriculture and ecotourism: Land cover/land use change projections for a natural protected area in the northeastern Yucatan Peninsula, Mexico. *Landscape and Urban Planning, 83*(2-3), 137-153.
Genc, L., Inalpulat, M., Kizil, U., & Aksu, S. (2014). *Detemination of Paddy Rice Field Using Landsat 8 Images*. Paper presented at the International Conference on Biological, Civil and Environmental Engineering.
Geneletti, D., & Gorte, B. G. H. (2003). A method for object-oriented land cover classification combining Landsat TM data and aerial photographs. *International Journal of Remote Sensing, 24*, 1273-1286.
Gervin, J. C., Kerber, A. G., Witt, R. G., Lu, Y. C., & Sekhon, R. (1985). Comparison of level I land cover classification accuracy for MSS and AVHRR data. *International Journal of Remote Sensing, 6*, 47-57.
Gillespie, A., Rokugawa, S., Matsunaga, T., Cothern, J. S., Hook, S., & Kahle, A. B. (1998). A temperature and emissivity separation algorithm for Advanced Spaceborne Thermal

Emission and Reflection Radiometer (ASTER) images. *IEEE transactions on geoscience and remote sensing, 36*(4), 1113-1126.
Gillies, R. R., & Carlson, T. N. (1995). Thermal remote sensing of surface soil water content with partial vegetation cover for incorporation into climate models. *Journal of Applied Meteorology, 34*(4), 745-756.
Gluch, R., Quattrochi, D. A., & Luvall, J. C. (2006). A multi-scale approach to urban thermal analysis. *Remote Sensing of Environment, 104*(2), 123-132.
Goshayeshi, D., Shahidan, M. F., Khafi, F., & Ehtesham, E. (2013a). A review of researches about human thermal comfort in semi-outdoor spaces. *European Online Journal of Natural and Social Sciences, 2*(4), 516-523.
Goshayeshi, D., Shahidan, M. F., Khafi, F., & Ehtesham, E. (2013b). A review of researches about human thermal comfort in semi-outdoor spaces. *European Online Journal of Natural and Social Sciences, 2*, 516-523.
Gottshe, F.-M., & Olesen, F. S. (2001). Modelling of diurnal cycles of brightness temperature extracted from METEOSAT data. *Remote Sensing of Environment, 76*, 337-348.
Grimmond, S. U. E. (2007). Urbanization and global environmental change: local effects of urban warming. *The Geographical Journal, 173*(1), 83-88.
Gronlund, C. J., Berrocal, V. J., White-Newsome, J. L., Conlon, K. C., & O'Neill, M. S. (2015). Vulnerability to extreme heat by socio-demographic characteristics and area green space among the elderly in Michigan, 1990-2007. *Environmental Research, 136*, 449-461.
Grossman-Clarke, S., Zehnder, J. A., Loridan, T., & Grimmond, C. S. B. (2010). Contribution of Land Use Changes to Near-Surface Air Temperatures during Recent Summer Extreme Heat Events in the Phoenix Metropolitan Area. *Journal of Applied Meteorology and Climatology, 49*(8), 1649-1664.
Guan, K. (2011). Surface and ambient air temperatures associated with different ground material: a case study at the University of California, Berkeley. *Environmental Science, 196*, 1-14.
Guerra Santin, O., Itard, L., & Visscher, H. (2009). The effect of occupancy and building characteristics on energy use for space and water heating in Dutch residential stock. *Energy and Buildings, 41*, 1223-1232.
Guhathakurta, S., & Gober, P. (2007). The Impact of the Phoenix Urban Heat Island on Residential Water Use. *Journal of the American Planning Association, 73*(3), 317-329.
Gusso, A., Cafruni, C., Bordin, F., Veronez, M. R., & Lenz, L. (2014). Multitemporal Analysis of Thermal Distribution Characteristics for Urban Heat Island Management. On *4th WOrld Sustainability Forum*: Multidisciplinary Digital Publishing Institute.
Gutman, G., & Ignatov, A. (1998). The derivation of the green vegetation fraction from NOAA/AVHRR data for use in numerical weather prediction models. *International Journal of remote sensing, 19*(8), 1533-1543.
Hallegatte, S., & Corfee-Morlot, J. (2010). Understanding climate change impacts, vulnerability and adaptation at city scale: an introduction. *Climatic Change, 104*(1), 1-12.
Hamdi, R. (2010). Estimating Urban Heat Island Effects on the Temperature Series of Uccle (Brussels, Belgium) Using Remote Sensing Data and a Land Surface Scheme. *Remote Sensing, 2010*(2), 2773-2784.
Han, T., & Nelson, J. (2015). Mapping hydrothermally altered rocks with Landsat 8 imagery: A case study in the KSM and Snowfi eld zones, northwestern British Columbia. *Geological Fieldwork 2014, British Columbia Ministry of Energy and Mines, British Columbia Geological Survey, 2015*(1).

Hansen, A., Bi, L., Saniotis, A., & Nitschke, M. (2013). Vulnerability to extreme heat and climate change: is ethnicity a factor? *Global Health Action, 6*(1), 21364-21371.

Harlan, S. L., Brazel, A. J., Prashad, L., Stefanov, W. L., & Larsen, L. (2006). Neighborhood microclimates and vulnerability to heat stress. *Social Science and Medicine, 63*, 2847-2863.

Harlan, S. L., Declet-Barreto, J. H., Stefanov, W. L., & Petitti, D. B. (2013). Neighborhood effects on heat deaths: Social and environmental predictors of vulnerability in Maricopa county, Arizona. *Environmental Health Perspectives, 121*, 197-204.

Hartmann, D. L., Tank, a. M. G. K., & Rusticucci, M. (2013). *IPCC Fifth Assessment Report, Climatie Change 2013: The Physical Science Basis.* Paper presented at the IPCC.

Haruna, I. U., Musa, I., Tikau, M. I., & Yerima, M. (2014). Improvement Of Thermal Comfort In Residential Buildings. *International Journal of Scientific & Technology Research, 3*, 180-183.

Hasanlou, M., & Mostofi, N. (2015). Investigating Urban Heat Island Estimation and Relation between Various Land Cover Indices in Tehran City Using Landsat 8 Imagery. On *1st International Electronic Conference on Remote Sensing.* . Multidisciplinary Digital Publishing Institute.

Hashem, N., & Balakrishnan, P. (2015). Change analysis of land use/land cover and modelling urban growth in Greater Doha, Qatar. *Annals of GIS, 21*(3), 233-247.

Hassan Radhi, Fayze Fikry, & Stephen Sharples. (2013). Impacts of urbanisation on the thermal behaviour of new built up environments: A scoping study of the urban heat island in Bahrain. *Elsevier, Landscape and Urban Planning 113*, 47– 61.

Heaton, M. J., Sain, S. R., Greasby, T. A., Uejio, C. K., Hayden, M. H., Monaghan, A. J., Boehnert, J., Sampson, K., Banerjee, D., Nepal, V., & Wilhelmi, O. V. (2014). Characterizing urban vulnerability to heat stress using a spatially varying coefficient model. *Spatial and Spatio-temporal Epidemiology, 8*, 23-33.

Heinl, M., & Tappeiner, U. (2012). The benefits of considering land cover seasonality in multi-spectral image classification. *Journal of Land Use Science, 7*(1), 1-19.

Henry, J. A., Dicks, S. E., Wetterquist, O. F., & Roguski, S. J. (1989). Comparison of satellite, ground-based, and modeling techniques for analyzing the urban heat island. *Photogrammetric Engineering and Remote Sensing, 55*, 69-76.

Hirano, Y., Imura, H., & Ichinose, T. (2009). *Effects of the heat island phenomenon on energy consumption in commercial and residential sectors of metropolitan Tokyo*. Paper presented at the In 7th International Conference on Urban Climate (ICUC7), Yokohama, Japan.

Ho, H. C., Knudby, A., & Huang, W. (2015). A Spatial Framework to Map Heat Health Risks at Multiple Scales. *International Journal of Environmental Research and Public Health, 12*, 16110–16123.

Hoffmann, P., Krueger, O., & Schl??nzen, K. H. (2012). A statistical model for the urban heat island and its application to a climate change scenario. *International Journal of Climatology, 32*, 1238-1248.

Hsiang, S. M. (2010). Temperatures and cyclones strongly associated with economic production in the Caribbean and Central America. *Proceedings of the National Academy of sciences, 107*(35), 15367-15372.

Hu, Y., & Jia, G. (2010). Influence of land use change on urban heat island derivedfrom multi-sensor data. *International Journal of Climatology, 30*, 1382-1395.

Hua, L., Man, W., Wang, Q., & Zhao, X. (2013). AWERProcedia Information Technology & Computer Science A New Decision Tree Classification Approach for Extracting Urban Land from Landsat TM in a Coastal City , China. On *AWER Procedia Information Technology and Computer Science*.

Huete, A. R. (1988). A soil-adjusted vegetation index (SAVI). *Remote sensing of environment*, *25*(3), 295-309.
Humphreys, M. (1978). Outdoor temperatures and comfort indoors Outdoor temperatures and comfort indoors. *Batiment International, Building Research and Practice*, *6*, 92-105.
Humphreys, M. (2015). Outdoor temperatures and comfort indoors Outdoor temperatures and comfort indoors. *Batiment International, Building Research and Practice*, *6*, 92-105.
Hung, T., Uchihama, D., Ochi, S., & Yasuoka, Y. (2006). Assessment with satellite data of the urban heat island effects in Asian mega cities. *International Journal of Applied Earth Observation and Geoinformation 8*, 34-48.
Iied. (2011). Climate change and the urban poor : 15 of the world ' s most vulnerable cities. 24.
IPCC. (2007). Climate change 2007: the physical science basis. *Intergovernmental Panel on Climate Change, Fourth assessment report*.
Isaac, M., & van Vuuren, D. P. (2009). Modeling global residential sector energy demand for heating and air conditioning in the context of climate change. *Energy Policy*, *37*, 507-521.
Jackson, T. J., Chen, D., Cosh, M., Li, F., Anderson, M., Walthall, C., Doriaswamy, P., & Hunt, E. R. (2004). Vegetation water content mapping using Landsat data derived normalized difference water index for corn and soybeans. *Remote Sensing of Environment 92*, 475–482.
Jalan, S., & Sharma, K. (2014). Spatio-temporal Assessment of Land Use/ Land Cover Dynamics and Urban Heat Island of Jaipur City using Satellite Data. *ISPRS - International Archives of the Photogrammetry, Remote Sensing and Spatial Information Sciences, XL-8*, 767-772.
Jenerette, G. D., Harlan, S. L., Brazel, A., Jones, N., Larsen, L., & Stefanov, W. L. (2007). Regional relationships between surface temperature, vegetation, and human settlement in a rapidly urbanizing ecosystem. *Landscape Ecology*, *22*(3), 353-365.
Jensen, J. R. (1983). Urban/suburban land use analysis. *Manual of Remote Sensing, R.N. Colwell (Ed)*, 1571–1666.
Jia, K., Wei, X., Gu, X., Yao, Y., Xie, X., & Li, B. (2014). Land cover classification using Landsat 8 operational land imager data in Beijing, China. *Geocarto International*, *29*(8), 941-951.
Jiang, J., & Tian, G. (2010). Analysis of the impact of Land use/Land cover change on Land Surface Temperature with Remote Sensing. *Procedia Environmental Sciences*, *2*, 571-575.
Jiang, J., Zhou, J., Wu, H., Ai, L., Zhang, H., Zhang, L., & Xu, J. (2005). Land cover changes in the rural–urban interaction of Xi'an region using Landsat TM/ETM data. *Journal of Geographical Sciences*, *4*, 423-430.
Johnson, D., Webber, J. J., Ravichandra, K. U. B., Lulla, V., & Stanforth, A. C. (2014). Spatiotemporal Variations in Heat-Related Health Risk in Three Midwestern U.S. Cities Between 1990 and 2010. *Geocarto International*, *29*, 65-84.
Johnson, D. P., Stanforth, A., Lulla, V., & Luber, G. (2012). Developing an applied extreme heat vulnerability index utilizing socioeconomic and environmental data. *Applied Geography*, *35*, 23-31.
Johnson, D. P., Wilson, J. S., & Luber, G. C. (2009). Socioeconomic indicators of heat-related health risk supplemented with remotely sensed data. *Int J Health Geogr*, *8*, 57.
Juan-juan Li, Xiang-rong Wang, Xin-jun Wang, Wei-chun Ma, & Hao Zhang. (2009). Remote sensing evaluation of urban heat island and its spatial pattern of the Shanghai metropolitan area, China. *Elsevier, Ecological Complexity 6*, 413–420.

Kahle, A. B. (1987). Surface emittance, temperature, and thermal inertia derived from Thermal Infrared Multispectral Scanner (TIMS) data for Death Valley, California. *Geophysics, 52*(7), 858-874.

Kahn, M. E. (2009). Urban Growth and Climate Change. *Annual Review of Resource Economics, 1*(1), 333-350.

Kaloustian, N., & Bechtel, B. (2016). Local climatic zoning and urban heat island in Beirut. *Procedia Engineering, 169*, 216-223.

Kamusoko, C., Gamba, J., & Murakami, H. (2013). Monitoring Urban Spatial Growth in Harare Metropolitan Province, Zimbabwe. *Advances in Remote Sensing, 2* 322-331.

Karlson, M., Ostwald, M., Reese, H., Sanou, J., Tankoano, B., & Mattsson, E. (2015). Mapping Tree Canopy Cover and Aboveground Biomass in Sudano-Sahelian Woodlands Using Landsat 8 and Random Forest. *Remote Sensing, 7*, 10017-11041.

Katayama, R., Shozi, M., & Tokiya, Y. (2000). A Research On The Urban Disaster Prevention Plan Concerning Earthquake Risk Forecast By Remoto Sensing in The Tokyo Bay Area. *ISPRS, Vol, Part B7, P6 62, 669*.

Kawakubo, F. S., Morato, R. G., & Luchiari, A. (2013). Use of fraction imagery , segmentation and masking techniques to classify land-use and land-cover types in the Brazilian Amazon. *International Journal of Remote Sensing, 34*, 5452-5467.

Kawamura, M., Jayamamana, S., & Tsujiko, Y. (1997). Comparison of Urbanization and Environmental Condition in Asian Cities using Satellite Remote Sensing Data. *GIS Development, Proceeding ACRS (1997)*.

Kawamura, M., Jayamana, S., & Tsujiko, Y. (1996). Relation between social and environmental conditions in Colombo Sri Lanka and the urban index estimated by satellite remote sensing data. *Int. Arch. Photogramm. Remote Sens, 31*, 321-326.

Ke, Y., Im, J., Lee, J., Gong, H., & Ryu, Y. (2015). Characteristics of Landsat 8 OLI-derived NDVI by comparison with multiple satellite sensors and in-situ observations. *Remote Sensing of Environment, 164*, 298-313.

Kealy, P. S., & Hook, S. J. (1993). Separating temperature and emissivity in thermal infrared multispectral scanner data: Implications for recovering land surface temperatures. *IEEE Transactions on Geoscience and Remote Sensing, 31*(6), 1155-1164.

Keramitsoglou, I., Kiranoudis, C. T., Ceriola, G., Weng, Q., & Rajasekar, U. (2011). Identi fi cation and analysis of urban surface temperature patterns in Greater Athens , Greece , using MODIS imagery. *Remote Sensing of Environment, 115*, 3080-3090.

Kerchove, R. V. D., Lhermitte, S., Veraverbeke, S., & Goossens, R. (2013). Spatio-temporal variability in remotely sensed land surface temperature , and its relationship with physiographic variables in the Russian Altay Mountains. *International Journal of Applied Earth Observation and Geoinformation, 20*, 4-19.

Kharat, S. A., & Musande, V. B. (2015). Cotton Crop Discrimination Using Landsat-8 Data. *International Journal of Computer Science and Information Technologies, 6*(5), 4381-4384.

Klein Rosenthal, J., Kinney, P. L., & Metzger, K. B. (2014). Intra-urban vulnerability to heat-related mortality in New York City, 1997-2006. *Health and Place, 30*, 45-60.

Klok, L., Zwart, S., Verhagen, H., & Mauri, E. (2012). The surface heat island of Rotterdam and its relationship with urban surface characteristics. *Resources , Conservation and Recycling, 64*, 23-29.

Kusaka, H., Hara, M., & Takane, Y. (2012). Urban Climate Projection by the WRF Model at 3-km Horizontal Grid Increment: Dynamical Downscaling and Predicting Heat Stress in the 2070's August for Tokyo, Osaka, and Nagoya Metropolises. *Journal of the Meteorological Society of Japan, 90B*, 47-63.

Kwong, Q. J., Adam, N. M., & Sahari, B. (2014). Thermal comfort assessment and potential for energy efficiency enhancement in modern tropical buildings: A review. *Energy and Buildings, 68*, 547-557.

Lam, K. F., Mui, H. W., & Yuen, H. K. (2001). A note on minimizing absolute percentage error in combined forecasts. *Computers and Operations Research, 28*(11), 1141-1147.

Larsen, K., & Gunnarsson-Östling, U. (2009). Climate change scenarios and citizen-participation: Mitigation and adaptation perspectives in constructing sustainable futures. *Habitat International, 33*, 260-266.

Larsen, P. H., Goldsmith, S., Smith, O., Wilson, M. L., Strzepek, K., Chinowsky, P., & Saylor, B. (2008). Estimating future costs for Alaska public infrastructure at risk from climate change. *Global Environmental Change, 18*(3), 442-457.

Li, H., & Liu, Q. (2008). Comparison of NDBI and NDVI as indicators of surface urban heat island effect in MODIS imagery. *International Conference on Earth Observation Data Processing and Analysis (ICEODPA), 7285*, 728503-728503-728510.

Li, P., Jiang, L., & Feng, Z. (2013). Cross-Comparison of Vegetation Indices Derived from Landsat-7 Enhanced Thematic Mapper Plus (ETM+) and Landsat-8 Operational Land Imager (OLI) Sensors. *Remote Sensing, 6*(1), 310.

Li, Y.-y., Zhang, H., & Kainz, W. (2012). Monitoring patterns of urban heat islands of the fast-growing Shanghai metropolis, China: Using time-series of Landsat TM/ETM+ data. *International Journal of Applied Earth Observation and Geoinformation, 19*, 127-138.

Li, Z., Liu, W. Z., Zhang, X. C., & Zheng, F. L. (2011). Assessing the site-specific impacts of climate change on hydrology, soil erosion and crop yields in the Loess Plateau of China. *Climatic Change, 105*, 223-242.

Lin, B., Wang, Z., Liu, Y., Zhu, Y., & Ouyang, Q. (2016). Investigation of winter indoor thermal environment and heating demand of urban residential buildings in China ' s hot summer e Cold winter climate region. *Building and Environment, 101*, 9-18.

Liu, H., & Weng, Q. H. (2009). Scaling Effect on the Relationship between Landscape Pattern and Land Surface Temperature: A Case Study of Indianapolis, United States. *Photogrammetric Engineering and Remote Sensing, 75*, 291-304.

Liu, H. Q., & Huete, A. (1995). A feedback based modification of the NDVI to minimize canopy background and atmospheric noise. *IEEE Transactions on Geoscience and Remote Sensing, 33*(2), 457-465.

Liu, J. Y., Zhuang, D. F., Luo, D., & Xiao, X. (2003). Land-cover classification of China: integrated analysis of AVHRR imagery and geophysical data. *International Journal of Remote Sensing, 24*(12), 2485–2500.

Lo, C. P., & Choi, J. (2004). A hybrid approach to urban land use/cover mapping using Landsat 7 Enhanced Thematic Mapper Plus (ETM +) images. *International Journal of Remote, 25*, 2687-2700.

Lo, C. P., Quattrochi, D. A., & Luvall, J. C. (1997). Application of high-resolution thermal infrared remote sensing and GIS to assess the urban heat island effect. *International Journal of Remote Sensing, 18*(2), 287-304.

Loehle, C. (2011). Climate Change Attribution Using Empirical Decomposition of Climatic Data. *The Open Atmospheric Science Journal, 5*(1), 74-86.

Lu, D., & Weng, Q. (2005). Urban Classification Using Full Spectral Information of Landsat ETM + Imagery in Marion County , Indiana. *Photogrammetric Engineering & Remote Sensing, 71*, 1275-1284.

Lu, D., & Weng, Q. (2006). Spectral mixture analysis of ASTER images for examining the relationship between urban thermal features and biophysical descriptors in Indianapolis, Indiana, USA. *Remote Sensing of Environment, 104*(2), 157-167.

Lu, N., Hernandez, A. J., & Ramsey, R. D. (2015). Land cover dynamics monitoring with Landsat data in Kunming, China: a cost-effective sampling and modelling scheme using Google Earth imagery and random forests. *Geocarto International, 30*(2), 186-201.

Luber, G., & McGeehin, M. (2008). Climate Change and Extreme Heat Events. *American Journal of Preventive Medicine, 35*, 429-435.

Ma, Y., Kuang, Y., & Huang, N. (2010). Coupling urbanization analyses for studying urban thermal environment and its interplay with biophysical parameters based on TM / ETM + imagery. *International Journal of Applied Earth Observation and Geoinformation, 12*, 110-118.

Madhumathi, A. A., & Sundarraja, B. M. C. (2012). Experimental study of passive cooling of building facade using phase change materials to increase thermal comfort in buildings in hot humid areas. *International Journal of Energy and Environment, 3*, 739-748.

Maeda, E. E. (2015). Downscaling MODIS LST in the East African mountains using elevation gradient and land-cover information. *International Journal of Remote Sensing, 35*, 3094-3108.

Maier, G., Grundstein, A., Jang, W., Li, C., Naeher, L. P., & Shepherd, M. (2014). Assessing the Performance of a Vulnerability Index during Oppressive Heat across Georgia, United States. *Weather, climate, and society, 6*(2), 253-263.

Mallick, J., Rahman, A., & Kumar, C. (2013). Modeling urban heat islands in heterogeneous land surface and its correlation with impervious surface area by using night-time ASTER satellite data in highly urbanizing city , Delhi-India. *Advances in Space Research, 52*, 639-655.

Manandhar, R., Odeh, I. O., & Ancev, T. (2009). Improving the accuracy of land use and land cover classification of Landsat data using post-classification enhancement. *Remote Sensing, 1*(3), 330-344.

Manatsa, D., & Mukwada, G. (2012). Rainfall Mechanisms for the Dominant Rainfall Mode over Zimbabwe Relative to ENSO and/or IODZM. *The Scientific World Journal*, 15.

Manatsa, D., Morioka, Y., Behera, S. K., Yamagata, T., & Matarira, C. H. (2013). Link between Antarctic ozone depletion and summer warming over Southern Africa. *Nature Geoscience, 6*, 934-939.

Manatsa, D., Mushore, T., & Lenouo, A. (2017). Improved predictability of droughts over southern Africa using the standardized precipitation evapotranspiration index and ENSO. *Theoretical and Applied Climatology, 127*(1-2), 259-274.

Manatsa, D., Unganai, L., Gadzirai, C., & Behera, S. (2012). An innovative tailored seasonal rainfall forecasting production in Zimbabwe. *Natural Hazards*, 1-21.

Mann, H. B., & Whitney, D. R. (1947). On a test of whether one of two random variables is stochastically larger than the other. *The annals of mathematical statistics*, 50-60.

Marland, G., Pielke, R. a., Apps, M., Avissar, R., Betts, R. a., Davis, K. J., Frumhoff, P. C., Jackson, S. T., Joyce, L. a., Kauppi, P., Katzenberger, J., et al. (2003). The climatic impacts of land surface change and carbon management, and the implications for climate-change mitigation policy. *Climate Policy, 3*, 149-157.

Matongera, T. N., Mutanga, O., Dube, T., & Sibanda, M. (2017). Detection and mapping the spatial distribution of bracken fern weeds using the Landsat 8 OLI new generation sensor. *International Journal of Applied Earth Observation and Geoinformation, 57*, 93-103.

Mazon, J. (2013). The influence of thermal discomfort on the attention index of teenagers: an experimental evaluation. *International Journal of Biometeorology, 58*(5), 717-724.

Mazvimavi, D. (2010). Investigating changes over time of annual rainfall in Zimbabwe. *Hydrology and Earth System Sciences, 14*, 2671-2679.

Mcalpine, C. a., Syktus, J. I., Deo, R. C., Lawrence, P. J., Mcgowan, H. a., Watterson, I. G., & Phinn, S. R. (2007). Modeling Impacts of Vegetation Cover Change on Regional Climate Change. *Change*.

McCarthy, M. P., Best, M. J., & Betts, R. a. (2010). Climate change in cities due to global warming and urban effects. *Geophysical Research Letters, 37*, 1-5.

McDonald, R. I., Green, P., Balk, D., Fekete, B. M., Revenga, C., Todd, M., & Montgomery, M. (2011a). Urban growth, climate change, and freshwater availability. *Proc Natl Acad Sci U S A, 108*(15), 6312-6317.

McDonald, R. I., Green, P., Balk, D., Fekete, B. M., Revenga, C., Todd, M., & Montgomery, M. (2011b). Urban growth, climate change, and freshwater availability. *Proceedings of the National Academy of Sciences of the United States of America, 108*, 6312-6317.

McFarland, M. J., Miller, R. L., & Neale, C. M. U. (1990). Land surface tempera- ture derived from the SSM/I passive microwave brightness temperatures. *IEEE Transactions on Geoscience and Remote Sensing, 28*, 839-845.

McFeeters, S. K. (1996). The use of the Normalized Difference Water Index (NDWI) in the delineation of open water features. *International journal of remote sensing, 17*(7), 1425-1432.

McLeod, R. S., Hopfe, C. J., & Kwan, A. (2013). An investigation into future performance and overheating risks in Passivhaus dwellings. *Building and Environment, 70*, 189-209.

McMichael, A. J., & Confalonieri, U. (2012). *Environment, climate change, social factors and the implications for controlling infectious diseases of poverty*. World Health Organization (WHO Press). World Health Organization.

McMillin, L. M. (1975). Estimation of sea surface temperatures from two infrared window measurements with different absorption. *Journal of Geophysical Research, 80*(36), 5113-5117.

Ministry of mines environment and tourism. (1998). *Zimbabwe's Initial National Communication. Prepared for the United Nations Framework Convention on Climate Change*: Climate Change Office, Zimbabwe.

Mlambo, A. (2008). Historical antecedents to operation Murambatsvina. *The hidden dimensions of operation Murambatsvina in Zimbabwe*, 9-24.

Mohamed, A. A., Odindi, J., & Mutanga, O. (2016). Land surface temperature and emissivity estimation for Urban Heat Island assessment using medium- and low-resolution space-borne sensors: A review. *Geocarto International, 32*(4), 455-470.

Mohan, M., Gupta, A., & Bhati, S. (2014). A Modified Approach to Analyze Thermal Comfort Classification. *Atmospheric and Climate Sciences, 4*, 7-19.

Moyo, M., Mvumi, B. M., Kunzekweguta, M., Mazvimavi, K., & Craufurd, P. (2012). Farmer perceptions on climate change and variability in semi-arid Zimbabwe in relation to climatology evidence The year-to-year variability of rainfall is a significant constraint to the sustainability of rain- fed farming systems in poorer countries in s. *African Crop Science Journal, 20*, 317-335.

Mushore, T., Manatsa, D., Pedzisai, E., Muzenda-Mudavanhu, C., Mushore, W., & Kudzotsa, I. (2017). Investigating the implications of meteorological indicators of seasonal rainfall performance on maize yield in a rain-fed agricultural system: case study of Mt. Darwin District in Zimbabwe. *Theoretical and Applied Climatology, 129*(3-4), 1167-1173.

Mushore, T. D. (2013a). Climatic Changes, Erratic Rains and the Necessity of Constructing Water Infrastructure: Post 2000 Land Reform in Zimbabwe. *International Journal Of Scientific & Technology Research 2*(8), 304-310.

Mushore, T. D. (2013b). Uptake Of Seasonal Rainfall Forecasts In Zimbabwe. *IOSR Journal Of Environmental Science, Toxicology And Food Technology (IOSR-JESTFT), 5*(1), 31-37.

Mushore, T. D., Mutanga, O., Odindi, J., & Dube, T. (2016). Assessing the potential of integrated Landsat 8 thermal bands, with the traditional reflective bands and derived vegetation indices in classifying urban landscapes. *Geocarto International, 32*(8), 886-899.

Mushore, T. D., Mutanga, O., Odindi, J., & Dube, T. (2017a). Determining extreme heat vulnerability of Harare Metropolitan City using multispectral remote sensing and socio-economic data. *Journal of Spatial Science*, 1-19.

Mushore, T. D., Mutanga, O., Odindi, J., & Dube, T. (2017b). Linking major shifts in land surface temperatures to long term land use and land cover changes: A case of Harare, Zimbabwe. *Urban Climate, 20*, 120-134.

Mwaniki, M. W., Moeller, M. S., & Schellmann, G. (2015). A comparison of Landsat 8 (OLI) and Landsat 7 (ETM+) in mapping geology and visualising lineaments: A case study of central region Kenya. *The International Archives of the Photogrammetry, Remote Sensing and Spatial Information Sciences, XL-7/W3*.

Myint, S. W. (2001). A Robust Texture Analysis and Classification Approach for Urban Land-Use and Land-Cover Feature Discrimination. *Geocarto International, 16*, 1-12.

Namdar, M., Adamowski, J., & Saadat, H. (2014). Land-use and land-cover classification in semi-arid regions using independent component analysis (ICA) and expert classification. *International Journal of Remote Sensing, 35*, 8057-8073.

Nayak, S., & Mandal, M. (2012). Impact of land-use and land-cover changes on temperature trends over Western India. *Current Science, 102*, 1166-1173.

Newland, K. (2011). *Climate Change and Migration Dynamics*. Washington DC.

Odindi, J. O., Bangamwabo, V., & Mutanga, O. (2015). Assessing the value of urban green spaces in mitigating multi-seasonal urban heat using MODIS land surface temperature (LST) and landsat 8 data. *International Journal of Environmental Research, 9*, 9-18.

Ogashawara, I., & Bastos, V. (2012). A Quantitative Approach for Analyzing the relationship between Urban Heat Islands and Land Cover. *Remote Sensing, 4*(12), 3596-3618.

Ogrin, D., & Krevs, M. (2015). Assessing urban heat island impact on long-term trends of air temperatures in Ljubljana. *Dela, 43*, 41-59.

Okamura, N., Takeuchi, W., Akatsuka, S., & Oyoshi, K. (2014). Evaluating Thermal Comfort in City Life and Its Relation to Socio-Economic Activities. *Asian Journal of Geoinformatics, 14*(2).

Oke, T. R. (2004). Initial guidance to obtain representative meteorological observations at urban sites.

Omran, E.-S. E. (2012). Detection of Land-Use and Surface Temperature Change at Different Resolutions. *Journal of Geographic Information System, 04*(03), 189-203.

Oort, P. A. J. v. (2005). Improving land cover change estimates by accounting for classification errors. *International Journal of Remote Sensing, 26*(14).

Ormsby, J. P. (2007). Evaluation of natural and man-made features using Landsat TM data. *International Journal of Remote Sensing, 13*(2), 303-318.

Oumar, Z. (2015). Fire scar mapping for disaster response in KwaZulu-Natal South Africa using Landsat 8 imagery. *South African Journal of Geomatics, 4*(3).

Owen, T. W., Carlson, T. N., & Gillies, R. R. (1998). An assessment of satellite remotely-sensed land cover parameters in quantitatively describing the climatic effect of urbanization. *International Journal of Remote Sensing, 19*(9), 1663-1681.

Panah, S. K. A., Dapper, M. D., Goossens, R., & Massoudi, M. (2001). The Use of TM Thermal Band for Land Cover/Land Use Mapping in Two Different Environmental Conditions of Iran. *Agricultural Science Technology, 3*(27-36).

Papakostas, K., & Kyriakis, N. (2005). Heating and cooling degree-hours for Athens and Thessaloniki, Greece. *Renewable Energy, 30*, 1873-1880.

Parsons, K. (2014). *Human thermal environments: the effects of hot, moderate, and cold environments on human health, comfort, and performance*: Crc Press.

Pengra, B., Long, J., Dahal, D., Stehman, S. V., & Loveland, T. R. (2015). A global reference database from very high resolution commercial satellite data and methodology for application to Landsat derived 30m continuous field tree cover data. *Remote Sensing of Environment*.

Perera, N., & Emmanuel, R. (2016). A "Local Climate Zone" based approach to urban planning in Colombo, Sri Lanka. *Urban Climate*.

Peterson, T., Basist, A., & Williams, C. (2000). A blended satellite–in situ near–global surface temperature dataset. *Bulletin of the American Meteorological Society, 81*, 2157–2164.

Petropoulos, G. P., Kalaitzidis, C., & Vadrevu, K. P. (2012). Support vector machines and object-based classification for obtaining land-use/cover cartography from Hyperion hyperspectral imagery. *Comput. Geosci., 41*, 99-107.

Pielke, R. A., Pitman, A., Niyogi, D., Mahmood, R., McAlpine, C., Hossain, F., Goldewijk, K. K., Nair, U., Betts, R., Fall, S., Reichstein, M., et al. (2011). Land use/land cover changes and climate: modeling analysis and observational evidence. *Wiley Interdisciplinary Reviews: Climate Change, 2*(6), 828-850.

Pilli-Sihvola, K., Aatola, P., Ollikainen, M., & Tuomenvirta, H. (2010). Climate change and electricity consumption-Witnessing increasing or decreasing use and costs? *Energy Policy, 38*, 2409-2419.

Polydoros, A., & Cartalis, C. (2014). Assessing thermal risk in urban areas – an application for the urban agglomeration of Athens. *Advances in Building Energy Research, 8*(1), 74-83.

Potts, D. (2011). 'We Have A Tiger By The Tail': Continuities and Discontinuities in Zimbabwean City Planning and Politics. *Critical African Studies, 4*(6), 15-46.

Pu, R., Gong, P., Michishita, R., & Sasagawa, T. (2006). Assessment of multi-resolution and multi-sensor data for urban surface temperature retrieval. *Remote Sensing of Environment, 104*, 211-225.

Qiao, Z., Tian, G., & Xiao, L. (2013). Diurnal and seasonal impacts of urbanization on the urban thermal environment : A case study of Beijing using MODIS data. *ISPRS Journal of Photogrammetry and Remote Sensing, 85*, 93-101.

Qin, Z., Dall'Olmo, G., Karnieli, A., & Berliner, P. (2001). Derivation of split window algorithm and its sensitivity analysis for retrieving land surface temperature. *J. Geophys. Res, 106*(22), 655-622.

Rao, P. K. (1972). Remote sensing of urban heat islands from an environmental satellite. *Bulletin of the American Meteorological Society, 53*(7), 647-659.

Rasul, A., Balzter, H., & Smith, C. (2015). Spatial variation of the daytime Surface Urban Cool Island during the dry season in Erbil, Iraqi Kurdistan, from Landsat 8. *Urban Climate, 14*, 176-186.

Rawal, R., & Shukla, Y. (2014). *Residential Buildings in India : Energy Use Projections and Saving Potentials.Global building performance network (GBPN). technical report, 2014.* New Delhi, India.

Reddy, C. V., Kumara, M. P., & Mandlaa, V. R. (2014). *Influence of land surface temperature and CO2 on urban environment by using landsat-8*. Paper presented at

the ISPRS TC VIII International Symposium on “Operational Remote Sensing Applications: Opportunities, Progress and Challenges”.
Reid, C. E., Mann, J. K., Alfasso, R., English, P. B., King, G. C., Lincoln, R. A., Margolis, H. G., Rubado, D. J., Sabato, J. E., West, N. L., Woods, B., et al. (2012). Evaluation of a Heat Vulnerability Index on Abnormally Hot Days: An Environmental Public Health Tacking Study. *Environmental health perspectives, 120*, 715-720.
Reid, C. E., O'Neill, M. S., Gronlund, C. J., Brines, S. J., Brown, D. G., Diez-Roux, A. V., & Schwartz, J. (2009). Mapping community determinants of heat vulnerability. *Environ Health Perspect, 117*(11), 1730-1736.
Rinner, C., Patychuk, D., Bassil, K., Nasr, S., Gower, S., & Campbell, M. (2010). The Role of Maps in Neighborhood-level Heat Vulnerability Assessment for the City of Toronto. *Cartography and Geographic Information Science, 37*, 31-44.
Rizwan, A. M., Dennis, L. Y., & Chunho, L. (2008). A review on the generation, determination and mitigation of Urban Heat Island. *Journal of Environmental Sciences, 20*(1), 120-128.
Roelofsen, P. (2015). A computer model for the assessment of employee performance loss as a function of thermal discomfort or degree of heat stress. *Intelligent Buildings International, 8*(4), 195-214.
Rossi, F., Pisello, A. L., Nicolini, A., Filipponi, M., & Palombo, M. (2014). Analysis of retro-reflective surfaces for urban heat island mitigation: A new analytical model. *Elsevier, Applied Energy 114*, 621–631.
Roy, D. P., Wulder, M. A., Loveland, T. R., C.E, W., Allen, R. G., Anderson, M. C., Helder, D., Irons, J. R., Johnson, D. M., Kennedy, R., Scambos, T. A., et al. (2014). Landsat-8: Science and product vision for terrestrial global change research. *Remote Sensing of Environment, 145*, 154-172.
Rozenstein, O., Qin, Z., Derimian, Y., & Karnieli, A. (2014). Derivation of land surface temperature for landsat-8 TIRS using a split window algorithm. *Sensors (Switzerland), 14*, 5768-5780.
Sailor, D. J., & Pavlova, A. A. (2003). Air conditioning market saturation and long-term response of residential cooling energy demand to climate change. *Energy, 28*, 941-951.
Saitoh, T. S., Shimada, T., & Hoshi, H. (1996). Modeling and simulation of the Tokyo urban heat island. *Atmospheric Environment, 30*, 3431-3442.
Salvati, A. (2015). *Urban Morphology and Energy Performance : the Direct and Indirect Contribution in Mediterranean Climate*. Paper presented at the PLEA 2015 Architecture in (R) Evolution–31st International PLEA Conference. Bologna 9-11 September. Building Green Futures
Salvati, L., & Sabbi, A. (2011). Exploring long-term land cover changes in an urban region of southern Europe. *International Journal of Sustainable Development & World Ecology, 18*(4), 273-283.
Santamouris, M., Papanikolaou, N., Livada, I., Koronakis, I., Georgakis, C., Argiriou, A., & Assimakopoulos, D. N. (2001). On the impact of urban climate on the energy consumption of buildings. *Solar Energy, 70*(3), 201-216.
Sarak, H. (2003). The degree-day method to estimate the residential heating natural gas consumption in Turkey: a case study. *Energy, 28*(9), 929-939.
Satman, A., & Yalcinkaya, N. (1999). Heating and cooling degree-hours for Turkey. *Energy, 24*(10), 833-840.
Sattari, F., & Hashim, M. (2014). A Breif Review of Land Surface Temperature Retrieval Methods from Thermal Satellite Sensors. *Middle-East Journal of Scientific Research 22*(5), 757-768.

Satterthwaite, D. (2008). Climate Change and Urbanization: Effects and Impliactions for Urban Governance. *United Nations Expert Group Meeting on Population Distribution, Urbanization, Internatl Migration and Development. New York , 21-23 January 2008.*, 29.

Sayemuzzaman, M., & Jha, M. (2014). Modeling of future land cover land use change in North Carolina using Markov chain and cellular automata model. *American Journal of Engineering and Applied Sciences*, *7*(3), 295.

Scherer, D., Fehrenbach, U., Lakes, T., Lauf, S., Meier, F., & Schuster, C. (2013). Quantification of heat-Stress related mortality hazard, vulnerability and risk in Berlin, Germany. *Erde, 144*, 238-259.

Schmugge, T., Hook, S., & Coll, C. (1998). Recovering surface temperature and emissivity from thermal infrared multispectral data. *Remote Sensing of Environment, 65*(2), 121-131.

Senanayake, I. P., Welivitiya, W. D. D. P., & Nadeeka, P. M. (2013). Remote sensing based analysis of urban heat islands with vegetation cover in Colombo city, Sri Lanka using Landsat-7 ETM+ data. *Elsevier, Urban Climate 5 (2013) 19–35, 5* 19–35.

Sertel, E., Ormeci, C., & Robock, A. (2011). Modelling land cover change impact on the summer climate of the Marmara Region, Turkey. *International Journal of Global Warming*, *3*(1/2), 194.

Setaih, K., Hamza, N., Mohammed, M. A., Dudek, S., & Townshend, T. (2014). CFD modeling as a tool for assessing outdoor thermal comfort conditions in urban settings in hot arid climates. *Journal of Information Technology in Construction*.

Seto, K. C., Güneralp, B., & Hutyra, L. R. (2012). Global forecasts of urban expansion to 2030 and direct impacts on biodiversity and carbon pools. *Proceedings of the National Academy of Sciences of the United States of America, 109*, 16083-16088.

Seto, K. C., & Kaufmann, R. K. (2005). Using logit models to classify land cover and land cover change from Landsat Thematic Mapper. *International Journal of Remote Sensing, 26*, 563-577.

Sha, B., & Ghauri, B. (2015). Mapping Urban Heat Island Effect in Comparison with the Land Use , Land Cover of Lahore District. *Pakistan Journal of Meteorology, 11*, 37-48.

Shahmohamadi, P., Che-ani, A. I., Ramly, A., Maulud, K. N. A., & Mohd-Nor, M. F. I. (2010). Reducing urban heat island effects : A systematic review to achieve energy consumption balance. *International Journal of Physical Sciences, 5*, 626-636.

Shapiro, S. S., & Wilk, M. B. (1965). An analysis of variance test for normality (complete samples). *Biometrika, 52*(3/4), 591-611.

Sharma, R., Ghosh, A., & Joshi, P. K. (2012). Analysing spatio-temporal footprints of urbanization on environment of Surat city using satellite-derived bio-physical parameters. *Geocarto International, 28*(5), 420-438.

Shastry, V., Mani, M., & Tenorio, R. (2016). Evaluating thermal comfort and building climatic response in warm-humid climates for vernacular dwellings in Suggenhalli (India). *Architectural Science Review*, *59*(1), 12-26.

Shoko, C., Clark, D., Mengistu, M., Dube, T., & Bulcock, H. (2015). Effect of spatial resolution on remote sensing estimation of total evaporation in the uMngeni catchment, South Africa. *Journal of Applied Remote Sensing, 9*(1), 095997-095997.

Shoko, C., Mutanga, O., & Dube, T. (2016). Progress in the remote sensing of C3 and C4 grass species aboveground biomass over time and space. *ISPRS Journal of Photogrammetry and Remote Sensing 120*(2016), 13–24.

Simone, G. D., Janeiro, R. D., Toronto, T. D., Jack, D., York, N., Toronto, J. P., & Rahman, M. (2011). Climate change and human health in cities Coordinating Lead Authors :

Lead Authors :. *Cities And Climate Change - First Assessment Report of the Urban Climate Change Research Network*, 179-213.

Sithole, K., & Odindi, J. O. (2015). Determination of Urban Thermal Characteristics on an Urban/Rural Land Cover Gradient Using Remotely Sensed Data. *South African Journal of Geomatics, 4*(4), 384-396.

Sivak, M. (2009). Potential energy demand for cooling in the 50 largest metropolitan areas of the world: Implications for developing countries. *Energy Policy, 37*(4), 1382-1384.

Smith, K. R., & Roebber, P. J. (2011). Green roof mitigation potential for a proxy future climate scenario in Chicago, Illinois. *Journal of Applied Meteorology and Climatology, 50*, 507-522.

Sobrino, J., & Raissouni, N. (2000). Toward remote sensing methods for land cover dynamic monitoring: application to Morocco. *International Journal of Remote Sensing, 21*(2), 353-366.

Sobrino, J. A., Jime´nez-Mun˜oz, J. C., & Paolini, L. (2004). Land surface temperature retrieval from LANDSAT TM 5. *Remote Sensing of Environment 90*, 434–440.

Sobrino, J. A., Oltra-carrió, R., Sòria, G., Bianchi, R., & Paganini, M. (2012). Impact of spatial resolution and satellite overpass time on evaluation of the surface urban heat island effects. *Remote Sensing of Environment, 117*, 50-56.

Song, Y., & Wu, C. (2015). Examining the impact of urban biophysical composition and neighboring environment on surface urban heat island effect. *Advances in Building Energy Research*.

Southworth, J. (2004). An assessment of Landsat TM band 6 thermal data for analysing land cover in tropical dry forest regions. *International Journal of Remote Sensing, 25*, 689-706.

Souza, L. C. L., Postigo, C. P., Oliveira, a. P., & Nakata, C. M. (2009). Urban heat islands and electrical energy consumption. *International Journal of Sustainable Energy, 28*, 113-121.

Spronken-Smith, R. A., & Oke, T. R. (1998). The thermal regime of urban parks in two cities with different summer climates. *International Journal of Remote Sensing, 19*(11), 2085-2104.

Srivanit, M., Hokao, K., & Phonekeo, V. (2012). Assessing the Impact of Urbanization on Urban Thermal Environment : A Case Study of Bangkok Metropolitan. *International Journal of Applied Science and Technology, 2*, 243-256.

Stathakis, D., Perakis, K., & Savin, I. (2012). Efficient segmentation of urban areas by the VIBI. *International Journal of Remote, 33*, 3661-6377.

Stathopoulou, M., & Cartalis, C. (2007). Daytime urban heat islands from Landsat ETM+ and Corine land cover data: An application to major cities in Greece. *Solar Energy, 81*, 358-368.

Stathopoulou, M., Cartalis, C., & Chrysoulakis, N. (2006). Using midday surface temperature to estimate cooling degree-days from NOAA-AVHRR thermal infrared data: An application for Athens, Greece. *Solar energy, 80*(4), 414-422.

Stathopoulou, M., Cartalis, C., & Keramitsoglou, I. (2004). Mapping micro-urban heat islands using NOAA/AVHRR images and CORINE Land Cover: an application to coastal cities of Greece. *International Journal of Remote Sensing, 25*(12), 2301-2316.

Steeneveld, G. J., Koopmans, S., Heusinkveld, B. G., & Theeuwes, N. E. (2013). Refreshing the role of open water surfaces on mitigating the maximum urban heat island effect. *Elsevier, Landscape andUrbanPlanning, 121*, 92–96.

Steeneveld, G. J., Koopmans, S., Heusinkveld, B. G., & Theeuwes, N. E. (2014). Landscape and Urban Planning Refreshing the role of open water surfaces on mitigating the maximum urban heat island effect. *Landscape and Urban Planning, 121*, 92-96.

Stewart, I. D., & Oke, T. R. (2012). Local climate zones for urban temperature studies. *Bulletin of the American Meteorological Society, 93*(12), 1879-1900.
Storey, J., Scaramuzza, P., Schmidt, G., Barsi, J., . (2005). LANDSAT 7 scan line corrector-off gap-filled product development. *Proceeding of Pecora 16*, 23-27.
Streutker, D. R. (2002). A remote sensing study of the urban heat island of Houston, Texas. *International Journal of Remote Sensing, 23*(13), 2595-2608.
Sun, L., & Schulz, K. (2015). The Improvement of Land Cover Classification by Thermal Remote Sensing. *Remote sensing, 7*, 8368-8390.
Sung, C. Y. (2013). Mitigating surface urban heat island by a tree protection policy: A case study of The Woodland, Texas, USA. *Elsevier, Urban Forestry & Urban Greening, 12*, 474-480.
Tanabe, S.-i., Haneda, M., & Nishihara, N. (2015). Workplace productivity and individual thermal satisfaction. *Building and Environment, 91*, 42-50.
Tanser, F. C., Sharp, B., & le Sueur, D. (2003). Potential effect of climate change on malaria transmission in Africa. *Lancet, 362*(9398), 1792-1798.
Tao, S., Yong, H., Hong, W., Chun-E, S., & Yuan-Jian, Y. (2015). Influence of urbanization on the thermal environment of meteorological station: Satellite-observed evidence. *Advances in Climate Change Research 6*(2015), 7-15.
Tao, Z., Santanello, J. A., Chin, M., Zhou, S., Tan, Q., Kemp, E. M., & Peters-Lidard, C. D. (2013). Effect of land cover on atmospheric processes and air quality over the continental United States – a NASA Unified WRF (NU-WRF) model study. *Atmospheric Chemistry and Physics, 13*(13), 6207-6226.
Terando, A. J., Costanza, J., Belyea, C., Dunn, R. R., McKerrow, A., & Collazo, J. A. (2014). The southern megalopolis: using the past to predict the future of urban sprawl in the Southeast U.S. *PLoS One, 9*(7), e102261.
Thomas, G., Sherin, A., Ansar, S., & Zachariah, E. (2014). Analysis of urban heat island in Kochi, India, using a modified local climate zone classification. *Procedia Environmental Sciences, 21*, 3-13.
Tomlinson, C. J., Chapman, L., Thornes, J. E., & Baker, C. J. (2011). Including the urban heat island in spatial heat health risk assessment strategies: a case study for Birmingham, UK. *Int J Health Geogr, 10*, 42.
Tonnang, H. E. Z., Kangalawe, R. Y. M., & Yanda, P. Z. (2010). Predicting and mapping malaria under climate change scenarios: the potential redistribution of malaria vectors in Africa. *Malaria journal, 9*, 111-121.
Torrance, J. (1981). Climate handbook of Zimbabwe. *Zimbabwe Meteorological Services, Harare*.
Tran, H., Uchihama, D., Ochi, S., & Yasuoka, Y. (2006). Assessment with satellite data of the urban heat island effects in Asian mega cities. *International Journal of Applied Earth Observation and Geoinformation, 8*, 34-48.
Tucker, C. J. (1979). Red and photographic infrared linear combinations for monitoring vegetation. *Remote Sensing of Environment, 8*, 127– 150.
Tucker, C. J., Townshend, J. R., & Goff, T. E. (1985). African land-cover classification using satellite data. *Science, 227*(4685), 369-375.
Tulandi, D., Pramoedyo, H., Yanuwiadi, B., & Rotinsulu, W. (2012). Thermal Comfort Assessment in the Boulevard Area in Manado CBD, North Sulawesi. *Change, 10*, p11.
Tursilowati, L. (2007). Urban Climate Analysis on The Land Use and Land Cover Change (LULC) in Bandung, Indonesia with Remote Sensing and GIS. *UN/Austria/ESA Symposium*

Uejio, C. K., Wilhelmi, O. V., Golden, J. S., Mills, D. M., Gulino, S. P., & Samenow, J. P. (2011). Intra-urban societal vulnerability to extreme heat: The role of heat exposure and the built environment, socioeconomics, and neighborhood stability. *Health and Place, 17*, 498-507.

UNFPA. (2007). The State of World Population 2007. United Nations Population Fund. *United Nations Publications*.

Unganai, L. S. (1996). Historic and future climatic change in Zimbabwe. *Climate Research, 6*, 137-145.

United Nations. (2014). World Urbanization Prospects: The 2014 Revision, Highlights. Department of Economic and Social Affairs. *Population Division, United Nations*.

USGS. (2016). Landsat 8 (L8) Data Users Handbook. *Department of the Interior U.S. Geological Survey, Version 2*.

Valsson, S., & Bharat, A. (2009). Urban heat island: Cause for microclimate variations. *Architecture-Time Space & People, 2125*.

van-Westen, C. J. Remote Sensing and GIS for Natural Hazards Assessment and Disaster Risk Reduction.

Vardoulakis, E., Karamanis, D., Fotiadi, A., & Mihalakakou, G. (2013). The urban heat island effect in a small Mediterranean city of high summer temperatures and cooling energy demands. *Solar Energy, 94*, 128-144.

Vaughan, R. G., Keszthelyi, L. P., Lowenstern, J. B., Jaworowski, C., & Heasler, H. (2012). Use of ASTER and MODIS thermal infrared data to quantify heat flow and hydrothermal change at Yellowstone National Park. *Journal of Volcanology and Geothermal Research, 233*, 72-89.

Vescovi, L., Rebetez, M., & Rong, F. (2005). Assessing public health risk due to extremely high temperature event: climte and social parameters. *Climate research, 30*, 71-78.

Vlassova, L., Perez-Cabello, F., Nieto, H., Martín, P., Riaño, D., & de la Riva, J. (2014). Assessment of methods for land surface temperature retrieval from Landsat-5 TM images applicable to multiscale tree-grass ecosystem modeling. *Remote Sensing, 6*(5), 4345-4368.

Voogt, J. A., & Oke, T. R. (2003). Thermal remote sensing of urban climates. *Remote Sensing of Environment, 86*, 370-384.

Wan, Z., Zhang, Y., Zhang, Q., & Li, Z.-L. (2004). Quality assessment and validation of the MODIS global land surface temperature. *International journal of remote sensing, 25*(1), 261-274.

Wang, C.-y., & Zhu, W.-p. (2011). Analysis of the Impact of Urban Wetland on Urban Temperature Based on Remote Sensing Technology. *Elsevier, Procedia Environmental Sciences, 10*, 1546 – 1552.

Wang, K., Liu, Q., & Liu, Q. (2010). *Localized land surface temperature retrieval from the MODIS Level-1b data using water vapor and in situ data.* Paper presented at the Geoscience and Remote Sensing Symposium (IGARSS), 2010 IEEE International. (pp. 2252-2254). Ieee.

Wang, X., Chen, D., & Ren, Z. (2010). Assessment of climate change impact on residential building heating and cooling energy requirement in Australia. *Building and Environment, 45*, 1663-1682.

Wania, A., Kemper, T., Tiede, D., & Peter Zeil, b. (2014). Mapping recent built-up area changes in the city of Harare with high resolution satellite imagery. *Applied Geography, 46*, 35-44.

Ward, D. S., Mahowald, N. M., & Kloster, S. (2014). Potential climate forcing of land use and land cover change. *Atmospheric Chemistry and Physics, 14*(23), 12701-12724.

Wei-wu, W., Li-zhong, Z., & Ren-chao, W. (2004). An analysis on spatial variation of urban human thermal comfort in Hangzhou, China. *Journal of Environmental Sciences, 16*, 332-338.

Weng, Q., Liu, H., & Lu, D. (2007). Assessing the effects of land use and land cover patterns on thermal conditions using landscape metrics in city of Indianapolis, United States. *Urban Ecosystems, 10*(2), 203-219.

Weng, Q., & Lu, D. (2008). A sub-pixel analysis of urbanization effect on land surface temperature and its interplay with impervious surface and vegetation coverage in Indianapolis , United States. *International Journal of Applied Earth Observation and Geoinformation, 10*, 68-83.

Weng, Q., Lu, D., & Schubring, J. (2004). Estimation of land surface temperature-vegetation abundance relationship for urban heat island studies. *Remote Sensing of Environment, 89*, 467-483.

Widyasamratri, H., Souma, K., Suetsugi, T., Hiroshi Ishidaira, Ichikawa, Y., Kobayashi, H., & Inagaki, I. (2013). Air Temperature Estimation from Satellite Remote Sensing to Detect the Effect of Urbanization in Jakarta, Indonesia. *Journal of Emerging Trends in Engineering and Applied Sciences, 4*(6), 800-805.

Wilhelmi, O. V., & Hayden, M. H. (2010). Connecting people and place: a new framework for reducing urban vulnerability to extreme heat. *Environmental Research Letters, 5*, 14021-14027.

Williams, C. N., Basist, A., Peterson, T. C., & Grody, N. (2000). Calibration and verification of land surface temperature anomalies derived from the SSM/I. *Bulletin of the American Meteorological Society, 81*, 2141-2156.

Wilson, J. W., & Brandes, E. A. (1979). Radar Measurement of Rainfall—A Summary. *Bulletin of the American Meteorological Society, 60*(9), 1048-1058.

Witt, R. G., Minor, T. B., & Sekhon, R. S. (2007). Use of HCMM thermal data to improve accuracy of MSS land-surface classification mapping. *International Journal of Remote Sensing, 6*(10), 1623-1636,.

Wolf, T., & McGregor, G. (2013). The development of a heat wave vulnerability index for London, United Kingdom. *Weather and Climate Extremes, 1*, 59-68.

World Meteorological Organization. (2000). Guidelines on Analysis of extremes in a changing climate in support of informed decisions for adaptation. *Climate Data and Monitoring, WCDMP*(No. 72).

World Meteorological Organization. (2007). The role of climatological normals in a changing climate. *WCDMP, No. 61*(WMO-TD No. 1377).

Wu, H., Ye, L.-p., Shi, W.-z., & Clarke, K. C. (2014). Assessing the effects of land use spatial structure on urban heat islands using HJ-1B remote sensing imagery in Wuhan , China. *International Journal of Applied Earth Observations and Geoinformation, 32*, 67-78.

Wu, S., Mickley, L. J., Kaplan, J. O., & Jacob, D. J. (2012). Impacts of changes in land use and land cover on atmospheric chemistry and air quality over the 21st century. *Atmospheric Chemistry and Physics, 12*, 1597-1609.

Xian, G., & Crane, M. (2005). An analysis of urban thermal characteristics and associated land cover in Tampa Bay and Las Vegas using Landsat satellite data. *Remote Sensing of Environment 104* ((2006)), 147–156.

Xian, G., Homer, C., Bunde, B., Danielson, P., Dewitz, J., Fry, J., & Pu, R. (2012). Quantifying urban land cover change between 2001 and 2006 in the Gulf of Mexico region. *Geocarto International, 27*(6), 479–497.

Xiao, R.-b., Ouyang, Z.-y., Zheng, H., Li, W.-f., Schienke, E. W., & Wang, X.-k. (2007). Spatial pattern of impervious surfaces and their impacts on land surface temperature in Beijing, China. *Journal of environmental sciences (China), 19*, 250-256.

Xu, H. (2006). Modification of normalised difference water index (NDWI) to enhance open water features in remotely sensed imagery. *International Journal of Remote Sensing, 27*, 3025-3033.

Xu, H. (2008). A new index for delineating built-up land features in satellite imagery. *International Journal of Remote Sensing, 29*, 4269-4276.

Xu, L. Y., Xie, X. D., & Li, S. (2013). Correlation analysis of the urban heat island effect and the spatial and temporal distribution of atmospheric particulates using TM images in Beijing. *Environmental Pollution, 178*, 102-114.

Yang, J. S., Wang, Y. Q., & August, P. V. (2004). Estimation of Land Surface Temperature Using Spatial Interpolation and Satellite-Derived Surface Emissivity. *Journal of Environmental Informatics*, 89-96.

Yang, L., Cao, Y., Zhu, X., Zeng, S., Yang, G., He, J., & Yang, X. (2014). Land surface temperature retrieval for arid regions based on Landsat-8 TIRS data : a case study in Shihezi , Northwest China. *Journal of Arid Land, 6*, 704-716.

Yang, W., Lin, Y., Wong, N. H., & Zhou, J. (2014). Thermal comfort requirements in the summer season in subtropical urban spaces. *Intelligent Buildings International, 6*, 224-238.

Yang Zhang, Chen Yiyun, Ding Qing, & Ping Jiang. (2012). Study on Urban Heat Island Effect Based on Normalized Difference Vegetated Index:A Case Study of Wuhan City. *Elsevier, Procedia Environmental Sciences 13* 574 – 581.

Yilmaz, S. (2007). Human thermal comfort over three different land surfaces during summer in the city of Erzurum, Turkey. *atmosfera, 20*(3), 289-297.

Yousif, T. A., & Tahir, H. M. M. (2013). Application of Thom's Thermal Discomfort Index in Khartoum State, Sudan. *Journal of forest products & industries, 2*(5), 36-38.

Yu, X., Zhang, A., Hou, X., & Li, M. (2013). Multi-temporal remote sensing of land cover change and urban sprawl in the coastal city of Yantai , China. *International Journal of Digital Earth*, 37-41.

Yuan, F., & Bauer, M. E. (2007). Comparison of impervious surface area and normalized difference vegetation index as indicators of surface urban heat island effects in Landsat imagery. *Remote Sensing of Environment, 106*, 375-386.

Yuen, B., & Kong, L. (2009). Climate change and urban planning in Southeast Asia. *SAPI EN. S. Surveys and Perspectives Integrating Environment and Society*, 1-20.

Zemba, A. (2010). Analysis of Urban Surface Biophysical Descriptors and Land Surface Temperature Variations in Jimeta City, Nigeria. *Global Journal of Human Social Science, 10*, 19-26.

Zha, Y., Gao, J., & Ni, S. (2003). Use of normalized difference built-up index in automatically mapping urban areas from TM imagery. *International Journal of Remote Sensing, 24*(3), 583-594.

Zhang, H., Qi, Z. f., Ye, X. y., Cai, Y. b., Ma, W. c., & Chen, M. n. (2013). Analysis of land use/land cover change, population shift, and their effects on spatiotemporal patterns of urban heat islands in metropolitan Shanghai, China. *Elsevier, Applied Geography 44*, 121-133.

Zhang, Q., Schaaf, C., & Seto, K. C. (2013). The Vegetation adjusted NTL Urban Index: A new approach to reduce saturation and increase variation in nighttime luminosity. *Remote Sensing of Environment, 129*, 32-41.

Zhang, Y., Odeh, I. O. A., & Han, C. (2009). Bi-temporal characterization of land surface temperature in relation to impervious surface area , NDVI and NDBI , using a sub-

pixel image analysis. *International Journal of Applied Earth Observation and Geoinformation, 11*, 256-264.
Zhang, Y., Yiyun, C., Qing, D., & Jiang, P. (2012). Study on Urban Heat Island Effect Based on Normalized Difference Vegetated Index:A Case Study of Wuhan City. *Procedia environmental sciences, 13*, 574 – 581.
Zhao, H., & Chen, X. (2005). *Use of normalized difference bareness index in quickly mapping bare areas from TM/ETM+*. Paper presented at the Proceedings. 2005 IEEE International Geoscience and Remote Sensing Symposium, 2005. IGARSS'05.
Zhou, X., & Wang, Y.-C. (2011a). Dynamics of Land Surface Temperature in Response to Land-Use/Cover Change. *Geographical Research, 49*(1), 23-36.
Zhou, X., & Wang, Y. C. (2011b). Spatial-temporal dynamics of urban green space in response to rapid urbanization and greening policies. *Landscape and Urban Planning, 100*, 268-277.
ZIMSTAT. (2012). *Census 2012, Provincial Report*.
Zinyama, L. M., Tevera, D. S., & Cumming, S. D. (1993). *Harare: the growth and problems of the city*: University of Zimbabwe Publications.
Zuvela-aloise, M., Bokwa, A., Dobrovolny, P., Gal, T., Geletic, J., & Gulyas, A. (2015). Modelling urban climate under global climate change in Central European cities. *EGU Conference Abstracts, 17*(2015), 21410222.
Zvigadza, S., Mharadze, G., & Ngena, S. (2010). Community Based Adaptation to Climate Change in Africa (CBAA) Communities And Climate Change: Building Local Capacity For Adaptation. *African Centre for Technology Studies*, 1-16.